Neural encoding of the vertical plane in freely-moving rats

Giulio Casali

Thesis submitted to University College London for the degree of Doctor of Philosophy in Neuroscience

Declaration

I, Giulio Casali, confirm that the work presented in this thesis is my own. Where information has been derived from other sources, I confirm this has been indicated in the thesis.

Acknowledgements

I would like to thank a number of people for providing great support throughout four long years of exciting science culminating in this thesis. First, a special thank you goes to Kate Jeffery (my secondary PhD supervisor) for being an excellent mentor and leading me through the meanders of the hippocampal circuits. I would also like to thank Francesca Cacucci (my primary PhD supervisor) for her precious advice and Daniel Bush for the fruitful exchange of ideas throughout this journey. I would also like to acknowledge other great scientists such as Caswell Barry, Robin Hayman, Neil Burgess and Daniel Bendor for the many conversations and advice I received. Moreover, a great thank goes to many colleagues whom I have come across during my stay at the IBN, in particular Liz, Shaz, Gioia, Freyja, Laurenz, Josh, Jonathan, Yave, Dot, Pierre, Sophie, James, Han, Amir, Catherine, Souraya, Eleonore, Roddy, Jonas. I would also like to thank my mighty football team Dynamo Francone for the little but nonetheless great time spent together as well as my dearest roman friends Marco, Riccardo, Nicola, Vittorio and Filippo. And last but not at all least, my brother Paolo and my parents require a special thank for the huge support during my stay abroad. However, the greatest thank you of all goes to my girlfriend, Silvia, for her amazing talent for bearing with me; your kindness, patience and support will be always remembered and very much appreciated.

Abstract

Grid cells produce a periodic hexagonal array of firing fields when the rat navigates on a horizontal 2D surface, and such regularity supports the hypothesis that they encode distances covered by the animal. This computation is thought to form the neural basis for path integration, and the medial entorhinal cortex (MEC), where grid cells are mostly found, is now believed to play a major role for the establishment of a cognitive map in the brain. However, while grid cells on the horizontal plane are invariant across different environments (they provide fixed spatial metrics), it is currently not known whether those distances vary in 3D space. Previous findings suggested that grid cells may be substantially incapable to perform path integration in the vertical plane and this thesis aimed to test a number of hypothesis to explain such an impairment. These results show that grid cells are not affected by experience with 3D locomotion; they are modulated by the orientation of the locomotion plane and on a climbing wall they display heavily distorted firing patterns with expanded but fewer fields. Based on these findings, the hypothesis that the inconsistency between horizontal and vertical maps may be due to the miscomputation of instantaneous speed was suggested. Preliminary results support the view that the speed signal carried by speed cells (single-unit level) and LFP theta oscillation (large ensembles) was substantially reduced suggesting an underestimation of speed during climbing. Put together these results support the hypothesis that the speed signal plays a crucial role for the generation of a regular grid. In the vertical dimension the speed signal is reduced and such impairment drives grid cells to expand and become more irregular. Overall these results demonstrate that the neural representation of space is therefore not symmetrical across dimensions but is instead anisotropic.

Table of Contents

List of abbreviations

ADN	Antero-dorsal thalamic nuclei
A-P	Anterior-posterior
CA (1-4)	Cornu ammonis
CANM	Continuous attractor network model
DG	Dentate gyrus
D-V	Dorsal-ventral
EC	Entorhinal cortex
EEG	Electroencephalogram
FCC	Face centred cubic
GC	Grid cell
HCP	Hexagonal close pack
HD	Head direction
HF	Hippocampal formation
HP	Hippocampus proper
HPC	Hippocampus
LFP	Local field potential
LTD	Long term depression
LTP	Long term potentiation
MEC	Medial entorhinal cortex
MS	Mossy fibers
MS-DBB	Medial septum and diagonal band of Broca
MTL	Medial temporal lobe
OIM	Oscillatory interference model
PAR	Parasubiculum
PC	Place cell
PRE	Presubiculum
PER	Perirhinal cortex
PHR	Parahippocampal region
POR	Postrhinal cortex
POS	Postsubiculum
PP	Perforant path
PV^+	Parvalbumin positive
RSC	Retrosplenial cortex

SC	Schaffer collateral
S-R	Stimulus-response
S-T	Septal-temporal
SUB	Subiculum
V-R	Virtual reality

Index of figures

Part 1

Introduction

1 Overview of spatial cognition

For every freely-moving animal, the capacity to localize itself in space is essential. This is because environments challenge an individual's survival for a number of reasons, including predators and lack of supplies. Therefore, in order to overcome such threats, animals need to determine their position as well as the goal location at any given time and be capable of drawing an imaginary vector connecting them. If an animal is capable of doing so, its movements in space will then be both efficient (the shortest path is taken) and flexible (robust to environmental changes) and the exhibited spatial behaviour is called navigation. What makes animals perform navigation is a matter addressed by scientists ever since the dawn of experimental psychology and such endeavours have been termed spatial cognition. Two sets of information or cues are used by an animal to orientate itself in space. On the one hand, cues coming from outside the animal's body, such as external landmarks, are used for navigation. They are processed by sensory systems (sight, touch, smell etc.) and are referred to as allothetic cues. On the other hand, cues generated from inside the animal are known as idiothetic, and depend on the whole set of senses perceiving body movements (vestibular, proprioceptive, motor efference copy etc.). The ability to integrate both allothetic and idiothetic information results in optimal navigation. The following example might help to explain this process.

It is a well-known experience to get back home late at night and need to reach a particular room without turning the lights on. The lack of visual information makes it challenging but it is eventually possible to accomplish the task and navigate to the light switch successfully. The strategy adopted usually requires one to mentally imagine the surrounding space and update self-position based on the perception of body movements (direction, speed). This example shows that self-motion cues can be sufficient to keep track of the path one has taken through space, and such computation is known as "path integration" or "dead reckoning" (Etienne and Jeffery, 2004). However, relying on idiothetic cues only is not accurate due to error accumulation. Continuing with the "moving-in-the-dark" example, it is also common to experience the feeling of uncertainty about ones current position after a number of steps in a dark room. However, bumping into objects (chairs, doors, furniture) may help in determining ones current location. Recognizing an object depends on sensory systems (touch in this example) and, if it is both familiar and fixed in space, it acts as a landmark re-setting position estimate. Therefore, accurate position is solved by integrating allothetic (when available) with idiothetic cues. How the

brain computes this is an unsolved question in neuroscience.

Since the dawn of modern ethology, animal navigation has received lots of interest (Darwin, 1873). However, initial studies mostly involved behavioural experiments (Shepard, 1933; Thinus-Blanc, 1996), because the neural substrate of spatial cognition could not be fully addressed until the development of electrophysiology *in vivo* recording methods. This technique ultimately led to the discovery of place cells in rodent hippocampus (O'Keefe and Dostrovsky, 1971). Since then, a wealth of evidence has been collected showing that the hippocampus, in concert with a large network of brain areas, performs computations necessary for spatial cognition and thus supports navigation. Importantly, thanks to a number of studies (most of which have been conducted in rodents), a coherent theoretical framework on spatial cognition is nowadays at our disposal. However, it should be pointed out that the majority of evidence comes from experiments where animals were allowed to navigate in simple horizontal environments (such as a small square box with a single cue card). In contrast, the complexity of real environments poses several additional challenges which the brain must be able to cope with. For instance, natural terrains where animals move are not just flat horizontal planes but rather a continuum of tilted and irregular surfaces. Few studies have specifically explored the functioning of these neural networks known for supporting spatial cognition during locomotion on non-horizontal surfaces. The broad question that this thesis aims to answer is whether in the rat brain, the circuits performing spatial cognition also encode spatial information during movements on the vertical plane and to see if such representations do not substantially differ from those in the horizontal. This can be seen as the first step towards the more general investigation of 3D encoding of space in the rodent brain. Preliminary evidence in rats suggested that movements along gravity dramatically impaired spatial coding (Hayman et al., 2011), but several factors could have contributed to the lack of spatial representation on the vertical plane. Specifically, the aim of this thesis was to test whether factors, such as previous experience with 3D locomotion or the orientation of the body relative to the surface, affect spatial coding. These questions were addressed by raising animals in enriched cages where rats spontaneously learned how to climb. The neural activity was then recorded in a variety of environments where a number of hypotheses generated from previous studies could be tested. Put together, these findings provide relevant insights into the topic of 3D spatial representation in the rodent.

The aim of this chapter is to briefly introduce the principles of spatial cognition along

with the pioneering experiments which addressed this fascinating matter.

1.1. Tolman and the cognitive map

Tolman, undoubtedly a pioneer in experimental psychology, tested rats' spatial skills in a number of circumstances (Tolman, 1948). Indeed, in his most famous "sunburst" experiment, he trained rats to run from a start box across a circular area and then down a corridor at the end of which was placed a reward (see Figure 1-1A). After several trials, the experiment was repeated but the central corridor was blocked and several radiating paths added (see Figure 1-1B). What he observed was a significant preference for the corridor that pointed towards the same place in the room to where the reward had been placed before. This result supported the hypothesis that rats not only learned the correct behaviour to perform in order to get the reward, but they developed a more comprehensive representation of space allowing them no navigate flexibly in it. Given that rats flexibly adopted the shortest path to reach a goal location following the change in the setup, Tolman proposed that rats had an allocentric map-like representation of the environment, which he called a "cognitive map" (Tolman, 1948). In order to be a map, it had to be "allo-centric" – i.e. world-centred, and so dependent on the spatial relationships within the environment– rather than "ego-centric" – i.e. body-centred thus anchored to the subject's position. This aspect of Tolman's theory conflicted greatly with the views of

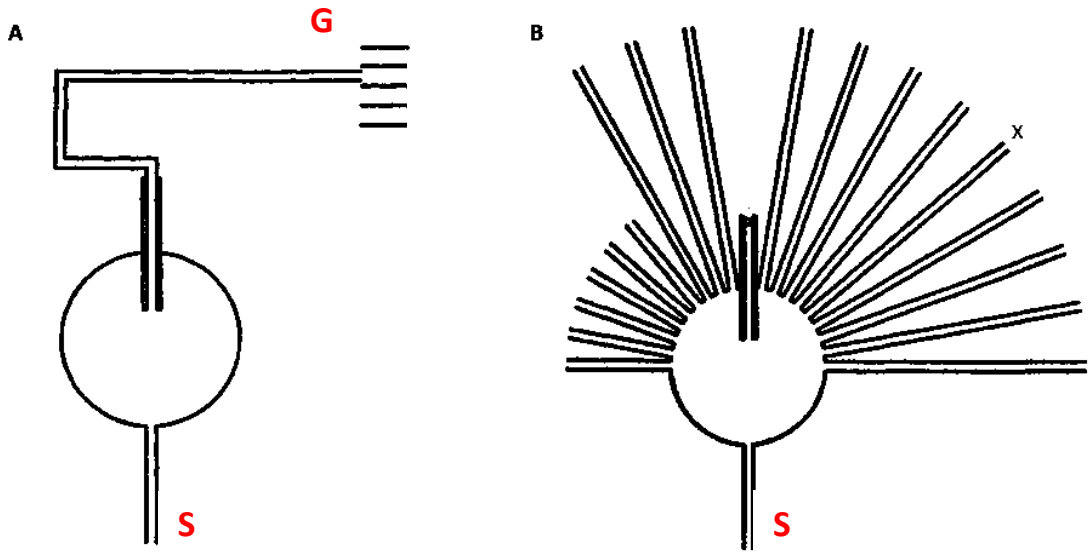

Figure 1-1 Sunburst maze designed to assess spatial behaviour of rats.

(**A**) Configuration of the maze during training. Rats placed at the start of one corridor (S), learned to cross the circular arena and follow the sets of continuous corridors to reach goal location (G).
(**B**) Configuration of the maze during probe. Among many corridors, rats chose the one pointing to the G location. Adapted from Tolman, 1948.

"behaviourism", the most prominent school of thought in psychology in vogue at that time. What this theory postulated was that complex behaviours, such as those exhibited by rats to navigate, are elicited by any form of cue (visual, auditory, kinaesthethic etc) functioning as a *stimulus (S)* which becomes progressively linked with a precise behaviour, the *response (R)*, aimed to obtain a reward. Therefore, according to behaviourists, spatial behaviour is generated as a chain of correct responses to environmental stimuli which are selected upon a "trial and error" learning process (Thorndike, 1898).

Even though Tolman at the beginning of his career was a behaviourist, his "cognitive map" theory was broadly in disagreement with the S-R paradigm postulated by behaviourism. Indeed, the capacity of rats to perform flexible behaviour clashes with the fixed S-R chain posited by behaviourists. In addition, the motivational state of the animal, as well as the presence of reinforcements, were not prerequisites for the formation of the cognitive maps, and these aspects heavily disagreed with the principles of behaviourism. Moreover, still relevant for the current investigation of spatial cognition is Tolman's early insight of the link between the representation of the space that the animal computes and the learning processes. In agreement with Tolman's theory, the information represented during a spatial experience can be retrieved in a subsequent exposure to the same environment; therefore, this process is thought to be dependent on the recalling of previous memory in the frame of a broad learning mechanism defined by the authors as "latent learning" (Tolman, 1948). Therefore, overall Tolman's theory must be considered not just as a new point of view on the debate over spatial cognition, but rather as a broader rethink of the neural learning processes. Indeed, the investigation of navigational abilities today offers us relevant clues toward the understanding of the mechanisms by which animals and humans learn.

1.2. The hippocampus functions as cognitive map

After the publication of the "Cognitive maps in rats and men" (1948), the issue over "cognitive map theory" almost disappeared from the debate among researchers. Partially this was due to the predominance of behaviourism and the relative weakness of experimental results supporting the Tolmanian cognitive map theory. However, a new epoch in the study of spatial cognition started in the early 1970s when a new generation of researchers radically changed the history of the field. Indeed, seminal studies were conducted with the aim of elucidating the mechanisms by which the brain supports navigation. This neurobiological approach was possible following the seminal study by

Scoville and Milner (1957) who examined a number of patients with medial temporal lobe (MTL) lesions, the most famous of which, H.M., underwent bilateral resection of the MTL as an attempt to cure severe drug-resistant epilepsy (Scoville and Milner, 1957). After the surgery, epileptic seizures decreased but H.M. begun exhibiting profound anterograde memory deficits – i.e. an incapacity to form new memories – as well as semantic and spatial deficits (Corkin, 2002; Corkin et al., 1997). Subsequent studies revealed a substantial loss of the hippocampus, even though recent examination showed severe loss of entorhinal cortex, amygdaloid complex and perirhinal cortex as well (Corkin, 2002). This finding suggested that the hippocampal formation in mammals may be one of the neural substrates involved in learning and memory, at least in humans, and this led to a new era of investigation of the hippocampus in animals. Compelling evidence for the hippocampal involvement for learning and memory came after the discovery of place cells (O'Keefe and Dostrovsky, 1971), neurons located in principal layer of the hippocampus showing spatially-selective firing while an animal explores space (see 3.2.1 for a thorough description of place cell properties). Since then the hippocampus and place cells have been extensively investigated, and a flourishing line of research has risen since the publication of the "Hippocampus as a Cognitve Map", in which it was proposed by O'Keefe and Nadel that the primary role of rodent hippocampus is for spatial memory (O'Keefe and Nadel, 1978). According to the authors, the hippocampus is the brain area responsible for spatial navigation since it hosts the neural representation of the environment, defined by Tolman (1948) as the "cognitive map". This book provided a coherent framework with which to study spatial cognition and has been seminal in the field of spatial cognition. A wealth of studies concomitant with the "Hippocampus as Cognitive Map" theory were conducted using a variety of tasks, protocols and manipulations (Day and Schallert, 1996; Eichenbaum et al., 1990; Jarrard, 1983; Morris, 1981; Morris et al., 1982; Olton and Papas, 1979; Olton and Samuelson, 1976; Olton et al., 1978; Winocur, 1982). Taken together, these results agreed with the principles of the Tolmanian cognitive map theory, but represented a step forward for having identified the neural substrate supporting spatial cognition: the hippocampus.

1.3. Hippocampus and plasticity

The attention that hippocampal research gained grew exponentially during those years, and particularly the fact that neural substrates of learning and memory could be investigated. It should also be mentioned that parallel to the spatial cognition field, a new

line of research suggested a causal link between the hippocampus and memory: the discovery of long term potentiation (LTP; Figure 1-2). The seminal studies by Bliss and Lomo in the 1970s revealed a striking feature of hippocampal circuits, which is that they are extremely plastic (i.e. adaptable). Bliss and Lomo showed that repetitive high-frequency train stimulation of the perforant path – the bundle of fibres projecting from the entorhinal cortex to the dentate gyrus – induced a long-lasting increased post-synaptic response (Bliss and Gardner-Medwin, 1971; Bliss and Lomo, 1970; Bliss and Lømo, 1973; Lomo, 1971a, 1971b). Further studies revealed a number of cellular mechanisms inducing LTP throughout the hippocampal circuit (Bliss and Collingridge, 1993; Brown et al., 1990). Similar to LTP, a related phenomenon, long term depression (LTD) was subsequently discovered (see Figure 1-2). This occurs when low-frequency stimulation is applied for a long time such that both pre-synaptic and post-synaptic mechanisms contribute to the weakening of the synapses involved (Bear and Abraham, 1996; Citri and Malenka, 2008).

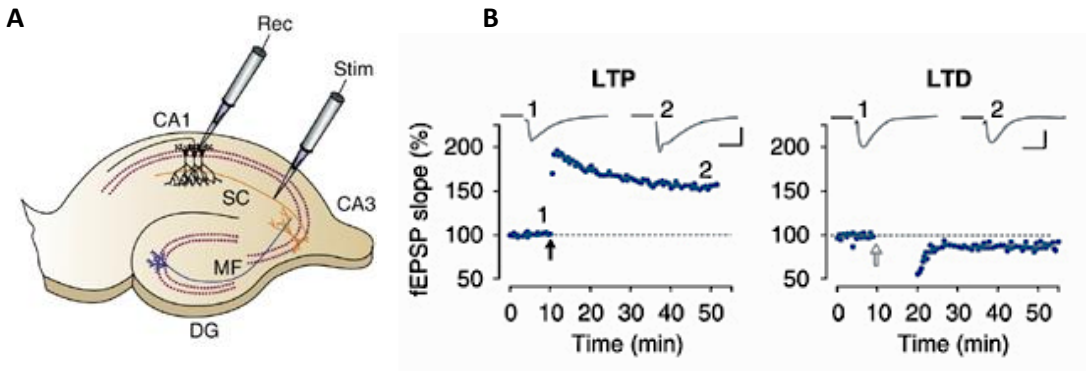

Figure 1-2 Synaptic plasticity in the hippocampal slice preparation.

A) Schematic representation of the experimental setup for measuring plasticity in a preparation of rodent hippocampal slice. Note the mossy fibres (MS) from DG inputting CA3 pyramidal neurons which project to CA1 via Schaffer collaterals (SC).

B) The strength of synaptic connections is measured as the slope of the field excitatory post-synaptic potential (fEPSP) across time (min). LTP (left) is induced following 100 Hz stimulation for 1s (black arrow), whereas LTD (right) is induced following 5 Hz stimulation for 3 minutes (white arrow). Note the enhanced response for LTP in contrast to decreased response (LTD). Adapted from Citri and Malenka, 2008.

The overall feature of hippocampal circuits to adapt by strengthening/weakening reciprocal connections very much resembles the theoretical model proposed by Hebb (1949). In this seminal work, he hypothesized that the simplest trace of memory in the brain can be established by the strengthening of synaptic connections between two cells, so that the pre-synaptic firing of cell A increases the firing's probability of the postsynaptic cell B (Hebb, 1949). This model of neural memory has since then been referred to as Hebbian plasticity. Three requirements were described in Hebb's classical model for the

establishment of memory, sometimes defined as Hebb's rule: activity dependence (since the firing activity is required for both the cells), associativity (only cells with a high co-firing index are strengthened) and specificity (only the synapses simultaneously active are strengthened, but not the ones belonging to same cells but forming synapses with other cells). As proposed by Hebb, this mechanism could foster the coupling of cellular events taking place in a short time window in light of simple forms of learning, such as the conditioned responses to stimuli. The model proposed by Hebb was experimentally confirmed by the seminal studies carried out by Kandel and colleagues who investigated the neural basis of learning in the snail Aplysia (Kandel and Tauc, 1965a, 1965b). These authors reported forms of learning dependent on a similar mechanism in which a third cell, a modulatory interneuron, is required for potentiation, a phenomenon referred to as hetero-synaptic plasticity. Moreover, the subsequent discoveries of LTP and LTD in the hippocampal circuits by Bliss and Lomo (Bliss and Lømo, 1973) further confirmed the Hebbian model and corroborated the hypothesis that synaptic plasticity may contribute to the establishment of memory traces in the hippocampus.

In summary, experimental evidence demonstrated a remarkable degree of plasticity occurring in the hippocampus, and such features have been interpreted as the underlying biological mechanism for the storage of information. However, it should be pointed out that sometimes the expression "learning and memory" is misleadingly associated to the concept of "plasticity", broadly referred to as the mechanism by which neurons modify their synaptic connections and/or other relevant properties in response to stimuli (such as activation, signals etc.). It must be noted that memory and plasticity are not synonymous; indeed, memory is the subject's faculty of being able to remember past experiences and efficiently make use of them (learning), whilst plasticity is the neuronal property of changing features, for instance the currents flowing between cells forming a given circuit - for an exhaustive review on plasticity and its contribution to several functions see Citri and Malenka (2008). Decades of research in the field have demonstrated that plasticity is a general mechanism of neural circuits, which takes place in several phases of ones life span (neurogenesis, development) and for different processes, such as sensory perception, pain, reward, motivation, addiction etc. However, plasticity has been hypothesized to be a relevant property allowing the storage of information and thus is thought to explain the formation of memories at a neuronal level. Indeed, synaptic mechanisms such as LTP and LTD in the hippocampus were proposed to play relevant roles in light of memory formation. Many findings support this hypothesis and it is now becoming clear how LTP

and LTD, which have been discovered as cellular electrical responses to artificial stimulation, occur *in vivo* in the hippocampus. Therefore, they are the most powerful models of information storage at a cellular level to help understanding the neurobiology of memory.

1.4. From the hippocampus to the network

Ever since the pioneering studies conducted by Tolman, the question of how animals perform navigation has been tightly bound to the investigation of learning and memory. Indeed, the principles of the cognitive map theory proposed by Tolman (1948) strongly disagreed with the "behaviourism" paradigm, according to which behaviour, including navigation, emerges as a sequence of S-R events acquired during "trial and error" learning processes (Thorndike, 1898). The bond between space and memory became even stronger once the investigation of the hippocampus was commenced. Indeed, altogether the three following observations generated a coherent theoretical framework in which hippocampal functioning was crucial for the computation of space and memory:

i) the hippocampus was involved in acquiring new memories (H.M.);
ii) neural plasticity obeying Hebbian rules allowed the storage of information;
iii) hippocampal place cells functioned like a cognitive map.

Still nowadays, the precise function of the hippocampal system is disputed, with different schools of thought postulating spatial vs. more declarative processing (Bird and Burgess, 2008; Cohen and Eichenbaum, 1991; Eichenbaum, 2000; Eichenbaum et al., 1992). The question of whether or not the hippocampus processes non-spatial information goes beyond the scopes of this thesis and will not be addressed here. However, decades of investigation have largely improved our knowledge of the spatial computation by the hippocampus, and the early hypothesis proposed by O'Keefe and Nadel in 1978 has been mostly confirmed. Indeed, it is not just the hippocampus where place cells are mostly found, but also a large network of brain areas centered on the hippocampal formation that have been shown to contribute to the representation of space. Compelling evidence came from the discoveries of several functionally-defined cell-types which, similar to place cells, convey spatially-relevant information (so-called spatially-modulated neurons, see 3.2). However, differently to place cells, they do not encode location in space. Indeed, neurons initially recorded from the post-subiculum showed allocentric encoding of head direction

and for this reason the term “head direction cells” was coined (Ranck, 1984; Taube, 2007; Taube et al., 1990a, 1990b). These cells play a major role in navigation, as they are believed to act like a compass, providing an internal sense of direction.

Another fundamental discovery in the field was made in the laboratory of Edward and May-Britt Moser in the early 2000s. A new functionally defined cell-type was identified and termed “grid cell” for its periodic hexagonal-array of firing which tessellates across the whole available space (Fyhn et al., 2004; Hafting et al., 2005; Sargolini et al., 2006). The spatial period shown by these cells suggested that they perform odometry (i.e. the computation of distance-measuring) and therefore they encode distances travelled (Moser and Moser, 2008; Rowland et al., 2016). Most recently, yet another functional cell-type has been also identified showing accurate encoding of speed and for this reason they have been named “speed cells” (Kropff et al., 2015). The understanding of the neural mechanisms of spatial representation is now one of the most interesting as well as investigated questions in neuroscience. The large interest it received ultimately led to the award of the most prestigious Nobel Prize to John O’Keefe (UCL, London, UK) shared with Edward and May-Britt Moser, co-directors of the Kavli Institute for Systems Neuroscience, Center for Neural Computation in Trondheim, Norway.

To conclude, since the initial discovery of place cells dated 1971 and the subsequent “hippocampus as a cognitive map theory” dated 1978, a large body of evidence has shown that an orchestra of brain areas centered around the hippocampus functions in concert in order to represent allocentric space as firstly proposed by Tolman (1948) and then O’Keefe and Nadel (1978). In this thesis the term “spatial cognitive system” will be repetitively used to refer to this large system including hippocampal formation and parahippocampal areas such as presubiculum, parasubiculum etc. In the following chapters, firstly the anatomy (Chapter 2) of this complex network will be overviewed. The following chapter will summarise the physiology of the neural correlates of space (Chapter 3). At the end, the limited investigation of the 3D encoding of space will be also summarized (Chapter 4).

2 Anatomy of the spatial cognitive system

In the previous chapter a brief introduction to the field of spatial cognition was provided, along with the early studies pointing to the hippocampus as the brain area hosting the Tolmanian cognitive map (Tolman, 1948). Indeed, a wealth of evidence collected in the last few decades has clearly shown the importance of the hippocampus along with many surrounding areas for the establishment of a map-like representation of space useful for navigation. However, the complexity of the network, as well as the sometimes misleading nomenclature, overall make the comprehension of these structures somewhat difficult. Therefore the aim of this chapter is to describe the anatomy of the spatial cognitive system.

The essential terminology of the spatial system, as well as the connectivity of the hippocampal formation and parahippocampal cortices, will be briefly presented in the following paragraphs. As reference, the terminology used in van Strien et al., (2009) is the one adapted throughout this thesis which classifies the whole spatial system into two main networks:

a) The hippocampal formation (HF), which includes the hippocampus proper, the dentate gyrus and the subiculum;
b) The parahippocampal region (PHR), which includes the presubiculum, parasubiculum, entorhinal cortex, perirhinal cortex and postrhinal cortex.

Given that the results presented in this thesis mostly focus on place cells from the hippocampus, and grid and speed cells from the entorhinal cortex, most attention will be given to these two brain areas. However, for a thorough anatomical understanding of the whole spatial cognitive system, the following readings are highly recommended: (Amaral and Lavenex, 2006; Amaral et al., 2007; Burwell and Agster, 2008; Neves et al., 2008; Witter and Amaral, 2004) and the most recent work by van Strien et al., (2009).

2.1 The hippocampal formation

The HF is a bilateral structure which occupies the caudal part of the rat brain (Figure 2-1). While the two HFs are well apart from each other at the most caudal end, they

progressively converge along the A-P axis until joining together and forming the hippocampal commissure.

The term “hippocampus” was given by the anatomist Arantius (Aranzi, 1587) who identified the hippocampal structure and gave this term for its C-shape which resembles a seahorse. As mentioned before, overall the HF is formed by the hippocampus proper (HP), sometimes referred to as the *cornu ammonis*, which in turn is formed by 4 subfields named CA1-4, the dentate gyrus (DG) and the subiculum (SUB).

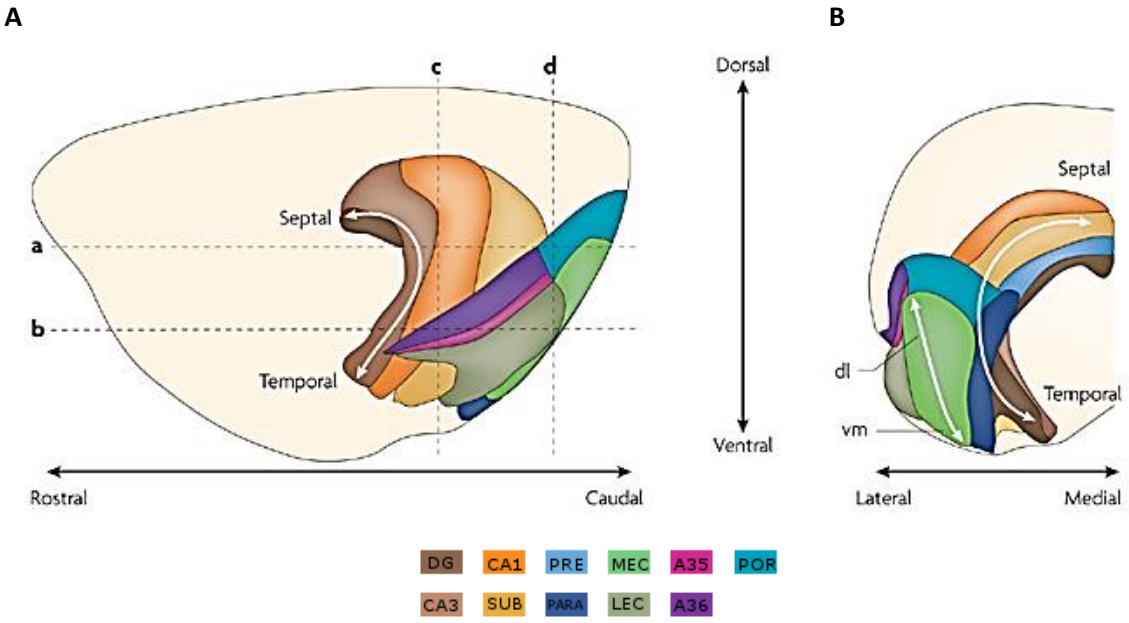

Figure 2-1 Anatomy of the hippocampal system.

Overview of the anatomy of the spatial-cognitive system from sagittal sections view showing (**A**) rostro-caudal (same as antero-posterior) extent and (**B**) coronal view showing medio-lateral extent.
Note the HF formed by CA1 (orange), CA3 (light brown), DG (dark brown) and SUB (light yellow). Surrounding areas form the PHR including EC (medial portion in light green and lateral in dark green), PRE (light blue), PAR (dark blue), POR (turquoise) and perirhinal cortex formed by Broadmann areas A35 (light purple) and A36 (dark purple). Adapted from van Strien et al. (2009).

2.1.1 Major bundles

The HF possesses a number of large bundles of fibres connecting the structures both commissurally and with external areas, in particular those forming the PHR. These bundles are:

a) The alveus: a thin sheet of white matter including both afferent and efferent projections located in the deepest part of the HF. All together these fibres collectively form the fimbria, located near the midline under the corpus callosum, and then becomes the fornix as it leaves the HF to reach the forebrain (Amaral and Lavenex, 2006).

b) Dorsal hippocampal commissure, formed by afferent and efferent projections to

PRE, PAR and EC (Amaral and Lavenex, 2006).

c) Ventral hippocampal commissure, which connects both homotopic (same) and heterotopic fields of the contralateral HF (Amaral and Lavenex, 2006).

d) The angular bundle, which is formed by both afferent and efferent commissural fibres of EC, PRE and PAR along with a number of cortical and subcortical areas. Importantly, the angular bundle also represents the main connection from the EC to all the septo-temporal levels of the HF (Amaral and Lavenex, 2006).

2.1.2 Laminar arrangement

As stated before, the HF as a whole is formed by three structures: the DG, the HP - which is divided into three subfields (CA1, CA2, CA3 and CA4) - and the SUB. The common property shared by these three structures is the laminar arrangement into three identified layers, representing the crucial difference from the PHR areas (Figure 2-2). Depending on the region, the three layers are labelled differently (Andersen et al., 1971). The deepest layer comprises both afferent and efferent fibres as well as interneurons and it is called the polymorphous layer (pol) or hilus in the DG and stratum oriens (so) in the CA subfields. The intermediate layer is the principal cell layer as is formed by principal cells, as well as interneurons. In the DG, the principal layer sits on top of the polymorphous layer and is termed the granular layer, as it is densely packed by granule cells. In the CA subfields, the principal layer mostly contains pyramidal neurons and hence is termed the pyramidal layer. Finally, the most superficial layer is termed the molecular layer in the DG and SUB, whereas in the HP it forms multiple sublayers, which are most distinguishable in CA3. They are: the, stratum lucidum, receiving afferents from the DG; stratum radiatum, which is formed by the apical dendrites of the pyramidal neurons underneath, and stratum lacunosum-moleculare, which is formed by the apical tufts

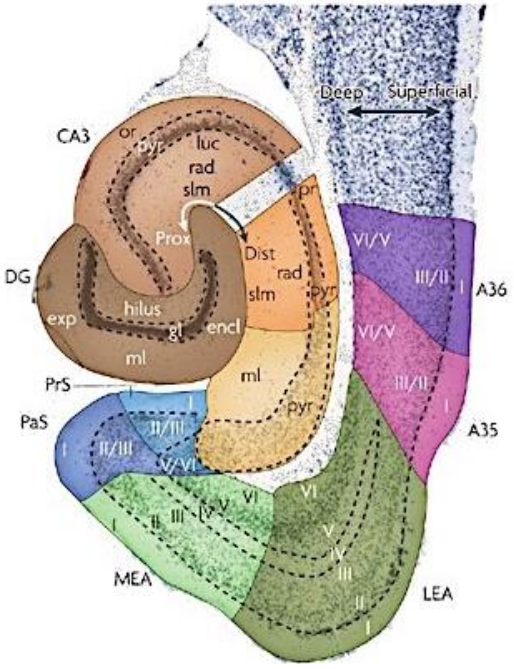

Figure 2-2 Laminar organization of the HF and PHR.

Horizontal section (section **b** from Figure 2-1) of the hippocampal system revealing three-layered organization in HF compared to the six-layered one in the PHR. Colour-coded the same way as Figure 2-1. Adapted from van Strien et al. (2009).

of the pyramidal dendrites (Figure 2-3). Importantly, this is the layer where the fibres from the PP lie and synapses with the HP neurons.

Intensive investigation of the HF anatomy has enabled mapping of the connections taking place between areas inside of the HF (intrinsic connections) as well as brain areas outside of the HF (extrinsic connections). In the next paragraphs, a brief overview of the intrinsic and extrinsic connectivity will be introduced and the functional implications discussed.

2.1.3 Intrinsic connectivity of HF

The projections connecting areas within the HF are termed "intrinsic" and can be summarized into two large categories: those forming the so-called "tri-synaptic pathway" and the ones forming the back-projections in the HF.

2.1.3.1 *Tri-synaptic pathway*

A large portion of information within the HF is known to travel through the tri-synaptic pathway, a unidirectional route from the EC to the HP (Figure 2-3). The first step of the circuit is formed by those axons departing from layer II and III of the EC and organized in a large bundle termed the perforant path (PP) which then contacts granular cells of the DG. Here, projections from the granule cells of the DG form the "mossy fibres" (MF) and target pyramidal cells of CA3. Here, projections from CA3 form the "Schaffer collaterals"

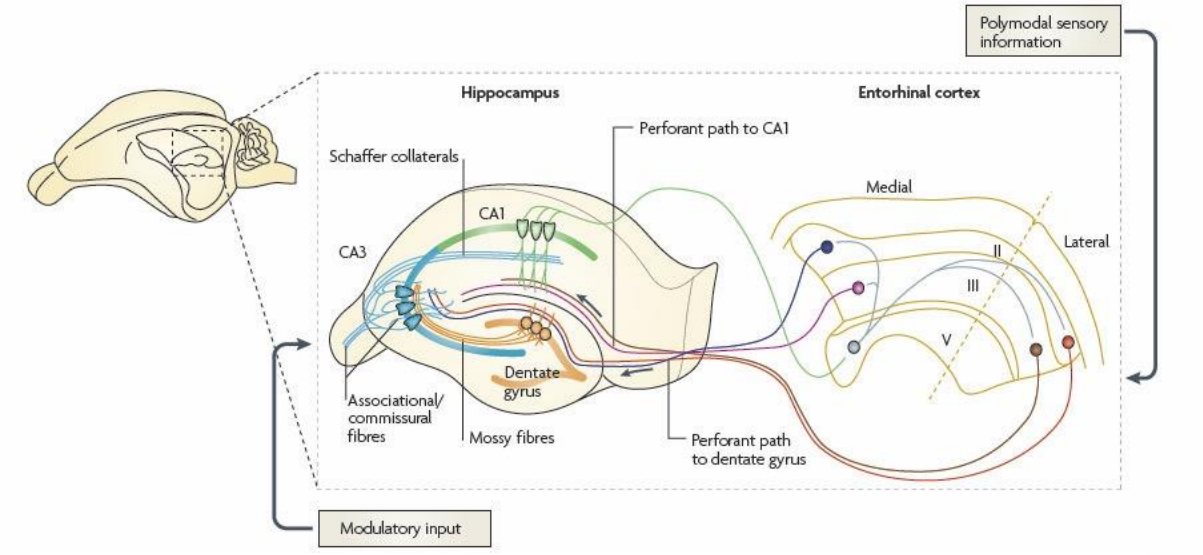

Figure 2-3 Tri-synaptic pathway.

Schematic representation of the connections between EC and HF forming the tri-synaptic pathway (PP from EC to DG, MF from DG to CA3 and SC from CA3 to CA1). Adapted from Neves et al., 2008.

(SC) reaching CA1 pyramidal cells. Remarkably, this component of the circuit shows an interesting topographical pattern along the transverse axis. Specifically, an inverse gradient takes place between the proximal-distal axis of the CA3-to-CA1 connections: the distal portion of CA3 neurons target proximal portion of CA1 neurons and vice versa (Ishizuka et al., 1990; Laurberg, 1979; Laurberg and Sørensen, 1981). CA1 principal layer is considered the output region of the whole HF, as it integrates direct (from EC) and indirect signals (via the tri-synaptic circuit) and then projects to several target areas including deep layers (V and VI) of the EC thus closing the loop between EC and HF. A large number of axons from CA1 stay within the HF, reaching principal layers of the SUB, forming what is sometimes referred to as the "fourth" connection of the tri-synaptic pathway. Again, an inverse topographical pattern is present here, with the proximal neurons of CA1 projecting to the distal ones of SUB and vice versa (Amaral et al., 1991; Ishizuka et al., 1990; Naber et al., 2001; Swanson et al., 1981; Tamamaki and Nojyo, 1990).

2.1.3.2 ***Back-projections***

The circuit presented above is sometimes referred as the "standard model" (van Strien et al., 2009) and it represents a very simplified outline of HF connectivity. Indeed, a number of back-projections have been identified from SUB to DG:

a) CA3 pyramidal neurons project to the DG hilus and inner molecular layer with no septotemporal gradient observed (Buckmaster et al., 1993; Laurberg, 1979);
b) CA1 inhibitory cells of the stratum radiatum and stratum oriens have been found to back-project to the same layers of CA3 (Amaral et al., 1991; Laurberg, 1979; Swanson et al., 1981);
c) SUB pyramidal projections have also been identified to input to all CA1 layers (Finch et al., 1983; Jackson et al., 2014; Köhler et al., 1978).

Moreover, recurrent collateral connections are widely found throughout the HF:

a) In CA3, pyramidal neurons target each other via recurrent collaterals. Such connectivity shows a particular organization along the septo-temporal axis in that each neuron targets cells nearby. The quantity and complexity of such connections has been estimated to be the major source of CA3 input itself (Witter and Amaral, 2004), raising several questions about its putative functions.

b) In DG, granule cells target mossy cell dendrites in the polymorphous layer which back-project to other granule cell dendrites in the molecular layer (Laurberg, 1979; Laurberg and Sørensen, 1981; Segal and Landis, 1974).

c) In CA1, pyramidal neurons also form recurrent collaterals and similarly in CA3 (although less abundant), cells target local neurons along the septo-temporal axis (van Strien et al., 2009).

It appears that the "standard model", according to which the flow of information within the HF travels unidirectionally, fails to capture the complexity of the whole circuit. Indeed, back-projections as well as local collateral circuits, have been found at all levels of the pathway.

2.1.4 Extrinsic connections of the HF

The projections to the HF that originate outside of it are termed extrinsic connections. It is well known that a substantial part of these connections is represented by the PHR input from the EC: a large bundle of fibres which is called the "perforant path" (PP) projects throughout the septo-temporal extent of the DG. In addition, a number of subcortical structures also reach the HF such as thalamus, basal forebrain, hypothalamus and locus coeruleus (van Strien et al., 2009). The basal nucleus of the amygdaloid complex targets CA1, CA3 and SUB, whereas glutamatergic, cholinergic and GABAerigc fibres from the medial septum and diagonal band of Broca (MS-DBB) are well documented to reach HP and MEC (Borhegyi et al., 2004; Gonzalez-Sulser and Nolan, 2017; Robinson et al., 2016; Vandecasteele et al., 2014). Relevant to the results of this thesis, many studies have shown that reciprocal connections from MS-DBB to HF and PHR are crucial for the generation of theta rhythm throughout the entire HF (Buzsáki, 2002; Fuhrmann et al., 2015).

2.1.5 Cell types of HF

As mentioned before, the HF shows the typical three-layered laminar organization (see Figure 2-2 and Figure 2-3) and the distribution of the cell-types follows such an arrangement. In the HP and SUB, the principal cell layer is populated by pyramidal neurons. Consistently, these cells show large pyramidal-shaped cell bodies and bipolar dendritic arborisation: apical trees extend towards the stratumn radiatum and stratum lacunosum moleculare (superficial layer), while the basal trees project towards the stratum oriens in all CA subfields and in the pyramidal layer in the SUB (Figure 2-4). Fine morphological

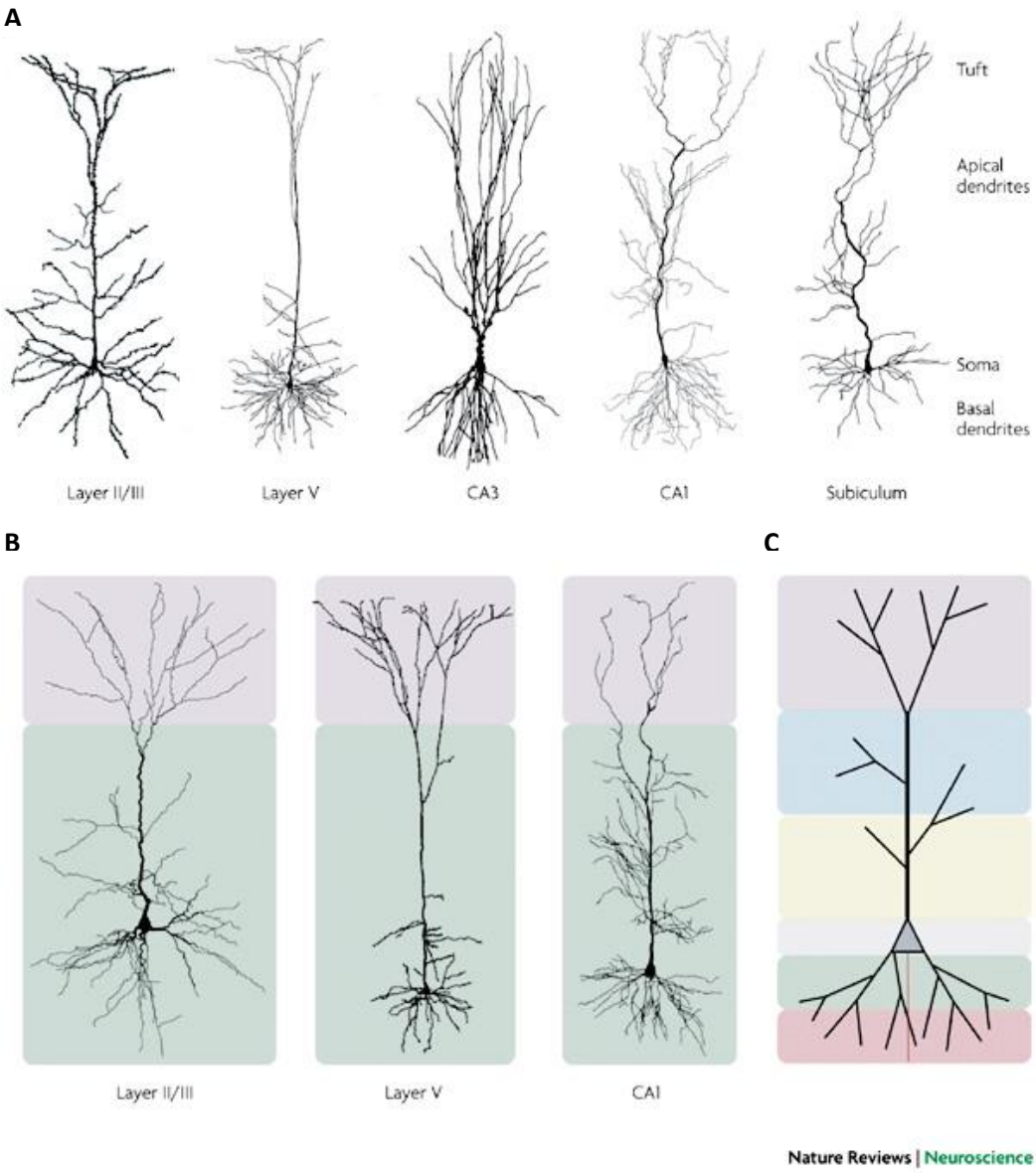

Figure 2-4 Structure of the pyramidal neurons

(**A**) Examples of pyramidal neurons from neocortex (layer II/III and V) and HF (CA3, CA1 and SUB). Note the differences in the morphology and size of the cell body, dendritic branches and dendritic tufts. (**B**) Based on synaptic inputs, pyramidal neurons are divided into functional domains: apical tufts usually receiving excitatory inputs (purple background) and basal and proximal dendrites (green background). (**C**) Schematic drawing of a pyramidal neuron representing the functional domains identified based on synaptic inputs. Adapted from Spruston et al., 2008.

differences are also shown by pyramidal cells across HP subfields (Spruston, 2008). For instance, CA2 pyramidal neurons show a characteristic pattern of dendritic branching which is used to define CA2 borders (Bartesaghi and Ravasi, 1999; Caruana et al., 2012). Moreover, fine differences also exist between CA3 and CA1 pyramidal cells: CA1 cell bodies are smaller and more densely packed with the whole dendritic arborisation being smaller (Amaral et al., 1990; Spruston, 2008).

The principal layer of the DG instead shows a peculiar cell-type known as “granule

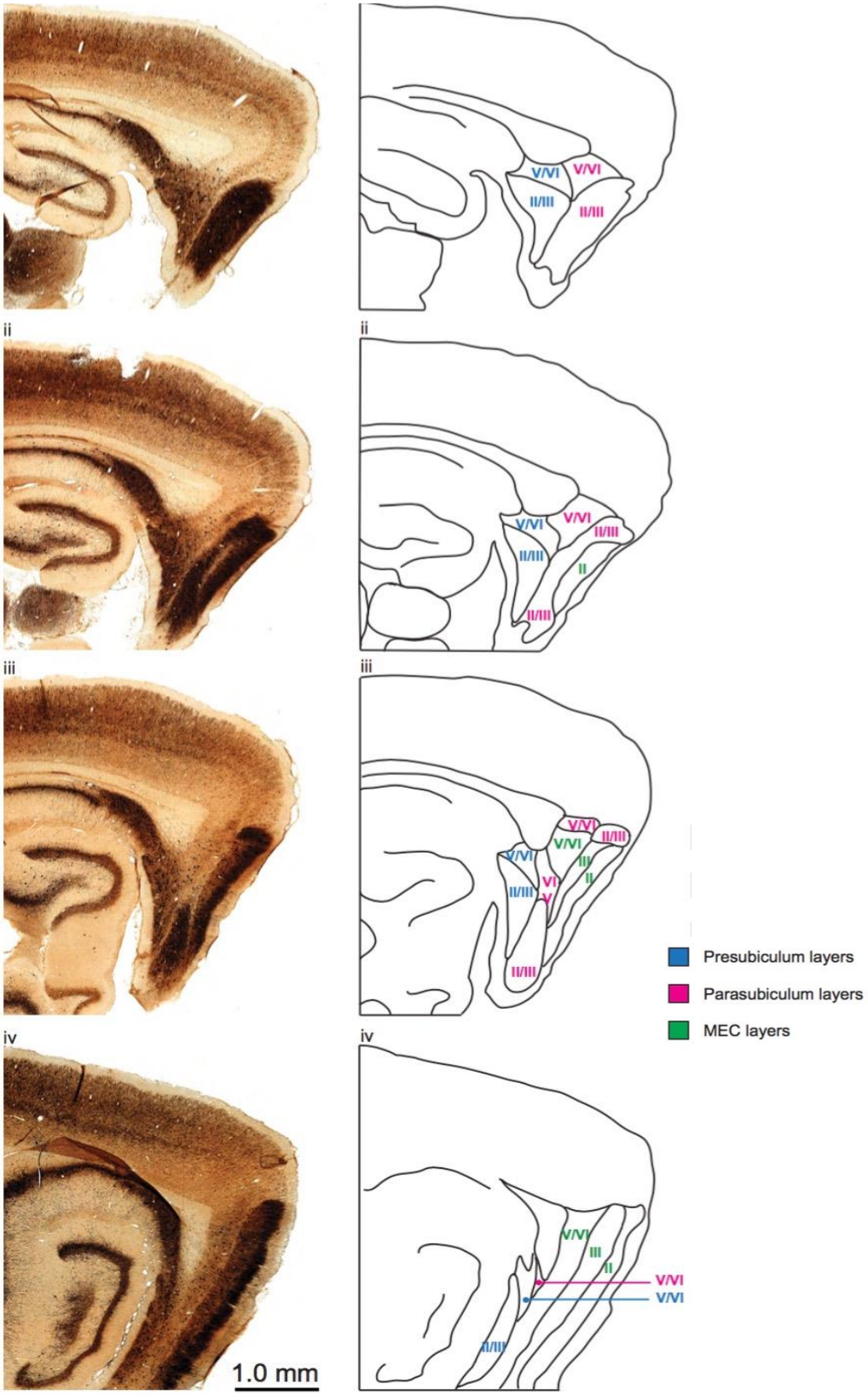

Figure 2-5 Anatomy of the PHR.

Series of sagittal slices from medial (top) to lateral (bottom), representing MEC, PRE and PAR with corresponding laminar organization (left: parvalbumin staining; right: schematic drawing). Adapted from Boccara et al., 2010.

cells". These neurons show medium-size elliptical cell bodies and typical cone-shaped

dendritic trees, which protrude out of the DG and project towards the molecular layer (where the perforant path from EC makes most of its connections in the DG). The granule cells represent the only population of neurons projecting outside of the DG, and it is the bundle of these fibres which form the mossy fibres targeting CA3.

Far more complicated is the description of a large variety of cell types which go under the general category of "interneurons". Attempts to classify them into subtypes have been several (Freund, 2003; Freund and Buzsáki, 1996; Klausberger et al., 2003; Petilla Interneuron Nomenclature Group et al., 2008; Somogyi and Klausberger, 2005) and mostly reflect the techniques used to characterize them based on connections, morphology, the layer they are mostly found in, neurochemical markers and electrophysiological properties such as theta-phase locking. However, it has been estimated that up to 92% of the HF interneurons are GABAergic neurons which target dendritic trees of pyramidal cells (Megías et al., 2001). Other examples of cells described in the literature are basket cells, which target pyramidal cell bodies and proximal dendrites (Klausberger et al., 2002; Tukker et al., 2013) and axo-axonic cells, which target the pyramidal cell axons at their initial segments and are likely to further modulate pyramidal neuronal activity (Klausberger, 2009; Somogyi et al., 2014). An overview of the functional connectivity between long-range projections from MS-DBB and local HF interneurons responsible for theta generation will be provided ahead in the next chapter.

2.2 The parahippocampal cortices

As mentioned before, the PHR is a large network of brain areas including the EC, consisting of a medial MEC and lateral LEC portion, PRE, PAR, PER and POR (Figure 2-5). A shared property of the PHR network is the typical six-layered structure of its cortices which, in contrast to the three-layered structure of the HF, is used as a criterion to separate SUB from PRE, and hence draw boundaries between HF and PHR (van Strien et al., 2009). In this section, the general anatomy, cyto-architecture and map of the major connections of the PRE, PAR and MEC will be summarised.

2.2.1 Presubiculum and parasubiculum

The PRE marks the borders between HF and PHR as it is located between the SUB, retrosplenial cortex and PAR. Sometimes, its dorsal part is referred to as post-subiculum and it is one region where head direction cells can be recorded in rats (Taube et al., 1990a, 1990b). The PAR is bordered by the PRE, POR and MEC and its clear differentiation

between superficial layers (layer II and III) is used as criteria for PRE and PAR distinction.

Both PRE and PAR receive projections from a number of areas outside of the PHR system and most importantly from putatively involved visuo-spatial processing areas, such as retrosplenial cortex, anterior thalamic nuclei and visual cortex. Noteworthy, in most of these areas, the presence of head direction cells as well as grid cells has been reported (Boccara et al., 2010; Finkelstein et al., 2015). In addition, PRE and PAR share inputs from the SUB, and such connections are thought to re-insert the HP pyramidal output into the whole hippocampal loop. Indeed, PRE and PAR project to many regions of the HF and PHR such as:

a) layer III of the MEC which receives bilateral projections from PRE (Haeften et al., 1997);
b) layer II of MEC and LEC received from all layers of PAR (Haeften et al., 1997; Witter and Amaral, 2004);
c) most regions of the HP, including the molecular layer of the DG, receive connections from the PRE (Amaral and Lavenex, 2006).

Local associational connections have also been reported within the PRE and PAR circuits. PRE layer II cells from ventral areas project to dorsal ones, whereas deep layers project to the ventral PRE cells.

2.2.2 Entorhinal cortex

The term “entorhinal” was coined to name the structure enclosed by the rhinal sulcus, and based on the cyto-architecture it is broadly divided into two subregions, medial and lateral (Burwell and Amaral, 1998; Witter and Amaral, 2004; Witter et al., 2000). This nomenclature roughly follows anatomical positions as the LEC occupies the rostro-lateral portion of the structure, and the MEC the caudal-medial region (Burwell and Agster, 2008). Different classifications can be made following different criteria and it is worth mentioning that based on the connectivity, some authors have divided the EC into six subregions, 4 of which form the LEC and 2 the MEC (Insausti et al., 1997). However, such a detailed level of analysis goes beyond the scope of this thesis, so throughout this study the EC will be only subdivided into medial and lateral regions.

2.2.2.1 *Laminar organization*

As a component of the PRH, the EC also shows the 6-layered laminar organization typical of neocortex (Figure 2-5). The layers are called: i) molecular layer; ii) stellate-cell layer; iii) superficial pyramidal-cell layer; iv) lamina dissecans; v) deep pyramidal cell-layer and vi) polymorph layer (Burwell and Agster, 2008). The density, morphology and connectivity of the neurons substantially changes across the layers and these differences are used to mark the layer boundaries.

The molecular layer is a relatively sparse layer with few interneurons (mostly GABAergic with projections to the DG) and transversely-oriented fibres projecting onto layer II neurons. The stellate-cell layer traditionally takes its name from the most abundant class of principal cells found here, stellate cells (Klink and Alonso, 1997) although a recent study showed that four classes of excitatory neurons are found in layer II and they are stellate and pyramidal cells along with two "new" classes termed "intermediate stellate cells" and "intermediate pyramidal cells" (Fuchs et al., 2016). In contrast, three sets of interneurons are found in layer II and depending on their biochemical markers they are classified as PV+, SOM+ and 5-HT3A+ neurons. Importantly, differential connections occur between inhibitory and principal neurons, some of which have been hypothesized to support attractor network dynamics for grid cell pattern formation (Fuchs et al., 2016). The high density of the neurons in layer II helps in marking the boundaries to the deeper layer III, where sparse medium-sized pyramidal cells are mostly found. Other cell-types located in layer III are fusiform, stellate, horizontal and bipolar cells.

Layer IV is a sparse layer with almost no cells to be found other than a few fusiform and pyramidal cells whose dendritic trees reach the fibres in layer I. Layer V contains multiple cell types such as pyramidal cells, horizontal cells and polymorphic cells (Amaral and Lavenex, 2006; Gloveli et al., 2001; Hamam et al., 2000) projecting to superficial layers and forming mostly excitatory asymmetrical synapses (Gray, 1959) onto pyramidal as well as stellate cells and interneurons (van Haeften et al., 2003). A recent study revealed that layer V neurons show different molecular profiles, dendritic trees and connections and overall form two distinct sublayers, 5a and 5b (Sürmeli et al., 2015). For instance, only layer 5a neurons have been shown to project to a number of cortical and subcortical brain areas whereas layer 5b neurons are likely to act locally in the MEC circuit. Moreover, differential input also occurs as only layer 5b neurons have been shown to receive layer II stellate cell projections (Sürmeli et al., 2015). Importantly, conjunctive grid-by-head-direction cells are found in layer III and V of the MEC (Sargolini et al., 2006) and their discovery supported early versions of continuous attractor network models (CANMs, see 3.2.3.2) (McNaughton

et al., 2006; Samsonovich and McNaughton, 1997). A detailed understanding of the local circuitry will help in answering several questions concerning the emergence of grid cell firing.

The structure of Layer VI is substantially less clear, with a large spectrum of cell-types found. Similarly to layer V, connections to superficial as well as deeper layer neurons occur in layer VI (Amaral and Lavenex, 2006). In addition, it should be mentioned that GABAergic interneurons have been found to spread-out across all layers of the EC, although the vast majority seem to lie in the superficial layers (Amaral and Lavenex, 2006).

2.2.2.2 *Connections between EC and HF*

The EC represents the major source of cortical projections to the HF and for this reason is sometimes referred as the "gateway" to the HC. Indeed, the EC integrates multi-modal information converging from a variety of cortical areas (e.g. parietal, temporal, prefrontal) which is in turn transferred to the HF (Canto et al., 2008). By far the largest bundle from the EC to the HF is the PP connecting both MEC and LEC to the DG and other regions of the HF (see Figure 2-3) and such connectivity follows a laminar organization. For instance, the EC to DG connections make contacts onto different sublayers within the DG molecular layer, with the LEC contacting the most superficial third of the dendritic tree and the MEC contacting the middle third (Amaral and Lavenex, 2006; Amaral et al., 2007). Similar lamination patterns of projections to the MEC and LEC has been reported for CA3

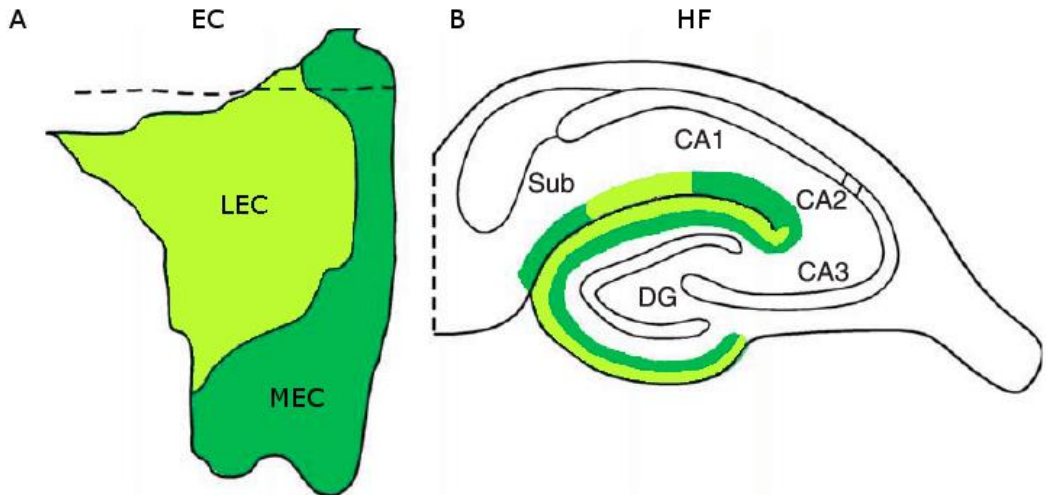

Figure 2-6 Tographical organization of the EC-HF connections.

Schematic drawings representing the connections between from EC and HF. (**A**) Anatomical subdivision of the EC into medial portion (MEC, dark green) and lateral portion (LEC, light green). Dashed line indicates the rhinal sulcus. **(B)** Drawing of a coronal section of the HF indicating the topography and laminar organization of the areas targeted by MEC and LEC. Projections from layer II of the EC target the HF in a laminar fashion; LEC inputs reach the molecular layer of the DG and the stratum lacunosum-moleculare of CA3, whereas MEC projections terminate deeper (same color code as in A). Projections from layer III of LEC input distal CA1 and proximal SUB) whereas, layer III MEC projections target proximal CA1 and distal SUB. Adapted from Burwell and Agster, 2008.

connections as well, with the LEC fibres contacting the superficial dendrites of CA3 stratum lacunosum-moleculare and the MEC fibres contacting the deeper ones. Moreover, most of the afferents to DG and CA3 from both MEC and LEC originate from layer II while direct projections to CA1 and SUB depart from layer III (Figure 2-6). The latter, in contrast to EC projections to DG and CA3, follow a topographical rather than lamellar organization (Figure 2-6). Layer III fibres from LEC contact the distal portion of CA1 (closest to the DG) as well as the proximal SUB (closest to the rhinal sulcus) whereas those from MEC target proximal CA1 and distal SUB (Burwell and Agster, 2008). PP fibres are thought to form excitatory synapses onto the dendritic spines of DG granule cells and CA pyramidal cells, and the majority of them have been shown to be asymmetric and hence excitatory (Witter, 2007).

Therefore, the EC signal is transferred to the HF mainly via the PP, and here it is integrated in a multi-step fashion (see Figure 2-3 and 2.1.3.1) in concert with those direct fibres targeting different sub-regions of the HF. Even though, as mentioned earlier, a substantial number of back-projections exist within the HF (see 2.1.3.2), the majority of the information is thought to flow uni-directionally towards CA1 and SUB pyramidal layer cells, where their axons project outside of the HF including back to the EC. The majority of EC return-projections from HF reach deep layers (layer V and VI), although some fibres have been shown to also target layer I (Kloosterman et al., 2003; Naber et al., 2001). The organization of these back projections to EC follows a topographical scheme, in which two parallel circuits between EC and HF take place simultaneously. Specifically, those CA regions receiving afferents from MEC return projections to MEC, whereas those receiving from LEC project to LEC. This segregation of the input-output connections has been hypothesized to enable independent and parallel processing of spatial information and non-spatial information (Hargreaves et al., 2005).

2.2.2.3 *Intrinsic connectivity*

Fine analysis of EC structure also revealed the existence of three associational connections organized into 3 “bands” along the rostromedial-caudolateral axis, termed medial, intermediate and lateral (Dolorfo and Amaral, 1998). This finding suggests that relevant information in the EC is simultaneously integrated within each band and segregated between bands. The associational connections within the band are mediated by both superficial layers, mostly targeting superficial layers, and deep layers, equally targeting superficial and deep layers. This associational pattern is maintained from EC to DG. Thus, different bands of the EC project to different S-T regions of the DG (Dolorfo and

Amaral, 1998) with the lateral band targeting the most septal DG, the intermediate band targeting the middle region and the medial band targeting the temporal region. As expected, the segregation of these routes is conserved across the entire pathway within the HF, with local connections within bands but no connections between them. This and other findings led to the hypothesis that different computations are achieved within the hippocampal system and lesion studies support this view (Moser et al., 1995). Traditionally, the dorsal region of the HP has been linked to spatial representation (Moser et al., 1995; O'Keefe and Dostrovsky, 1971), even though spatial activity in the ventral HP is well documented (Jung et al., 1994; Poucet et al., 1994). Importantly, the spatial scale of grid cells increases along the D-V extent of MEC, and a similar increase occurs in place cells along the S-T axis of the HP (Hafting et al., 2005; Jung et al., 1994). Therefore, the organization of the associational bands between EC and HF correlates with the spatial tuning of grid and place cells. This finding supports the notion that parallel processing occurs in different regions of the EC-HP network, with the lateral band of the EC mostly targeting the dorsal HP where spatial processing is primarily computed. However, it should be noted that the borders of the bands do not follow the canonical medial vs. lateral borders of the EC. Therefore, it is likely that a "mix" of different information is integrated, possibly following topographical gradients, even though medial and lateral sub-regions have been thought to execute different functions.

2.2.2.4 *Parallel processing within EC*

Consistent with the segregated-functions hypothesis, medial and lateral entorhinal cortices display different connectivity. The LEC is reciprocally inter-connected with the PER which is believed to integrate multi-sensory information. In addition, piriform and insular cortex project to the LEC as well as the amygdala and other areas involved in olfactory processing (Hargreaves et al., 2005; Kerr et al., 2007; Knierim et al., 2006). It is thus now generally believed that the LEC encodes "non-spatial", but "contextual" information including those of emotional valence. This view is consistent with the electrophysiology data showing poor spatial processing by LEC neurons (Deshmukh and Knierim, 2011; Hargreaves et al., 2005; Yoganarasimha et al., 2011) in contrast to the MEC where a large number of spatially-modulated neurons are found (Fyhn et al., 2004; Hafting et al., 2005; Sargolini et al., 2006; Solstad et al., 2008). Consistent with these findings, the MEC receives extrinsic projections from different areas compared to LEC. Visual-processing areas, posterior parietal and cingulate cortices are well-known afferents to MEC (Kerr et al., 2007;

van Strien et al., 2009). In addition, the dorsal thalamus – and particularly the midline, dorso-lateral and anterior dorsal nuclei – project to the lateral and intermediate bands of the MEC. Importantly, these thalamic nuclei are known to host head direction cells (see 3.2.5.1) and are thought to represent the internal sense of head direction and thus act as a neural compass (Peyrache et al., 2015; Taube, 2007; Taube et al., 1990a, 1990b). Additional afferents to the lateral and intermediate bands of the MEC come from the POR which is broadly involved in visuo-spatial processing.

To conclude, anatomical as well as electrophysiological studies convincingly support the notion that two large entorhinal sub-regions, termed medial and lateral, can be identified and parallel processing, subsequently reaching the HF through the PP, occurs within the EC. While the MEC is mostly involved in spatial processing, the LEC conveys non-spatial information. It should be pointed out though that: a) spatial and non-spatial encoding is still combined within the associational bands before entering the HF and the nature of this integration is not yet understood; b) MEC and LEC are mutually interconnected, with MEC layers II, III, V and VI sending projections to superficial LEC layers while layers II and V from LEC project onto MEC superficial layers, and layers II and VI project to both superficial and deep MEC layers (Dolorfo and Amaral, 1998).

2.3 Summary

The aim of this chapter was to briefly review the anatomy of a large network of brain areas centred on the hippocampal system, which is believed to support spatial navigation. A wealth of anatomical studies helped to build a theoretical framework in which the circuitry involved can be simplified as the following loop $EC_{superficial}$->DG->CA3->CA1->SUB->EC_{deep} with the flow of information being unidirectional and integrated in a multi-step fashion. The EC thus acts as a "gateway" to the HF, and its highly organized structure reveals two sub-regions carrying parallel computations, one for spatial encoding (MEC) and one for non-spatial and probably contextual/emotional valence (LEC). In addition, three associational bands have been found within the EC with a mixture of medial and lateral sub-regions co-existing with same associational bands. Noteworthy, topographical projections from EC bands target the DG as well as the HP possibly explaining the remarkable correlation between the increase of the firing field size by grid cells along the D-V axis in the MEC and by place cells along the septo-temporal axis of the HF. In the next chapter, the properties of the place and grid cell system will be discussed.

3 Physiology of the spatial cognitive system

In this chapter, the physiology of the spatial cognitive system will be overviewed in order to make comprehension of the results section possible for the reader. Firstly, the prominent oscillation (7-11 Hz) termed "theta" recorded with the local field potential (LFP) throughout the hippocampal formation will be described. Secondly, the main properties of the so-called "spatially-modulated" neurons will be overviewed, with particular attention to those cell-types investigated in this thesis.

3.1 Theta oscillation

The extracellular current generated by the post-synaptic activation emitted by a large ensemble of neurons can be recorded with the LFP (Andersen et al., 2006). Compared to single-unit activity, where the firing of a single cell can be examined, LFP reveals the sum of the population activity occurring in a small volume of tissue centred on the recording electrode (Buzsáki, 2002). In other words, recordings of the extracellular LFP can be used as an estimate for the efficacy of postsynaptic activation due to both excitatory and inhibitory synaptic activity from a large ensemble of neurons (O'Keefe, 2006).

Extracellular LFP recordings in HF reveal rhythmical activity, which is thought to arise from the synchronised firing of the neural ensemble generating the LFP signal (Bland, 1986;

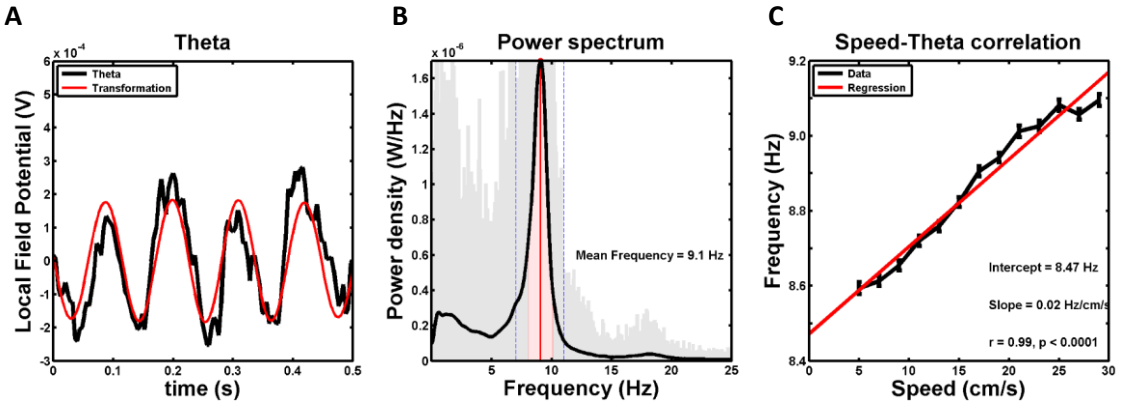

Figure 3-1 Theta oscillation in the hippocampus.

Theta oscillation is the most prominent oscillation recorded with the LFP in the hippocampus and surrounding brain areas. (**A**) Theta oscillation (black trace) shows a regular sinusoidal pattern which can be filtered (red trace) with the Hilbert transform. (**B**) Power spectrum analysis shows a clear peak in theta band (7-11 Hz, blue dashed line) and the mean frequency oscillation (9.1 Hz) as the frequency at which the power maxima is detected. (**C**) The frequency of theta oscillation correlates with running speed and the analysis of the fitted regression line reveals the intercept and slope of the correlation as modeled by Burgess (2008). Data collected and analyzed by the author.

Green and Arduini, 1954; Vanderwolf, 1969). This phenomenon is most evident in cortical structures, where the rhythmical firing, coupled with the parallel organization of the dendrites and the axons causes large amplitude extracellular potential fluctuations (Buzsáki, 2002). The periodicity of the recorded signal has been thoroughly analysed, and based on its frequency, different patterns have been described. The most prominent rhythm in the HP is a regular sinusoidal oscillation termed theta with a clear peak in the power spectrum between 7 to 11 Hz (Figure 3-1). Although theta oscillation is typical of the HP and is often used as a hippocampal landmark for in vivo recordings, it is also recorded across several PHR areas including EC, PAR, PRE, POS (Buzsáki, 2002) and outside the PHR such as the olfactory bulb. Moreover, theta has been identified in many species but since the frequencies can vary across mammals it is hard to make reliable comparative studies (Buzsáki, 2002).

3.1.1 Functional dissection of theta oscillation

The first report of a neural oscillation in the HF was made by Jung and Kornmüller (1938) in the rabbit (Jung and Kornmüller, 1938) but the work by Green and Arduini (1954) provided deeper insights into the matter (Green and Arduini, 1954). The oscillatory pattern exhibited by theta has been linked to a variety of hippocampal functions, from anxiety/anxiolytic-drug action (Gordon et al., 2005; Gray et al., 1975; Seidenbecher et al., 2003; Shin et al., 2009) to memory processing (Hasselmo et al., 2002; Lever et al., 2010) and spatial cognition (Brandon et al., 2011; Koenig et al., 2011; O'Keefe, 2006). Indeed, theta frequency has been shown to be modulated by a number of variables of all kinds, from navigational ones, such as running speed (Jeewajee et al., 2008a; McFarland et al., 1975), to psychological states, such as attention and arousal of the animal (Kramis et al., 1975; Sainsbury et al., 1987), and physical factors such as temperature (Whishaw and Vanderwolf, 1971) and age (Wills et al., 2010). Initial observations that theta shows different frequencies during navigation and immobility states led researchers to classify theta into two subgroups: type I, or "movement/related", occurring during locomotion (walking, running, swimming) and type II, or "alert immobility-related", which is linked to attention, anxiety and arousal state (Vanderwolf, 1969). Importantly, this classification reflects pharmacological sensitivity and therefore is based on different neurobiological substrates: type I theta is resistant to atropine, a cholinergic antagonist of muscarinic

receptors, while type II is modulated by it.

3.1.1.1 *Theoretical dissection*

As mentioned before, the frequency of theta oscillation has been shown to correlate with the animal's running speed (McFarland et al., 1975) and computational studies have linked this phenomenon to path integration mechanisms (Burgess et al., 2007; O'Keefe and Recce, 1993). Burgess (2008) proposed the following model for theta frequency as a linear function of speed:

$$f_\theta(t) = f_0 + \langle\beta\rangle\, s(t)$$

In such terms, $\langle\beta\rangle$, representing the slope of the correlation, modulates the increase of frequency depending on speed. This factor simulates the firing of "velocity-controlled-oscillators" hypothesised to be located in the septum, MEC and thalamus (Welday et al., 2011) as well as in place cells (Geisler et al., 2007) and grid cells (Jeewajee et al., 2008a). Such a signal is linked with theta type I, and is thought to be dependent on MEC. The second factor, termed f_0, corresponds to the baseline frequency, and represents the intercept of the speed-theta correlation on the frequency axis during immobility. This frequency is therefore linked to theta type II.

3.1.1.2 *Experimental validation of the model*

The hypothesis that theta oscillation is supported by two parallel systems corresponding to theta type I and II has been experimentally validated by a comprehensive study by Wells and colleagues (2013) who demonstrated the dissociation of $\langle\beta\rangle$ from f_0. Following anxiolytic administration, f_0 was reduced while $\langle\beta\rangle$ was not affected by the anxiolytic drugs (Wells et al., 2013). In contrast, environmental novelty caused the opposite effect: it did not affect f_0, but decreased $\langle\beta\rangle$, though it recovered over repeated exposures (Wells et al., 2013). These results are consistent with previous findings showing reduced theta frequency during novelty (Jeewajee et al., 2008b) and provide a number of theoretical implications for computational models of grid cell firing (Barry et al., 2012a; Brandon et al., 2011; Burgess, 2008; Koenig et al., 2011; McNaughton et al., 2006).

As mentioned above, the type I speed-theta correlation has been linked to path integration mechanisms, and the reduction of its slope suggests an underestimation of rats' physical displacement in space (i.e. speed). Intuitively, the underestimation of speed causes

the underestimation of distance. Indeed, all models for grid cell firing require an invariant speed input, and if this input is down-regulated, as observed during novelty, then the neural metrics for distance should reflect this impairment. Consistent with this theoretical framework, grid cells during novelty have been shown to expand their grid scale (Barry et al., 2012a), suggesting that they underestimate distances in a unfamiliar environment. Importantly, similar to speed-theta slope recovery over repeated exposures, grid cells metrics "shrank" back to their regular scale with experience (Barry et al., 2012a). Therefore, this and other findings suggest that at least the type I component of theta oscillation, might be involved in path integration (Brandon et al., 2011; Geisler et al., 2007; Hafting et al., 2008; Jeewajee et al., 2008a; Koenig et al., 2011; McNaughton et al., 2006).

The features of theta type II are still not well characterized. It is known to occur during alert immobility and it is dependent on arousal and anxiety (Green and Arduini, 1954). Indeed, anaesthetised animals show low theta frequency (4-6 Hz) (Klausberger et al., 2003; Kramis et al., 1975) whereas immobile animals engaged in avoidance tasks (Bland et al., 2006, 2007) or fixation in a nose-poking task (Takahashi et al., 2009) show theta frequency consistent with the values reported by Wells and colleagues (2013).

3.1.2 Circuits underlying theta oscillation

Since the early reports of regular rhythms in the HF, unravelling the anatomy of the circuits generating theta has been the goal of a number of studies. Decades of investigation revealed a complex network of brain areas, including cortical as well as subcortical nuclei, involved in theta oscillation. A large body of evidence collected in the last few decades suggested that the medial septum and diagonal band of Broca (MS-DBB) are fundamental for theta generation (Buzsáki, 2002; Vertes and Kocsis, 1997). Indeed, large ensembles of neurons from MS-DBB show typical theta modulated firing (Stewart and Fox, 1989a, 1989b, 1989c) and lesions of the MS-DBB dramatically impair theta in the HP (Green and Arduini, 1954; Lee et al., 1994; Petsche et al., 1962; Yoder and Pang, 2005). However, recent studies have challenged this model showing in vitro intrinsic theta oscillation in CA1 and reversal of theta rhythm from SUB to CA1 and CA3 (Jackson et al., 2014), demonstrating a bidirectional flow of information within the HP (see 2.1.3.2 for back projections in the HP anatomy). Nonetheless, the MS-DBB is generally thought to act as a "pacemaker" by providing temporal synchronisation for the whole hippocampal and para-hippocampal network. Several studies have aimed to characterise the local circuits within the MS-DBB as well as the reciprocal connections with the HF. In particular, the identification of cell-types,

morphology, connectivity, and neurotransmission has been thoroughly assessed, and a complicated picture of the network has started to emerge. There is now a general consensus regarding the central role played by the interconnected inhibitory GABAergic neurons throughout the HF for generation of theta (Buzsáki, 2002). However, while these neurons could functionally serve as a scaffold for the emergence of theta oscillation, other cell-types have been shown to deeply influence theta frequency such as cholinergic and glutamatergic neurons (discussed below) as well as noradrenergic (Hajós et al., 2003) and histamine-releasing neurons (Hajós et al., 2008). In the following paragraphs, a brief overview of three sets of cell-types, grouped on a neurotransmitter basis, will be provided. However, for a deeper comprehension of the matter, the following articles are suggested: (Freund, 2003; Freund and Buzsáki, 1996; Stoiljkovic et al., 2015).

3.1.2.1 *GABAergic projections*

Projections from the MS-DBB to HP are well documented, and a large proportion of them depend on long projecting GABAergic neurons which have been shown to target local GABAergic interneurons in the HP (Freund and Antal, 1988; Klausberger and Somogyi, 2008). Many in vitro studies have shown that long projecting GABAergic neurons of the septal area express parvalbumin (PV+) and their firing in vivo is locked to the peak and trough of the on-going theta oscillation (Borhegyi et al., 2004; Varga et al., 2008). Subsequent studies proved that septal PV+ neuronal firing precedes hippocampal dynamics and act as pacemakers, supporting the hypothesis of septal control on hippocampal theta (Hangya et al., 2009). Which class of neurons in the hippocampus projecting PV^+/GABAergic neurons target is still not completely elucidated. Indeed, as mentioned earlier, hippocampal interneurons form a large and heterogeneous population, differing in morphology, connectivity and neurotransmitter (Freund and Buzsáki, 1996; Klausberger and Somogyi, 2008). In addition, their firing has been shown to respond differently to theta phase (Klausberger et al., 2003; Somogyi and Klausberger, 2005) reflecting differential connections from septal GABAergic input (Eyre et al., 2007).

While the MS-DBB connections to the HP are well established, less investigated is the pathway to the EC. Recent studies shed light on this matter showing a strong innervation from septal GABAergic neurons onto local GABAergic interneurons across all MEC layers (Fuchs et al., 2016; Gonzalez-Sulser et al., 2014). Importantly, PV^+ long-range projecting neurons target both fast and non-fast spiking interneurons (Fuchs et al., 2016) so that a very similar scheme of connectivity is found between MS-DBB and HP (Freund and Antal,

1988) and it has been hypothesized that these temporal dynamics play a relevant functional role in synchronizing the HP and MEC (Buzsáki, 2002).

3.1.2.2 *Cholinergic projections*

The cholinergic innervation of the HP from MS-DBB is well documented, along with its putative role in modulating theta oscillation (Buzsáki, 2002; Frotscher and Léránth, 1985; Kramis et al., 1975; Lawrence, 2008). In anaesthetized animals, levels of Ach correlate with hippocampal theta power but does not modulate the frequency (Kinney et al., 1999; Lee et al., 1994; Monmaur et al., 1997). The study by Vandecasteele and colleagues (2014) using optogenetic stimulation of septal cholinergic projections to the HP confirmed the lack of frequency modulation of theta (Vandecasteele et al., 2014). However, cholinergic projections have been shown to suppress sharp-wave ripples and generally reduce the power of other competing oscillations (Vandecasteele et al., 2014). These findings corroborate the view of two on-going mechanisms generating theta, one dependent on cholinergic system and one independent (Kramis et al., 1975). The lack of frequency modulation following stimulation of cholinergic fibres is consistent with the slow action of the second messenger via metabotropic muscarinic receptors, resulting instead in an enhanced theta power by increasing the discharge rates of septal neurons (Vandecasteele et al., 2014).

Further insights on the contribution of MS-DBB cholinergic neurons for theta oscillation comes from the recent work of Dannenberg and colleagues (2015). Consistent with the study by Vandecasteele et al (2014), optogenetic stimulation of MS-DBB ACh neurons have been shown to induce theta oscillation in HP and inhibit CA3 pyramidal neurons where sharp-wave ripples are thought to originate (Dannenberg et al., 2015). In addition, two distinct MS-DBB ACh pathways have been hypothesized and partially validated (Dannenberg et al., 2015): one depending on local interneurons inside of the MS-DBB, and one depending on neurons projecting outside of the MS-DBB. The former consists of MS-DBB neurons targeting PV^+/GABAergic neurons (see above), which in turn target inhibitory hippocampal interneurons (Dannenberg et al., 2015). Consistent with the study by Vandecasteele et al (2014), cholinergic trasmission is mediated via muscarinic signaling, explaining the lack of theta frequency modulation by ACh (Dannenberg et al., 2015). The long-projecting pathway consists of ACh fibres targeting a variety of hippocampal interneurons (Nagode et al., 2011, 2014), but they are not thoroughly documented.

3.1.2.3 *Glutamatergic neurons*

Recent descriptions of the whole MS-DBB population revealed a large number of glutamatergic excitatory neurons (Danik et al., 2005) with very heterogeneous firing patterns and post-synaptic targets (Huh et al., 2010; Robinson et al., 2016), including both local cholinergic and GABAergic neurons within MS-DBB and pyramidal cells in CA3 (Colom et al., 2005; Huh et al., 2010). The recent observation that most of the glutamatergic neurons display theta-modulated firing suggests they play an important contribution to theta oscillation (Huh et al., 2010) and a proposed mechanism is to synchronize GABAergic as well as cholinergic population within the MS-DBB (Robinson et al., 2016). Further evidence suggesting a pivotal role of glutamatergic transmission for theta oscillation come from two recent studies. The first study is from Fuhrmann and colleagues (2015) which showed that glutamatergic projections from MS-DBB to the hippocampus drive locomotion onset, entrain theta frequency in the hippocampus and their firing correlates with running speed. By targeting (mostly) oriens-lacunosum moleculare interneurons, glutamatergic projections in the hippocampus have been shown to modulate the overall network activity in concert with the SC and PP input to pyramidal cells in CA1. In such a theoretical framework, place cell speed modulation is consistent with feedforward disinhibition mechanisms caused by glutamatergic MS-DBB afferents to the hippocampus (Fuhrmann et al., 2015).

The second study is by Justus and colleagues (2017) who show that MS-DBB glutamatergic projections entering MEC and target several cell-types including pyramidal, stellate and interneurons of layer II/III convey speed-modulated signals which are likely to be integrated within MEC circuits for path integration-based mechanisms. Moreover, computational modelling suggests that due to their membrane electrophysiological properties, pyramidal cells are the most suitable class of cells capable of integrating glutamatergic MS-DBB projections and generate rate-coded speed signals. In contrast, fast-spiking interneurons may be that class of cells which thanks to glutamatergic MS-DBB projections generates a speed modulated theta-rhythmic signal (Justus et al., 2017).

Together, these results are consistent with the observation that speed-modulated signals have been found across several cortical and subcortical brain areas (Hinman et al., 2016; King et al., 1998; Kropff et al., 2015; Saleem et al., 2013) by means of a rate-coded signal as well as theta modulation. Moreover, it is also possible that spatial firing in MEC results from the integration of these two independent speed inputs (Gonzalez-Sulser and Nolan, 2017; Hinman et al., 2016; Justus et al., 2017).

3.1.3 Summary

Together, the findings at our disposal support the notion that many brain areas produce local oscillations within the theta range (Goutagny et al., 2009; Jackson et al., 2014; Manseau et al., 2008) but the MS-DBB is the structure where theta oscillation is thought to be primarily generated and transmitted throughout the HF (Dannenberg et al., 2015; Fuhrmann et al., 2015). In particular, septo-hippocampal projections, formed by GABAergic, cholinergic and glutamatergic neurons, mostly target local interneurons and such connections enhance theta locking and synchronization among brain areas. In this simple model, back projections from the HF to the MS-DBB further enhance the synchronization within the network (Takács et al., 2008; Tóth et al., 1993).

3.2 Spatially modulated neurons

Ever since the discovery of place cells (O'Keefe and Dostrovsky, 1971), hippocampal function has been linked to the cognitive map as postulated by Tolman (Tolman, 1948). This was made possible thanks to *in vivo* recordings in freely-moving animals, which allows investigators to couple single-unit activity to behaviour. Further investigations then revealed a number of neurons encoding unique (or the conjunction of) information relevant for spatial navigation such as position, distances, direction, geometry and speed

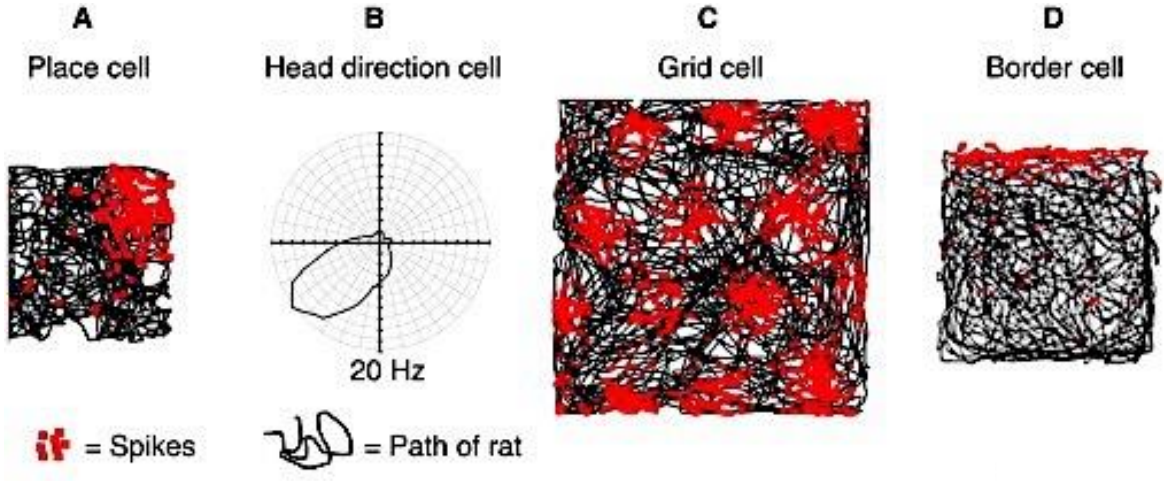

Figure 3-2 Spatially modulated neurons.

Across the HF and PHR, there is a variety of neurons whose firing is shown to convey information relevant for navigation and for this reason they are called spatially modulated neurons. (**A**) Example of the spatial activity exhibited by hippocampal place cell during 10 minutes exploratory session (red dots represent spikes discharged, black line the cumulative path). Note the spatial clustering of the spikes in the top right corner of the box forming a unique place in space where the cell fires termed "place field". (**B**) Differently from place cells encoding position, head direction cells convey heading direction as shown by the directional tuning curve representing the firing rate of the cell across allocentric directions faced by the animal during exploration. (**C**) Similarly to place cells, grid cells also form place fields but rather than being a single one, each cell produces a number of equidistant place fields arranged in an hexagonal array termed "grid" tessellating the whole available space. (**D**) Border cells from MEC also form spatial place field but they are located along boundaries of the environment and are therefore thought to provide information about the geometry of the environment. From Marozzi and Jeffery, 2012.

(Figure 3-2). Therefore, the evidence collected in the last few decades has helped build a coherent theoretical framework supporting the notion that the hippocampal system, as a whole, forms, updates and retrieves a map-like representation of space which is believed to support navigation. Given the relevance for the results section, in the next paragraphs the general properties of place cells, grid cells and the most recently characterized speed cells will be overviewed, with head direction cells and border cells briefly mentioned. It is worth mentioning at this stage though that given the large interest that the field received in the last decade, a thorough description of the spatial cognitive system cannot be provided here as it goes beyond the scope of this thesis - but the following reviews are recommended for a more general description of the field (Hartley et al., 2014; Moser et al., 2008). Moreover, recent technologies such as the use of 1- or 2-photon microscopes, intra-cellular and/or juxta-cellular recordings, virtual reality and optogenetics have enabled scientists to reveal new fundamental aspects of the systems of interest and greatly helped to understand functioning of the neural circuits involved. However, given that the technology used to collect data presented in this thesis is based on electrophysiological recordings, it is mostly these findings that will be focused on.

3.2.1 Place cells

The existence of a population of neurons in the rat hippocampus which fire with respect to the position of the animal while moving in a box represents the great discovery made by O'Keefe and Dostrovsky (1971). These neurons, located in CA1/CA3 pyramidal layer, show several key features: a) they discharge complex spikes - i.e. intermittent bursts of spikes of decreasing amplitude (Ranck, 1973) they fire when the animal is in a discrete portion of space - termed the "cell receptive place field" or simply "place field" - and fire almost no spikes outside of it (Figure 3-2A and Figure 3-3). Because of the spatial response, these neurons were aptly named "place cells". Since then, hippocampal place cells have also been identified in mice (Cacucci et al., 2008; Tonegawa et al., 1996) (Tonegawa et al., 1996; Cacucci et al., 2008), monkeys (Rolls et al., 1989), bats (Rubin et al., 2014; Ulanovsky and Moss, 2007, 2011; Yartsev, 2013), pigeons (Bingman et al., 1996) and humans (Ekstrom et al., 2003). After more than 4 decades of intense investigation, a number of characteristic features are now at our disposal to describe place cell firing. Below is brief summary of place cell properties and hypothesised functioning.

3.2.1.1 *Firing properties*

Place cells exhibit a number of features for which they differ from other neurons in the hippocampal formation. First, place cells show relatively long periods of low rates of spiking alternated with intermittent "bursts" of activity in which several action potentials are discharged with decreasing amplitude (Muller and Kubie, 1987; Muller et al., 1987; Speakman and O'Keefe, 1990). This spiking pattern is referred to as complex-spiking (Ranck, 1973). This and other evidence allowed researchers to identify place cells as pyramidal neurons in the principal layer of the hippocampus (Dombeck et al., 2010; Harris et al., 2001; Harvey et al., 2009). Moreover, as shown by temporal autocorrelation, place

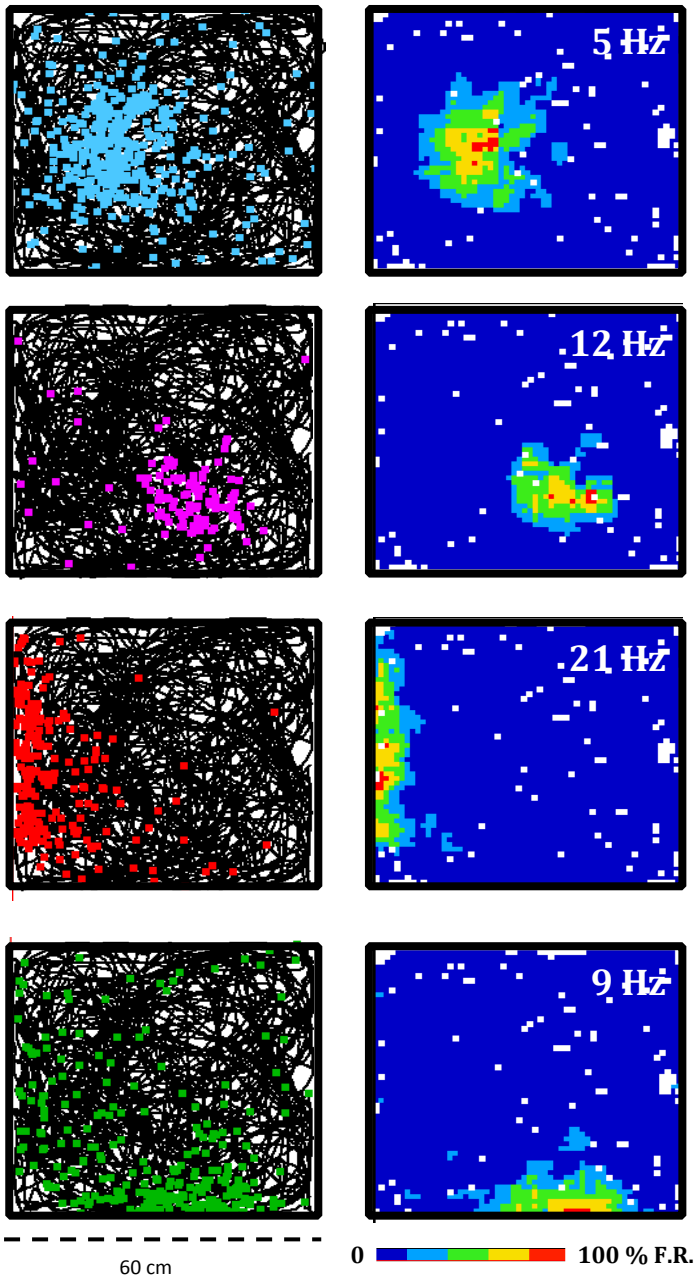

Figure 3-3 Place cells from the hippocampus.

Example of 4 place cells recorded in a square-shaped screening box (60 cm) during a 10 minutes screening trial are shown as spike plots (left column) and rate maps (right column). Black line represents cumulative path of the animal and coloured dots the location of the action potentials discharged by each cell. Rate maps represent the firing rate of the cell across space as heat map from 0 (blue) to 100% (red) of the peak firing rate (top right in white). Data collected by the author.

cell firing shows theta modulation but at a slightly higher frequency than ongoing theta (see 3.2.1.3).

3.2.1.2 *Spatial properties*

The most striking feature of place cells is the peculiar propensity to fire when the animal is in a discrete region of the environment referred to as "receptive field" or "place field". Far from this place, the firing rate of the cell is virtually zero and it increases as the animal approaches this area, reaching a peak firing rate which varies between cells. Consistently, place fields exhibit a concentric increase of firing rate toward its maximum (Figure 3-3). Accordingly, place fields have a unique maximum whose peak usually ranges from 5 to 30 Hz and their firing can be approximated as a two-dimensional Gaussian (O'Keefe and Burgess, 1996). However, it should be said that firing rate is typically represented as simply the number of spikes occurring in a given spatial bin divided by the dwell time in it. Indeed, fine-scale analysis of individual traversals within place fields reveals that the firing rate of a cell is not always consistent but rather variable (Fenton and Muller, 1996). This feature has been termed "overdispersion," and the attentional state of the animal is the proposed explanation for this variation (Fenton et al., 2010).

3.2.1.3 *Temporal properties*

As mentioned before, place cell firing follows a rigid temporal organization: action

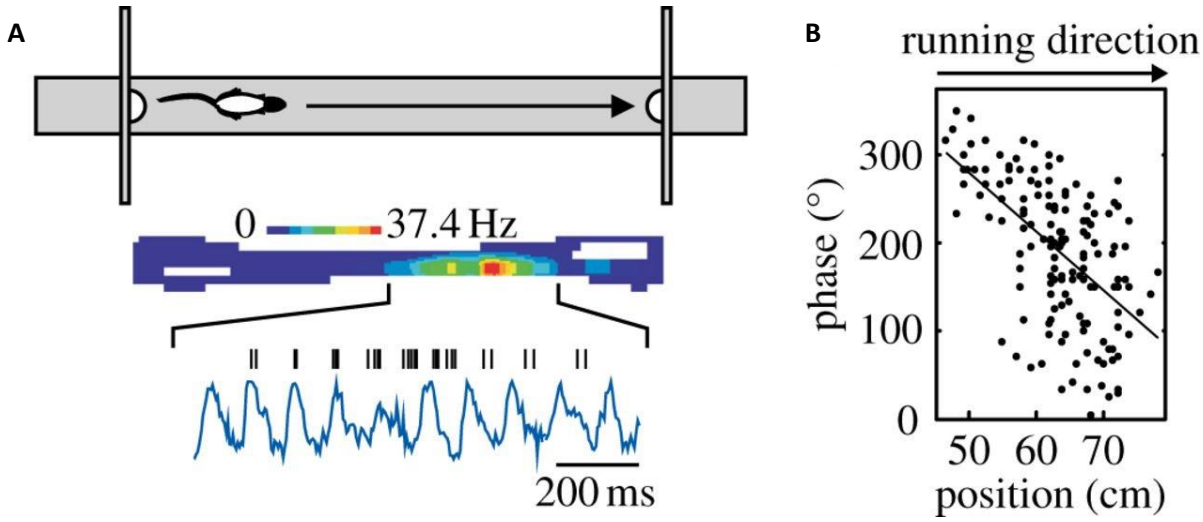

Figure 3-4 Phase precession by hippocampal place cells.

(**A**) During locomotion (top), hippocampal place cells exhibit typical spatial activity revealed as a rate map (middle) showing the firing rate of cell across space as heat map. During running, theta oscillation (bottom, blue trace) is the most prominent signal recorded with LFP and temporal analysis of place cell spiking (bottom, black line) reveals phase precession.
(**B**) Scatter plot showing the position of where the action potentials were fired on the track (**A**) against the phase of LFP theta. The negative slope reveals that as the animal ran through the field, the spikes were discharged at earlier phases of the ongoing theta. Adapted from Hartley et al., 2014.

potentials are discharged in intermittent bursts but their occurrence is theta modulated. Interestingly the frequency at which bursts are released is slightly higher than that of the ongoing theta oscillation. This apparent desynchronisation between two oscillators causes action potentials by place cells to be discharged in bursts at progressively earlier phases of the theta cycle (Figure 3-4). This phenomenon, termed phase precession (O'Keefe and Recce, 1993) has been hypothesised to serve as a mechanism for spatial decoding within the place field, and has inspired many computational models for place cell firing (Burgess and O'Keefe 2011; Lengyel, Szatmáry, and Érdi 2003; John O'Keefe and Recce 1993).

3.2.1.4 *Representation in stable environments*

Standard recordings of place cells are usually made in open field environments where animals are free to move in two dimensions. In such circumstances, place cells have been shown to be omni-directional, meaning that they fire as the animal approaches the centre of a field regardless of the direction the animal is facing. However, in constrained environments where the animal runs in one direction only, such as on linear tracks, place fields are usually directional (McNaughton et al., 1983). In general, place fields are widely-distributed around the available space (Muller et al., 1987) although a tendency to represent areas near the walls and barrier is documented (Hetherington and Shapiro, 1997). Even though place cells are detected from the unique locus of activity, well described in the literature are examples of double fields, i.e. the same place cell exhibiting distinct place fields within the same environment. The frequency of place cells showing two fields ranges from 5-10% in apparatus such as cylindrical open fields (Muller and Kubie, 1987; Muller et al., 1987) and the properties of two place fields of one cell (size, shape, peak firing rate) are not consistent, indicating that even if exhibited by the same cell, the representation is independent.

When multiple cells are simultaneously recorded, properties of the population ensemble can be examined. Firstly, the anatomical position of the cells does not correlate with place field location, meaning that there is no topographical representation (Alme et al., 2014; Dombeck et al., 2010; Wilson and McNaughton, 1993). Moreover, it has been estimated that about 130 place cells are sufficient to determine an animal's location with an accuracy of 1 cm in a 60 x 60 cm square box (Wilson and McNaughton, 1993) even though it has been calculated that about one third of CA1-3 place cells actively contribute to spatial representation, with the majority simply staying silent (Alme et al., 2014; Guzowski et al., 1999; Leutgeb et al., 2004; Thompson and Best, 1989). Taken together,

these results support that notion that individual place cells form neural maps of space and the ensemble as a whole encodes animal self-location during navigation. Further evidence in favour of this hypothesis comes from the observation that these spatial maps stay stable across time. Thompson and Best (date) recorded the activity of ensembles of place cell in a familiar and unchanged environment across weeks in rats, and neural maps were found to persist for up to 153 days (Thompson and Best, 1989; Ziv et al., 2013). This evidence supports the view that place cell firing contributes to the formation of episodic memory by providing spatial information in stable environments.

Since their discovery in early 70s, place cell firing was largely investigated to explain mechanisms driving spatial response. Greatest insights were achieved by testing spatial firing following environmental manipulations of a variety of modalities such as visual, olfactory, tactile and auditory (Muller et al., 1987; Paz-Villagràn et al., 2002; Save et al., 1998). Early studies showed that place cell firing response is strongly influenced by distal landmarks; the rotation of cue cards drives place fields to rotate accordingly (Muller and Kubie, 1987; O'Keefe and Conway, 1978) . Similarly, in rats blinded after birth, tactile information functions as prominent landmarks and is able to control place cell firing (Save et al., 1998). However, significant changes in the environment drive place cells to alter their firing response. This phenomenon is broadly referred to as "remapping" (Bostock et al., 1991; Muller and Kubie, 1987) and it may include:

i) changes in rate coding with no change in the location of place fields (i.e. rate remapping);
ii) changes in location of some but not all place fields (i.e. partial remapping);
iii) re-arrangement of the whole place cell ensemble with changes in location of place fields as well as the switching on/off of some cells (i.e. global remapping).

The functional meaning of remapping is not clear yet although it has been proposed that having two completely independent representations following changes in the environment may help distinguish between the two conditions, a computation referred to as "pattern separation" (Leutgeb and Leutgeb, 2007). When subtle changes take place, usually rate remapping is likely to occur (Leutgeb et al., 2005) whereas when prominent features of the environment are changed, global remapping seems to take place. For instance, the combination of olfactory and visual cues generates different "contexts" which modulate place cells responses (Anderson

and Jeffery, 2003). Similarly, when the animal is exposed to a completely different environment, place cell representation is re-organized, with a large portion of cells simply staying silent and a new ensemble becoming active (Muller, 1996). The capacity for hippocampal encoding has been recently challenged in 11 recording rooms and CA3 place cells showed independent representation with almost no overlapping between comparisons (Alme et al., 2014).

Strong modulation of place cell firing is caused by the environmental boundaries as shown by O'Keefe and Burgess (1996). Indeed, geometrical deformation of an enclosure, such as the stretching or squashing the walls, induces parametric deformation of the place field demonstrating direct control of the boundaries on place cells (O'Keefe and Burgess, 1996). This and other findings led to the formulation of the boundary-vector cell model proposed by Barry and colleagues to explain the generation of place cells' spatial responses (Barry et al., 2006).

3.2.1.5 *Relevance for path integration*

The experiments mentioned above largely investigated the effects of a variety of allothetic cues onto place cells firing. Firstly, place cell firing is stable in complete darkness (O'Keefe, 1976; Quirk et al., 1990) and occurs in blinded rats as well (Save et al., 1998). Moreover, if a landmark is perceived as unstable, their influence onto place cells is degraded (Jeffery et al., 1997). Consistently place cell firing is robust to the removal of prominent landmarks (Muller and Kubie, 1987). Convincing evidence for place cell computation of self-motion cues comes from Gothard et al. (1996) where rats were trained to run along a linear track with a moveable start box and fixed goal at the end to create a mismatch between allothetic and idiothetic cues (Gothard et al., 1996). The results showed that for a significant portion of the track, place cell firing was modulated by the integration of self-motion cues rather than external landmarks, demonstrating that internal sense of position is updated by path-integration mechanisms (Gothard et al., 1996).

3.2.1.6 *Summary*

In conclusion, a large body of evidence has shown that a combination of allothetic and idiothetic cues modulate place cell firing. Taken together, overall these results show that, consistent with the "hippocampus as a cognitive map theory", the place cell system acts like an internal signal encoding the allocentric representation of space.

3.2.2 Grid cells

Investigations driven by the interest in place cells led to the discovery of another cell-type implicated in self-localisation and path integration termed “head direction cells” (Ranck, 1984; Taube, 2007; Taube et al., 1990a, 1990b). These neurons appear to encode an animal’s direction of facing in allocentric coordinates (see 3.2.5.1 for a brief description of head direction cells). Therefore, the theoretical framework in which place cells encode location and head direction cells encode the direction of travelling was hypothesized to support path integration during navigation (McNaughton et al., 2006). However, a number of questions required answers. In particular, outstanding questions were: how do place cells determine current location? How are self-motion cues integrated with allothetic ones? How do place cells know about the distances travelled?

The break-through discovery of grid cells from the Mosers’ lab in Trondheim, Norway, accounts for many of these questions (Fyhn et al., 2004; Hafting et al., 2005; Sargolini et al., 2006). These studies explored the medial entorhinal cortex (MEC) and described a new class of neurons which, similarly to place cells, show clear spatial activity. However, differently from place cells, these neurons revealed several equidistant *foci* of firing organized as a regular hexagonal lattice. The striking regularity of the firing pattern tessellating the whole available space led the authors to coin the term “grid cells” (see Figure 3-2 and Figure 3-5).

Ever since their discovery, grid cells have received a large amount of attention and their firing properties have been deeply investigated across species. They have been identified in the homologue areas of mice (Fyhn et al., 2008), bats (Yartsev et al., 2011), monkeys (Killian et al., 2012) and humans (Doeller et al., 2010). Below is a short overview of their main properties but the following readings are strongly recommended for a deeper understanding of the matter (Buzsáki and Moser, 2013; Derdikman and Moser, 2010; Jeffery and Burgess, 2006; McNaughton et al., 2006; Moser and Moser, 2008; Moser et al., 2008; Rowland et al., 2016).

3.2.2.1 ***Firing properties***

Similar to place cells, grid cells mostly show low firing rate intermingled with short epochs of high firing displaying bursts of spikes during field crossing (Figure 3-5). Grid cells were initially discovered in layer II of the MEC (Fyhn et al., 2004; Hafting et al., 2005) but they have been found across different layers in MEC even though they are most abundant in layer II (Sargolini et al., 2006). Further studies revealed the presence of grid cells also in surrounding brain areas such as PRE and PAR (Boccara et al., 2010). Given that stellate cells

are most abundant in layer II, they were hypothesized to be grid cells (Burgalossi et al., 2011). However pyramidal neurons from superficial layers with grid-like firing has been also demonstrated and it now appears hat grid cells do not correspond to a single cell-type but they are both stellate and pyramidal cells (Domnisoru et al., 2013; Ray et al., 2014; Schmidt-Hieber and Häusser, 2013; Tang et al., 2014). Identifying the characteristics and differences between the two classes of neurons is matter of future investigation.

3.2.2.2 *Temporal properties*

Similar to place cells, grid cells also show rigid temporal organization: action potentials are discharged in intermittent bursts during field crossings whereas the firing rate outside the fields is negligible (Fyhn et al., 2004; Hafting et al., 2005; Sargolini et al., 2006). Most grid cells also show theta modulation and a relevant proportion of them also display phase precession, although its occurrence differs across layers (Domnisoru et al., 2013; Schmidt-Hieber and Häusser, 2013). Noteworthy, the observation of phase precession in grid cells (Climer et al., 2013; Domnisoru et al., 2013; Hafting et al., 2008; Jeewajee et al., 2014) has led to a number of computational models based on theta oscillation and designed to support path integration (Burgess, 2008; Burgess and O'Keefe, 2011; Burgess et al., 2007; Jeewajee et al., 2008a).

3.2.2.3 *Spatial properties*

The striking feature of grid cells is the periodic firing producing a regular hexagonal array of fields in horizontal 2D environments. Indeed, similar to place cells, grid cells form rounded place fields; areas of space where the cells reliably fire. However rather than firing in a unique place, each cell shows a number of fields organized in a hexagonal array or "grid" (Hafting et al., 2005). For the majority of grid cells, firing occurs during field crosses regardless of the animal's speed or direction but grid cells from layer III and V are directionally modulated and thus display conjunctive grid-directional firing (Sargolini et al., 2006).

A quantitative description of grid cell firing was implemented by Hafting and colleagues (2005) who extracted a number of grid features after computing spatial autocorrelograms (Hafting et al., 2005). Nowadays, this represents a well-established method in the field. Simply, one grid cell rate map (template) is auto-correlated in a loop a number of times with its own replica (copy) after shifting it by one bin along either the –x or -y coordinate. For each shift, a single correlation value (for the overlapping bins only) is

computed and stored forming a 2D matrix highlighting the periodicity of the template firing rate map (see also Sargolini et al., 2006 for a thorough description of the algorithm). From the spatial autocorrelogram matrix, it is then possible to extract a number of features such as the scale or wavelength (the average distance between surrounding peaks), the orientation of the grid (referenced to the x-axis or the south wall of the open field box), and the phase of the grid (the position of the peaks along the orientation axis). In addition, an estimate of the regular pattern can be quantified by calculating a grid score index (method which unfortunately does not unequivocally detects grid cells from a random population but is at the moment the best criteria for selecting grid cells - see below for criteria used in this thesis).

Intense investigation of grid cells revealed the functional importance of these features. Since their initial discovery, the scale of grid cells has been shown to increase

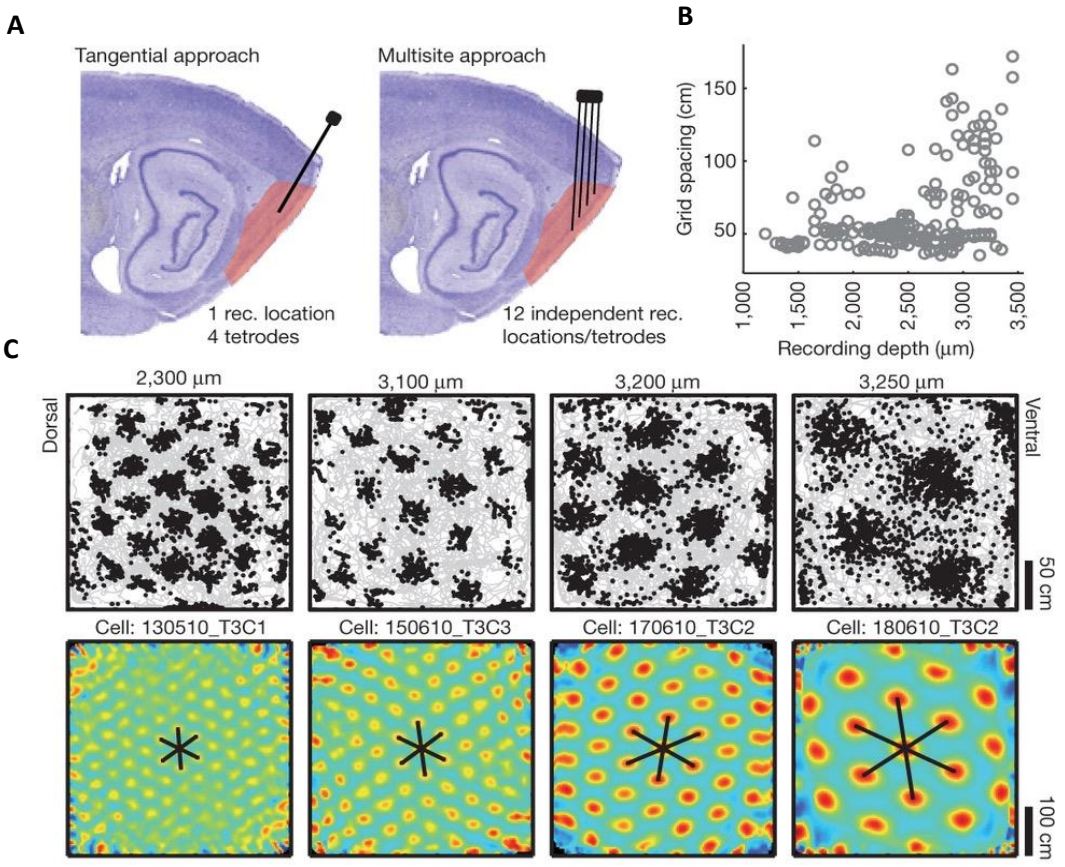

Figure 3-5 Grid cells along the D-V extent of the MEC.

Large ensemble recordings revealed modular organization of grid cells as distinct anatomical clusters with independent spatial properties along the D-V extent of the MEC. (**A**) Sagittal slices of posterior portion of the rat brain showing different methods used to implant tetrodes for large ensemble recording of grid cells: tangential (left) and multisite approach allows to sample large areas of the MEC (red shade area). (**B**) Scale of grids (cm) recorded across D-V extent (µm) of the MEC. (**C**) Four examples of grid cells belonging to different modules recorded at different depths of the MEC D-V extent. Spike plots (top row) with relative spatial autocorrelogram (bottom row) showing spatial properties exhibited by grid cells of different modules. Note the increasing scale and field size as well as different grid orientation across modules. Adapted from Stensola et al., 2012.

along the dorsal-ventral extent of the MEC (Figure 3-5). Relevant for this thesis, there is a strong correlation between the size of grid fields and the scale of the grid (Hafting et al., 2005). (Barry et al., 2007) hypothesized an incremental increase in grid scale along the D-V axis, and this was confirmed by Stensola's study (2012) in which the activity of a large number of grid cells (overall 968 grid cells from 15 rats, up to 186 cells from a single animal) was examined. Grid cells were shown to be anatomically clustered into modules along the D-V extent (Figure 3-5). Interestingly, within each module grid cells seem to share most of their properties (orientation, theta modulation, field size, response to boundaries) with just the position of the fields differing relative to each other (different phases). In contrast, grid cells across modules behaved very differently, suggesting that grid cell encoding is supported by local independent networks rather than a global homogenous system (Stensola et al., 2012).

3.2.2.4 *Hypothesized function*

Since being discovered, the capacity for grid cells to measure distance has meant they are the ideal candidate to perform to path integration (Hafting et al., 2005). The idea mostly comes from the fact that grid fields are equidistant to each other as if they "marked" 6 equidistant places from each firing field. Importantly, the six-fold symmetry pattern is a widespread geometrical organization in nature – being the most efficient way for packing non-overlapping circles of the same size on a plane (C. Gauss, 1831). The hypothesis that grid cells play a major role in path integration was initially supported by a number of experiments. For instance, early studies showed that grid cells were anchored to external landmarks but their regular pattern was stable in darkness and persisted following landmark removal (Fyhn et al., 2007; Hafting et al., 2005). These observations supported the hypothesis that grid cell firing patterns were generated by integrating self-motion cues. Consistent with this view, passive exploration does not elicit regular grid patterns - action potentials are discharged but in a disorganized fashion (Winter et al., 2015a). In contrast, more recent studies showed that the grid firing pattern is disrupted during darkness in mice (Chen et al., 2016) and, in the similar circumstances, severely impaired in rats - though weak distance coding was preserved (Pérez-Escobar et al., 2016). As such, the extent to which grid firing is dependent upon visual cues, and the mechanism by which such cues might be processed to generate regular firing patterns requires further investigation.

Similarly to place cells, grid cells also show rearrangement of their fields following

spatial (Fyhn et al., 2007) and non-spatial manipulation (Marozzi et al., 2015a). However, differently from place cells, remapping-inducing manipulations always produce regular grids (so grid cells never turn off). Most importantly the remapped grids are oriented along the same direction and show the same scale, meaning that grid cells are "set" to determine fixed distances across environments in a context-invariant fashion (Marozzi et al., 2015). Consistently, grid cells recorded on linear tracks exhibit repetitive firing patterns in 1D only (Hafting et al., 2008) and the apparent weaker periodicity is consistent with a slice through a 2D lattice (Yoon et al., 2016).

Overall these findings can be generalized by saying that the grid cell code is invariant across environments and this fixed scheme has been hypothesized to act as universal metric of space. Indeed, the rigid response to movements exhibited by grid cells may be functional for the general computation of distance during navigation (Jeffery and Burgess, 2006; Moser and Moser, 2008). Exact mechanisms of how this is achieved is far from being clear but theoretical studies have started to tackle the question (Barry and Bush, 2012; Bush et al., 2015; Erdem and Hasselmo, 2012; Rowland et al., 2016).

3.2.2.5 ***Dynamic grid***

The claim which accompanied the discovery of grid cells that they are the neural substrate for path integration received general consensus considering the striking regularity displayed by grid fields. However, the results from a series of studies challenges this notion. The first result inconsistent with the model is the one obtained by Barry and colleagues (Barry et al., 2007). The authors replicated the experimental design conducted by O'Keefe and Burgess (1996) showing the control of place cell firing by boundaries (O'Keefe and Burgess, 1996). Similarly, grid cells responded parametrically to the geometrical manipulation (they stretched/squashed by the same amount) showing that they are under similar control of boundaries (Barry et al., 2007). Therefore, in this circumstance, grid cells failed to perform invariant odometry as the resulting grid map deformed and not by the same scale. One possible explanation is that maybe grid cell firing is initially generated by the integration of self-motion cues and once established it becomes anchored to external cues such as boundaries (Ólafsdóttir and Barry, 2015). This hypothesis is supported by the following study in which the grid cell firing pattern was produced for the first time in a novel environment (Barry et al., 2012a). Interestingly, at first exposure, grid cells showed increased field size and scale compared to a familiar control with a generally less regular arrangement too, a phenomenon which has been termed "grid

expansion". However, with repeated exposures, the firing pattern became more regular and the grid scale shrinks to the standard scale. This result revealed an important feature of grid cells: they are more dynamic than previously thought, with undergoing plasticity processes as plausible mechanisms (Barry et al., 2012a). A theoretical study proposed grid expansion as an optimal response in spatial uncertainty due to novel conditions (Towse et al., 2014) signalled by an increased level of acetylcholine in the HF (Hasselmo, 2006).

Dynamical encoding by grid cells has also been demonstrated in a longitudinal study in which grid cells where recorded from animals exploring two adjacent square boxes connected by an external corridor (Carpenter et al., 2015). Initially grid cells formed identical grids in each box (local reference) but over time they differed and formed coherent grid maps of both enclosures (global reference). This finding again demonstrates how flexible grid firing can be and also that grid cells are eventually capable of encoding distances over large spaces in a coherent fashion as well as across multi-compartments (Carpenter et al., 2015). This result is somewhat in disagreement with previous results obtained by Derdikman and colleagues (2009) who recorded place and grid cells from animals running on a highly mutli-comparmentalized hairpin maze (Derdikman et al., 2009). Under such circumstances, grid cells lost their hexagonal symmetry in favour of a mosaic of fragmented submaps as they showed repeated firing pattern every other lap of the maze when rats were running along the same direction. However, when rats were trained to perform stereotypic behaviour in a large open field, grid cells showed the regular hexagonal pattern suggesting that the fragmentation in the hairpin maze could be driven by the geometry of the environment (Derdikman et al., 2009). In the follow-up study, head direction cells were not affected during running in the hairpin maze, even though the whole grid cell system showed loss of hexagonal symmetry (Derdikman et al., 2009). Taken together these two studies suggest that:

i) the head direction system is not affected by grid cell representation indicating maybe they may be upstream of grid cells in the spatial network;
ii) while head direction cells are relatively independent of environmental geometry, grid cells are heavily influenced by it.

3.2.2.6 *Influence of geometry on grid cell firing*

Among many topics in the field of spatial cognition, the exploration of the relationship between grid cell firing and environmental boundaries has been one of the

most flourishing ones. Indeed, the rescaling (Barry et al., 2007) as well as fragmentation of grids (Derdikman et al., 2009) highlights the strong influence of geometry on the spatial representation system. In addition, further evidence for the strong role of geometry came from the discovery of "border cells", found in MEC which fire along boundaries and may signal the overall geometry of an environment (Solstad et al., 2008).

A recent study by Hardcastle (2015) showed that when an animal is far from boundaries over a long time, grid representation becomes inaccurate probably due to the accumulation of path integration errors (Hardcastle et al., 2015). However, proximity to boundaries re-sets grid cells so that accurate the hexagonal firing pattern can be re-established. Computational modelling suggests that the border-grid cell network could be responsible grid cell re-setting (Hardcastle et al., 2015). This view suggest that grid firing may be dependent on an internally-generated signal driving grid cells to fire. Such a signal is probably linked to path-integrator process which is more prone to errors over time (Winter et al., 2015a). However, whether this is sufficient to produce effective grids or whether visual information is necessary is still not fully understood (Chen et al., 2016; Hafting et al., 2005; Pérez-Escobar et al., 2016). Moreover, grid cell firing seems to be dependent on an external source of information, most likely provided by the environmental geometry encoded by border cells (Barry et al., 2007; Hardcastle et al., 2015). Further investigation on how the integration of external and internal signals is achieved will help answer the many questions remaining regarding grid cell firing.

Two recent studies shed light onto the relationship between boundaries and the internally-generate grid. Krupic and colleagues (2015) examined a number of grid cell features in a trapezoidal enclosure and found that regularity, scale and field size of the grids was severely altered compared to the square box (Krupic et al., 2015). These results suggest that in a 2D environment with two non-parallel boundaries – likely to be encoded by border cells – the grid is strongly distorted (Krupic et al., 2015). Two alternative hypotheses can be drawn: either the validity of the grid cells as a universal metric for space hypothesis is to be rejected, or maybe grid cells provide a metric system but the trapezoidal geometry affects them and thus the perception of space is altered (Krupic et al., 2015). Deeper insights on this matter came from the study of Stensola and colleagues (2015) who analysed the alignment of the grid relative to the boundaries (Stensola et al., 2015). A theoretical study suggested that grid orientation followed environmental boundaries (Krupic et al., 2014). However, finer analysis showed that grids tend to orient 7.5° either direction from one or more walls of the environment and such rotation occurs

with elliptic deformation of the grid (Stensola et al., 2015). However, grid distortion does not appear in novel environments but develops over repeated exposures, perhaps together with grid shrinkage (Barry et al., 2012a). The process by which grids rotate and become more elliptical has been termed “shearing” and it is likely to be generated by repulsive forces from boundaries via border cells. The functional role for shearing and 7.5° alignment is still not clear but minimizing symmetry between the environmental geometry and the grid lattice could be optimal for avoiding errors in self-localization (Stensola et al., 2015). Future experiments testing such hypotheses will help to explain the mechanisms behind grid shearing.

3.2.3 Models of grid cell firing

Since their discovery, grid cells were hypothesized to be the neural substrate of path integration. Moreover, their regular firing attracted the attention of many computational neuroscientists and a number of models have been proposed to explain how the six-fold symmetry is generated. The majority of the models can be grouped into two main classes, broadly referred as oscillatory interference models and continuous attractor networks (Giocomo et al., 2011a; Rowland et al., 2016; Zilli, 2012). Additional models have been also proposed to explain grid cell pattern formation (Kropff and Treves, 2008; Mhatre et al., 2012). Here, a brief summary of the oscillatory interference and continuous attractor network models will be provided.

3.2.3.1 *Oscillatory interference models (OIMs)*

Since the early report of phase precession in place cells, the putative role of theta oscillation in path integration was proposed and its involvement for place field generation postulated (O’Keefe and Recce, 1993). However, OIMs posit periodic firing by place cells, a prediction which was never validated until phase-precessing grid cells in MEC were reported (Hafting et al., 2008). Since then, a variety of studies proposed that the repetitive pattern could be generated due to the interference of two oscillatory signals afferent to one grid cell. Simply, one oscillator acts as a baseline and has a frequency in the theta band (7-11 Hz) and is modulated by running speed like that exhibited by theta oscillation in the LFP (Figure 3-6A). The second oscillation also has a frequency in the theta band and in addition to being modulated by running speed it is also modulated by preferred firing direction in cosine-tuned fashion - i.e. velocity-controlled oscillators (VCO) (Burgess, 2008; Burgess et al., 2007; Jeewajee et al., 2008a). Neurons with such properties have been

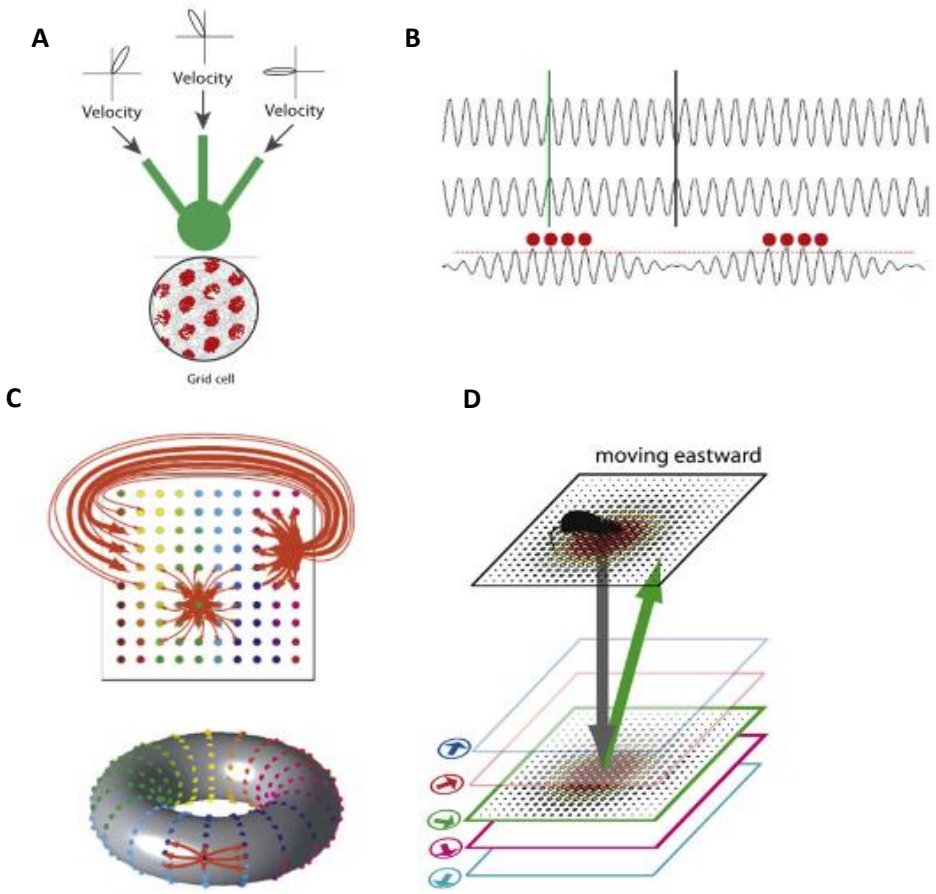

Figure 3-6 Computational models for grid cells firing.

Two classes of models have been proposed to explain the regular firing pattern exhibited by grid cells. (**A**) OIMs posit that theta modulated units with speed and directional modulation along with other baseline theta frequency units input grid cell soma. (**B**) In the grid cell soma the two out of phase oscillators generate a regular interference pattern which triggers grid cells to fire periodically. (**C**) Attractor network-based models rely on the circuit architecture and posit that a Mexican hat connectivity (top) represented with the strength of the arrows in the sheet of neurons of a 2D version of an attractor drives grid cells firing. Because neurons at the edge of the sheet connect to those on the opposite side, the circuit is hypothesized to follow a toroidal pattern of connections (bottom). (**D**) The bump in the attractor is moved thanks to the activity of a hidden layer of neurons which reflects both speed and direction of the animal in space. Adapted from Giocomo et al., 2011.

found in the hippocampus, medial septum and anterior thalamus (Welday et al., 2011). When the animal runs along the VCO's preferred firing direction, the two oscillators input at the same time to the grid cell, though the VCO has a slightly higher frequency than the baseline oscillator. The interference between these two signals is sufficient to produce an intracellular membrane potential oscillation triggering periodic spiking (Figure 3-6B). Computational studies showed that simulated neurons receiving from 6 VCOs with preferred firing direction 60° apart, together with baseline oscillators, display the typical firing pattern of grid cells (Burgess, 2008; Burgess et al., 2007; Hasselmo et al., 2007; Jeewajee et al., 2008a; Welday et al., 2011).

Several pieces of evidence support the OIMs. For instance, medial septum

inactivation, where theta oscillation is thought to be generated and transmitted to MEC, abolishes regular grid cells firing (Brandon et al., 2011; Koenig et al., 2011). Moreover, passive movements fail to elicit regular firing patterns by grid cells and, consistent with OIMs, the speed to theta relationship does not persist (Winter et al., 2015a). However, the presence of grid cells in crawling bats with no undergoing theta oscillation represents a major challenge to most OIMs (Yartsev et al., 2011), although the low speed of animals has been suggested as a potential bias (Barry et al., 2012b).

3.2.3.2 *Continuous attractor network models (CANMs)*

Conversely to OIMs, CANMs rely on the network-based property of the whole MEC architecture. They posit that the regularity in grid cell firing arises as a result of the recurrent connectivity of the circuit in which grid cell firing represents the animal's current location by functioning as continuous attractors (Fuhs and Touretzky, 2006; McNaughton et al., 2006; Samsonovich and McNaughton, 1997; Shipston-Sharman et al., 2016; Zilli, 2012). Original models hypothesized a "Mexican hat" scheme of connections between grid cells (McNaughton et al., 2006; Samsonovich and McNaughton, 1997), according to which grid cells sharing similar phases strongly excite each other, while those with different phases are instead reciprocally inhibited (Figure 3-6C). Therefore, within the MEC, a "bump of activity" is formed and stabilized thanks to the recurrent architecture. In order to follow animal movements in physical space, the bump is hypothesized to "move" around the neural sheet thanks to heading and speed information encoded within the structure (Burak and Fiete, 2009; Fuhs and Touretzky, 2006; Guanella et al., 2007) or via the interaction between conjunctive directional grid cells from layer III and V (Sargolini et al., 2006) and "pure" grid cells of layer II (Figure 3-6D) (McNaughton et al., 2006; Samsonovich and McNaughton, 1997; Shipston-Sharman et al., 2016).

A number of experimental results support CANMs for grid cell firing. For instance, the organized connections in the circuit postulated by CANMs predict a high degree of homogeneity across cells in response to external perturbation. This prediction has been validated by remapping studies showing coherent response by grid cells ensemble (Fyhn et al., 2007; Marozzi et al., 2015). Similarly, grid cells maintained spatial relationship to each other following geometrical changes in the environment (Yoon et al., 2013). Moreover, the observation of conjunctive grid cells in layer III and V (Sargolini et al., 2006), is consistent with early versions of CANMs (McNaughton et al., 2006; Samsonovich and McNaughton, 1997). It should be mentioned that more recent CANMs do not require conjunctive grid

cells for moving the bump of activity across the cells forming the attractor (Burak and Fiete, 2009; Fuhs and Touretzky, 2006; Guanella et al., 2007; Pastoll et al., 2013).

Recent studies investigated stellate cells' mutual connections and showed no excitatory connection (Couey et al., 2013; Fuchs et al., 2016; Pastoll et al., 2013) so CANMs only depending on inhibitory connections have been also proposed (Bonnevie et al., 2013; Burak and Fiete, 2009; Couey et al., 2013; Pastoll et al., 2013). Optogenetic dissection of the MEC circuit revealed that parvalbumin positive (PV^+) GABAergic cells, considered the most-likely candidate to perform phase-specific inhibition, receive input from grid cells with all phases (Buetfering et al., 2014) in contrast to what dictated by some CANMs (Burak and Fiete, 2009) but not all (Shipston-Sharman et al., 2016; Solanka et al., 2015).

3.2.3.3 ***Hybrid models***

Recent technological advancements allowed scientists to perform whole-cell *in vivo* patch-clamp recording in head-fixed animals running in virtual reality. Schmidt- Hieber and Hausser (2013) found that stellate cells membrane potentials during field crosses exhibited sustained intracellular depolarization consistent with CANMs but also display phase precession as predicted by OIMs (Schmidt-Hieber and Häusser, 2013). Similarly, Domnisoru and colleagues (2013) found intracellular signatures of both theta-like oscillation and slow depolarization during field crossing (Domnisoru et al., 2013). Therefore, some relevant features predicted by both classes of models seem to be partially validated experimentally. Therefore a new generation of hybrid models has been recently released, taking into account recurrent architecture of the network, theta oscillation and phase precession occurring at the same time (Bush and Burgess, 2014; Domnisoru et al., 2013; Schmidt-Hieber and Häusser, 2013). Further experiments are therefore needed to elucidate the precise mechanisms generating grid cell firing patterns.

3.2.3.4 ***Summary***

In conclusion, a number of studies corroborated the original hypothesis that grid cells may provide a fixed spatial metric for space. Experimental and theoretical evidence suggest that grid firing can be driven via path-integrator processes (Hafting et al., 2005; Winter et al., 2015a), although whether allothetic information is necessary (Chen et al., 2016; Pérez-Escobar et al., 2016) and how it is integrated are still outstanding questions.

In new environments, expanded maps with grids parallel to boundaries are quickly formed, but shrinking to standard size, shearing and elliptic deformation of the grid are

dynamical processes that progressively occur with experience (Barry et al., 2012a; Ólafsdóttir and Barry, 2015; Stensola et al., 2015). What function this serves and how this is that achieved will be matter of future investigation.

In general, much speculation has been propounded about what spatial metric provided by grid cells can be functional for. In contrast to place cells, the firing pattern exhibited by a single grid cell is ambiguous for decoding position due to the multiple fields homogenously tessellating the available space. However, at least theoretically, the grid cell population ensemble provides two useful sets of information for navigation: current position and distance to or from any point in space. Computational studies have shown that current position can be determined if the ensemble includes cells from different modules with independent grid features like scale and orientation (Bush et al., 2015; Fiete et al., 2008; Mathis et al., 2012). Moreover, a distance vector can be extracted from two sets of cells signalling two reference points in space. However, whether an actual decoding process occurs downstream of the grid cell signal and how this is read-out still remains to be determined (Bush et al., 2015; Fiete et al., 2008).

3.2.4 Speed cells

As mentioned before, most models for path integration require a stable, reliable and invariant speed signal. This is true for CAN models positing the bump of activity being translated between grid cells to reflect animal movements (McNaughton et al., 2006).

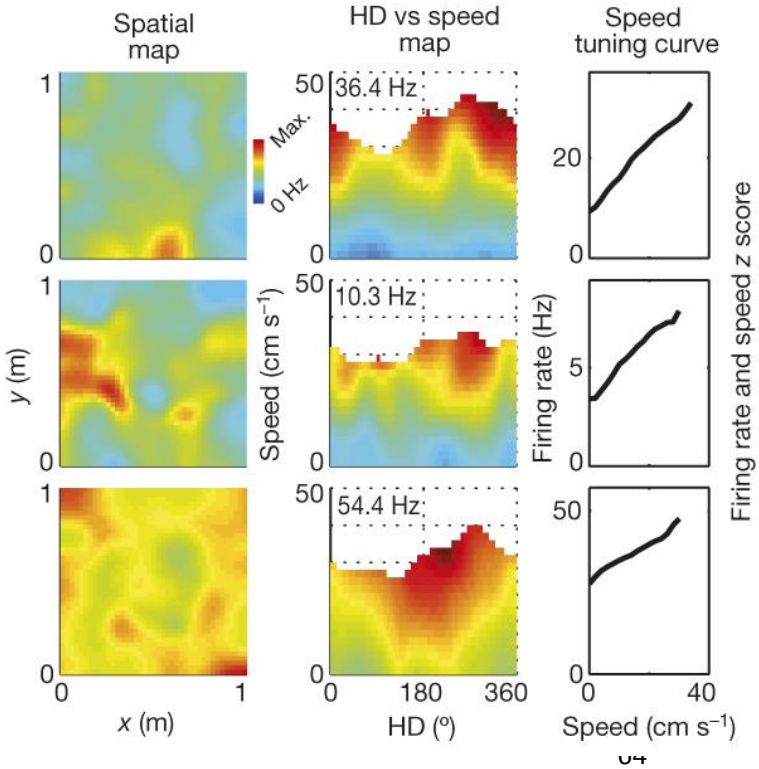

Figure 3-7 Speed cells in the MEC

Three examples of speed cells (each row) recorded in the MEC showing no spatial activity (i.e. they fire everywhere, left column) as well as directional information (i.e. the firing rate is modulated by running speed and not by orientation, middle column) but encode speed information as revealed by the speed lines (i.e. the firing rate increase with running speed, right column) representing mean firing rate across speed. Adapted from Kropff et al., 2015.

Similarly, OIMs posit speed modulation for both basal and velocity-controlled oscillators (Burgess, 2008; Burgess et al., 2007). Indeed, miscomputation of speed would drive grid cells to flicker in space and/or ultimately to break down the hexagonal symmetry. Therefore, on one hand, theoretical models predicted the existence of a speed signal useful for path integration. On the other hand, experimental evidence corroborated this hypothesis. Indeed, LFP theta frequency was known to correlate with running speed (Jeewajee et al., 2008a), suggesting that the ensemble of neurons could be modulated by running speed (Figure 3-1). Moreover, many studies reported neurons with a positive correlation between firing rate and instantaneous speed (Buetfering et al., 2014; King et al., 1998; Welday et al., 2011), as well as place cells and grid cells, which have also been shown to be modulated by running speed (Geisler et al., 2007; Sargolini et al., 2006). However, the description of a separate population of neurons encoding instantaneous speed (and henceforth called "speed cells"), comes from a recent study by Kropff and colleagues (2015). Based on the results, a brief overview of speed cell features is provided here (Kropff et al., 2015).

3.2.4.1 *Firing properties*

Detailed descriptions of speed cell firing is lacking given the limited available data. The little that is known speaks for tonic firing typical of interneurons which differs from the bursts of spikes released by place and grid cells. A substantial proportion of speed cells shows typical theta modulation and preliminary evidence suggests that at least many of the speed cells may be inhibitory PV^+ cells (Cao et al., 2015) like those investigated by Buetfering and colleagues (Buetfering et al., 2014).

3.2.4.2 *Spatial properties*

Speed cells linearly increase their firing rate with animal running speed. This property is revealed by speed lines representing mean firing rates across different speeds (Figure 3-7). There is a large variability across cells with respect to average firing rate, strength of the speed modulation, baseline firing and slope of the speed tuning curve. Speed cells have been found across many layers of the MEC but also in the hippocampus. Importantly, speed cells do not carry additional information (spatial, directional) so they form a neural population on their own separated from grid, place and head direction cells (Kropff et al., 2015).

3.2.4.3 *Hypothesized function and theoretical considerations*

The speed lines exhibited by speed cells suggest that they may be encoding instantaneous speed and such signals feed into the MEC networks for path integration. Evidence supporting this notion comes from a number of observations:

a) Speed cells are context-invariant: at the single cell level, the relationship between speed and firing rate is stable within and across sessions. Moreover, the relationship persists also across different environments, dimensions (linear track and open field), and tasks. Consistently, speed modulation is also preserved in darkness, ruling out the hypothesis that they may be signalling optic flow instead.
b) While speed cells largely differ in a number of features (firing rate, slope, baseline, theta modulation), at a population ensemble they carry a very coherent signal which can be used to decode the animal's running speed.
c) A substantial subset of speed cells showing theta modulation exhibit prospective encoding, though only in the MEC. Importantly, speed cells and grid cells share similar prospective bias (~50-80 ms) and such a finding is consistent with the hypothesis that speed cells may be upstream to grid cells.

Even though only a few studies investigated speed cell firing properties (Hinman et al., 2016; Kropff et al., 2015), the findings at our disposal strongly argue that that these neurons may encode instantaneous speed and this information could be used for path integration. Further experiments are necessary to test this hypothesis, however some theoretical considerations, relevant to the results section of this thesis, can be made at this point.

The working hypothesis stated by Kropff et al. (2015) posits that speed cells may be upstream of grid cells such that the speed signal is integrated by grid cells to compute the sense of distance (Kropff et al., 2015). Perhaps one way of testing this hypothesis would be to analyse the speed lines of speed cells during novelty, where the grid firing patterns are known to expand (Barry et al., 2012a). The natural prediction is that the firing rate of speed cells is decreased, namely that the instantaneous speed is underestimated and that drives grid cells to underestimate distances thus driving expansion. Similarly, a second test can be proposed, which is to examine the firing pattern by speed cells during passive movements as in the study by Winter et al. (2015). Passive movements cause disruption of the regular firing pattern by grid cells, suggesting that the system is dependent on efferent motor copy

(Winter et al., 2015a). Two alternative scenarios can be imagined:

a) speed cell tuning curves become flat, suggesting that they are dependent on self-generated movements only and their impaired signal may explain grid cells firing disruption. This finding would unequivocally show that speed cells depend on the proprioceptive system.
b) speed cells maintain their speed encoding. In which case, the hypothesis that speed cells integrate self-generated movements would need to be rejected, shifting the focus to other systems such as the vestibular system. In particular, the otolith organs, comprising the saccule and utricle, are known to encode linear acceleration along the vertical and horizontal axis respectively (Angelaki and Cullen, 2008). Theoretically, the utricle could be the first step of a long pathway where horizontal linear acceleration is primarily encoded. This signal is then conveyed to upper-level stations in the midbrain where this is transformed into speed detection and ultimately displacement by grid cells in the MEC (Jacob et al., 2014).

Future investigation will help test these hypotheses. Moreover, the following questions remain to be asked:

a) is the speed signal generated locally or outside the MEC and conveyed from other brain areas?
b) are speed cells also modulated by allothetic information? In which case, how is that information integrated?
c) what is the source of the speed signal? Which system is required for the generation of the speed signal? Does it depend on the vestibular system or proprioception?

Further investigations of speed cell features and particularly a detailed characterization of the upstream pathway will help answering a number of questions on the nature of the grid cell system and the circuits for path integration.

3.2.4.4 *Summary*

Taken together the results obtained by Kropff and colleagues (2015) argue for the existence of a distinct population of cells which encode instantaneous speed. The context-

invariance of their encoding resembles the fixed spatial metrics carried by grid cells and for this reason they have been linked to path integration mechanisms (Kropff et al., 2015). As mentioned before, at least a large fraction of speed cells seem to fall under the category of PV^+ inhibitory neurons (Cao et al., 2015), which, consistent with previous results, have been shown to increase their firing rate with running speed (Buetfering et al., 2014). Based on experimental evidence showing lack of excitatory connections between stellate cells, recent CANMs with recurrent inhibitory connections have been proposed (Bonnevie et al., 2013; Couey et al., 2013; Pastoll et al., 2013). However, the study by Buetfering and colleagues (2014) challenge the notion that PV^+ cells, which are reciprocally interconnected to stellate cells, mediate the phase-specific inhibition that some authors believe are a necessary component of CANMs (Buetfering et al., 2014) – a contrary view is presented by (Solanka et al., 2015). Understanding where and how the speed signal is computed, along with its functional role, will be pivotal to understanding how grid cell firing is generated.

3.2.5 Other spatial cell types

In the results section of these thesis, the spatial activity of place, grid and speed cells on the vertical wall is described. As such, a large section of this chapter has been dedicated to describing their main properties relevant for the understanding of the results presented in this thesis. However, in addition to these cell types, there are other functionally identified cells falling under the category of spatially-modulated neurons. A brief mention of these will be provided in the next paragraphs along with the main literature for a deeper comprehension of the matter.

3.2.5.1 *Head direction cells*

The ability to integrate self-motion, as described above, is clearly an important information source for freely moving animals. Since the discovery of place cells, the neural mechanism supporting path integration has been widely sought in the brain, resulting in the discovery of a new cell-type in the post-subiculum (POS) by Ranck (Ranck, 1984). These neurons, termed “head direction cells” (HDCs), show allocentric encoding of an animals’ heading direction and became the broad research theme investigated by J. Taube since early 90’s (Taube et al., 1990a, 1990b). Further studies revealed the presence of HD cells in a number of other brain areas including anterior dorsal thalamic nuclei (ADN) (Taube, 1995), lateral mammillary nuclei (Stackman and Taube, 1998), retrosplenial cortex (Chen et al., 1994; Cho and Sharp, 2001; Jacob et al., 2016) and MEC (Giocomo et al., 2014; Sargolini

et al., 2006) among others.

The properties of HDCs have been widely investigated and a thorough description of them goes beyond the scope of this thesis. A large body of evidence shows that they rely on allothetic as well as idiothetic information to encode direction (Goodridge and Taube, 1995). In the absence of external sensory cues, HDCs maintain relatively stable preferred firing directions, drifting only slowly. For a thorough review of HD cells and their contribution to path integration see McNaughton et al., (2006) and Taube (2007). Taken together, the results suggest that HDCs encode allocentric direction and for this reason they are hypothesized to act as an internal compass fundamental for efficient navigation (Taube, 2007). However, it must be said that HDC firing has been shown to best correlate with the direction of the head of the animal rather that the heading direction, which instead corresponds to the direction of the movements (Raudies et al., 2015). Therefore, whether and how the brain encodes heading direction are still outstanding questions in the field.

3.2.5.2 *Border cells and boundary vector cells*

Following the discovery of grid cells in the MEC, many experiments have investigated this brain area and along with the report of HDCs in this structure (Giocomo et al., 2014; Sargolini et al., 2006), another functionally identified cell-type, termed “border cells” have also been described in the MEC (Solstad et al., 2008). These cells increase their firing rate when an animal approaches or is located near the border of an environment. They are predominantly located in the middle and deep layers of the MEC and are thought to provide information about the geometry of the environment. However their activity and their influence on grid cell firing is poorly characterized but they are likely to mediate the effects of environmental geometry previously described (see 3.2.2.6).

Another functional cell-type with border-related activity, termed boundary vector cells, have been reported in rat SUB (Lever et al., 2009) and has been hypothesized to represent an important input to place cells (Barry et al., 2006). These cells fire at specific distances from boundaries and at specific directions, although their firing can also be elicited by edges and by the absence of walls. Future experiments will help understand their contribution to place cell firing and how border/direction information is integrated to form place fields in the hippocampus (Barry et al., 2006).

In this chapter, a short introduction to the neural systems encoding space has been

provided to give the reader the essential information to broadly understand the topic. In the next chapter, the literature addressing the neural encoding of the 3D world.

4 Towards 3D encoding of space

The way the brain represents space is one of the key questions in systems neuroscience. However, as the general picture of the neural encoding in flat (2D) environments is becoming clearer, an issue that still remains fairly unexplored is the way that the brain encodes 3D (and thus more realistic) space. The aim of this chapter is to review the evidence collected in the last decade addressing the question of how the mammalian brain encodes and navigatates in 3D space (Jeffery et al., 2013a, 2015). Firstly, the scientific terminology used to describe movements in 3D throughout this thesis will be introduced. Secondly, findings collected from two animal models (rats and bats) will be summarised. Finally, a cross-species summary will be proposed in order to provide a global theoretical framework for understanding the scientific questions investigated and presented in this thesis.

4.1 Terminology for 3D movements

In order to review the experimental evidence collected in the last decade on the 3D encoding of space, it is necessary to firstly accurately describe the terminology used to determine position, movements and orientation in 3D. To begin with, two related variables need to be defined and are:

1. dimension, which refers to "*the number of parameters needed to specify a point in a space*" (Jeffery et al., 2015);
2. the frame of reference, which refers to the collective sum of all the "*fixed parts of the space from which the parameters are measured*" (Jeffery et al., 2015).

For instance, when a rat runs back and forth on a linear track, the position can be assessed by excluding lateral movements and using one dimension only – i.e. the position along the axis specified by the track. Movements can only be linear (translation) and categorized like left-right or North-South. Accordingly, in this context the reference frame can be set as the linear track itself.

Slightly more complicated becomes describing planar navigation, for instance during a standard free-foraging task carried in large environments such as 100 cm square boxes. In such a configuration, movements happen in two dimensions, so two numbers (-*x* and -*y*

coordinates) are needed to describe position in space. Movements can be linear or angular (also termed rotations), and the orientation of these is determined by using the angle the animal is facing (termed azimuth) referenced to an arbitrary axis (in rectilinear environments the edges are generally used for the x-reference axis). In such a scenario, the surface of the environment is defined as the reference frame (Jeffery et al., 2015).

When an animal explores volumetric space, movements occur in 3D and it is evident that three coordinates (*-x, -y* and *-z*) are needed to describe the position. Furthermore, rather than a unique angular rotation, three rotations can occur in 3D and each one is specified by a single plane. The rotation on the x-y plane is the azimuth, while rotation along the vertical plane is termed pitch, and the angle to define orientation of the animal along its longitudinal axis is termed roll (Figure 4-1).

Moreover, as well as the allocentric definitions, it is also worth specifying the egocentric rotations in 3D. The rotation in the plane of the animal's feet is termed yaw – and such rotations is what determines the azimuth. In contrast, the rotation in the plane orthogonal to yaw is termed pitch, while the one in the coronal plane is termed roll (Figure 4-1).

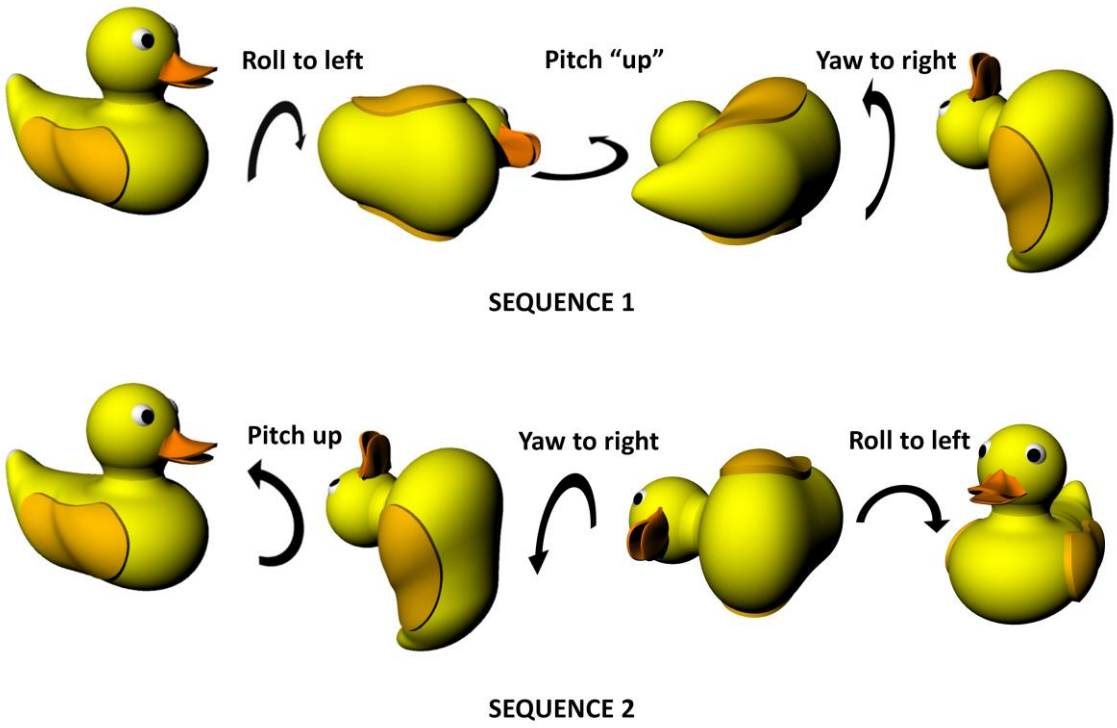

Figure 4-1 Non-commutativity of 3D rotations

Roll, pitch and yaw represent the possible rotations an animal can perform in 3D. An important feature is the non-commutativity of those rotations, meaning that depending on the order they computed, different outcomes would be generated. For instance compare sequence 1 (top row) [Roll to Left – Pitch up – Yaw to right] with sequence 2 (bottom row) [Pitch up – Yaw to right – Roll to Left] where the duck in the example turns out in two different positions and facing different angles. Adapted from Jeffery et al., 2015.

It should be noted that in rotating on a single plane - which is a 2D entity – requires two dimensions and given that there are altogether three dimensions, rotations occurring in perpendicular planes “share” one of their dimensions. In other words, differently from linear motion, rotations in 3D cannot be completely independent as the rotation in one plane alters the axis of rotation in another. This property has two natural consequences for rotations in 3D:

a) they are non-commutative, i.e. they are order-dependent;

b) two following rotations in the orthogonal planes result in a rotation also on the third plane (Figure 4-1).

Therefore, the complexity generated by movements in 3D space poses several challenges for brain in order to perform effective navigation. In particular, maintaining a stable compass signal, measuring travelled distances, determining self-position and ultimately performing route-planning is a complex cognitive skill that the neural circuits for spatial coding must compute. The next paragraphs will briefly introduce and discuss the experimental evidence of spatial activity in 3D from rats and bats.

4.2 Spatial representation in rodents

Since the dawn of experimental psychology, rats have been intensively tested in a variety of cognitive tasks including spatial navigation. Furthermore, since the discovery of place cells in rat hippocampus (O’Keefe and Dostrovsky, 1971), rodents have become the model species for electrophysiology *in vivo*. Accordingly, initial attempts to elucidate 3D representation of space in mammals were carried out in rats. In this chapter, the activity of spatially modulated neurons in rodents in 3D space will be. It should be noted however, that given that rats are surface-dwelling animals, all the experiments presented in this chapter do not precisely test 3D movements given that they cannot fly. Instead, the experiments presented here shortly focus on spatial coding on the vertical plane, therefore still on a 2D map but with the z-coordinate (height) tested.

4.2.1 Place and grid cells on the pegboard

One pioneering study aimed to elucidate the 3D representation by place cells was carried out by Knierim and McNaughton (2001) who recorded place cells from animals running on a flat rectangular linear track and compared the firing patterns observed on it to

the ones displayed by the same cells after tilting portions of the track by 45° (Knierim and McNaughton, 2001). The results showed that place cells broadly responded to movements in 3D but with no evidence for metric encoding probably due to the saliency of the available cues on the flat portions of the track.

The study by Hayman and colleagues (2011) addressed the neural representation of vertical space in rodents (Hayman et al., 2011). These authors recorded both place and grid cells from rats trained to navigate on a pegboard, a vertical board with embedded projecting pegs onto which animals were trained to climb while foraging for food (Figure 4-2A-B). By comparing the neural maps between the pegboard and a flat arena as a control, grid cells on the pegboard produced vertical stripes spanning along the entire height of the apparatus (Figure 4-2C) suggesting a dramatic drop in the ability to perform path integration in the vertical dimension. Moreover, grid cells on the pegboard showed a significant increase in the length of the major but not the minor axes of the fields, as well as an increase in the aspect ratio (major/minor axis) and preferential orientation of the stripes along the vertical axis compared to the horizontal control. Similar results were also

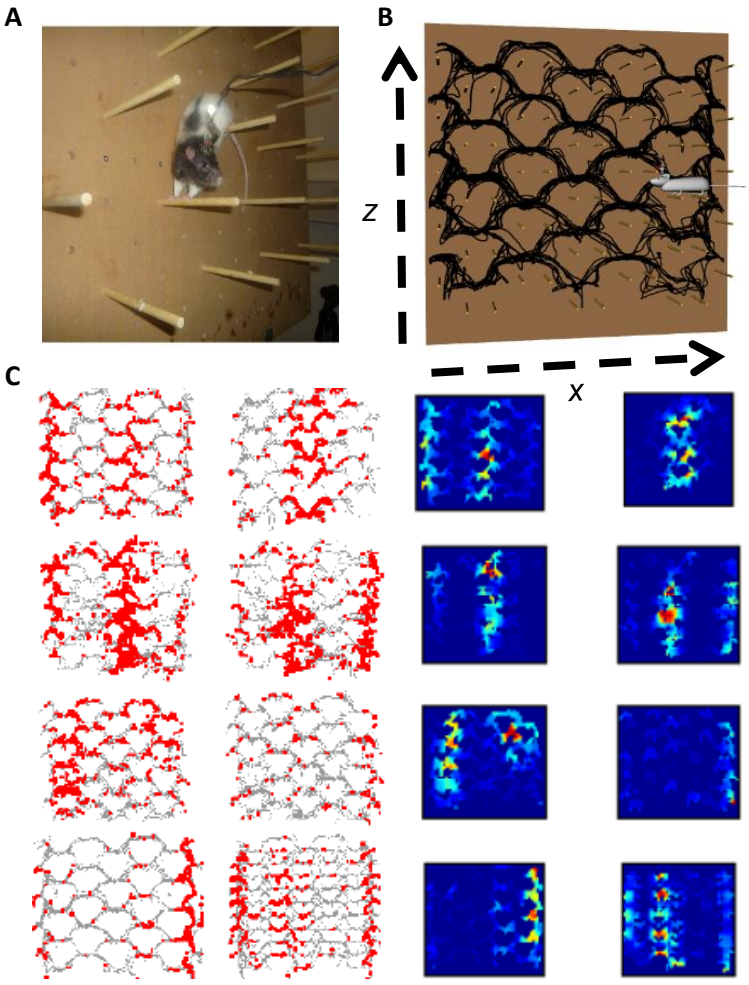

Figure 4-2 Vertical stripes of firing by grid cells on the pegboard.

Grid cells during navigation on the pegboard produced vertical stripes of firing. (**A**) Photo taken by R. Hayman showing a rat walking across the horizontal pegs embedded onto the pegboard apparatus. (**B**) Schematic drawing representing the rat cumulative path on the pegboard. (**C**) The vertical stripes of firing by 8 grid cells recorded on the pegboard are represented as spike plots (left columns) and rate maps (right columns). Adapted from Hayman et al., 2011.

shown by place cells, which produced columnar firing on the pegboard, suggesting that the grid and place cell systems responded coherently to vertical locomotion.

Overall this study showed an impaired capacity by grid and place cells to perform accurate spatial representation in the vertical dimension and thus that they encode the horizontal and vertical dimensions differently (Hayman et al., 2011). These results led the authors to formulate a number of hypotheses (see also 4.5.1):

a) the lack of experience of navigating in the vertical dimension by lab-housed rats prevents them from encoding vertical movements (referred to as the experience-dependent hypothesis, see 4.5.1.1);
b) there is a general insensitivity to vertical movements (referred to as the anisotropic hypothesis, see 4.5.1.2).
c) the topology of the environment orienting the rats body parallel to the horizontal earth-reference acts as an explanation for the horizontal but not vertical spatial firing (referred to as the reference frame hypothesis, see 4.5.1.3);

Among these three hypotheses, Hayman et al. 2011 opted for the second one and thus proposed that the mammalian cognitive map is insensitive to height and thus anisotropic (Hayman et al., 2011), suggesting that the general representation of space is two-dimensional rather than volumetric (Jeffery et al., 2013b)

4.2.2 Grid cells on the tilted plane

One step forward towards a deeper understanding of 3D encoding comes from the follow-up experiment by Hayman and colleagues (Hayman et al., 2015). In this study, the activity of grid cells was recorded while animals freely navigated between a horizontal and 40° tilted slope joined together as a continuous surface (Figure 4-3). This was done to test: a) whether the odometry signal carried by grid cells was impaired for movements on the slope; b) whether the firing pattern by grid cells on the slope was consistent with the 3D optimal packing predicted by a number of computational models (Horiuchi and Moss, 2015; Mathis et al., 2015; Stella and Treves, 2015). The results showed that grid cells maintained the capacity of forming discrete firing fields on the slope surface and they displayed no differences (field size, scale orientation) when compared to the ones on the horizontal plane except for a weak but significant reduction in the hexagonal arrangement (“gridness”). This finding shows that on the slope local maps are quantitatively similar to

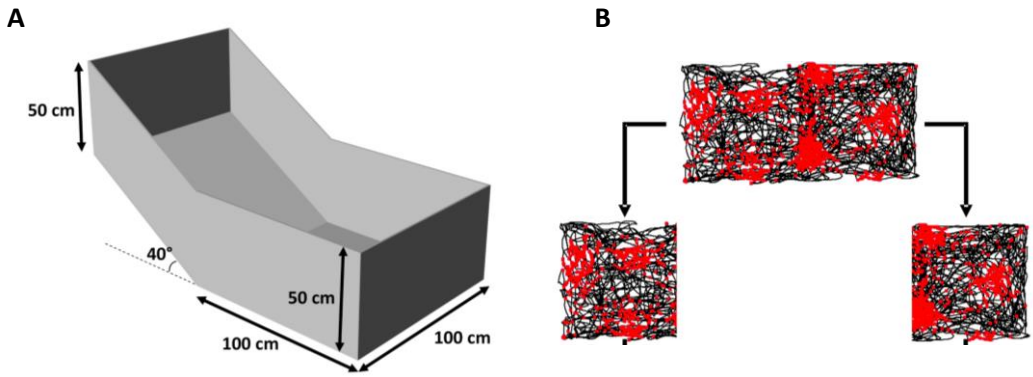

Figure 4-3 Grid cells representation on the tilted plane.

(**A**) Schematic drawing representing the experimental apparatus formed by two continuous surfaces, one horizontal (right) and one tilted 40° upwards (left). (**B**) One example of grid cell recorded on both surfaces (top) showing characteristic grid arrangement on both surfaces (bottom). Adapted from Hayman et al., 2015.

the ones on the flat horizontal plane. Further analyses addressing whether the speed-to-theta relationship was altered on the tilted plane showed that both the slope and the intercept of the speed-to-theta correlation displayed no differences between the titled and horizontal plane (Hayman et al., 2015). Therefore, similarly to the encoding of distance by single grid cells, the encoding of instantaneous speed by theta was unaffected on the tilted plane.

Overall these results show that on the slope grid cells mostly maintained their quantitative firing properties and the speed-signal encoded by the LFP theta oscillation stayed stable on both planes (Hayman et al., 2015). However, the decreased regularity in the grid arrangement observed on the slope led the authors to hypothesize that the firing pattern on the tilted plane was consistent with any 3D optimal packings (Horiuchi and Moss, 2015; Mathis et al., 2015; Stella and Treves, 2015) rather than a local grid map. To test this hypothesis, Hayman et al. 2015 simulated both the face centred cubic (FCC) and hexagonal close pack (HCP) lattice of spherical fields in 3D (see also 4.3.3 for a description of them) and sliced these volumes both at 0°and 40° (Hayman et al., 2015). This was done to respectively visualize the firing pattern of an ideal grid on the floor and slope and compare these to the experimental results. The comparisons showed that none of the parameters observed matched the predicted firing on the slope, neither for the HCP nor for the FCC lattice. Therefore, the results returned by simulations ruled out the hypothesis that at least on the slope, the field organization followed the arrangement of optimal packing. Accordingly, although indirectly, these results speak against the hypothesis that grid cells could produce 3D optimal packing (Hayman et al., 2015).

4.2.3 The mosaic hypothesis

As shown by Hayman et al. (2015), grid cells on the tilted plane exhibited local maps which maintained the same spatial metrics as on the horizontal plane (Hayman et al., 2015). Importantly, the pattern on the slope not only was qualitatively the same as on the horizontal plane, but also showed radically different patterns from what expected for 3D optimal packing. Jeffery and colleagues proposed a different way for the brain to represent 3D space (Jeffery et al., 2013b, 2015). Rather than being a continuous volumetric representation, the authors hypothesized that the mammalian brain, at least in surface-dwelling animals such as rats, may instead "*construct a mosaic of maps that are locally planar but related to each other by their relative distances and directions*" (Jeffery et al., 2015). Accordingly, the encoding of a volumetric distance could be achieved by "stitching" together the local maps. What remains to be elucidated though is if each of these local maps shares the same reference frame or not. If the answer is yes, it is possible to think of the earth-horizontal plane (detected by the gravity vector) as crucial to determine such a reference plane (i.e. the earth-reference hypothesis). In contrast, if each map had a local reference, then it has to be able to flexibly "orient" to the surface angle and hence to the orientation of the animal body. It follows that a likely candidate for the local reference frame would be the one parallel to the locomotion plane (body-orientation hypothesis). Unfortunately, the experiment conducted by Hayman and colleagues (Hayman et al., 2015) was not suitable to address this question: the 40° angle used in the study made the plane for the animals to walk on very steep, but it was not enough for test the earth-reference vs. body-orientation hypotheses. Future experiments aimed to test these hypotheses are therefore needed and, as discussed below (see 4.5), this thesis aims to elucidate this matter.

1.1.1 Head direction cells on the vertical plane

It has been previously mentioned that the HDC system is thought to provide the sense of heading direction acting as an internal compass for navigation (see 3.2.5.1). This notion has been well supported by a variety of experiments and it seems to be valid also on the vertical plane. The first study to investigate this topic was carried out by Stackman and colleagues (2000) in which head direction cells from ADN and PoS in rats were recorded in a cylindrical enclosure with high walls covered with mesh which animals could climb on. The results showed that head direction cells showed regular preferred firing directions on the horizontal floor as well as during climbing in the vertical plane (Figure 4-4). Importantly,

head direction cells fired during upwards climbing only on the wall the preferred firing direction on the floor was oriented to as well as during downwards climbing on the opposite side (180° apart). This result shows that the head direction cell network translated the sense of direction found on the floor onto the cylindrical walls and therefore kept a stable and consistent reference frame throughout the maze (Stackman et al., 2000). It should be said that in this study only linear acceleration was truly tested in this apparatus as no yaw rotation was involved during climbing.

A study by Taube et al. (2013) addressed this matter and showed that in the vertical plane head direction cells also responded to yaw rotations (Taube et al., 2013). Interestingly, the preferred firing direction of head direction cells in the vertical was consistent with the horizontal one, a finding which corroborates the hypothesis that the horizontal reference frame was maintained throughout the maze (Stackman et al., 2000). However, further experiments revealed that while head direction cells responded on the vertical plane, they did not do so while animals walked upside-down. Calton and Taube (2005) reported that 47% of the head direction cells lost directional information, while the remaining ones produced much noisier turning curves (Calton and Taube, 2005). The dramatic impairment observed by head direction cells under inverted navigation may explain the behavioural deficits exhibited by rats on a simple spatial task while inverted (Gibson et al., 2013; Valerio et al., 2010).

In conclusions, head direction cells in rodents have shown to function on the vertical plane as good as on horizontal and its functioning is equally robust during linear as well as angular movements. Relevant for this thesis, the consistency between horizontal and

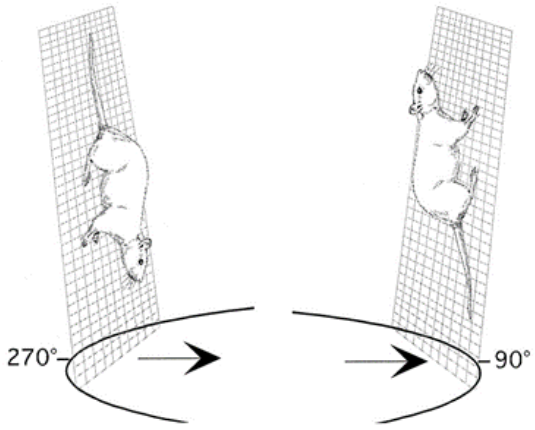

Figure 4-4 Head direction cells on the vertical plane.

Schematic representation of a rat climbing downwards (left) and upwards (right) on two opposed climbing walls after crossing central arena on the floor. The arrows represent the preferred firing direction of a single HD cell pointing 270° (downwards on the left wall) and 90° (upwards on the right wall) showing that the HD system translated the horizontal sense of direction onto the vertical plane. Adapted from Stackman et al., 2000.

vertical movements suggest a shared reference frame which may underlie a fully 3D system to encode direction undertaken in volumetric space.

4.3 Spatial representation in bats

Since the early pioneers, neuroscientists have taken advantage of several animal models to understand neural circuits underpinning behaviours. Among many, rodents have been the most successful group for a number of reasons and especially in the spatial cognition field, mice and rats had been intensely used since the dawn of this discipline. In particular, since the pioneering studies by Tolman (Tolman, 1948), rats were tested in a number of spatial tasks and such investigations ultimately led to many fundamental discoveries in the rat hippocampus. In parallel, the recent developing of transgenic technologies associated with neural circuits in mice has greatly enhanced our understanding of the neural subtrates of navigation. However, over the last decade, bats have received a great deal of interest thanks to a series of studies conducted in Ulanovsky's lab based at the Weizman Institute in Tel Aviv, Israel. Indeed, neurons acting like place cells (Ulanovsky and Moss, 2007, 2011; Yartsev and Ulanovsky, 2013), grid cells (Yartsev et al., 2011) and head direction cells (Finkelstein et al., 2015) were reported in the homologous brain structures of bats (Geva-Sagiv et al., 2015). Taken together, these findings showed that the neural circuits relevant for spatial cognition are mostly conserved across mammalian *phyla*. Moreover, although the majority of studies in the hippocampal field are still conducted in rodents, bats represent a suitable species for investigating spatial cognition. In particular, addressing whether and how 3D representation of space is achieved in bats is appropriate given that:

a) they fly and thus spontaneously perform 3D navigation;

b) in the wild they cover long distances so must have evolved efficient navigational strategies requiring path integration (Geva-Sagiv et al., 2015).

In the following paragraphs, the findings obtained in bats will be briefly reviewed with the aim to show that:

a) the neural circuits for navigation are mostly conserved across *phyla*;

b) the highlighted differences between *phyla* could help improve our knowledge of these neural circuits.

4.3.1 Place and grid cells in crawling bats

The first study addressing neural circuits for spatial navigation in bats was conducted by Ulanovsky and Moss (2007). The authors reported units in the principal layer of echo locating big brown bats (*Eptesicus fuscus*) showing clear place fields (Figure 4-5A) while they were freely crawling onto a tilted surface (Ulanovsky and Moss, 2007, 2011). This initial finding thus showed that place cells in the hippocampus were also conserved in bats. Importantly, LFP theta oscillation differed from the rat counterpart. Indeed, the oscillation detected in theta band did not occur during locomotion (when this is most prominent in rodent LFP) but during echolocation epochs. Moreover, rather than being a continuous signal, it appeared to be rather intermittent during short bouts (Ulanovsky and Moss, 2007, 2011).

The study of Yartsev and colleagues (2011) provided further evidence on bat hippocampal functioning. Firstly, the authors replicated previous findings by showing place cell activity in the hippocampus of the crawling Egyptian fruit megabat (*Rousettus aegyptiacus*). Importantly, like the big brown bats, theta oscillation appeared not to be continuous but rather intermittent in short bouts (Yartsev et al., 2011). Secondly, the authors addressed whether grid-like firing could exist without continuous theta. Similar to the rodent, bat MEC was demonstrated to host a variety of spatially modulated neurons including grid cells, head direction cells and border cells (Figure 4-5B). In addition, further anatomical investigation showed a high degree of fidelity across MEC layers too, suggesting that both the anatomy and physiology of the structure is highly conserved across those mammalian *phyla* (Yartsev et al., 2011). However, if on one hand these results indicated great similarities between rats and bats, key differences between them were also found. Indeed, the temporal analysis of grid cell firing in bats showed that although the spatial six-fold symmetry was evident, none of the units displayed clear theta modulation nor LFP theta oscillation (Yartsev et al., 2011). Therefore, consistent with previous studies (Ulanovsky and Moss, 2007, 2011), these observations challenge those computational models linking theta oscillation with path-

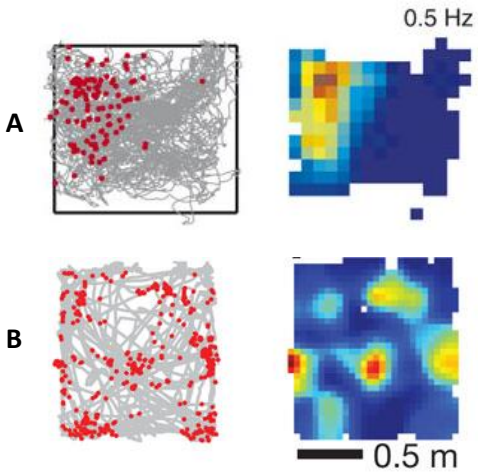

Figure 4-5 Place and grid cells from crawling bats.

Example of one place cell (**A**) and grid cell (**B**) represented as spike plot (left) and rate map (right). Adapted from Ulanovsky and Moss, (2007) and Yartsev et al., (2011).

integration mechanisms (Burgess, 2008; Burgess and O'Keefe, 2011; Burgess et al., 2007) and it has often been used as argument to disproving them (Barry et al., 2012b; Yartsev et al., 2011). The discussion on the critiques addressed on this controversial matter will not be reviewed here as it goes beyond the scopes of this chapter.

To conclude, overall these results show that even in bats, a mammalian group phylogenetically distant from rodents, the representation of space is conserved and encoded within the hippocampal formation thanks to a number of functionally-identified cell types which are likely to contribute to the formation of the spatial cognitive map.

4.3.2 Place and head direction cells during flight

It has been mentioned before that the initial attempts to assess spatial representation in bats were carried while animals crawled on a horizontal or tilted plane (Ulanovsky and Moss, 2007, 2011; Yartsev et al., 2011). These studies revealed in bats the presence of a number of spatially modulated neurons in the homologue brain areas of rats. However, the lack of continuous theta modulation reported during crawling was proposed to be due to the slow speed of the animals (Barry et al., 2012b). Moreover, it should be pointed out that crawling is not the appropriate behaviour to investigate navigation as the bats natural locomotion pattern is flight. Accordingly, addressing spatial coding in free-flying bats remained as natural question to be asked.

The follow-up study by Yartsev and Ulanovsky (2013) shed light on this matter as

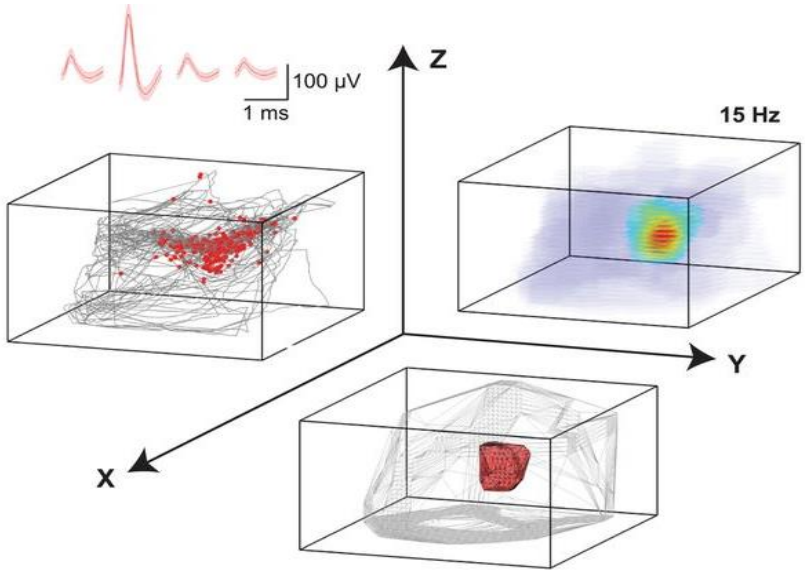

Figure 4-6 Place cell in free flying bats.

Example of place cell recorded during flight in a large cuboid is represented as spike plot (left), rate map (right) and volume (bottom). Adapted from Yartsev and Ulanovsky (2013).

they recorded the activity of hippocampal place cells in freely flying bats. Similar to rodents' place cells on the horizontal plane, the majority (75%) of hippocampal neurons from bats fired every time the animal flew through a restricted volume of the whole available space (i.e. a 3D place field, Figure 4-6). Moreover, consistent with the literature on rodents, bats volumetric fields showed a high degree of spatial tuning, different sizes and stability throughout the experimental sessions (Yartsev and Ulanovsky, 2013). However, differently from the vertical elongation displayed by place cells on the pegboard in rats (Hayman et al., 2011), place cell representation was isotropic, i.e. symmetrical across all dimensions. Indeed, 3D place fields did not display any significant elongation in the x-,y-,and z- axes and more than 90% of them were not significantly different from that expected from an underlying sphere used at chance level (Yartsev and Ulanovsky, 2013). Therefore, these results showed that even in bats, a mammalian group phylogenetically distant from rodents, the representation of space is conserved and encoded within the hippocampus thanks to the presence of place cells encoding self-location. Importantly, the resolution by which place fields are formed is the same at all possible directions, showing that the bat representation of space is symmetrical across dimensions and is therefore volumetric (Yartsev and Ulanovsky, 2013). Moreover, consistent with previous reports in crawling bats (Ulanovsky and Moss, 2007, 2011; Yartsev et al., 2011), complete lack of spike-train theta modulation was again observed during flight and the role of theta oscillation for spatial coding questioned (Yartsev and Ulanovsky, 2013).

The 3D firing by hippocampal place cells led authors to hypothesize the existence of a 3D head direction signal in bats too. Finkelstein and colleagues (2015) reported HD cells in the PRE of bats (a brain area where HD cells have been reported previously in rats (Boccara et al., 2010)), trained in a variety of tasks including 3D free flight (Finkelstein et al., 2015). Interestingly, some neurons showed tuning curves with respect to yaw (azimuth), but also to pitch and roll movements (Figure 4-7). Moreover, some units displayed conjunctive encoding of 2 and 3 Euler angles and seemed to follow an anatomical gradient along the A-P axis of the PRE. Interestingly and differently from rats (Calton and Taube, 2005), yaw-responsive HD cells in inverted bats showed a 180° flip in the preferred firing direction. This result led the authors to propose a toroidal model of head direction coding formed by two 360°-ranged and independent cycles representing azimuth and pitch at the same time (Finkelstein et al., 2015).

In summary, recent investigation of the bat hippocampal formation revealed that:

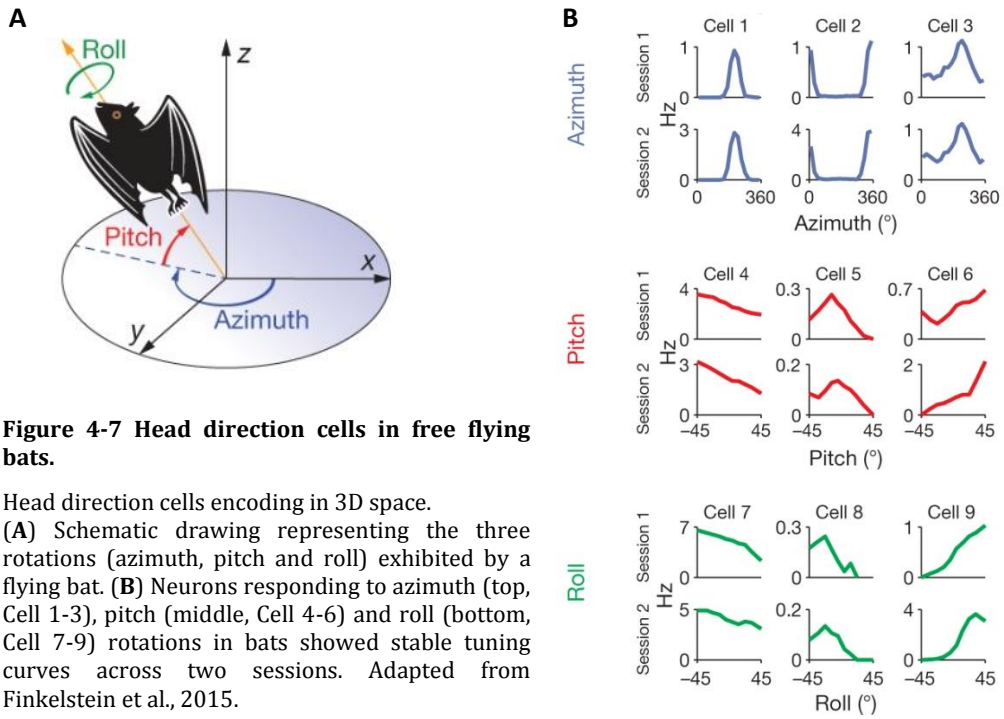

Figure 4-7 Head direction cells in free flying bats.

Head direction cells encoding in 3D space.
(**A**) Schematic drawing representing the three rotations (azimuth, pitch and roll) exhibited by a flying bat. (**B**) Neurons responding to azimuth (top, Cell 1-3), pitch (middle, Cell 4-6) and roll (bottom, Cell 7-9) rotations in bats showed stable tuning curves across two sessions. Adapted from Finkelstein et al., 2015.

1. the neural circuits for navigation are conserved across mammals;
2. the spatially modulated neurons found in rodents are also present in bats and share most of their properties;
3. the lack of intrinsic theta rhythm in bats is not speed-dependent and challenges oscillatory-based mechanisms for path integration;
4. those studies addressing volumetric encoding in bats suggest that the representation can be truly 3D and not planar as suggested for rodents.

It appears clear that, in this theoretical framework, the missing link is to unveil the 3D encoding by grid cells during flight. Initial attempts have been made already and preliminary data speak for a relatively regular organization of 3D firing by grid cells during free flight (Ginosar et al., 2014, 2015). Therefore, it is only a matter of time before these and others studies will shed light onto this fascinating question. In the next paragraph, a brief overview of theoretical considerations and computational studies focused on the 3D encoding by grid cells will be presented.

4.3.3 Grid cells in flying bats: speculations and theoretical predictions.

As mentioned above, the hexagonal array exhibited by grid cells supports the notion that grid cells provide spatial metrics by determining travelled distances. Indeed, as a result of the hexagonal arrangement, the distance between each of the six surrounding peaks from an arbitrary central field defines the cell scale (or wavelength). Interestingly, mathematical studies (C. Gauss, 1831) showed that the hexagonal pattern represents the optimal lattice, i.e. the most efficient way for packing non-overlapping circles of the same size on a plane. Therefore, given that grid fields are usually circular, the hexagonal lattice exhibited by grid cells is the optimal neural mechanism for representing 2D space most accurately. However, real environments are 3D and even surface-dweller animals, such as rodents, are known to navigate not only along horizontal planes (earth-reference frame) but also climb and/or move through underground tunnels and burrows. Moreover, many mammal phyla, such as cetaceans, seals, otters, and bats navigate in 3D environments, raising one important question: did evolution shape the neural circuits responsible for representation of space for the encoding of volumetric navigation? The recent reports of purely volumetric place cells (Yartsev and Ulanovsky, 2013) as well as 3D head direction cells (Finkelstein et al., 2015) led to an increasing interest focused on 3D encoding by grid cells in free flying bats.

This topic has been addressed by theoretical studies (Mathis et al., 2015; Stella and Treves, 2015) which linked grid cell firing patterns to mathematics, where the problem of

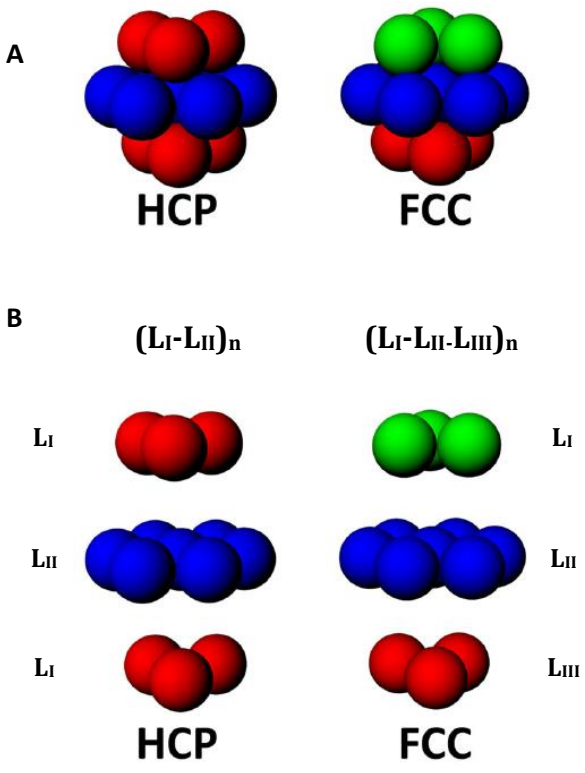

Figure 4-8 Optimal packing of spheres in 3D space.

(**A**) Schematic representation of 13 equidistant spheres forming an optimal 3D packings termed HCP (left) or FCC (right). The difference between HCP and FCC is highlighted in (**B**) where the lattice organization is described: HCP is formed by two layers $(L_I\text{-}L_{II})_n$ as shown by the identical position of the red spheres at the top and bottom layer. In contrast, FCC is formed by three layers $(L_I\text{-}L_{II}\text{-}L_{III})_n$ with top and bottom spheres placed in different positions and highlighted with different colors (red and green). Adapted from Jeffery et al., 2015.

sphere packing in a volume represents a challenging question. It is known since the time of Gauss that only two arrangements represent regular solutions to the sphere-packing problem (C. Gauss, 1831) and they are termed the face-centered-cubic (FCC) lattice, and the hexagonal-close packed arrangement (HCP). Indeed, conceptually similar to the hexagonal lattice being optimal for tiling 2D space, the FCC and HCP lattices are the densest packings for filling a volume with non-overlapping spheres (Figure 4-8A). In other words, in order to maximize the packing ratio of spheres in 3D, several layers of hexagonally arranged spheres laid on a plane need to be stacked up as tightly as possible. Therefore, both FCC and the HCP are based on a series of layers of spheres arranged in a hexagonal pattern, with each layer being offset and thus being stacked upon the other with a given phase. Importantly, FCC and HCP differ for the sequence of the phases in each layer of spheres: for instance, if we arbitrarily define one of these layers as L_I there will be only two possible arrangements (L_{II} and L_{III}) on the layer above L_I which sets all the spheres at the same distance from their neighbours (Jeffery et al., 2015). The maximum packing of spheres is then obtained by stacking layers following two rules (Figure 4-8B):

a) FCC = L_I-L_{II}-L_{III}-L_I-L_{II}-L_{III} -L_I-L_{II}-L_{III}; FCC = $(L_I\text{-}L_{II}\text{-}L_{III})_n$

b) HCP = L_I-L_{II}-L_I-L_{II} -L_I-L_{II}; HCP = $(L_I\text{-}L_{II})_{n;}$

Simply, the FCC and HCP packings differ for the existence of a "third" layer (L_{III}) being offset (different coordinates on the *x*-*y* plane) to the ones underneath, so that whereas the HCP only exhibits a sequence of two layers $(L_I\text{-}L_{II})_n$, the FCC has sequences of three layers $(L_I\text{-}L_{II}\text{-}L_{III})_n$. It seems that these two ways of placing the spheres in a volume are actually very similar; simply by taking into account a set of 13 spheres - i.e. one central field + 12 surrounding spheres - they differ for the position in only 3 spheres (Stella and Treves, 2015). However, given that an HCP cannot be simply described by three vectors (it is formed by two instead of three layers), mathematically it is not defined as a lattice even though it is packed as tightly as a FCC, which instead is a proper packing lattice. Therefore, the firing pattern recorded by grid cells in animals moving on a flat surface strongly resembles the hexagonal array known to be the optimal planar packing. However, while there is only one arrangement that represents space most accurately in 2D, two patterns are known to return the highest packing score: these are the HCP and the FCC, and as hypothesized by Mathis and colleagues (2015) both these structures are the most likely candidates for metric representation of volumetric space by grid cells in free flying bats.

It must be pointed out that this theoretical prediction, i.e. grid cells in 3D exhibit either a HCP or FCC pattern, relies on a model where grid cell firing emerges from an isotropic representation, meaning that the computation of odometry is computed with equal resolution along all possible directions of movements. Consistent with this view, place cells form isotropic fields (Yartsev and Ulanovsky, 2013), and HD cells in bats can be responsive to yaw (rotation along the horizontal plane), pitch (rotation along sagittal plane) as well as conjunctive yaw + pitch rotations (Finkelstein et al., 2015). Accordingly, it is fair to say that, in bats at least, thanks to an adapted head direction system providing information along all the allocentric directions in 3D, grid cells are very likely to receive spatial input detecting displacement in all directions with substantially equal resolution.

The study by Stella and Treves (2015) corroborates the hypothesis that both FCC and HCP could be valid firing patterns for grid cell activity in a volumetric space. Previous works by these authors suggested that the typical hexagonal grid pattern could emerge spontaneously over time as a result of an adaptation process involving synaptic plasticity (Kropff and Treves, 2008; Rowland et al., 2016). A version of this model was implemented and results showed that both HCP and FCC result in grid cell firing patterns that closer to the ones predicted by the model, with no apparent structure dominating the other (Stella and Treves, 2015). Moreover, additional evidence suggests that the FCC could indeed be the 3D pattern formed by grid cells in bats. Horiuchi and Moss (date) have implemented the grid cell CANM (McNaughton et al., 2006) with an additional fourth ring-integrator for movements along the z-axis (Horiuchi and Moss, 2015) and obtained an FCC lattice by grid cells in 3D. Therefore, given the convergence of the theoretical predictions provided by these studies (Horiuchi and Moss, 2015; Mathis et al., 2015; Stella and Treves, 2015), it is sensible to argue that grid cells in free flying bats are likely to exhibit a type of spatial firing which strongly resembles either the FCC or the HCP pattern. Time will tell which of the two predictions turns out to be correct.

4.4 Synthesis and conclusions

In the last paragraphs, the main studies addressing the neural representation of 3D space in rats and bats have been separately overviewed and compared, but a synthetic approach has not yet been provided. In this final paragraph, a general discussion of the overall findings from both groups will be attempted.

As previously pointed out, 3D experiments in rats are behaviourally challenging as they neither fly nor swim in deep waters. However, in the wild they dig underground

tunnels as well as climb onto trees. Therefore, it is reasonable to say that they move along the gravity vector too as they do not just move on horizontal planes. Addressing 3D spatial coding in rats has been possible by recording cells from animals moving onto a variety of non-horizontal planes (Hayman et al., 2011, 2015). Even though this approach did not fully answer the question, it still yielded important results. In contrast, bats naturally perform 3D movements as they fly during both light and darkness and also make use of echolocation to orient themselves. They also crawl onto horizontal or tilted surfaces so occasionally perform 2D navigation too. Therefore, a comparison of the findings from both animals can be attempted bearing in mind that one assumption has to be made, which is that the rat encoding along z-axis on the vertical plane would be quantitatively the same as if the animal could move in an ideal 3D space. Therefore, for a rigorous comparison between rats and bats, that assumption should be first verified: to do that, the ultimate experiment would be to assess spatial coding from rats moving on the lattice maze, a 3D lattice where rats have been already tested for behavioural experiments. For now, the following considerations can be made:

- It appears evident that, at least from a histological and physiological point of view, rats and bats share the same neural substrates of space. Indeed, place, head direction, grid and border cells have been found in the homologue brain areas of both groups – suggesting that perhaps those circuits are widely conserved across all mammals.
- One crucial difference between rat and bat spatial coding depends on the lack of theta rhythm (both at LFP and single cell level) in bats. Such findings argue against models linking oscillations to periodic firing of grid cells and poses several questions about the role of the theta oscillation itself in rodents. As stated before, this matter is beyond the purpose of this thesis and it will not be discussed further. However, the lack of theta itself can be simply mentioned as an important key difference in the physiology of the local circuit addressed.
- While the studies in crawling bats (Ulanovsky and Moss, 2007, 2011; Yartsev et al., 2011) essentially replicate the findings of the spatially modulated neurons in 2D in rats, the recordings of place and head direction cells in 3D substantially increased our understanding of navigation in volumetric space (Finkelstein et al., 2015; Yartsev and Ulanovsky, 2013). With respect to place cells, the anisotropic encoding by place cells on the pegboard (Hayman et al., 2011) seemed

inconsistent with the globular firing emitted by free-flying bats. However, several hypotheses were raised to explain the insensitivity for the vertical dimension and this thesis too aimed to investigate this matter.

- Similar considerations made for place cells apply for the head direction cell system. Indeed, data from bats revealed 3D head direction cells along with a sub-population of pitch- and roll-dependent neurons, sometimes showing conjunctive encoding as well (Finkelstein et al., 2015). It is likely that cells with similar responses are also found in rats' homologue brain areas. Therefore, future experimentation will help answering the question.
- What is the nature of 3D grid cell encoding? This question still remains unanswered given the lack of available data and only theoretical considerations can be made at this point. The findings so far collected on the pegboard suggest anisotropic encoding (Hayman et al., 2011) but no bat counterpart is currently known. The main goal of this thesis was to unveil grid cell encoding while rats climb on a vertical wall (see below), so the results presented here will be discussed later. However, as repetitively mentioned before, regardless of how grid cells look n the vertical plane, it is not guaranteed that it would also be the same during volumetric movements. Investigation of grid cells in in rats moving on the lattice maze as well as in free flying bats will answer several questions, for instance: is the grid cell system anisotropic or symmetric across dimensions? If the latter, is the 3D arrangement an array of "blobs" or a regular pattern? And if regular, is it a 3D optimal packing - as predicted by several computational models - or not? These and other questions regarding the function of theta oscillation and temporal encoding will be the object of the further studies to come.

In conclusion, a brief introduction to the available literature on the 3D representation of space in mammals has been provided here. In the next paragraphs the general goals of the present study are highlighted, along with the hypotheses formulated, the experiments designed to test them and predictions drawn.

4.5 Aims of the project

The specific question that this thesis aimed to answer was to reveal the nature of the firing pattern by place and grid cells when rats climbed on a vertical wall. The most influential work which originally motivated this study was the study by Hayman et al.,

(2011) where both place cells and grid cells showed a severe impairment in computing odometry along the vertical dimension. This result therefore showed that the representation of space is not symmetrical across dimensions, and that at least in rodents the representation of 3D space is not supported. In order to explain this result, the authors provided a number of valid and testable hypotheses. The work explored in this thesis conceptually follows the study from Hayman and colleagues (2011) and Taube and Shinder (2013). In the following sections these hypotheses will be reviewed together with a brief overview of the experiments that will be carried out.

4.5.1 Hypotheses

The results reported by Hayman et al., 2011 provided relevant insights for the building of a complex theoretical framework which will be briefly described here and followed throughout this section. Two main sets of hypotheses were formulated and are categorized as:

a) experience-dependent hypothesis, i.e. the representation of space changes depending on the familiarity/experience of rats' locomotion in 3D;

b) experience-independent hypotheses, which are here termed as:

i) anisotropic encoding hypothesis, i.e. intrinsic and irreversible lack of encoding along height;

ii) reference frame hypothesis, i.e. the locomotion plane orients the reference frame.

4.5.1.1 *Experience-dependent*

A sensible observation proposed in the study of Hayman and colleagues (2011) postulated that the limited amount of experience with 3D navigation given to rats housed in laboratory cages negatively biased the spatial encoding in vertical space. Consistently, the following hypothesis, termed experience-dependent, was formulated according to which the spatial representation is a function of the experience. In particular, as stated by Hayman et al., (2011) the authors could not rule out the possibility that the lack of vertical odometry on the pegboard was due to a general unfamiliarity with the vertical dimension, because rats normally used in laboratories are born in small cages and are always housed in environments with no chance of experiencing navigation in the vertical dimension. The hypothesis posits that due to the poor experience of vertical navigation, the capacity to measure vertical distances is dramatically reduced, causing the continuous stripes of firing

seen on the pegboard. In contrast, animals with extensive experience of 3D navigation can represent vertical space more accurately or the same as in the horizontal one.

4.5.1.2 *Anisotropic encoding*

The original hypothesis proposed by Hayman and colleagues (2011) was termed "anisotropic encoding" and it posits an intrinsic lack of encoding by place and grid cells for movements along the vertical dimension. In other words, the circuits underpinning spatial representation are insensitive to movements in the vertical plane, so no odometry along height is computed by place and grid cells. It follows that the spatial maps are therefore constitutively both planar (2D) and horizontally-referenced. Consistently, on the pegboard which is a 2D surface, the planar map is reduced to 1D as the vertical movements are not integrated and the reference frame is set along the horizontal earth-reference. Under these theoretical constraints, the vertical stripes of firing on the pegboard should be viewed as a vertical extension of multiple linear-track-like laps along the horizontal axis on the pegboard. One distinctive piece of evidence supporting this hypothesis is the consistency with the other result from Hayman and colleagues (2011) on the helical maze: grid and place cells seemed to intrinsically lack vertical encoding on this apparatus too so both results could be generalized into a single theoretical framework. However, it should be said that the helical maze displays major topological differences (it is 1D track) and the repetitive firing displayed across the coils could be instead due to visual cues.

4.5.1.3 *Reference frame*

As firstly mentioned by Hayman et al. (2011) and then pointed out by Taube and Shinder (2013) the columns of firing observed by grid cells on the pegboard could also be explained by a second hypothesis termed "reference frame". According to this second and equally valid view, in each given environment the navigational reference frame is set parallel to the locomotion plane, i.e. body orientation. During regular navigation in the horizontal plane, the body of the animal is parallel to the plane the animal moves on, so the reference frame and the locomotion plane coincide (Figure 4-9). In contrast, on the pegboard despite animals moving in both horizontal and vertical directions, the body orientation was mostly kept horizontal given the rats were moving across the protruding pegs. Therefore, according to this hypothesis, during navigation on the pegboard the reference frame was set to horizontal causing the emergence of the vertical stripes (Taube and Shinder, 2013).

To summarize, the three hypotheses mentioned above take into account either the intrinsic lack of encoding for movements in the vertical plane regardless of body orientation or experience (i.e. anisotropic encoding) or posit that the locomotion plane (i.e. reference frame) or experience (experience-dependent hypothesis) are key modulators of place and grid cells responses during vertical navigation. In the next paragraph the experiments designed for testing these hypotheses will be put forward.

4.5.2 Tests and predictions

In order to test the hypotheses previously mentioned (see above), two sets of experiments were conceived. The first set, termed "experienced pegboard experiment", were mostly designed to test the experience-dependent hypothesis (4.5.1.1). The second set, termed "floor-wall experiment" was designed to test the anisotropic encoding vs. reference frame hypotheses.

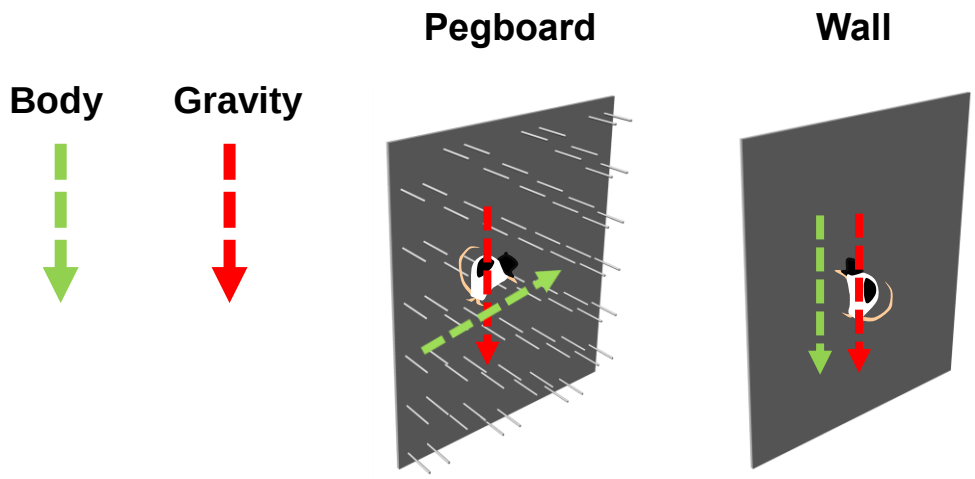

Figure 4-9 Body axis and gravity vector on the vertical plane

Schematic representation of the body axis (green arrow) and the gravity (red arrow) during locomotion on the pegboard and climbing wall. Note the two vector being orthogonal on the pegboard in contrast to the wall where they are parallel.

4.5.2.1 *The "experienced pegboard" experiment*

While reviewing all the hypotheses formulated explaining the lack of vertical encoding by place and grid cells, Hayman et al. (2011) proposed that the spatial representation might be function of experience. In particular, as stated by Hayman et al., (2011) the experience-dependent hypothesis posits that the lack of vertical odometry on

the pegboard could have been due to a general unfamiliarity with the vertical dimension given that tested rats were born and raised in flat small cages with no chance of navigation along the vertical dimension. In order to test this hypothesis, it would thus be necessary to record cells from different groups of animal, one raised in standard lab cages and one in a 3D enriched environment, and compare their respective firing patterns on the vertical plane. To test this hypothesis, animals were raised in two different environments:

1. standard laboratory cages where animals gain little experience of vertical locomotion (they will be termed naive animals throughout this thesis);
2. a large vertically-enriched environment (see Figure 5-1) where animals spontaneously developed efficient climbing skills and experienced vertical navigation (they will be called experienced animals throughout this thesis).

After electrode implantation, animals with grid cells would then be recorded while moving on the pegboard apparatus as in the study by Hayman and colleagues (2011). The experience-dependent hypothesis posits that animals raised in the 3D environment encode space differently from the ones raised in flat-horizontal cages. Therefore, a grid-like firing pattern by grid cells recorded from animals housed in the vertically enriched environment (i.e. experienced animals) is predicted by the experience-dependent hypothesis. In contrast, the vertical stripes reported by Hayman et al., (2011) is predicted to be displayed in the naïve animals.

In addition to replicate previous findings on the pegboard, one further experiment was conceived. In the study by Hayman et al., (2011), the pegs on the pegboard were placed in a manner such that it promoted mostly horizontal movements. To test whether the vertical stripes of firing displayed by grid cells could emerge also during non-horizontal movements, another arrangement of pegs on the pegboard which enhanced diagonal traversals across pegs was designed (5.2.2). Remarkably, this experiment was not designed to test the experience-dependent hypothesis but rather to test the anisotropic encoding hypothesis. Indeed, the anisotropic hypothesis only refers to the lack of vertical encoding along height, regardless of the behaviour displayed by the animal, therefore it predicts vertical column of firing similar to the ones obtained by Hayman et al., (2011). Any different result from the vertical stripes would be evidence against its validity.

4.5.2.2 *The ”floor-wall” experiment*

As previously described, the anisotropic encoding hypothesis posits the lack of encoding for movements along gravity in contrast to the reference frame hypothesis which posits that the orientation of the animal's body during navigation modulates place and grid cell firing.

According to the reference frame hypothesis, the locomotion plane of the animal sets the grid cell reference frame and that could explain the vertical stripes observed on the pegboard. Therefore, we needed an experiment that allowed us to tease apart the effect of gravity from body orientation on cell firing response. Therefore, an experiment where the activity of place and grid cells was recorded from animals climbing on the vertical plane was designed. Importantly, during climbing animals display the body orientation parallel to gravity rather than orthogonal as onto the pegboard. Therefore, the relationship between the locomotor and experimental plane stays the same on both the horizontal and vertical surfaces (unlike on the pegboard where the locomotor plane remained horizontal while the animal moved over the vertical surface). In order to rigorously compare the firing response by place cells and grid cells between horizontal and vertical navigation, an *ad hoc* experimental *apparatus* was built, made out of two perpendicular and same-size surfaces joined together at 90° where animals could move continuously between the horizontal and vertical plane (5.2.3) by running and climbing respectively. Under the constraints that the floor-wall experiment dictates, the anisotropic encoding and reference frame hypotheses yield two different and mutual predictions: the anisotropic hypothesis posits an impaired encoding of space along the vertical dimension regardless of the degree of experience or locomotion pattern used. Therefore, it predicts

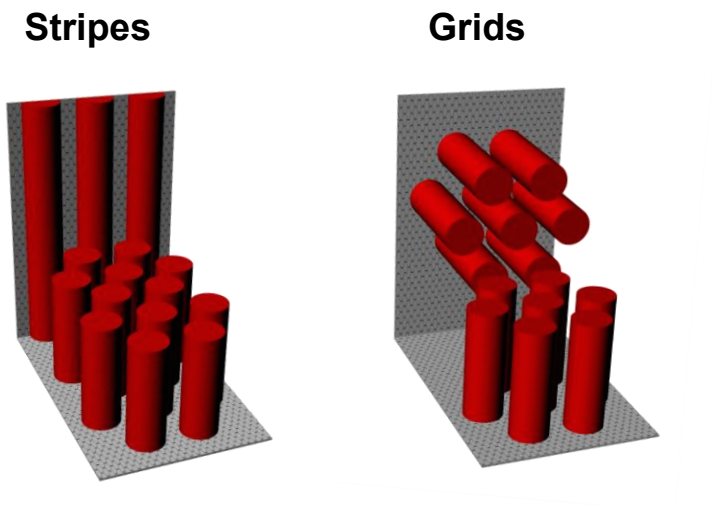

Figure 4-10 Theoretical predictions on the wall.

The anisotropic encoding and reference frame hypotheses predict two mutually exclusive results during climbing on the wall. While the former predicts vertical stripes on the wall, the reference frame hypothesis predicts grid-like firing on the wall similar to the horizontal plane.

the emergence of vertical stripes by place and grid cells from animals climbing on the wall with their body oriented along gravity (in other words the result predicted by the anisotropic hypothesis is the same as on the pegboard). In contrast, the reference frame hypothesis posits that when the animal climbs on the wall, the locomotor plane is relevant for orienting the reference frame parallel to the climbing wall. Therefore, the reference frame hypothesis predicts no major differences between horizontal and vertical maps for both place cells and grid cells and ultimately the emergence of rounded fields on the wall along with a hexagonal array (Figure 4-10). Accordingly, this hypothesis predicts a result opposite to the one reported by Hayman et al., (2011) given that no stripes should appear on the vertical wall.

Table 1 Summary of the tested hypotheses.

			Pegboard		**Wall**
			Configuration		
			Horizontal	*Diagonal*	
Experience-dependent	***Group***	*Naive*	Stripe	Stripe	Stripe
		Experienced	Grid	Grid	Grid
Anisotropic			Stripe	Stripe	Stripe
Reference frame			Stripe		Grid

In conclusion, a summary of the main scientific questions that this thesis aimed to answer was described and discussed together with the working hypotheses and predictions generated. In the following chapter the general materials along with the analyses used will be thoroughly described before reporting the results obtained following experimentation.

Part 2

Research project

5 Materials and methods

5.1 Subjects

Overall 37 male Lister Hooded rats provided by Charles-River, UK, have been used in this thesis. After one week of habituation in standard Perspex cages, cohorts of 4-10 animals from 2-5 weeks after weaning were then moved to the parrot cage set in a different room (5.1.2) representing the cohort of rats termed “experienced animals”. In contrast, only one animal (r621) was kept in standard Perspex cages throughout the whole experimentation and it represents the animal used to replicate findings on the pegboard which was then added to the cohort of animals termed “naïve animal” used in the Hayman et al., (2011) study. No power analysis to estimate the minimum number of observations (i.e. animals, cells etc.) was performed before conducting the experiments.

Throughout the entire time prior to surgery, animals were housed under a 12-hour light-darkness cycle at 21-23 degree Celsius with *ad libitum* access to food and water. One week after surgery animals were put on a food-restriction regime (90% of initial weight), and weighed and monitored daily. All the procedures were carried out according to the restrictions contained in the Animals (Scientific Procedures) Act of 1986 and licensed by the UK Home Office.

5.1.1 Experimental groups

Out of the overall number of 37 animals used in this study, 6 rats were implanted in the HPC and 31 in the MEC. Out of the 6 rats implanted in the HPC, 4 passed criteria for place cell detection (5.6.8) and were then used in the floor-wall experiment. Out of the

Table 2 Summary of the 15 rats implanted in the MEC included in this study.

				Rats Group	
				Naïve	**Experienced**
Experiment	**Experienced-pegboard**	Conditions	Horizontal	*R621*	*R654*
			Diagonal		*R604 R605*
	Floor-wall	Conditions	Large wall		*R617*

					R553 R563 R589 R604 R605 R631 R633 R634 R644 R647 R654 R655

31 rats implanted in the MEC, 15 passed criteria for either grid or speed cell detection and so were then used in the experienced-pegboard or floor-wall experiment (Table 2).

5.1.2 Parrot cage

A parrot cage was used to create the large vertically enriched environment needed to house animals in the experienced animals group. The parrot cage was a large cage (160 x 260 x 220 cm) designed for housing birds, whose surfaces such as walls and the roof on top were covered with chicken-wire mesh (see Figure 5-1). This was done in order to prevent

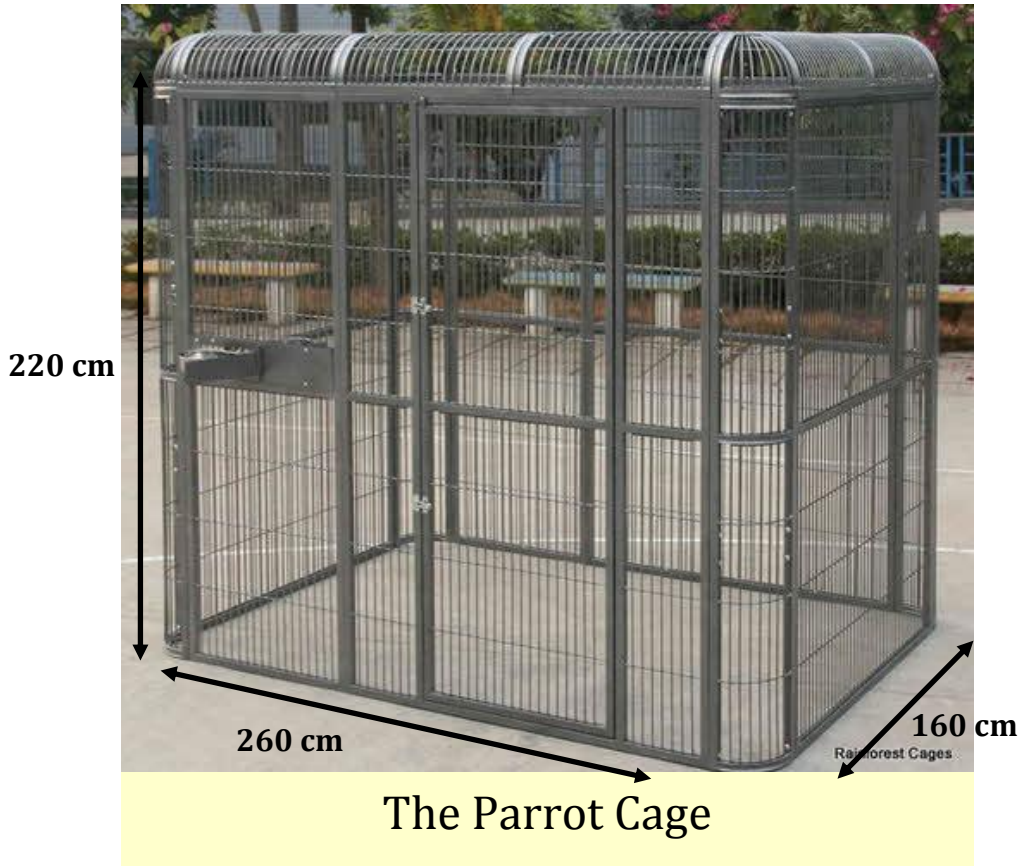

Figure 5-1 Photo of the parrot cage.

Animals from the cohort of rats termed "experienced animals" were raised in this large cage designed for housing birds. All the surfaces forming walls and ceiling were covered with chicken-wire mesh and the floor with sawdust sand. Additional objects, such as barriers, beams and ropes were placed into the cage in order to promote spontaneous exploration.

animals from escaping through the bars. During housing in the parrot cage, the animals were monitored daily but their behaviour was neither recorded nor quantified. During the first week of habituation steamed rice was scattered often (2-3 times a week) on to the walls of the cage in order to encourage climbing. The rats spontaneously developed efficient climbing skills and learned to reach the top of the walls – from two weeks after introduction to the cage, rice was only placed at the junction between the wall and roof of the cage. Putative differences in rat climbing skills, as well as the time spent climbing during housing in the parrot cage, was not quantified.

5.2 Experimental apparatus

In the present study, HPC and MEC i*n vivo* electrophysiological recordings were conducted in rats foraging in four different environments (open field, pegboard, floor-wall, large wall) which differed in size, colour, texture and orientation relative to the earth-horizontal reference. Recordings in the open field (5.2.1) were mostly used for screening purposes (see below) and were conducted for both the experienced dependent experiment (Chapter 6) and the floor-wall experiment (Chapter 7). In contrast, recordings on the pegboard apparatus (5.2.2) were used only for the experienced dependent experiment (Chapter 6), whilst those on the floor-wall apparatus (5.2.3) were used only for the floor-wall experiment (Chapter 7). A pilot study termed large-wall experiment (7.2.4) was also conducted on a large vertical surface termed “large wall”.

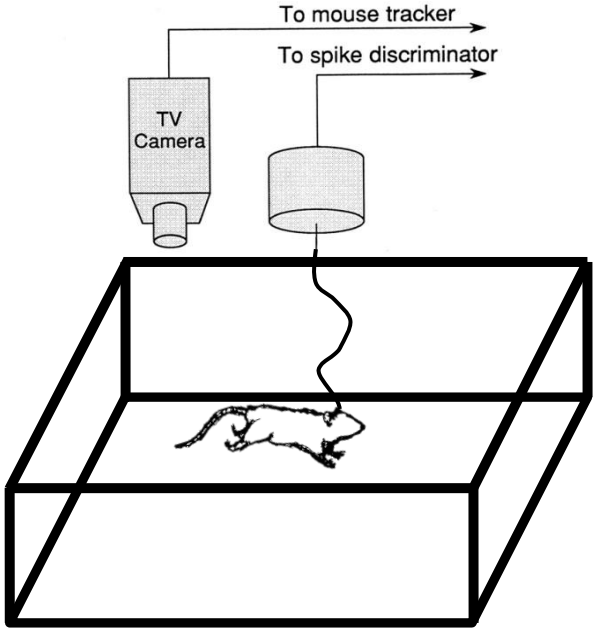

Figure 5.2 Schematic representation of the open field arena.

The open field box was used in this study to conduct screening recordings. It was made out of a 120 cm wooden surface surrounded by 80 cm high walls, painted in black and placed in the centre of the experimental room with no curtains.

5.2.1 Open field

The open field apparatus (Figure 5.2) was used for screening purpose and placed in the centre of one room with no surrounding curtains so that distal cues such as the desk, chair and shelves were visible from the rat’s perspective. The arena was made out of a 120 cm square piece of wood surrounded by walls (80 cm high) restraining the animal’s path. Both

the horizontal surface and the walls were painted black and a white cue card was placed on top of one wall as a polarizing cue.

5.2.2 Pegboard

The pegboard apparatus was made out of a single 120 x 120 cm square piece of wood, painted in white and attached onto one wall of the open field room dedicated for screening. On its surface, a number of rounded holes (1 cm diameter) were made where cylindrical wooden pegs (15 cm length) could be inserted (Figure 5-3A). In this thesis, two arrangements of the pegs have been used: a horizontal configuration and a diagonal configuration (Figure 5-3B-C). In the horizontal configuration, pairs of pegs were located at the same height of the pegboard alternated with other pairs at different heights (below and above them). This arrangement of the pegs was the one mostly used in the study by Hayman and colleagues (2011) and, thanks to the pairs of pegs being located at the same height, animals could then walk across them displaying horizontal movements (Figure 5-3B). In contrast, in the diagonal configuration, pegs were not arranged in horizontal pairs but in a diagonal fashion with an angle of 45° referenced to the horizontal axis (Figure 5-3C). Given that rats from one peg could not reach another peg at the same height, rats could not perform horizontal movements and instead performed mostly diagonal runs.

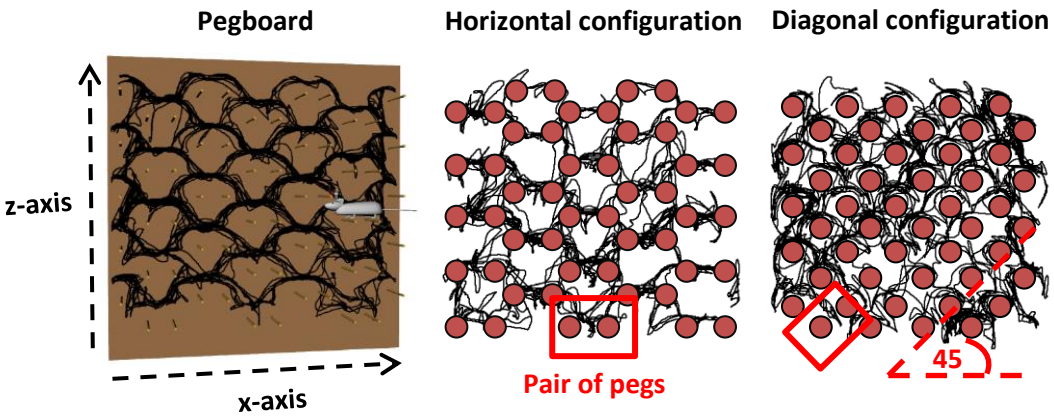

Figure 5-3 The pegboard apparatus.

Schematic representation of the pegboard apparatus and peg configurations used in this study. (**A**) The pegboard apparatus is a vertical wooden surface with embedded pegs allowing animals to walk across them. An example of path exhibited by animal (black line overlaid) on the horizontal configuration. (**B**) The arrangements of the pegs (brown circles) in the horizontal configuration along with the path of the animal (black line) is shown. Note the horizontal pair of pegs (highlighted in the red box) thanks to which animals could walk across and display horizontal movements. (**C**) In contrast, in the diagonal configuration, there were no longer horizontal pairs so animals had to perform diagonal movements (highlighted in the red box) rather than horizontal passes.

5.2.3 Floor-wall

The floor-wall apparatus was made out of two rectangular pieces of wood (120 x 80 cm), painted in black and joined together at a 90° angle forming a horizontal (floor) and vertical (wall) surface (Figure 5-4). On the wall, a number of thin beams were hung horizontally on which chicken-wire mesh identical to that used in the parrot cage was stapled. Due to the small gaps between the wall and the mesh rats could grip onto this

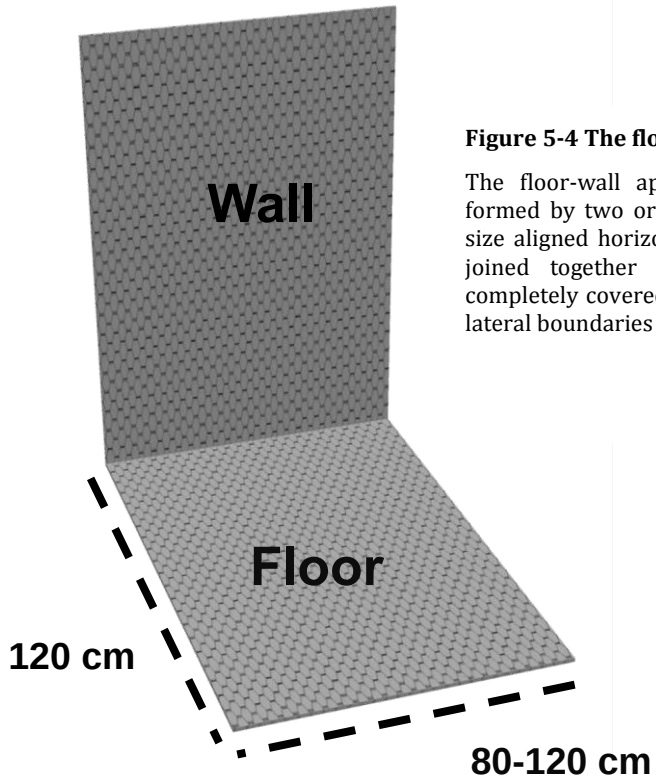

Figure 5-4 The floor-wall apparatus.

The floor-wall apparatus is an L-shaped construction formed by two orthogonal wooden surfaces of the same size aligned horizontally (floor) and vertically (wall) and joined together with 90° angle. Both planes were completely covered with chicken wire and surrounded by lateral boundaries (not shown).

apparatus relatively easily, and was effective for the experienced animals to climb on the wall. Moreover, additional wooden panels (80 cm high) were placed at the edges of both floor and wall boundaries in order to restrain the animal's path.

5.2.4 Large wall

Similar to the vertical surface of the floor-wall apparatus, the large wall apparatus consisted of a large square piece of wood (200 x 200 cm) that was on the wall of the experimental room and covered with the same chicken wire mesh used in the floor-wall apparatus (Figure 5-5). Different from the floor-wall apparatus, there was no horizontal counterpart but instead a narrow corridor (20 cm wide) at the bottom of the wall with lateral pieces of plastic sheets (30 cm high) to restrain the animal's path. At the lateral edges of the wall, two metal stripes were screwed in the wall of the room so that four small wooden platforms (5 × 10 cm) could be easily attached/detached by inserting the magnets

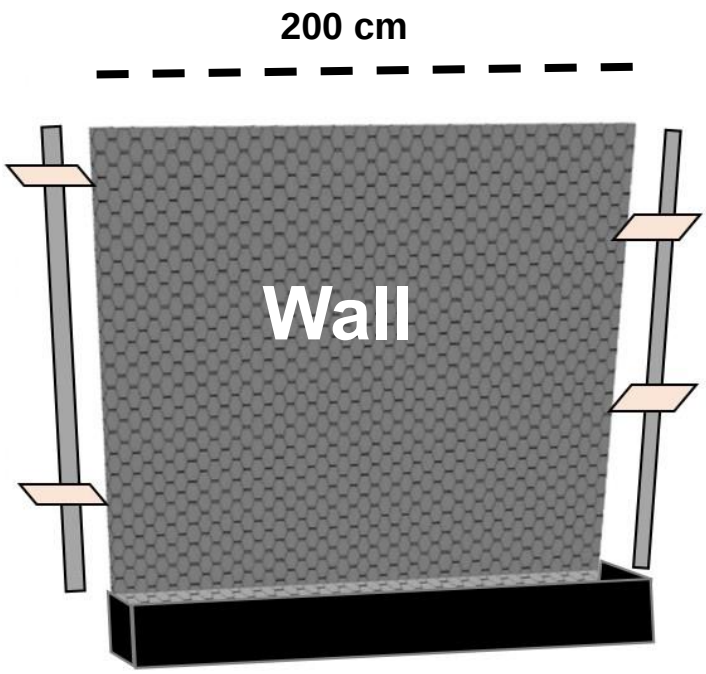

Figure 5-5 The large wall apparatus.

Schematic representation of the large wall apparatus.
The large wall apparatus is a large vertical square surface covered with chicken wire mesh similar to the one used for the floor-wall apparatus and. At the bottom of the wall there was a narrow corridor where the animal could rest in between climbing phases. At the edge of the wall moveable platforms were placed to encourage the animal to rest instead of reaching the bottom corridor.

onto two embedded metal brackets. This was done to encourage the animal to rest on the lateral platforms instead of moving downwards to the bottom of the wall so that a new climbing phase would begin. The position of the lateral platform was randomly changed during the recordings.

5.3 Surgical procedures

Overall 37 animals underwent surgical implantation: 6 animals were implanted in the left hippocampus and 31 animals in the left MEC. Throughout surgery, animals were kept under anaesthesia with isofluorane/O_2 (Abbott, UK). The anaesthetic induction took place in a chamber set in a separate room where animals were subsequently injected with pain killer (0.1ml/100 g/rat weight of 1/10 diluted Vetergesic® buprenorphine 0.3mg/ml, Alstoe UK) and then placed into a stereotaxic frame. For hippocampal implants, bregma was used as a reference landmark on the skull and the implant site determined by using the following coordinates: A.P. (antero-posterior) = 4.0 mm; M.L (medio-lateral) = 2.5 mm; D.V. (dorso-ventral) = 1.5 mm. In contrast, for MEC implants lambda was used as a reference landmark on the skull and the implant site determined by using the following coordinates:

A.P. = 1.2 mm; M.L. = 4.5 mm; D.V. = 1.5 mm, angle = 8-10°. The transverse sinus was used as a further landmark for A.P. tetrode implantation for MEC surgeries. Once the tetrodes were implanted in the targeted area, the microdrive was attached to the skull by spreading liquid dental cement (Simplex rapid, Associated Dental Products, LTD, UK) on the bone around 6 screws that had been previously inserted. Once dried out, the cement anchored the microdrive to the skull permanently, allowing stable recordings. All surgeries were carried out under sterile conditions and 7 days recovery was given to rats after surgery and prior to food restriction.

5.4 Single-unit electrophysiology *in vivo*

5.4.1 Electrodes and microdrive

17-25 µm (diameter) insulated platinum wires (California Fine Wire, CA, USA) were twisted together and manually cut, forming 4 strands of electrodes (tetrodes). This procedure optimized the separation of units (see 5.6.3.1). Sets of either 4 or 8 tetrodes were then inserted into the microdrive cannula (Axona Ltd, St. Albans, UK) connected to a moveable screw allowing tetrode advancements in steps of as little as 25 µm. Each strand of the tetrodes was then connected to the corresponding wires of the microdrive and covered with nail varnish for electrical insulation and to prevent mechanical damage. In order to lower and standardise the impedance of the tetrodes, electroplating in a platinum solution was carried out by using a NanoZ device (Neuralinx, USA) on the same day of the surgery (each channel was plated to 150kOhms impedance and measured for a 1kHz signal).

5.4.2 Extracellular recording

Rats were removed from the Perspex cage in the holding room and brought into the room for the recording (i.e. either screening room or floor-wall room). Here the microdrive implanted on the rat' head was connected to the multichannel recording equipment (Axona Ltd., St Albans, UK) by plugging the head-stage to 2-4m lightweight wires (Axona Ltd, St Albans, UK).

The neural signal (extracellular potential) recorded from the tips of the tetrodes was firstly passed through a RC-coupled, unity gain operational amplifier embedded on the head-stage device (Axona Ltd, St Albans, UK). Each channel was then amplified (8000-38000 times), bandpass filtered (500Hz to 7kHz) and referenced against another channel

belonging to a different tetrode. Before the recordings started, a user-defined voltage threshold was set for each channel - action potentials exceeding this value, along with the surrounding 1ms of signal, were saved for further analysis. Specifically, the waveform was sampled at a frequency of 50 kHz and for each recorded action potential the voltage was sampled 50 times and saved together with the corresponding timestamps (0.2ms pre-threshold and 0.8ms afterwards). Before setting the trigger, the activity on each channel was visualised via a single unit oscilloscope display and listened via an audio amplifier (Axona Ltd, St Albans, UK). That was done to ensure that during the recordings, only the actual spikes were captured and filtered from the electrical noise. This process was repeated once every day before the recordings in the open field commenced. Once the settings for each channel were saved, all the experimental recordings (across different *apparatus* or rooms) of the same day were conducted using the same settings. For each recording, at least one channel was set to record the EEG.

5.4.3 Tracking

The position of the animal's head was detected by using an infra-red camera tracking 1 or 2 LEDs placed on the head-stage device (Axona Ltd, St Albans, UK) at the sampling frequency of 50 Hz and *post-hoc* synchronized with the neural signal (5.6.1). This represents a standard method in the field and compared to video tracking it allows accurate position and works also in darkness.

The majority (42/44) of the recordings were conducted using a single LED necessitating that head direction be inferred from the translation of the animal between sampling points. A single LED was preferred over a double 'boom' (Axona Ltd, St Albans, UK), because the larger two LED arrangement was prone to being caught in the chicken-wire mesh.

For tracking the animal's position on the floor-wall apparatus it was necessary to record with two cameras placed opposite to both surfaces (i.e. on the ceiling to record the floor and on another wall to record the wall). To do that, a time base corrector (Datavideo, TBC 5000) was used. It was set to receive the tracking signal detected from the two cameras and produce a combined output signal at the same sampling rate with alternated tracking from the two cameras (floor, wall, floor, wall, etc.). In other words, the temporal resolution for each camera was lowered from 50 to 25 Hz (i.e. the time between two consecutive points on the same surfaces rises from 20 to 40 ms). A custom-coded MATLAB script interpolating the missing points on both surfaces allowed the generation of a

continuous tracking dataset in the floor-wall apparatus at the sampling rate of 50 Hz which could be synchronized with the neural signal as in the open field (5.6.1).

5.5 Histology

Once electrodes were assessed to no longer be recording from the region of interest, or when spatially-modulated cells hadn't been recorded for at least two weeks, rats were anaesthetized with isofluorane before an interperitoneal injection with a lethal dose of sodium pentobarbital (~1.5 ml). Animals were perfused with a transcardiac injection of saline (~300 ml) followed by the same amounts of 4 % paraformaldehyde after breathing had ceased. Perfused brains were removed from the animal and placed in 4 % paraformaldehyde solution for a minimum of three days at the temperature of 4°. Each brain was placed in 20 % sucrose solution for at least 24 hours prior to sectioning or until it was shown to sink in solution. This was done for the coupled purpose of removing water from the brain tissue via osmosis and cryoprotection of the brain.

Slicing of the brain was conducted using a freezing Leica microtome set at 40 µm thicknesses either sagitally (MEC implanted rats) or coronally (HPC implanted rats). Brain slices were then wet-mounted onto superfrost plus slides (Thermo Scientific) and left to dehydrate for at least 2 days. Once dried out, a staining procedure was conducted in either Cresyl Violet or Thionin solution. After staining, slides were left in histoclear solution for 10-20 minutes before cover slides were secured over the slices using DPX mountant (Sigma-Altrich) and left to dehydrate for at least 24 hours. The slides were then examined under an Olympus microscope with an Xli digital camera (XL Imaging Ltd, Germany) so that the electrode tracks within the brain could be determined.

5.6 Analysis

In the following paragraphs, the description of all analyses used in this study will be provided. All the analyses regarding the behaviour of the animal (5.6.1), LFP theta (5.6.2) and single unit activity (5.6.3) were conducted in Matlab 2015a (Mathworks, Natwick, NA, USA).

5.6.1 Behaviour

5.6.1.1 *Position*

The LEDs mounted on the head-stage device allowed the position (raw data) of the

animal's head to be detected due to an infra-red camera (sampling rate was 50 Hz) placed opposite to the surface that the animal was moving on (see 5.4.3). The raw data in pixels was firstly converted into cm and then processed by using a 400ms boxcar smoothing factor which generated the smoothed position used for the all further analyses.

5.6.1.2 *Speed*

The instantaneous speed of the animal was calculated as the derivative of the position data and converted in cm/s. Data points with speeds higher than 100 cm/s were rejected as false data points.

5.6.1.3 *Direction*

For the majority of the recordings a single LED, as opposed to two, was mounted on the head-stage device (see 5.4.3). This was done to prevent the head-stage device from getting entangled in the chicken-wire mesh covering the wall during climbing in the floor-wall experiment. Therefore, the instantaneous direction was determined as the heading or displacement direction (i.e. angle which defines the direction of the movement between two contiguous data points) and calculated as follows:

$$dx_t = x_{t+1} - x_t$$
$$dy_t = y_{t+1} - y_t$$

where *dx* and *dy* are the derivative for the *xy* coordinates for each time sample *t*.

The instantaneous heading direction θ_t was obtained as follows:

$$\theta_t = arctan\left(\frac{dx_t}{dy_t}\right)$$

with θ_t subtracted to one arbitrary x-axis aligned to the edge of the apparatus as reference.

5.6.1.4 *iHeading differences on the pegboard*

In order to detect putative differences in the heading direction of animals while moving on the horizontal and diagonal configuration of the pegboard, the following analysis was conducted. For each session, the dwell time across directional bins (bin size =

6°) was first computed and then normalized by dividing the dwell time in each bin by the overall time of the session.

A directional autocorrelation was then conducted as follows:

$$r(\tau_\theta) = \frac{n\Sigma\lambda(\theta)\lambda(\theta-\tau_\theta) - \Sigma\lambda(\theta)\lambda(\theta-\tau_\theta)}{\sqrt{n\,\Sigma\lambda(\theta)^2 - (\Sigma\lambda(\theta))^2}\sqrt{n\Sigma\lambda(\theta-\tau_\theta)^2 - (\Sigma\lambda(\theta-\tau_\theta))^2}}$$

where $r(\tau_\theta)$ is the correlation coefficient between those bins with directional offset (τ_θ), $\lambda(\theta)$ is the normalized dwell time in the heading bin defined by angle θ, and n is the total number of heading bins. In other words, the heading dwell map is copied and correlated with itself a number of times in a loop after increasing the θ angle. Due to the periodic nature of the heading behaviour on the pegboard, the heading autocorrelogram displayed peaks of high-correlation and troughs of low correlations (Figure 5-6).

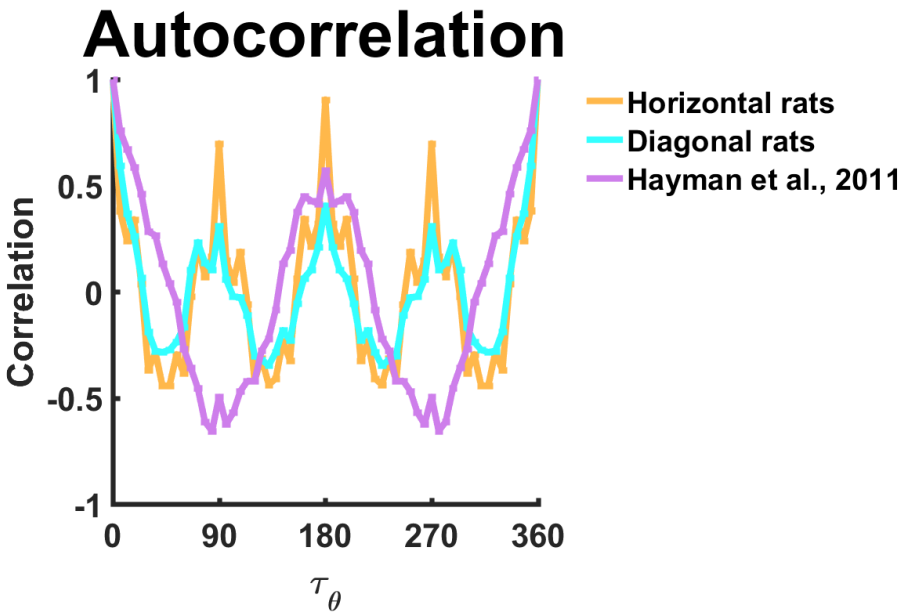

Figure 5-6 Directional autocorrelation on the pegboard

Example of heading autocorrelation of a single session across the three groups of rats. Note the different number of peaks between the horizontal configuration (4 peaks, orange and purple lines) compared to the diagonal configuration (2 peaks, turquoise line).

To quantify whether animals mostly showed a diagonal or horizontal heading bias, for each session a diagonal score and horizontal score was obtained as follows: the diagonal score was determined as the mean auto-correlation at 90° and 180° and

subtracted to the mean auto-correlation at 45° and 135°. The horizontal score was determined as the mean auto-correlation at 180° subtracted to the mean auto-correlation at 90°.

5.6.2 LFP Theta

5.6.2.1 ***Spectral analysis***

Power spectrum analysis of the LFP theta was conducted following methods described in Hayman et al., (2015) and Jeewajee et al., (2008b). Briefly, for each surface the LFP sequence was zero-padded to the next highest power of 2. The power density was obtained using fast Fourier transform and smoothed with a Gaussian kernel (standard deviation = 0.375 Hz).

5.6.2.1.1 Power spectrum

The power of theta frequency was determined as the peak in the power density in the theta band (7-11 Hz; Figure 3-1B for representative example of power spectrum analysis).

5.6.2.1.2 Mean theta frequency

The mean theta frequency was determined as the frequency showing the peak of the power density in the theta band (7-11 Hz; Figure 3-1B for representative example of power spectrum analysis).

5.6.2.1.3 The strength of the theta

The strength of the theta modulation was quantified as the signal to noise ratio between the power spectra $\pm$ 1 Hz from the theta frequency and the mean power of the whole spectrum between 1 and 125 Hz.

5.6.2.2 ***Theta frequency modulation by running speed***

As shown by a number of studies before (Jeewajee et al., 2008b; Wells et al., 2013), the linear relationship between running speed and theta frequency was explored by the following methods used in Hayman et al. (2015).

5.6.2.2.1 Theta filtering

First, the recorded LFP traces were analysed by applying a band-pass filter (0.34-125 Hz) and sampled at 250 Hz. Next, the LFP signal was processed by using a 251-tap Blackman windowed band-pass *sinc* (sine cardinal) filter in the theta range (7-11 Hz). Then, the analytic signal was obtained by applying a Hilbert transform and the instantaneous theta frequency (sampling rate 250 Hz) calculated as the difference in phase between consecutive points (Figure 3-1A for representative example of the LFP raw data and filtered data after Hilbert transformation).

5.6.2.2.2 Speed-theta frequency relationship

The linear relationship between speed and theta frequency was determined for each session across all surfaces. In order to compare the frequency of theta oscillation to the animal's running speed, theta frequency sampled at 250 Hz was down-sampled to 50 Hz by averaging over 5 consecutive values. The instantaneous speed and filtered theta frequency could then be correlated at 50 Hz and the nature of the speed-frequency relationship quantified. This was done for each session of each experiment (open field, pegboard, large wall) and replicated for the floor and wall data in the floor-wall experiment.

Firstly, the speed data was binned into 2 cm/s bin within the 2-20 cm/s speed range and the frequencies averaged for each bin, so that the *r* Pearson's correlation coefficient between speed bins and corresponding average frequency was determined along with the corresponding *p* value. To statistically compare the results of the *r* Pearson's correlation coefficients between surfaces, they were transformed into the *z* correlation values by using the Fisher transformation (Hayman et al., 2015; Jacob et al., 2014) which was calculated as follows:

$$z = \frac{1}{2} \ln \frac{(1+r)}{(1-r)}$$

In order to investigate the nature of the relationship, a regression line was then fitted to the data. For each recording session (and each surface in the floor-wall experiment), two values were then determined: (a) the intercept of the regression line, defined as the LFP theta frequency at speed = 0 cm/s; (b) the slope of the regression line, defined as the gradient of the speed-theta linear relationship (Figure 3-1C).

5.6.3 Single-unit

Following the recordings, the single unit activity of all the neurons recorded from a single tetrode was displayed offline using Tint, a custom-built cluster-cutting programme

provided by Axona Ltd., (St Albans, UK). All the recorded spikes were firstly plotted as a "cluster space" representing the peak-to-peak amplitude of each spike on one channel against the amplitude of the same spike on the other channels (Figure 5-7A).

5.6.3.1 *Spike sorting*

The spatial firing of the single cells was examined (see 5.6.4) after first isolating the spikes emitted by each neuron (i.e. spike sorting), this was done using the cluster-cutting software Tint (Axona, Ltd, St Albans, UK). Briefly, the recorded action potentials were automatically sorted to different neurons (clusters) using KlustaKwik (Kadir et al., 2014). This method employs an expectation-maximisation approach to identify spikes discharged by different neurons recorded on a single tetrode (Figure 5-7B). Specifically relying on the differences in voltage observed, for each action potential, on the four channels that

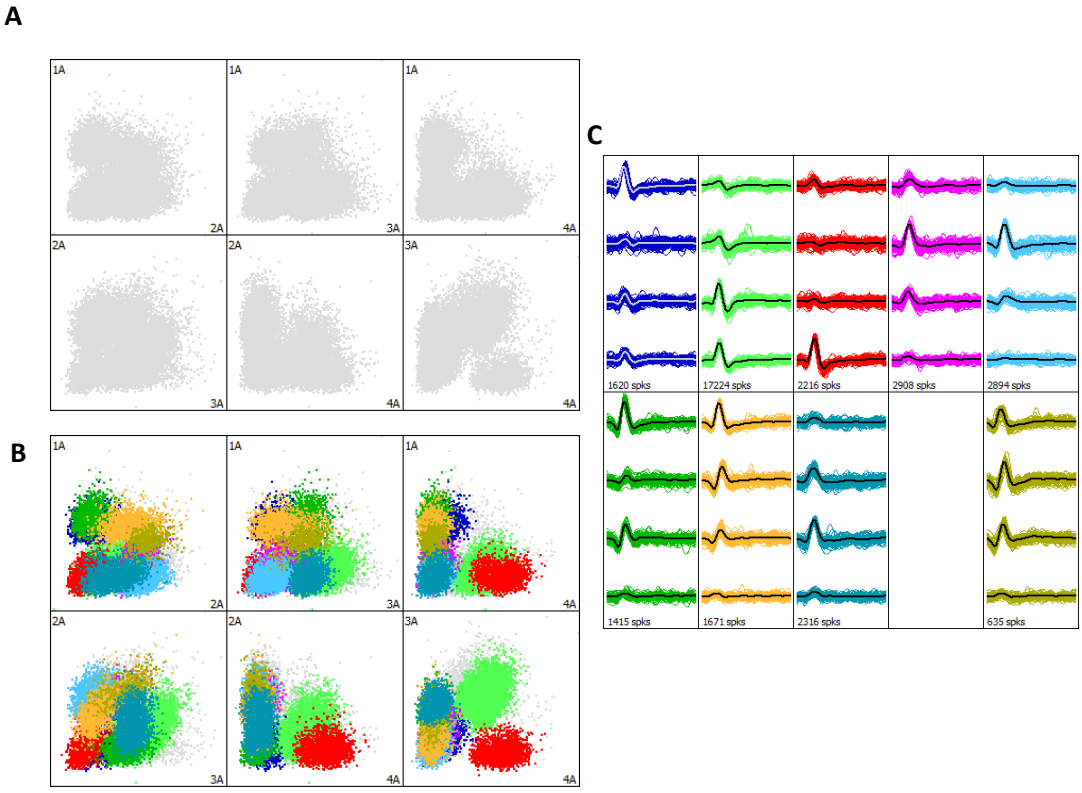

Figure 5-7 Spike-sorting procedure.

Representative example of the spike sorting procedure showing all the action potentials recorded from a single tetrode and plotted in the "cluster space".
A). For each tetrode 6 scatter plots were generated representing the peak-to-trough amplitude of the action potentials across pairs of channels (e.g. 1A vs 2A indicates channel 1 vs. channel 2). The spikes were then assigned to different clusters by using KlustaKwik (Kadir et al., 2014).
B) Similar to **A**, the same 6 scatter plots now represent the isolated clusters (n=9) following KlustaKwik procedure (Kadir et al., 2014). The spikes plotted with the same colour represent action potentials assigned to the same cluster.
C) The waveforms of the corresponding colour-coded 9 clusters identified in **B** are plotted across the channels of the same tetrode. Note the differences across clusters with respect to the shape and size of the corresponding waveforms.

comprise each tetrode – these in turn being approximately proportional to the distance between the tetrode tip and neuron (Figure 5-7C).

The results from the KlustaKwik (Kadir et al., 2014) algorithm tended to "overcut" cells (i.e. for a single cell several clusters were identified as different cells). Therefore, for each pre-identified cluster, additional checking was conducted. Two clusters were merged into a single one if they were overlapping in the cluster space, displayed similar waveforms across 4 channels, and showed no spiking in the 0-5ms window of the temporal cross-correlogram. The rationale for the latter criteria being that the temporal auto-correlation of a single cell shows no spiking in the 0-5ms window due to the refractory period of the cell.

The spike-sorting of the recorded spikes was done for each session across the three surfaces. Using the position of the clusters in the cluster space, as well as the waveform across the 4 channels, clusters were labelled as the same neurons and so they could be compared across surfaces.

5.6.4 Spatial analysis

In the following paragraphs, the description of the spatial analyses is provided.

5.6.4.1 *Rate map*

To reveal the spatial activity, for each cell the spatial rate map was produced by creating a 2 x 2 cm spatial bins matrix containing in each bin the average firing rate calculated by dividing the number of recorded spikes by the cumulative dwell time (Figure 5-8A). Additional smoothing was implemented by using 5 bins square boxcar smoothing (Figure 5-8B) in order to detect place fields (Figure 5-8C; see 5.6.5.1).

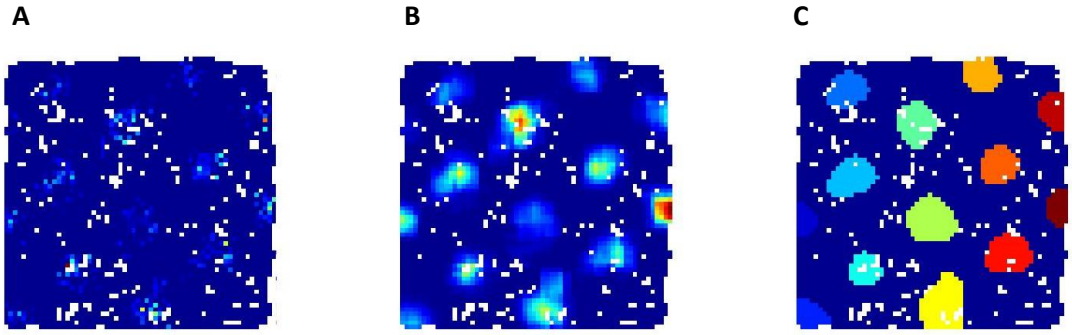

Figure 5-8 Rate map and field detection.

The spatial modulation of a place or grid cell can be revealed with a rate map. **A**) The unsmoothed rate map of a grid cell, obtained by diving the number of spikes in each spatial bin by the dwell, time is shown. **B**) Smoothed rate map (5 bins boxcar) highlighting spatial firing and regular grid displayed by a sngle grid cell. **C**) Firing fields detected from the smoothed rate map by using a "local-maxima"

5.6.4.2 *Spatial information*

As proposed by Skaggs et al., (1993) the extent to which place cell firing predicts location can be calculated as follows:

$$I(R|X) \approx \sum_i p(x_i)\ f(x_i)\ log_2\left(\frac{f(x_i)}{F}\right)$$

where $p(x_i)$ and $f(x_i)$ correspond to, respectively, the probability of the animal being in location (spatial bin) x_i and the firing rate of cell in location x_i. *F* is the overall firing rate. $I(R|X)$ corresponds to the amount of spatial information between firing rate *R* and location *X.* The spatial information in bits/spike was calculated by dividing the $I(R|X)$ by *F*(Skaggs et al., 1993) .

5.6.4.1 *Spatial coverage*

The spatial coverage was used as an estimate of the spatial firing extent of cells and was quantified as the number of the bins with a firing rate greater than 20% of the peak firing rate, divided by the total number of bins of the rate map.11

5.6.4.2 *Spatial autocorrelogram*

To quantify the regularity, scale (distance between surrounding fields) and orientation of the grid cell firing pattern, the spatial rate map of each cell was used to generate a spatial autocorrelogram (Hafting et al., 2005) which was obtained as follows:

$$r(\tau_x, \tau_y) = \frac{n\Sigma\lambda(x,y)\lambda(x-\tau_x, y-\tau_y) - \Sigma\lambda(x,y)\lambda(x-\tau_x, y-\tau_y)}{\sqrt{n\,\Sigma\lambda(x,y)^2 - (\Sigma\lambda(x,y))^2}\sqrt{n\Sigma\lambda(x-\tau_x, y-\tau_y)^2 - (\Sigma\lambda(x-\tau_x, y-\tau_y))^2}}$$

where $r(\tau_x, \tau_y)$ is the correlation coefficient between those bins with spatial offset τ_x and τ_y, $\lambda(x,y)$ is the firing rate in the spatial bin defined by coordinate x and y, and n is the total number of spatial bins. In other words, the smoothed rate map of a cell is copied and correlated with the original map a number of times in a loop after increasing the shift (τ_x, τ_y) each time along x and y (see Figure 5-9 for the generation of the autocorrelogram). Due to the periodic nature of their firing pattern, the spatial autocorrelogram of a grid cell displays a number of equidistant peaks (red circles in Figure

5-9) forming a hexagonal grid.

5.6.4.2.1 Grid score

Gridness (or grid score) a measure of the six-fold symmetry present in the spatial autocorrelogram, was calculated as follows. The region encompassing the 6 peaks closest to the origin of the spatial autocorrelogram was rotated in 30° steps – and the correlation between the rotated and un-rotated data found. Gridness was then defined as the highest correlation at rotations at 30°, 90° and 150° and subtracted from the lowest correlation at 60° and 120° (Figure 5-9). Following (Sargolini et al., 2006) grid scale was defined as the median distance from the central peak of the spatial autocorrelogram to the six closest peaks (Figure 5-9). Similar grid orientation was defined as the angle between the horizontal *x*-axis and the line joining the centre of the autocorrelogram and the closest peak anticlockwise from the reference line.

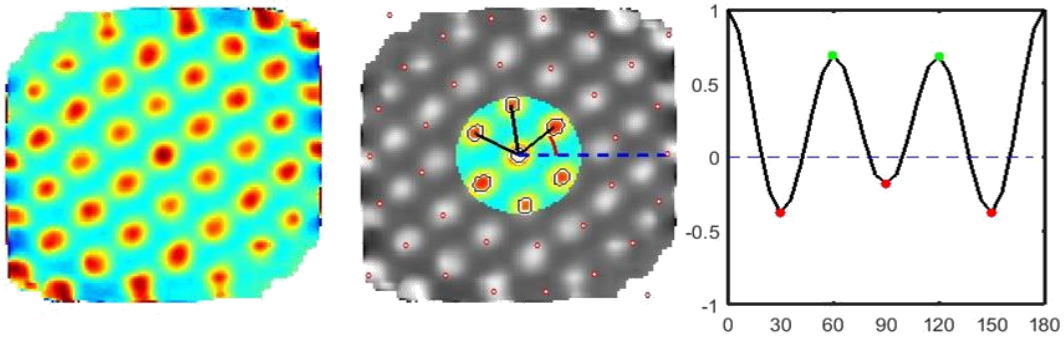

Figure 5-9 Spatial autocorrelogram and grid score.

The spatial autocorrelogram (left) is an analytical tool which allows to reveal the periodicity of the spatial firing pattern of grid cells. Based on the spatial autocorrelogram it is possible to determine a number of characteristics features of the grid (middle) such as the scale measured as the median distance between the three nearest peaks from the center (black lines), and orientation of the grid (angle in red between first peak grid from the x-axis as reference represented in dashed blue line). The grid score is determined as the lowest peak correlation at 60° and 120° (green dots) minus the highest peak at 30°, 90° and 150° (red dots).

5.6.4.2.2 Stripe score

A quantitative measure of the "stripeness" of grid firing on the pegboard was necessary to compare grid representations of experienced vs. naïve animals. Due to the lack of periodicity along the vertical dimension on the pegboard, the spatial autocorrelogram of the stripes returned stripes of high positive correlation values spanning almost the entire height of the autocorrelation map in contrast to the typical six peaks of a grid cell on the horizontal plane (Figure 5-10). Therefore, an index of the vertical vs. horizontal repetition was calculated as the ratio between the number of bins with a

correlation value higher than 0.2 (see also Figure 5-10) of the middle column (vertical axis) and the central row (horizontal axis).

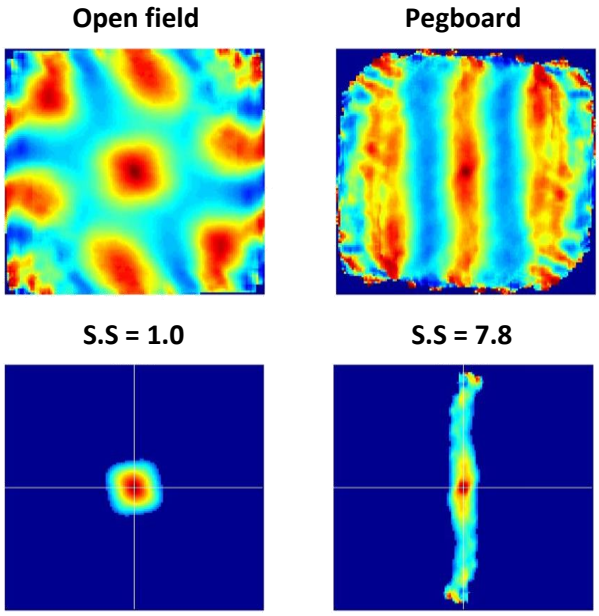

Figure 5-10 Stripe score between horizontal and pegboard.

The spatial autocorrelogram of a grid cell in the open field (left) reveals the typical six-fold symmetry pattern on horizontal plane in contrast to the vertical stripes on the pegboard (right). For rounded fields the stripe score is approximately 1, in contrast to high values of "stripeness" on the pegboard.

5.6.4.3 *Grid field metrics*

In order to describe grid field spatial metrics, the properties of the central field of the spatial autocorrelogram (correlation value higher than 0.2) were examined using the inbuilt Matlab (Mathworks, Natwick, NA, USA) function *regionpropos*. The field size was determined as the number of spatial bins forming the central field and then converted into cm^2. The length of the major and minor axis of the grid field was determined as the major and minor axis of the ellipse fitted onto the central place field and converted into cm. The orientation was determined as the angle between the major axis of the grid field and an arbitrary referenced *x*-axis set parallel to one of the boundaries of the environment. The shape of the grid field was determined as the aspect ratio of its axes (major/minor).

5.6.5 Place field analyses

The analyses on grid cells place fields have been conducted by applying a local-maxima approach as described in Hayman et al., (2015).

5.6.5.1 *Place field detection*

The peaks in the rate map were firstly detected by identifying all local maxima in the rate map (Figure 5-8B). Next, for each peak, the putative place field around it was

determined by including those bins with a firing rate higher than a threshold defined as 30% of each peak's firing rate (Figure 5-8). Finally, only those fields with size greater than 60 cm^2 (see below), peak firing rate greater than 1Hz, and a minimum number of spikes emitted in them (2% of the overall session), were included in the analyses.

5.6.5.2 *Place field characteristics*

Similar to the grid spatial metrics (5.6.4.3), the geometrical properties of place fields were addressed using the *regionprops* inbuilt function in Matlab (Mathworks, Natwick, NA, USA). The field size was computed simply by converting in cm^2 t11he number of bins (bin size = 2cm) forming each place field. The major axis of the field was determined as the length of the major axis of the ellipse fitted on the place field map and the minor axis simply the length of the orthogonal axis. The orientation of the field was determined as the angle between the major axis and a fixed arbitrary *x*-axis which was set to be parallel to one of the boundaries of the environment where the cell was recorded. Finally, to characterize the shape of the place field, the aspect ratio was simply determined as the ratio of its axes (major/minor).

5.6.6 Speed analyses

The speed modulation of each cell was addressed following two methods referred to as the "speed score" and the "speed line score".

5.6.6.1 *Speed score*

Firstly, the instantaneous firing rate of the cell across the entire session was obtained by creating a histogram of the spikes that occurred using the same sampling rate as the tracking camera (50 Hz) and then smoothed using a 260ms wide Gaussian smoothing curve. The speed score of the cell was then obtained simply by computing the Pearson correlation coefficient between the instantaneous speed of the animal and instantaneous firing rate of the cell. In order to compare the speed score across surfaces, the speed score was then transformed in the z-fisher coefficient (5.6.2.2).

5.6.6.2 *Speed line score*

In addition, the speed modulation of the cell was also quantified by examining the mean firing rate of the cell across 2 cm/s wide bins in the 2-20 cm/s range (Figure 5-11). Similar to the speed-theta correlation, the Pearson correlation coefficient between speed

bins and the mean firing rate was obtained (i.e. the speed line score) and a regression line fitted to obtain the slope and intercept of the speed line. Similar to the speed score (see above), the speed line score was then transformed in the z-fisher coefficient in order to compare across surfaces.

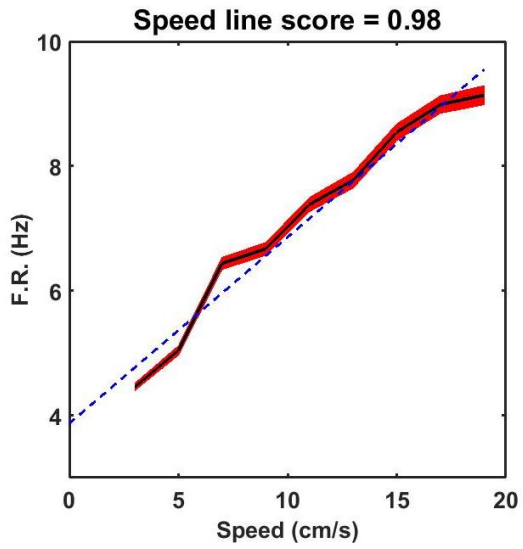

Figure 5-11 Speed line score.

An example of speed cell showing linear increase in the average firing rate (black line) ± standard error (red area) across speed.
The speed line score is computed as the Pearson correlation value between the speed bins (2 cm/s) and mean firing rate. The speed line allows to fit the regression line (blue dashed line) which also computes the intercept (3.8 Hz) and slope (0.3 Hz/cm/s).

5.6.7 Temporal analysis

In the following paragraphs, the methods addressing the spike-train rhythmicity will be provided.

5.6.7.1 *Intrinsic firing frequency*

The cell oscillatory spiking pattern was addressed by examining the spike-train during "runs" where instantaneous speed was higher than 2 cm/s for at least 0.5s (Jeewajee et al., 2008a). The intrinsic firing frequency of the cells was obtained by examining the power spectrum of the spike-train averaged temporal autocorrelogram. This was computed using "unbiased" normalization by the number of bins (bin width = 2 ms) and then averaging the autocorrelogram for each run after weighting by the length of the run (Jeewajee et al., 2008a). Secondly, it was truncated in the 0-500 ms temporal window and zero-padded to 2^{16} elements. The power density was then computed in the 0-125 Hz frequency range and smoothed using Gaussian kernel (sigma = 0.2 Hz).

The intrinsic firing frequency was determined as that frequency in the theta range (7-11 Hz) with the highest peak power (Figure 5-12). To quantify the strength of the theta modulation, a signal to noise ratio was determined as the mean power in the range of $\pm$ 1 Hz of the intrinsic frequency divided the mean power in the 0-125 Hz range. The signal to

noise ratio = 5 was set as cut-off threshold for a cell to be theta modulated (Wills et al., 2012).

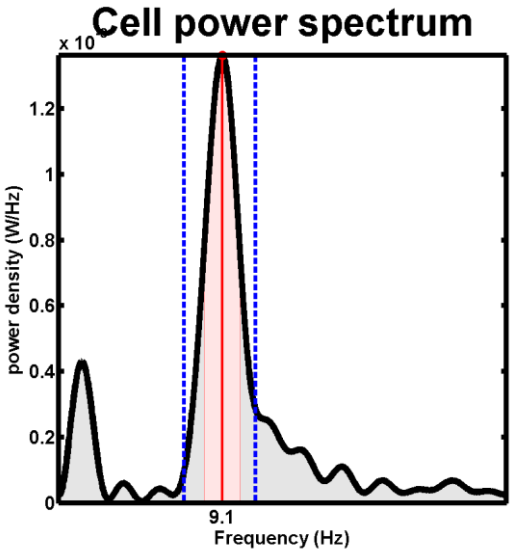

Figure 5-12 Spectral analysis of spike-train.

Power density analysis revealing putative oscillatory pattern. Black line represents power density (y-axis) across frequency (x-axis) in the 0-25 Hz range. The estimated intrinsic firing frequency was determined as the frequency (9.1 Hz) where power showed maximum peak (red line) in the theta range (7-11 Hz, blue dashed lines).

5.6.8 Cell categorization

In order to identify putative spatial cells from the whole ensemble of neurons (*n* = 1645), each recorded cell underwent spike-train random shift shuffling procedure to derive chance-level criteria in each surface (floor, wall and open field).

5.6.8.1 *Shuffling procedure*

Briefly, for each shuffle (*n* shuffles = 400), the spike-train was shifted forward by a random time interval (number between 30 seconds and the length of the entire session minus 30 seconds) and then wrapped around so that for each iteration the shuffled spike-train had the same number of spikes but not in register with the animal behaviour. For each iteration, all the spatial analysis described previously were carried and the grid score, speed score, speed tuning score and spatial modulation score determined. Finally, all the scores obtained from the shuffling procedure for each surface (floor, wall and open field) and analysis (grid score, speed score, speed line score and directional score) were pooled together and the cut-off significance threshold identified as 99 percentile derived from the shuffled distribution. The spatial scores used for cell detection were derived from shuffling procedure in addition to a number of criteria based on minimum firing rate.

5.6.8.2 *Cell criteria*

5.6.8.2.1 Place cells

The criteria used to identify place cells were adopted from the study of Grieves and colleagues (2016) where in order to be classified as place cell, a cell had to satisfy all the following criteria on at least one of the experimental surfaces (Grieves et al., 2016) :

1. mean firing rate greater than 0.5 Hz and less than 5 Hz;
2. peak firing rate greater than 1 Hz;
3. Skaggs spatial information greater than 0.5.
4. At least one place field detected.

5.6.8.2.2 Grid cells

A cell was classified as a grid cell once it satisfied all the following criteria on at least one of the experimental surfaces:

1. mean firing rate greater than 0.5 Hz and less than 5 Hz;
2. peak firing rate greater than 1 Hz.

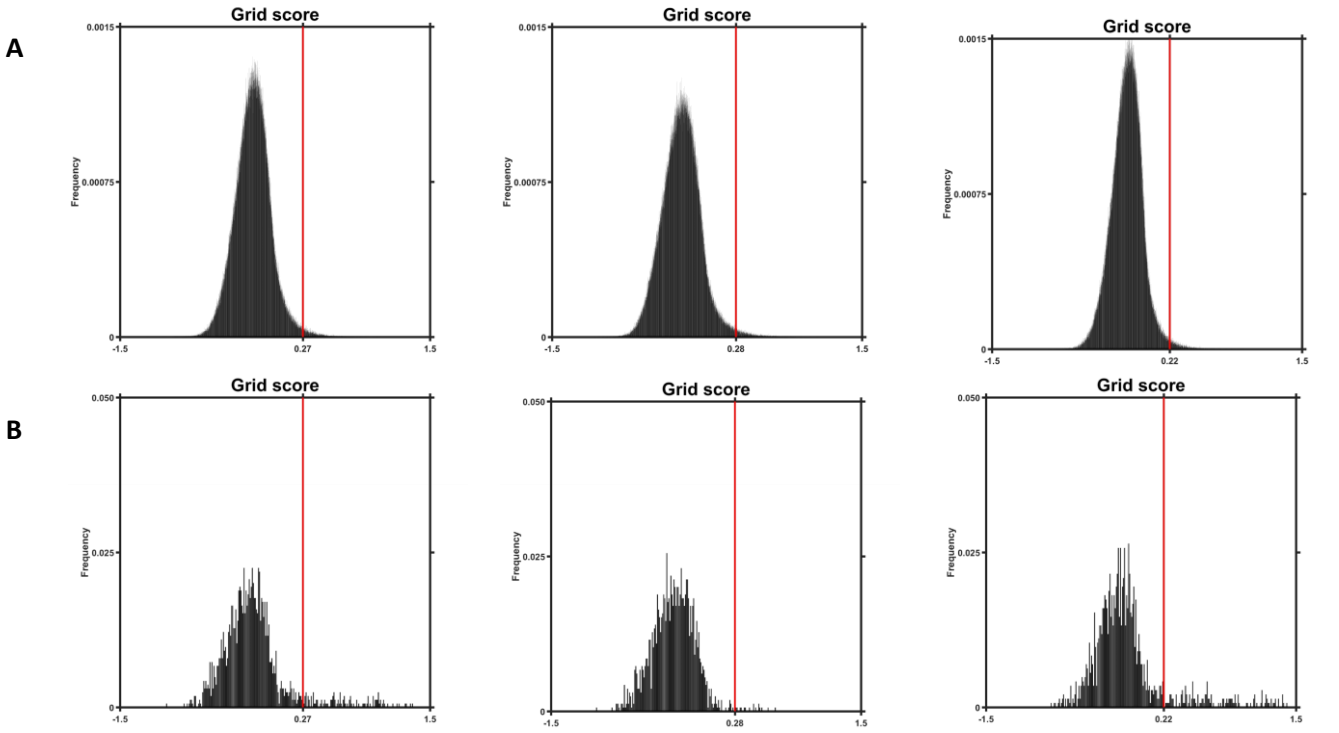

Figure 5-13 Shuffled and observed grid score distributions.

Results of grid score shuffling procedure across surfaces (floor = left, wall = centre, open field = right). (**A**) For each shuffle (n= 400) the grid score was calculated and pooled across cells returning a Gaussian distribution (top row) representing the grid score null distribution for each surface. The 99 percentile of the shuffled distribution was used to determine the grid score significant thresholds on each surface (red lines) which was 0.27 on the floor, 0.28 on the wall and 0.22 in the open field. (**B**) Distributions of the observed grid scores determined for each cell on each surface. The red lines represent significance grid score thresholds determined from shuffling.

3. grid score greater than cut-off threshold derived from $99^{perctile}$ shuffling (Figure 5-13; floor = 0.27, wall = 0.28, open field = 0.22);
4. At least one grid field detected.

5.6.8.2.3 Speed cells

A cell was classified as speed cell if it was not classified as grid cell and it satisfied all the three following criteria on at least one experimental surface (floor, wall, open field):

1. mean firing rate of the speed line at 19 $\pm$1 cm/s was greater than 1 Hz;
2. speed score greater than cut-off threshold derived from $99^{perctile}$ shuffling (Figure 5-14; floor = 0.035, wall = 0.033; open field = 0.030);
3. speed line score greater than cut-off threshold derived from $99^{perctile}$ shuffling (Figure 5-14B; floor = 0.88, wall = 0.89, open field = 0.88).

5.6.9 Statistical workflow

The results presented in Chapter 6 were conducted using a mixed two-way repeated measure ANOVA between surfaces (within subject factor) and across groups of animals (between subject factor). A Tukey-Kramer test was used *post-hoc* to determine significant effects.

The results presented in Chapter 7 comparing place cell firing between the floor and wall were conducted using both a two-tailed paired *t*-test (when the same cells were compared between surfaces) and an un-paired *t*-test (when different ensembles of cells between surfaces were compared). In contrast, all the analyses comparing the properties of grid cells, LFP theta, and speed cells were conducted using two-tailed paired *t*-tests. In addition, to compare the effects of running speed between surfaces on LFP theta power and speed cell firing rate, a two-way repeated measure ANOVA was used. Moreover, to compare categorical responses of cells between surfaces (i.e. marginal homogeneity), the McNemar's test was used throughout this thesis.

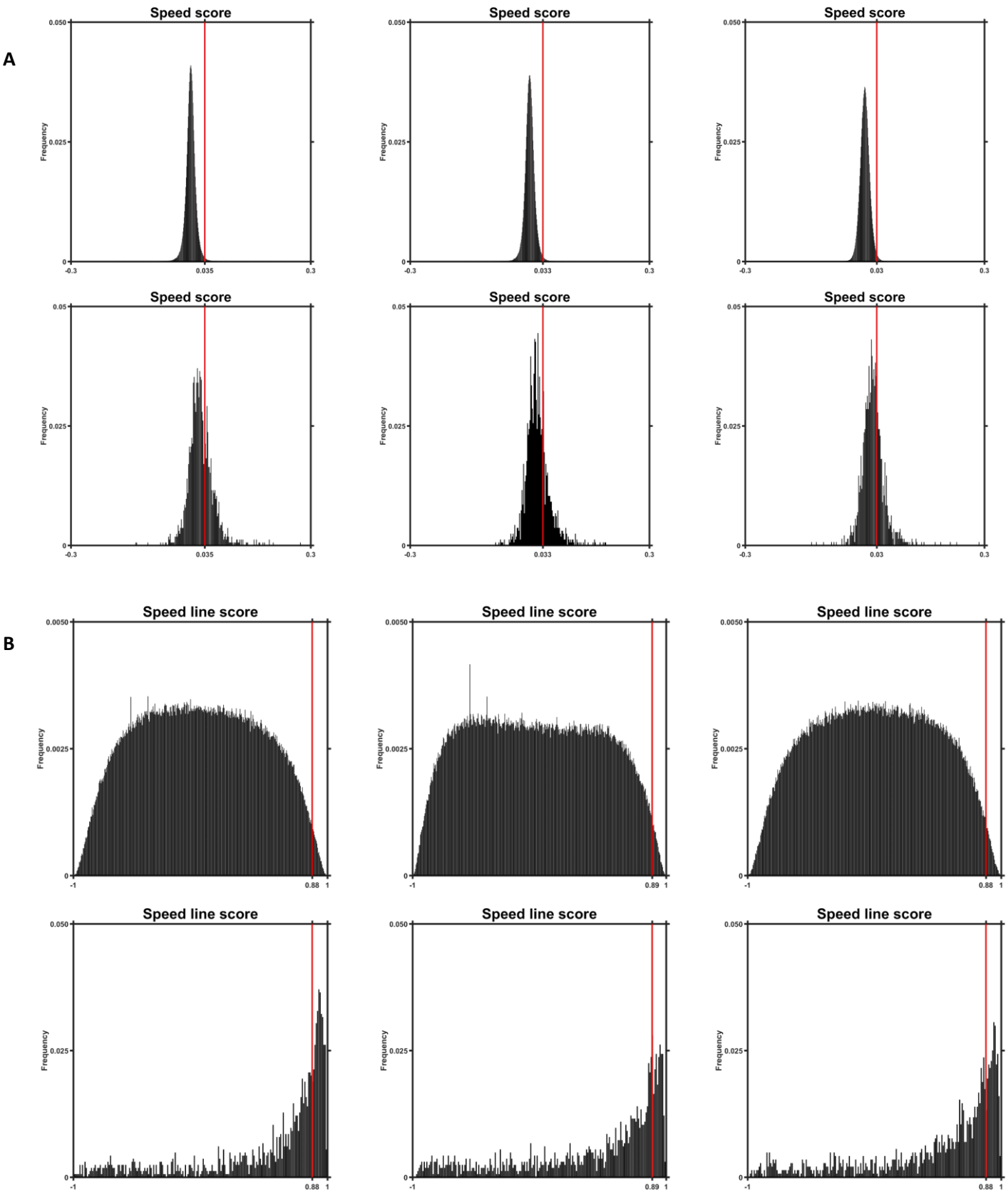

Figure 5-14 Shuffled and observed speed score and speed line score distributions.

Results of shuffling procedure on the floor (left), wall (centre) and open field (right). For each shuffle (n= 400) the speed score (**A**) and speed line score (**B**) were calculated and pooled across cells returning Gaussian distributions representing the corresponding null distributions for each surface (top rows). The 99 percentiles of the shuffled distributions were used as significant thresholds (red lines) of each surface to determine cells from the observed distribution (bottom) rows) passing criteria for speed cell detection.

6 Experienced pegboard experiment

The experienced-pegboard experiment is to be considered as a pilot study with the general aim of: a) testing the experience-dependent hypothesis (4.5.1.1 Experience-dependent) by replicating previous findings by Hayman et al., 2011; b) exploring whether different locomotor patterns affect grid cells firing response. To do that, two experimental conditions in which grid cells were recorded on the pegboard were conducted. Consistent with the study of Hayman et al., (2011), in the first condition termed "horizontal pegs condition", grid cells from 1 experienced and 1 naïve animal were recorded on the pegboard with the horizontal configuration. In contrast, in the second condition termed "diagonal pegs condition", grid cells from two experienced animals were recorded on the pegboard with the diagonal configuration.

6.1 Experimental design

Both conditions took place following the following protocol: on a regular basis, animals underwent at least one screening session a day (10-20 minutes) in a large and familiar room (see 5.2.1 Open field). Preliminary spike-sorting of the recorded data was done immediately after the session, and if at least one grid cell was identified, an experimental recording on the pegboard would be commenced straight after without unplugging the headstage device. The recordings on the pegboard took place in the same room as screening and lasted a variable time amount (between 20 and 30 minutes) until: a) sufficient spatial coverage on the pegboard was obtained; b) the animal showed spontaneous exploratory behaviour. Once completed, a second and longer (30 minutes) open field session took place immediately after in the open field box. In order to promote exploratory behaviour throughout all the recordings, steamed rice mixed with malt-paste (GimCat malt soft extra paste) was randomly placed at the proximal ends of the pegs (pegboard recording) or scattered around on the floor (open field). The depth of the recording sites where grid cells were detected varied between animals.

6.2 Results

6.2.1 Horizontal pegs condition

A total of 9 grid cells were recorded from 1 experienced animal (r654) and 22 grid

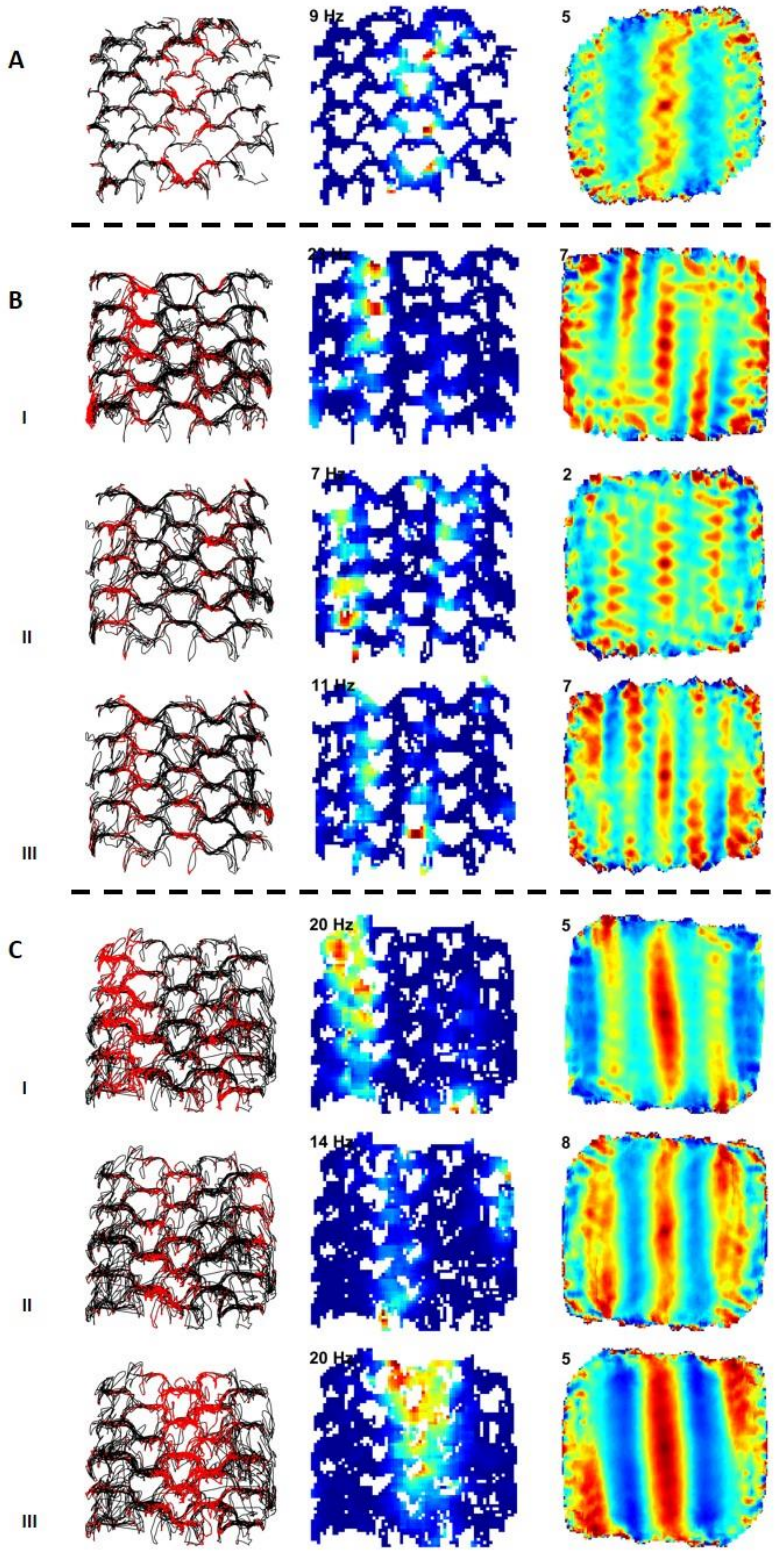

Figure 6-1 Grid cells on the horizontal condition of the pegboard.

Seven examples of grid cells recorded on the horizontal configuration of the pegboard from the three groups of rats showing vertical stripes as in the study by Hayman et al., 2011. Each row represents one example of cell with the spike plot (left), rate map (middle) and spatial autocorrelogram (right). The numbers in the top left corner of both rate maps and spatial autocorrelogram represent respectively the peak firing rate of the cell and the stripe score.
(**A**) One example of grid cell recorded from Hayman et al., 2011. (**B**$_{i\text{-}iii}$) Three grid cells recorded from the naïve animal (r621) and (**C**$_{i\text{-}iii}$) showing three grid cells from the experienced animal (r654).

cells from 1 naïve animal (r621). Similar to previous results (Hayman et al., 2011), grid cells

from the experienced animal produced vertical stripes of firing on the pegboard, most of which spanned the entire height of the apparatus (Figure 6-1). To compare whether grid cells from the experienced animal differed from the naïve one, the stripe scores on the pegboard and open field of both groups of animals were compared (experienced vs. naïve) with the dataset obtained by Hayman and colleagues (2011) comprising 17 grid cells from 4 animals (Figure 6-2). On the pegboard the stripe score was 5.2 ± 0.7 for the naïve animal, 4.7 ± 0.5 for the animals in Hayman et al., (2011) and 4.2 ± 0.5 for experienced animal. In contrast, on the open field, the stripe score was 1. ± 0.0 for the naïve animal, 1.2 ± 0.1 for the animals from Hayman et al., (2011) and 0.9 ± 0.1 for experienced animal. A two-way analysis of variance (ANOVA) comparing the stripe score across the three groups of animals (Hayman et al., (2011), naïve and experienced animals) and environment (pegboard vs. open field) revealed a significant effect of the environment ($F_{1,90}$ = 69,9, p < 0.0001) but no difference across groups ($F_{2,90}$ = 0.51, p = 0.60) and no interaction ($F_{2,90}$ = 0.56, p = 0.57). Therefore, these results showed no significant differences between the three groups of animals (Figure 6-2). Similarly, the grid score between groups of animals was compared across the environments. On the pegboard, the grid score was -0.37 ± 0.05 for the naïve animal, -0.52 ± 0.07 for the animals from Hayman et al., (2011) and -0.50 ± 0.04 for the experienced animal. In contrast, in the open field, the grid score was 0.9 ± 0.08 for the naïve animal, 0.56 ± 0.13 for the animals from Hayman et al., (2011) and 0.27 ± 0.20 for experienced animal. A two-way ANOVA revealed a significant effect of the environment ($F_{1,90}$ = 161, p < 0.0001) along with a significant effect of the experience ($F_{2,90}$ = 7.77, p < 0.001) but no significant interaction ($F_{2,90}$ = 0.33, p = 0.72). *Post-hoc* multi-comparison analysis adjusted with Bonferroni correction revealed no differences between the grid score across groups of animals on the pegboard (p = 0.28) but only a significant difference in the grid score in the open field between the naïve and experienced animals (p < 0.01).

In addition, the geometrical properties of the stripes were further investigated (Figure 6-2). The major axis on the pegboard was 89 ± 10 cm for the naïve animal, 121 ± 9 cm for the animals from Hayman et al., (2011) and 108 ± 10 cm for the experienced animal. In contrast, in the open field, the major axis length was 17 ± 1 cm for the naïve animal, 26 ± 4 cm for the animals from Hayman et al., 2001 and 46 ± 13 for the experienced animal. A two-way ANOVA returned a significant effect of the environment ($F_{1,90}$ = 108, p < 0.0001) and also a significant effect of experience ($F_{2,90}$ = 5.31, p < 0.01) but no significant interaction ($F_{2,90}$ = 1.82, p = 0.17). *Post-hoc* multi-comparison analysis adjusted with Bonferroni correction revealed a weak significant difference between the naïve animal and

the animal from Hayman et al., (2011) (p = 0.023). Similarly, the minor axis length was compared: on the pegboard it was 21 ± 4.7 cm for the naïve animal, 24 ± 3.8 cm for animals from Hayman et al., (20011) and 22 ± 1.5 cm for the experienced animal and in the open field it was 14 ± 0.5 cm for the naïve animal, 18 ± 2.0 cm for the animals in Hayman et al., (2011) and 30 ± 6.8 cm for the experienced animal. This time the two-way ANOVA returned no significant effect of the environment ($F_{1,90}$ = 0.27, p = 0.76) and no significant effect of experience ($F_{2,90}$ = 2.23, p = 0.11) nor interaction ($F_{2,90}$ = 1.65, p = 0.20). Finally, the aspect ratio (major/minor axes) was compared: on the pegboard it was 5.4 ± 0.6 for the naïve animal, 5.8 ± 0.5 cm for the animals from Hayman et al., (2011) and 4.9 ± 0.6 for the experienced animal, whereas in the open field it was 1.1 ± 0.0 for the naïve animal, 1.4 ± 0.0 for the animals from Hayman et al., (2011) and 1.4 ± 0.1 for the experienced animal. A two-way ANOVA revealed a significant effect of the environment ($F_{1,90}$ = 97, p < 0.0001) but no effect of experience ($F_{2,90}$ = 0.32, p = 0.73) and no interaction ($F_{2,90}$ = 0.37, p = 0.69).

Put together, these results, although from a limited number of cells and only from 1

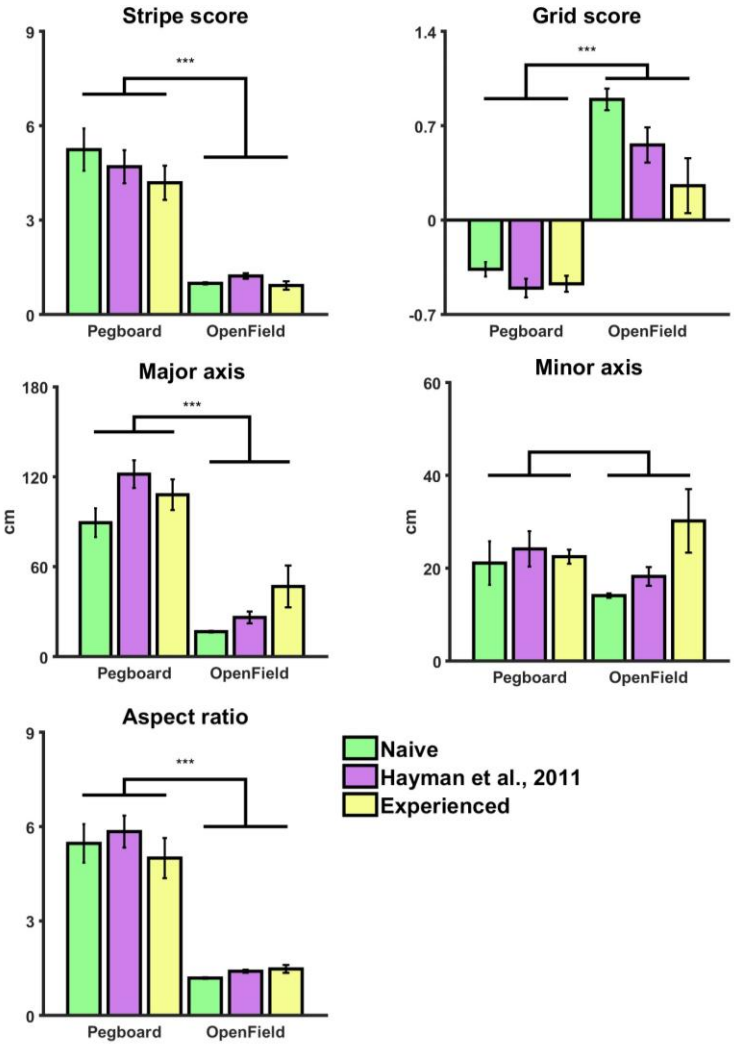

Figure 6-2 Comparisons between open field and pegboard across groups.

The spatial firing of grid cells across groups of rats has been compared between pegboard and open field. The analysis revealed that the stripe score was significantly greater on the pegboard than on the open field for all groups of rats in contrast to the grid score which instead was significantly lower on the pegboard compared to the open field for all group of rats. The geometrical properties of the stripes returned similar differences: the length of the major axis was greater on the pegboard than in the open field for all rats, although our analyses revealed a small significant difference between naïve animals and the one from Hayman et al., (2011) study. However, the length of the minor axis did not differ across environments nor groups of rats whereas the aspect ratio showed a significant effect of the environment but not of the experience.

animal for each group, suggest that grid cell representation is not affected by extensive experience of vertical locomotion and that the results of Hayman et al (2011) were not due to the restricted upbringing of rats.

6.2.2 Diagonal pegs condition

The findings from the horizontal pegs condition suggest that the prior experience with 3D navigation does not substantially affect grid cells firing on the pegboard. This result is inconsistent with the experience-dependent hypothesis and might be interpreted as additional evidence for the anisotropic encoding hypothesis. However, the columnar firing pattern of grid cells has been documented, to the best of our knowledge, only on the horizontal configuration of the pegboard. This observation motivated the following pilot study termed "diagonal pegs condition" (5.2.2). In this experiment the possibility that the stripe-like firing by grid cells would depend on the horizontal locomotor pattern was addressed. To test this hypothesis, a total of 22 grid cells were recorded from 2 experienced animals (r604 and r605) climbing on the pegboard with the pegs arranged in the diagonal configuration. Importantly, these animals were never exposed to the pegboard with the horizontal configuration prior to experiments.

6.2.2.1 *Heading direction on the pegboard*

First, in order to test whether the heading behaviour differed between rats tested on the horizontal- vs. diagonal-configuration of the pegboard, the normalized heading dwell map was computed. This highlighted the preferential diagonal heading on the diagonal-configuration of the pegboard in contrast to the horizontal bias on the horizontal configuration.

Next, the heading autocorrelation was computed for each session and that was used to determine both horizontal and diagonal scores which were then compared across groups of animals. The diagonal score significantly changed across groups of animals (diagonal score mean ± SEM: Hayman et al., (2011) = 0.19 ± 0.05, Horizontal rats = 0.30 ± 0.04, Diagonal rats = 0.52 ± 0.03; $F_{2,36}$ = 10.9, p < 0.001). A post-hoc Tukey-Kramer test revealed a significant increase in the diagonal score of Diagonal rats compared to both Horizontal rats (p < 0.01) and Hayman et al., (2011) rats (p < 0.001) and no differences between Horizontal rats and Hayman et al., (2011) rats (p = 0.24).

The horizontal score also significantly changed across groups of animals (horizontal score mean ± SEM: Hayman et al., (2011) = 0.40 ± 0.06, Horizontal rats = 0.26 ± 0.04,

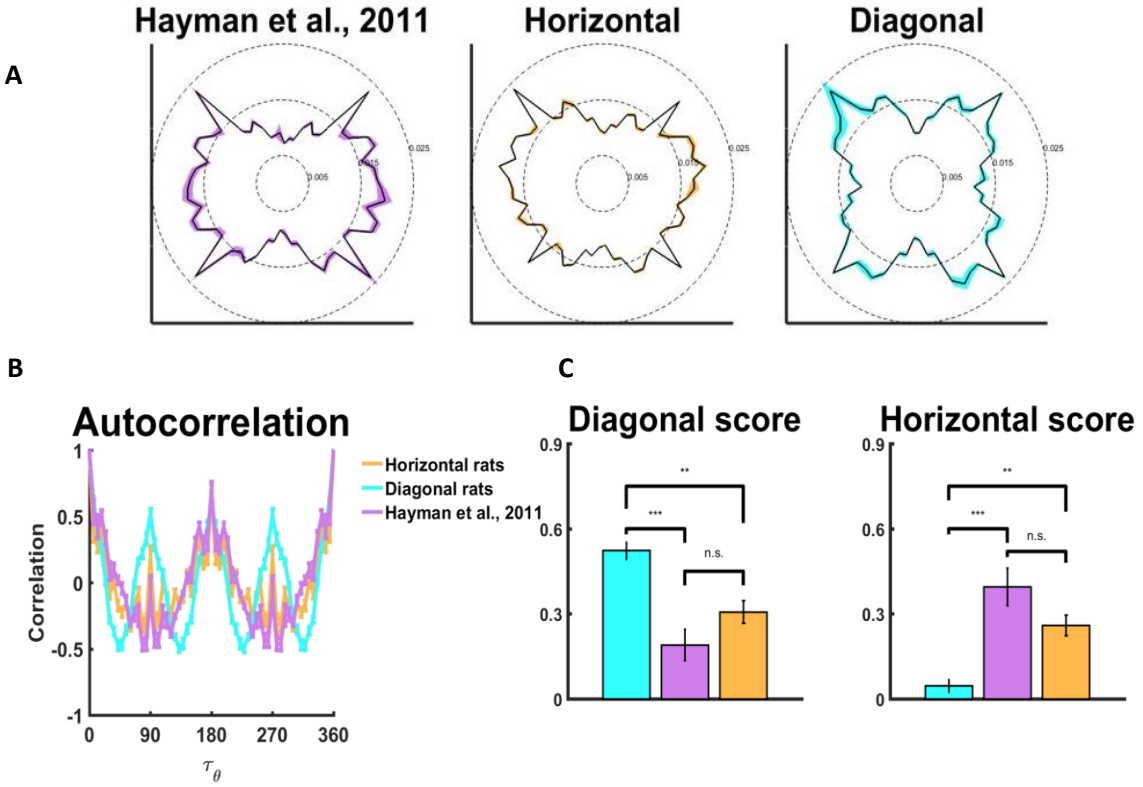

Figure 6-3 Heading direction on horizontal vs diagonal configuration of the pegboard.

(**A**) Polar plots showing the normalized directional dwell time across groups: Hayman et al., (2011), Horizontal and Diagonal. (**B**) The heading autocorrelogram reveals the different periodic pattern exhibited by rats: while Horizontal and Hayman et al., 2011 rats showed a peak at 180°, Diagonal rats exhibited peaks and 90° and 180°.These results suggest that while Hayman et al., 2011 and Horizontal rats mostly moved along 2 directions 180° apart, the Diagonal rats moved along 4 directions 90° apart. (**C**) The diagonal score (left) was significantly higher in Diagonal rats compared to both Hayman et al., 2011 and Horizontal rats. In contrast, the Horizontal score (right) was lower in Diagonal rats compared to both Hayman et al., 2011 and Horizontal rats.

Diagonal rats = 0.05 ± 0.02; $F_{2,36}$ = 13.1, p < 0.0001). A post-hoc Tukey-Kramer test revealed a significant decrease in the horizontal score of Diagonal rats compared to both Hayman et al., (2011) rats (p < 0.0001) and Horizontal rats (p < 0.01) and no differences between Horizontal rats and Hayman et al., (2011) rats (p = 0.18).

Together, these results thus suggest that between the horizontal and diagonal configuration of the pegboard, animals displayed different heading behaviours.

6.2.2.2 *Grid cell firing pattern*

Unlike grid cells recorded from both naïve and experienced animals on the horizontal configuration, grid cells on the diagonal configuration did not produce vertical stripes of firing but rather scattered firing across the whole pegboard (Figure 6-4). The stripe score on the diagonal configuration was compared to the horizontal one by pooling data from experienced and naïve animals (which were previously shown not to differ) and compared

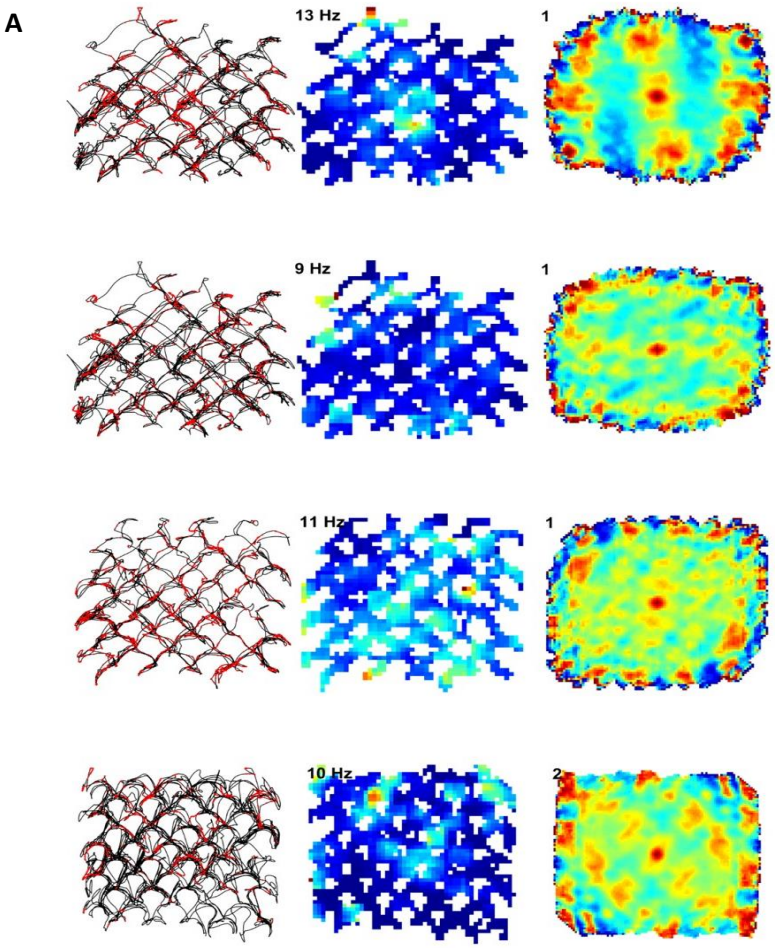

Figure 6-4 Grid cells on the diagonal configuration of the pegboard.

4 examples of grid cells recorded on the diagonal configuration of the pegboard represented as spike plots (left), rate map and peak firing rate (midle) and spatial autocorrelogram (right) with relative stripe score calculated. (B) The comparisons revealed a significant decrease in the stripe score of Diagonal rats compared to both Hayman et al., 2011 and Horizontal rats and no differences between them.

with previous data by Hayman et al., (2011) which were also collected on the horizontal configuration. The stripe score was 4.7 ± 0.5 for Hayman et al., (2011) animals, 4.9 ± 0.5 for experienced and naïve animals pooled together and 1.4 ± 0.3 for animals recorded on the diagonal configuration. A one-way ANOVA analysis revealed a significant difference between the three groups ($F_{2,70}$ = 16.9, p < 0.0001). *Post-hoc* analyses adjusted with Bonferroni correction revealed no significant difference between horizontal comparisons (p = 0.68) but a significant difference between data from the Hayman et al., (2011) study and the diagonal condition (p < 0.001) and horizontal and diagonal condition (p < 0.0001). Therefore, even though the results on the diagonal configuration come from a limited number of animals (n = 2) and limited number of cells (n = 22), these results convincingly suggest that the vertical stripes on the pegboard are not the only firing pattern on the pegboard, as it disappeared when using the diagonal configuration.

Accordingly, these findings suggest that the pattern of locomotion displayed by the animals substantially affects grid cell firing response.

6.3 Discussion

The principal aim of this set of experiments was to test the hypothesis that previous observations of impaired odometry by grid cells on the pegboard resulted from restricted environmental experience (experience-dependent hypothesis). To do that, the activity of grid cells from one experienced animal moving on the pegboard with the pegs arranged horizontally (horizontal condition) was recorded. Even though a low number of cells was recorded, and only from one experienced and one naïve animal, grid cells on the horizontal configuration showed strikingly similar stripe-like firing pattern when compared to the study of Hayman et al., (2011). The theoretical prediction generated by this hypothesis yielded a differential firing pattern between naïve and experienced animals, with no columnar pattern by the experienced animal. In contrast, empirical findings show that the same firing pattern on the pegboard condition is produced by grid cells regardless of prior experience with 3D locomotion. In fact, the spatial representation exhibited by grid cells in the horizontal condition from both experienced and naïve animal showed no significant differences from the results obtained by Hayman and colleagues (2011) with effectively naïve animals. This result, although preliminary, demonstrates that even though different subjects were used, different experimenter and, most importantly, different levels of experience with vertical locomotion prior to experience, previous findings were successfully replicated. Therefore, the fact that grid cells from experienced animals also produced vertical stripes during locomotion on the pegboard in the “horizontal pegs” condition, argues against the experience-dependent hypothesis as an explanation for the vertical stripes on the pegboard.

The results from the horizontal-pegs condition could be interpreted as further evidence for the anisotropic encoding of space given that, as predicted, vertical stripes also appeared from an experienced animal. However, findings from the diagonal pegs condition disagree with the prediction of the anisotropic encoding hypothesis given that, in contrast to the horizontal configuration, grid cells did not produce vertical stripes. Importantly, grid cell representation not only was not stripe-like on the diagonal configuration of the pegboard, but did not even show the typical six-fold symmetry which is normally observed on horizontal plane. In contrast, a clear organization of the firing pattern could not be identified by eye, an observation that, to the best of our knowledge, unless following

pharmacological inactivation of afferent brain areas (Bonnevie et al., 2013; Winter et al., 2015b) or passive movements (Winter et al., 2015a), has never been reported before in grid cells. In these cited experiments, grid cell representation was found to be heavily impaired following temporary inactivation of the hippocampus (Bonnevie et al., 2013) or ADN (Winter et al., 2015b) where place and head direction cells are found and are thought to interact with the grid cell system. A similar effect was found during passive transport of a rat placed in a clear transparent box (Winter et al., 2015a): in this situation head direction cells kept firing in the same way as during active exploration, while grid cells showed disorganized firing with no grid pattern. In our experiment, animals spontaneously learned how to climb across diagonally-arranged pegs in a standard free foraging task with no training required. Therefore, the lack of a regular six-fold symmetry (as well as stripe-like firing) is a "natural" response of grid cells during locomotion in this particular environment. Why do grid cells neither produce hexagonal grids nor vertical stripes in the diagonal configuration as in the horizontal one? A more general interpretation of these results will be provided in the overall discussion of this thesis (Chapter 9).

To summarise, three considerations can be made in light of the results shown here. The first consideration is that although with a limited number of data (1 rat, 9 cells), grid cells from the experienced animal clearly showed the same firing pattern as the naïve animals. Indeed, the naïve and experienced animals produced firing patterns similar to those displayed in Hayman et al., (2011), both from a qualitative (grid cells of all three groups showed columns on the pegboard but not in the open field) and quantitative point of view (there was no difference in the stripe score between the three groups). This result therefore allows us to generalise the findings from the naïve animals of Hayman et al., (2011) as being the natural spatial response of grid cells during locomotion in the horizontal condition of the pegboard regardless of prior experience with 3D navigation.

The second consideration is that the prediction provided by the anisotropic encoding hypothesis is met only in the horizontal condition and not in the diagonal one. The anisotropic encoding hypothesis posits an intrinsic lack of encoding for movements along the vertical dimension regardless of the locomotor pattern used. The fact that the vertical stripes appear in the horizontal configuration of the pegboard but not in the diagonal one, allows us also to reject the anisotropic encoding hypothesis.

Finally, the third consideration provided by results of the experienced pegboard experiment is that different configurations of the pegs on the pegboard substantially drive different firing responses by grid cells. Indeed, while grid cells from animals with different

experience with 3D navigation showed columns in the horizontal condition, in the diagonal condition there was no specific vertical bias in the firing response of grid cells. These results therefore suggest that the vertical stripes are linked to movements occurring in the horizontal condition. As postulated by the reference frame hypothesis, the orientation of the body, along to which locomotion is computed, affects spatial response of grid cells. Therefore, the vertical stripes observed in the horizontal configuration of the pegboard support the reference frame hypothesis. According to this view, grid cells do not perform odometry along height given that the vertical axis is orthogonal to the locomotor plane. The observation that grid cells in the diagonal configuration of the pegboard no longer produce vertical stripes is also consistent with the reference frame hypothesis as it shows that grid cells are modulated by the orientation of locomotion (horizontal vs. diagonal plane). One recent study by Hayman et al., (2015) showed that grid cells on a 2D slope (tilted 45°) maintain the capacity to produce fields and perform odometry as on the horizontal plane Hayman et al., (2015). This result may be interpreted as contradictory given that grid cells on the diagonal configuration did not produce clear firing patterns. It should be pointed out though that while rats on the slope of Hayman and colleagues (2015) navigated maintaining a single body orientation (i.e. parallel to the angle of the slope), animals on the pegboard kept two orthogonal, and maybe conflicting, body orientations.

In conclusion, the results from the pilot experiment “experienced pegboard”, consisting of two experimental conditions (horizontal pegs and diagonal pegs), provided preliminary evidence for rejecting two hypotheses (experience-dependent and anisotropic encoding) and supported the reference frame hypothesis. According to this view, a grid cells reference frame is modulated by the orientation of the body, so in a situation where animals move on the vertical plane upright, the grid cell firing pattern should be similar to the horizontal. The next experiment, termed floor-wall experiment, specifically addresses this question. The activity of grid cells from experienced animals was recorded during climbing on a vertical wall and compared to that on a horizontal plane. The results of this experiment will be described and discussed in the next chapter.

7 The floor-wall experiment

This experiment aimed to test the hypothesis that place and grid cells maintained their spatial firing responses during movements on a climbing wall. The results from the "experienced pegboard experiment" suggest that the vertical stripes produced by grid cells on the pegboard originally described by Hayman and colleagues (2011) may be linked to the horizontal orientation of the body. This observation led to the formulation of the reference frame hypothesis according to which grid cells fail to perform path integration along the direction orthogonal to the locomotion plane (Hayman et al., 2011; Taube and Shinder, 2013). In order to test this hypothesis, the so-called floor-wall experiment was conducted.

7.1 Experimental design

The floor-wall experiment took place using the following protocol: on a regular basis, animals underwent at least one screening session a day (10-20 minutes) in a large and familiar room (see 5.2.1). Preliminary spike-sorting of the recorded data was done immediately afterwards and if at least one place or grid cell was identified, an experimental recording session would be commenced (usually starting about 2 hours after the last screening session). The floor-wall recording took place in a different room and lasted a variable amount of ranging between 1 and 2.5 hours, until: a) sufficient spatial coverage of both floor and wall was obtained, and b) the animal showed spontaneous exploratory behaviour. Once the recordings on the floor-wall apparatus were completed, a second open field session (30 minutes) took place immediately after in the screening room. In order to promote foraging behaviour throughout all the recordings, rice mixed with pet-paste was scattered around on the floor and/or attached onto the wall mesh.

7.2 Results

In this section, all the results including the behaviour of the animal and electrophysiological results at single-cell level will be provided.

7.2.1 Behaviour

During the recordings, the animals displayed spontaneous exploratory behaviour on both floor and wall while searching for food scattered by the experimenter in order to let

the rat evenly sampling both surfaces. Thanks to the prior experience in the enriched environment (5.1.2) animals showed efficient climbing skills on the wall. However, they still seemed to prefer the horizontal surface compared to the vertical one, and movements during climbing seemed to be slower. These observations motivated a number of behavioural analyses (see below) aimed to investigate whether the locomotor pattern substantially changed between surfaces. A brief description of the behaviour exhibited by rats in this protocol will be provided in the following paragraphs. These results have been obtained by pooling together all the experimental sessions (n = 53) involving animals implanted in the hippocampus (4 rats, 11 sessions) and medial entorhinal cortex (12 rats, 42 sessions).

7.2.1.1 *Dwell time*

Rats spent a significantly greater amount of time on the floor compared to the wall (Figure 7-1A; dwell time: floor = 66 ± 3 minutes, wall = 39 ±21 minutes, t_{52} = 7.48, p < 0.0001). Electrophysiological results were robust to this behavioural bias when the floor data was down sampled to match dwell time on the wall.

7.2.1.2 *Speed*

The mean speed between floor and wall was compared and it was significantly greater on the floor compared to the wall (Figure 7-1B; dwell time: floor = 9.9 ± 0.3 cm/s, wall = 6.9 ±0.2 cm/s, t_{52} = 9.17, p < 0.0001). Importantly, this result was true despite the fact that rats spent a greater percentage of time resting (speed < 2 cm/s) on the floor

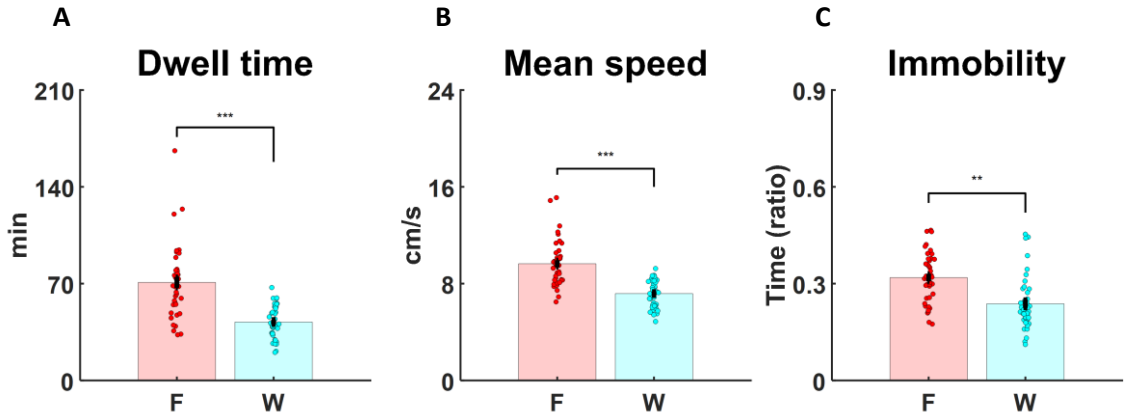

Figure 7-1 Behavioural differences between surfaces.

Rats on the floor-wall apparatus exhibited remarkable differences in their behaviour as shown by coloured bars representing the mean ± S.E.M. with superimposed dots for each data point between floor (F) and wall (W). Dwell time (**A**), mean speed (**B**) and immobility (**C**) were significantly increased on the floor compared to the wall.

compared to the wall (Figure 7-1C; immobility: floor = 32 ± 1.1 %, wall = 25 ± 1.3 %, t_{41} = 3.46, $p < 0.01$).

7.2.1.3 *Heading*

The hypothesis that rats during climbing showed heading bias (see Figure 7-2 for dwell time across heading directions) was addressed in two different ways. First the mean resultant vector length of the rat trajectory was compared between floor and wall and that was not significantly different (vector length: floor = 0.074 ± 0.006, wall = 0.082 ± 0.007: t_{52} = -0.77, p = 0.44) suggesting that rats did not show substantial heading bias between floor and wall.

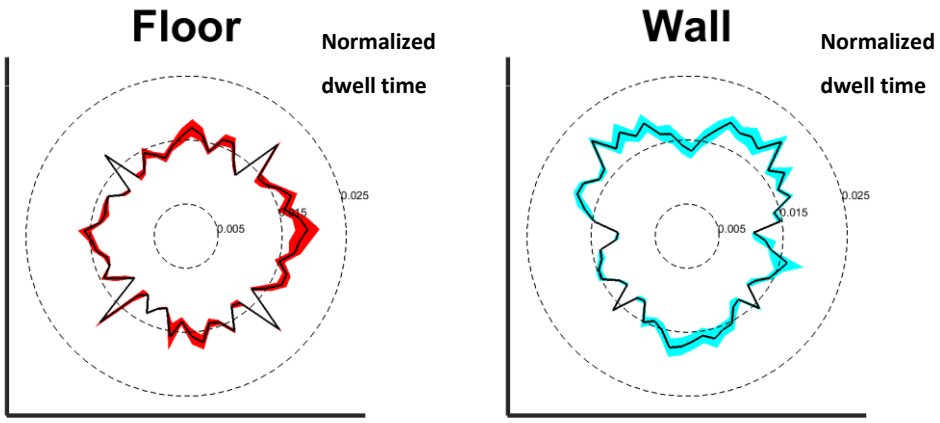

Figure 7-2 Dwell time across directional bins.

The directionality of the trajectories between floor and wall did not significantly differ. Polar plots representing the normalized mean dwell time ± standard error across directional bins between floor (left) and wall (right). The comparison of the mean vector length between floor and wall returned no statistical difference.

7.2.2 Place cells

Overall 100 neurons recorded from 4 experienced animals showed spatially modulated firing passing the criteria for inclusion in the place cell dataset (Figure 7.3). The analyses detected 60 place cells active only on the floor (60 %, Figure 7.3A, Figure 7.3A D), 14 place cells displaying place fields on both surfaces (14 %, Figure 7.3B), 18 place cells active on the wall but not on the floor (18 %, Figure 7.3C) and 8 silent place cells (8 %). McNemar's test determined that there was a statistically significant difference in the proportion of active place cells between floor and wall ($p < 0.0001$).

In the next paragraphs, all the results reported between surfaces were obtained by pooling place cells recorded from different animals (n = 4) (see 10.1 for extra analysis addressing place cell properties between animals).

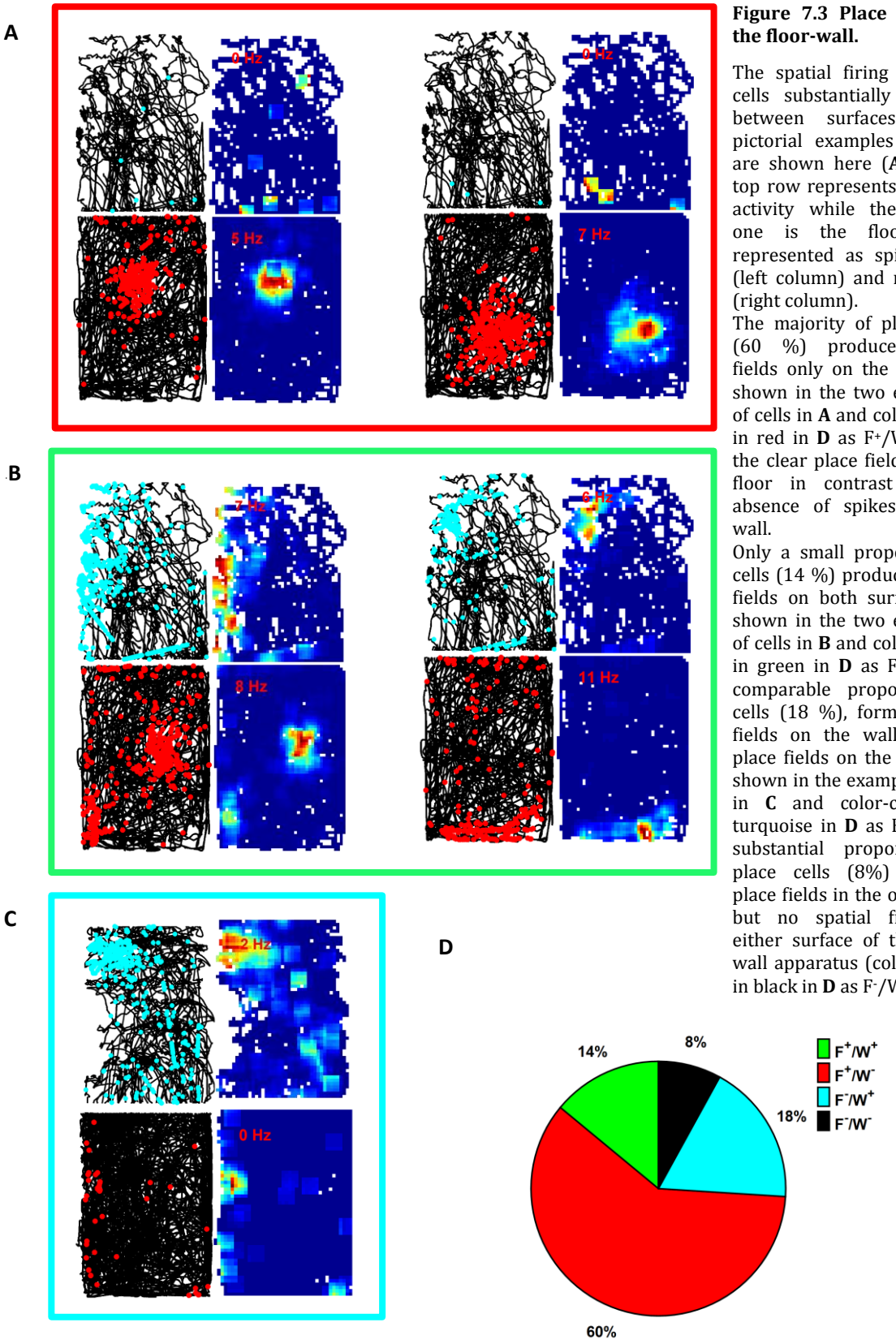

Figure 7.3 Place cells on the floor-wall.

The spatial firing of place cells substantially differed between surfaces. Seven pictorial examples of cells are shown here (**A-C**). The top row represents the wall activity while the bottom one is the floor, both represented as spike plots (left column) and rate map (right column).

The majority of place cells (60 %) produced place fields only on the floor (as shown in the two examples of cells in **A** and color-coded in red in **D** as F^+/W^-). Note the clear place fields on the floor in contrast to the absence of spikes on the wall.

Only a small proportion of cells (14 %) produced place fields on both surfaces (as shown in the two examples of cells in **B** and color-coded in green in **D** as F^+/W^+). A comparable proportion of cells (18 %), formed place fields on the wall but no place fields on the floor (as shown in the example of cell in **C** and color-coded in turquoise in **D** as F^-/W^+). A substantial proportion of place cells (8%) showed place fields in the open field but no spatial firing on either surface of the floor-wall apparatus (color-coded in black in **D** as F^-/W^-).

7.2.2.1 *Firing rate properties*

After describing the ensemble of active cells, further analyses addressed the firing properties of the cells. Consistent with the majority of place cells being silent on the wall, a significant drop in the mean and peak firing rate across all cells was observed (Figure 7-4A; mean firing rate: floor = 0.63 ± 0.07 Hz, wall = 0.33 ± 0.07 Hz, t_{99} = 3.28, p < 0.01; peak firing rate, Figure 7-4B; floor = 6.3 ± 0.5 Hz, wall = 4.3 ± 0.5 Hz, t_{99} = 3.05, p < 0.01). However, when only the subset of active cells on each surface were compared no significant difference was found (Figure 7-4C; mean firing rate: floor = 0.66 ± 0.08 Hz, wall = 0.81 ± 0.15, two-tailed unpaired: t_{104} = -0.97, p = 0.33; Figure 7-4D; peak firing rate: floor = 7.1 ± 0.6 Hz, wall = 9.2 ± 1.1 Hz, two-tailed unpaired, t_{104} = -1.90, p = 0.06). These results thus suggest that fewer place cells produced spatial firing on the wall compared to the floor (Figure 7.3D) but their firing rate properties were not altered during climbing on the wall.

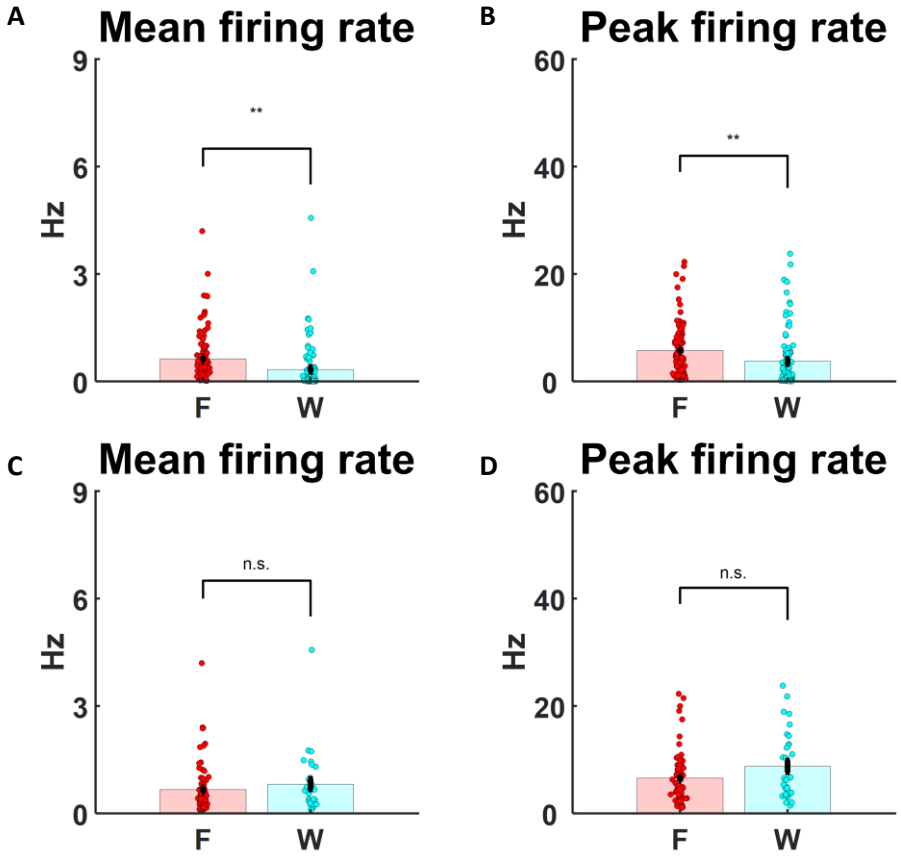

Figure 7-4 Firing rate properties of place cells between surfaces.

Firing rate properties as shown by coloured bars representing the mean ± S.E.M. with superimposed dots for each data point between floor (F) and wall (W). The mean (**A**) and peak firing rate (**B**) of all place cells significantly differed between floor and wall. However, this effect was due to the greater number of cells which stayed silent on the wall. The comparisons between only those cells active on each surface returned instead no significant difference for both the mean (**C**) and peak firing rate (**D**) between floor and wall.

7.2.2.2 *Spatial encoding properties*

After describing place cell firing properties, further analyses addressed the spatial

encoding between surfaces. First, the spatial information (5.6.4.2) between floor and wall was compared and it was significantly increased on the wall compared to the floor (Figure 7-5A left; floor = 1.2 ± 0.07 bit/spike, wall = 2.0 ± 0.13 bit/spike, t_{99} = -7.29, p < 0.0001). In contrast, the spatial coverage (5.6.4.1) was significantly greater on the floor compared to the wall (Figure 7-5B left; floor = 0.17 ± 0.01, wall = 0.10 ± 0.01, t_{99} = 5.53, p < 0.0001).

Importantly, it should be pointed out that the spatial information score can sometimes return abnormally high values when the firing rate of a cell is very low (as for the majority of place cells on the wall). Therefore, both the spatial information and coverage scores were also compared between active cells only. This time the spatial information was not significantly different (Figure 7-5A right; floor = 1.3 ± 0.05 bit/spike, wall = 1.3 ± 0.08 bit/spike, two-tailed un-paired: t_{104} = -0.01, p = 0.98). Similarly, the spatial coverage between active cells was not significantly reduced on the wall compared to the floor (Figure 7-5B right; floor = 0.15 ± 0.01, wall = 0.13 ± 0.03, two-tailed un-paired: t_{104} =

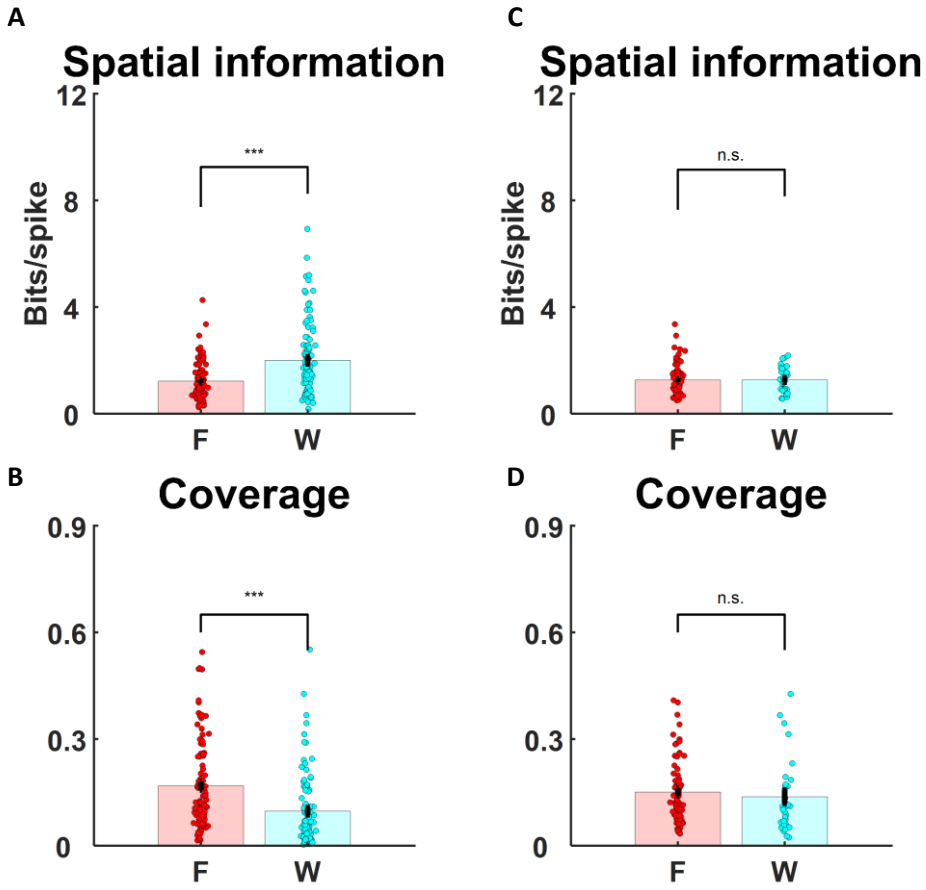

Figure 7-5 Spatial encoding by place cells between surfaces.

The spatial activity of place cells as shown by coloured bars representing the mean ± S.E.M. with superimposed dots for each data point between floor (F) and wall (W).
The spatial encoding of all place cells was compared between surfaces and both the spatial information (**A**) and coverage (**B**) was significantly different between surfaces. However, when only the subsets of active cells on each surface were compared, the spatial information (**C**) and coverage (**D**) were not significantly different between surfaces.

0.65, p = 0.51). Therefore, consistent with the mean and peak firing rate differences between floor and wall, these results suggest that the spatial firing by the subset of active place cells was not affected during climbing on the wall.

7.2.2.3 *Place field properties*

To rule out the hypothesis that place cell representations between floor and wall differed in their geometrical rather than spiking features, a number of place fields' features such as the field size, major and minor axes and the aspect ratio were compared. The analyses revealed a significant reduction in the size of fields and a mild reduction in the minor axis of the fields on the wall compared to the floor (Figure 7-6A, area: floor = 1115 ± 100 cm^2, wall = 681 ± 103 cm^2, two-tailed unpaired: t_{104} = 2.60, p = 0.010; Figure 7-6B, major axis: floor = 54.6 ± 3.20 cm, wall = 46.5 ± 3.49 cm, two-tailed unpaired: t_{104} = 1.51, p = 0.13; Figure 7-6C, minor axis: floor = 28.5 ± 1.54 cm, wall = 22.4 ± 2.1 cm, two-tailed unpaired: t_{104} = 2.26, p = 0.026; Figure 7-6D, aspect ratio: floor = 2.11 ± 0.15, wall = 2.58 ±

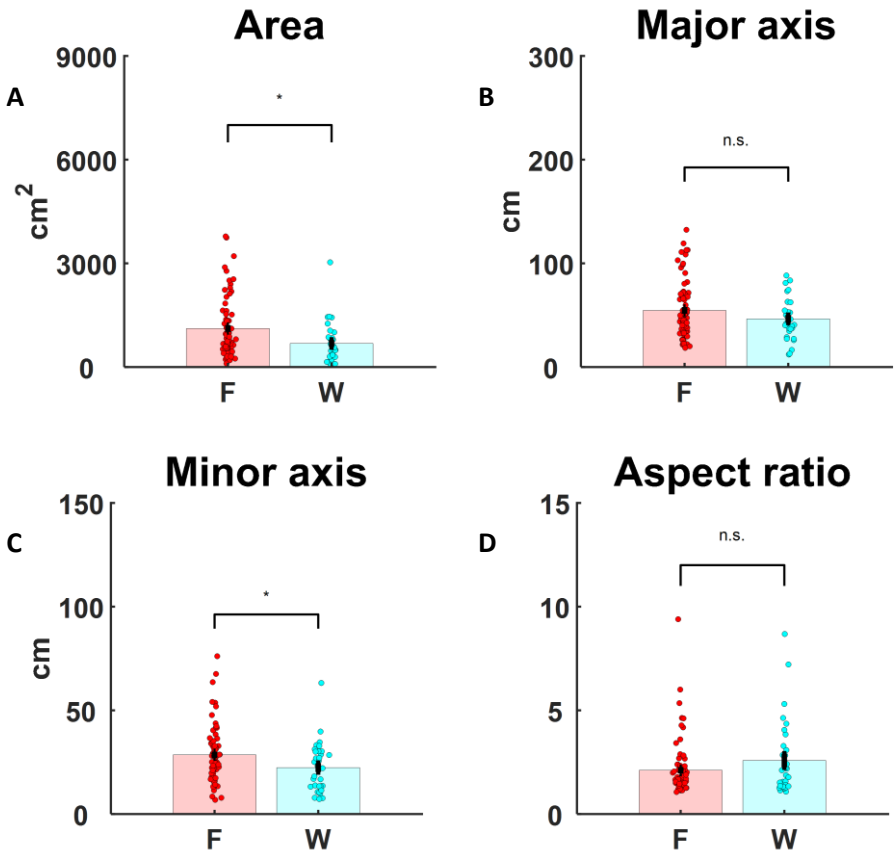

Figure 7-6 Place field properties between floor and wall surfaces

Place field properties are represented as coloured bars showing the mean ± S.E.M. with superimposed dots for each data point between floor (F) and wall (W). The size of the fields (**A**) was significantly reduced on the wall compared to the floor while the major axis (**B**) did not show significant differences between surfaces. Similarly, the minor axis (**C**) was reduced on the wall while the aspect ratio (**D**) did not show significant differences between floor and wall.

0.32, two-tailed unpaired: t_{104} = -1.49, p = 0.14). Put together, these results show that place cells were generally more silent on the wall than on the floor but the subset of active place cells produced place fields on the wall which were mostly similar to those on the floor.

7.2.3 Grid cells

An overall number of 119 neurons from 11 rats passed criteria for grid cells and were recorded on the floor and wall apparatus and subsequently in the open field. As expected, they showed the typical hexagonal firing pattern on the floor as well as in the open field but, despite the presence of large firing fields on the wall, they did not display the hexagonal grid-patterns on the vertical plane (Figure 7.8). Importantly, the spatial activity observed largely differed from the vertical elongation of the fields as previously reported by Hayman et al., (2011) and the first experiment on the pegboard (Figure 6-1).

In the next paragraphs, all the results between surfaces were obtained by pooling grid cells recorded from different animals (n = 11) (see 10.2 for extra analyses addressing grid cell properties between animals).

7.2.3.1 *Firing rate properties*

First, grid cell firing rate between surfaces was compared and it revealed significant decreases on the wall compared to the floor (Figure 7-7A, mean firing rate: floor = 1.13 ± 0.07 Hz, wall = 0.80 ± 0.06, t_{118} = 6.21, p < 0.0001; Figure 7-7B, peak firing rate: floor = 8.81 ± 0.56, wall = 6.85 ± 0.44, t_{118} = 4.56, p < 0.0001). Taken together, these initial results show

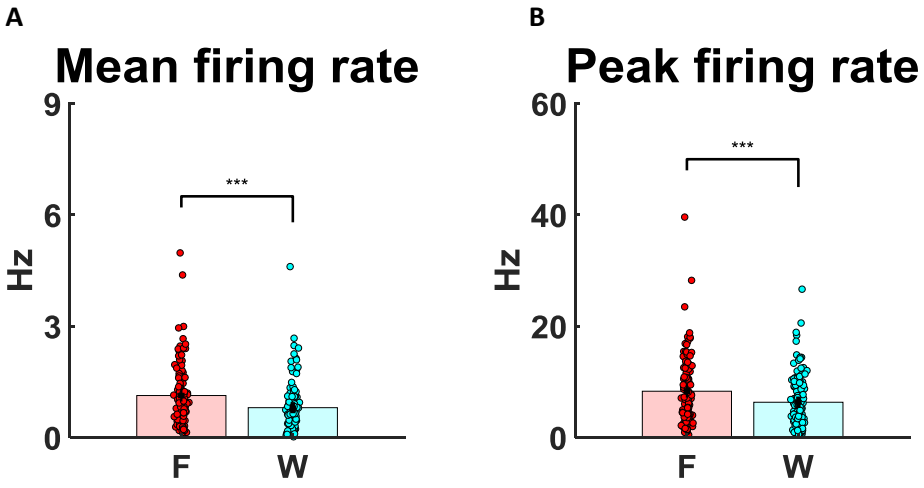

Figure 7-7 Firing rate properties of grid cells between surfaces.

Firing rate properties represented as coloured bars showing the mean ± S.E.M. with superimposed dots for each data point between floor (F) and wall (W). Both the mean firing rate (**A**) and peak firing rate (**B**) of grid cells were significantly reduced on the wall compared to the floor.

that the firing activity of grid cells was substantially decreased on the wall.

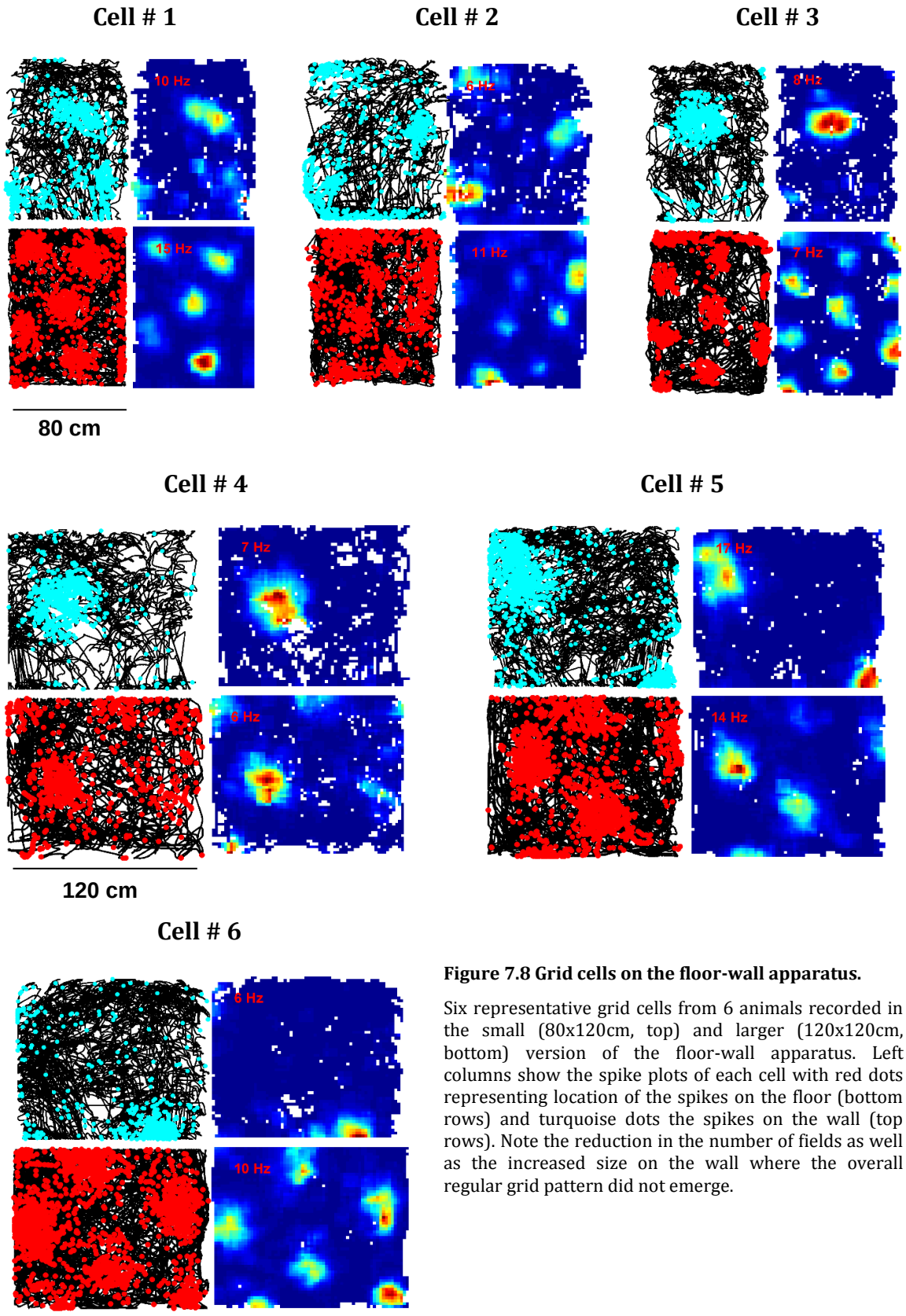

Figure 7.8 Grid cells on the floor-wall apparatus.

Six representative grid cells from 6 animals recorded in the small (80x120cm, top) and larger (120x120cm, bottom) version of the floor-wall apparatus. Left columns show the spike plots of each cell with red dots representing location of the spikes on the floor (bottom rows) and turquoise dots the spikes on the wall (top rows). Note the reduction in the number of fields as well as the increased size on the wall where the overall regular grid pattern did not emerge.

7.2.3.2 *Spatial properties*

After addressing grid cell firing, the spatial encoding of grid cells also was investigated. A number of spatial properties such as the grid score, stripe score, coverage and scale (Figure 7-9) were compared between floor and wall. The grid score was substantially decreased on the wall compared to the floor (Figure 7-9A, floor = 0.44 ± 0.04, wall = - 0.07 ± 0.02, t_{118} = 10.3, p < 0.0001) unlike the stripe score which was instead increased on the wall compared to the floor (Figure 7-9B, floor = 1.17 ± 0.05, wall = 1.68 ± 0.11, t_{118} = -4.08, p < 0.0001). The spatial coverage was not significantly different between surfaces (Figure 7-9C, floor = 0.26 ± 0.02, wall = 0.23 ± 0.02, t_{118} = 1.85, p = 0.066) whereas the scale of the spatial autocorrelogram was significantly decreased on the wall compared to the floor (Figure 7-9D, floor = 56.5 ± 1.9 cm, wall = 59.9 ± 1.69 cm, t_{118} = 2.90, p < 0.01).

Together these results suggest that the spatial activity of grid cells was substantially altered during climbing on the wall compared to running on the floor. Consistent with the

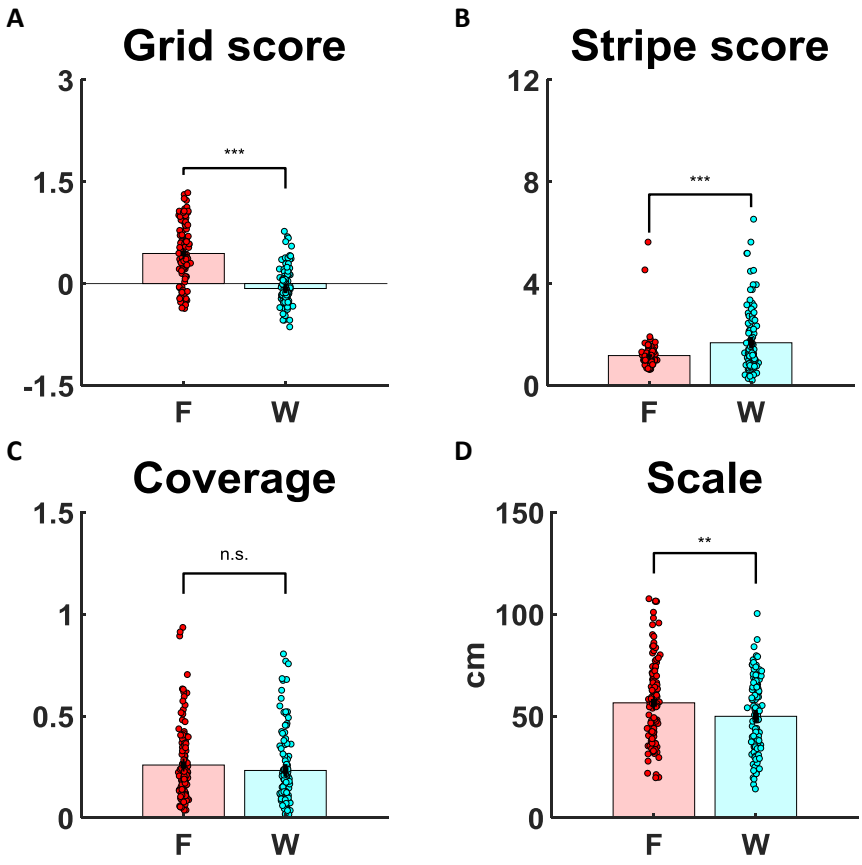

Figure 7-9 Spatial properties of grid cells between surfaces.

Spatial properties of grid cells represented as coloured bars showing the mean ± S.E.M. with superimposed dots for each data point between floor (F) and wall (W). The grid score (**A**) on the wall showed dramatic drop compared to the floor while the stripe score (**B**) was significantly increased on the wall compared to the floor. The spatial coverage (**C**) was not significantly different whereas the scale (**D**) was reduced on the wall compared to the floor.

horizontal configuration of the pegboard, the regular firing of grid cells was severely disrupted (grid score) and was more anisotropic (stripe score) on the wall compared to the floor, although the effect was less pronounced compared to the pegboard (see Figure 6-1 and Figure 7-9). The absence of a regular pattern by grid cells on the wall may explain why on the wall the scale of grid cells, as returned by the spatial autocorrelogram, did not show a significant increase. Indeed, the complete lack of spatial regularity *de facto* biases the measure of the spatial scale. However, previous studies highlighted a strong correlation between the scale of the grid and the size of the grid fields (Hafting et al., 2005). Therefore, to establish whether in the vertical plane there was a substantial expansion of the grid firing pattern, the spatial metrics of grid cells were examined by focusing on grid field properties between surfaces.

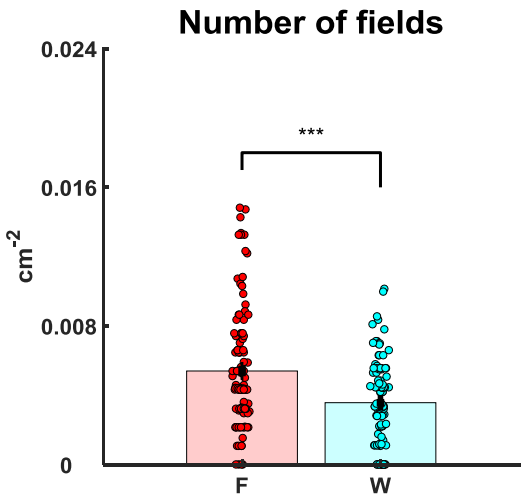

Figure 7-10 Number of grid fields between surfaces.

The number of grid fields (quantified as number of fields/available area) between surfaces is represented as coloured bars showing the mean ± S.E.M. with superimposed dots for each data point between floor (F) and wall (W). The comparisons reveal a significant decrease on the wall compared to the floor.

7.2.3.3 *Grid field properties*

After describing the firing properties of grid cells on the wall, the spatial characteristics of grid fields were addressed. First, the number of grid fields (normalized by the available area) was decreased on the wall compared to the floor (Figure 7-10, floor = $5.41 \pm 0.30 \times 10^{-3}$ cm^{-2}, wall = $3.58 \pm 0.22 \times 10^{-3}$ cm^{-2}, $t_{118} = 6.30$, $p < 0.0001$).

The next step was to assess differences in the spatial metrics of grid fields between planes (Figure 7.11A-D). To do that, two methods were applied, these returned similar results. The first method was to extract geometrical features of the field from the spatial autocorrelogram (see 5.6.4.3). The size of the grid fields was substantially increased on the wall compared to the floor (Figure 7.11A, floor = 1272 ± 136 cm^2, wall = 4196 ± 480 cm^2, t_{118} = -6.17, $p < 0.0001$). Consistent with the increase in the size of the fields, there was a

significant increase in the length of the major and minor axes of the fields on the vertical plane (Figure 7.11B, major axis: floor = 46.1 ± 3.58 cm, 109.9 ± 7.71 cm, t_{118} = -7.91, p < 0.0001; Figure 7.11C, minor axis: floor 31.1 ± 1.18 cm, wall = 45.8 ± 2.76 cm, t_{118} = -5.26, p < 0.0001). The increase in size and axes of grid fields on the wall demonstrated that even though the overall spatial activity of grid cells was not reduced – the spatial coverage was not significantly different (see Figure 7-9) – the spatial firing pattern was significantly enlarged on the wall. To test whether also the shape of the fields was affected on the wall, the aspect ratio (major/minor axis) across surfaces was compared and showed a significant increase on the wall (Figure 7.11D, floor = 1.45 ± 0.06, wall =2.34 ± 0.12, t_{118} = -5.91, p < 0.0001) suggesting that fields were more elongated on the wall compared to the floor. Consistent with the increase in the stripe score on the wall, the distribution of grid field orientations (see 5.6.4.3) differed significantly between floor and wall (Figure 7-12).

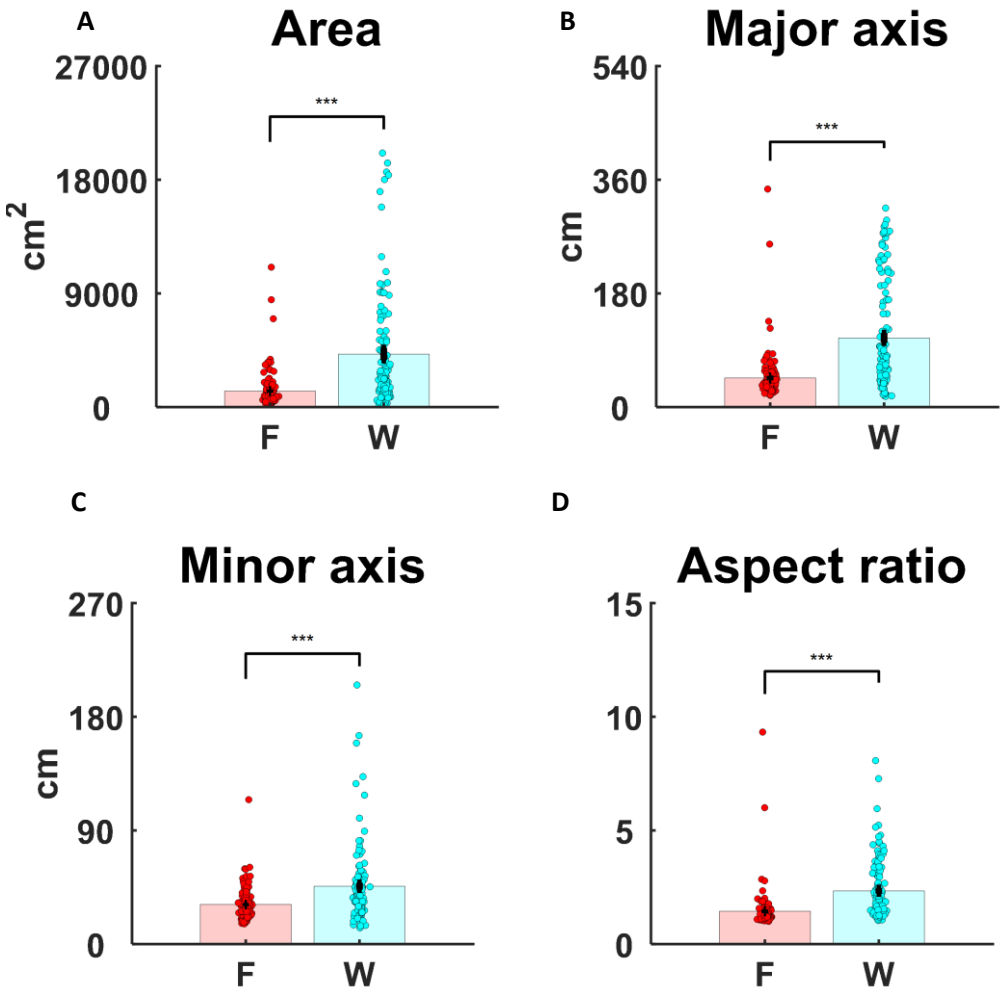

Figure 7.11 Grid fields properties between surfaces.

Grid field properties represented as coloured bars showing the mean ± S.E.M. with superimposed dots for each data point between floor (F) and wall (W). Error! Reference source not found.The omparisons revealed significant increase on the wall compared to the floor in the size of the fields (**A**), major axis length (**B**), minor axis length (**C**) and aspect ratio (**D**).

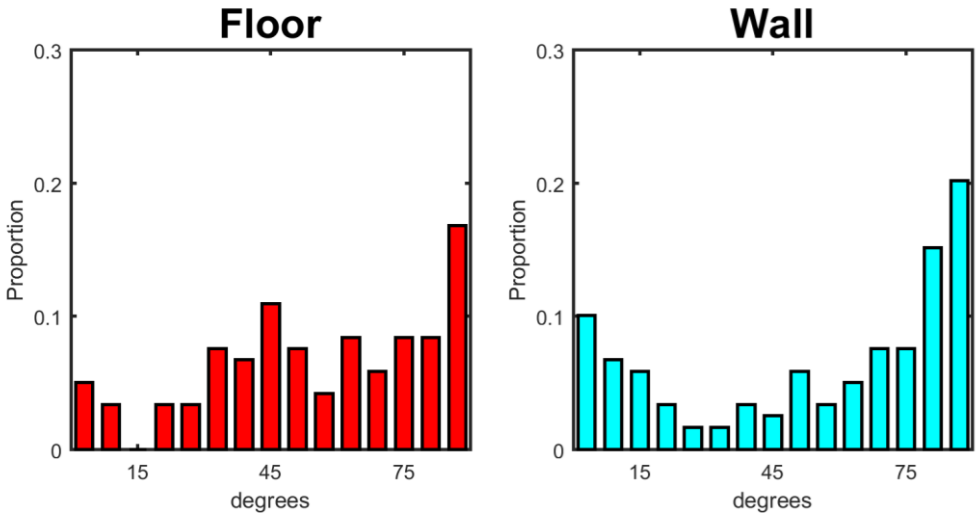

Figure 7-12 Grid field orientations.

Distributions of the grid field major axis orientations between floor (left) and wall (right). Note the peak on the wall distribution for the 90° angle corresponding to the vertical axis on the wall.

The second approach used to assess the spatial characteristics of grid fields was to repeat the analyses on grid fields directly (see 5.6.5). For each cell, the grid field with the highest firing rate was chosen as the representative example of the cell and compared across surfaces. These analyses returned results similar to those obtained with the spatial autocorrelogram method although with less pronounced effects (field size: floor = 572 $\pm$ 52 cm^2, wall = 685 $\pm$ 63 cm^2, t_{100} = -1.72, p = 0.089; major axis: floor = 33.3 $\pm$ 1.82 cm, wall = 38.8 $\pm$ 2.03 cm, t_{100} = -2.59, p = 0.011; minor axis: floor = 21.2 $\pm$ 0.95 cm, wall = 22.6 $\pm$ 1.00 cm, t_{100} = -0.87, p = 0.38; aspect ratio: floor = 0.96 $\pm$ 0.067 cm, wall = 1.75 $\pm$ 0.060 cm, t_{100} = -1.76, p = 0.082).

In summary, overall these results show that the grid cell spatial firing pattern was substantially affected between horizontal and vertical locomotion. These results, thus show that while the general grid code displays a substantially altered pattern in the firing rate (both the mean and peak firing rate of cells were reduced on the wall), spatial activity (grid score was reduced in contrast to the stripe score which was increased) and grid field characteristics (increased area, length of the axes and different shape). Put together, these results argue that the spatial metrics of grid cells are altered on the climbing wall.

7.2.4 Large wall experiment

The floor-wall experiment was originally designed to test the reference frame hypothesis, and specifically that the firing pattern of grid cells is modulated by the locomotion plane. In contrast to the vertical stripes reported on the pegboard (Hayman et

al., 2011), the reference frame hypothesis predicts a hexagonal firing pattern similar to that seen on the horizontal plane. The findings on the floor-wall experiment partially support the reference frame hypothesis as grid cells on the climbing wall did not produce the same pattern as on the pegboard (discussed below), but neither did they exhibit the hexagonal regular pattern (dramatic drop in the grid score) nor kept the same spatial properties (reduced coverage, reduced number of fields and increased field size). As mentioned before, these results argue that the general spatial metrics are altered on the climbing wall. However, it is not possible to rule out the hypothesis that on walls of larger size than the one tested in the floor-wall experiment (small size = 80 x 120 cm, large size = 120 x 120 cm, see displayed. This possibility was explored in the pilot study termed "large wall experiment".

7.2.4.1 *Experimental design*

One experienced rat was implanted in the MEC and recorded on the large wall (5.2.4 Large wall). Given the large extent of the wall (2 × 2 m) the rat did not sample the entire surface in a single session, so it was necessary to record multiple trials across days to obtain sufficient coverage of the wall. To ensure that the cell was present across days,

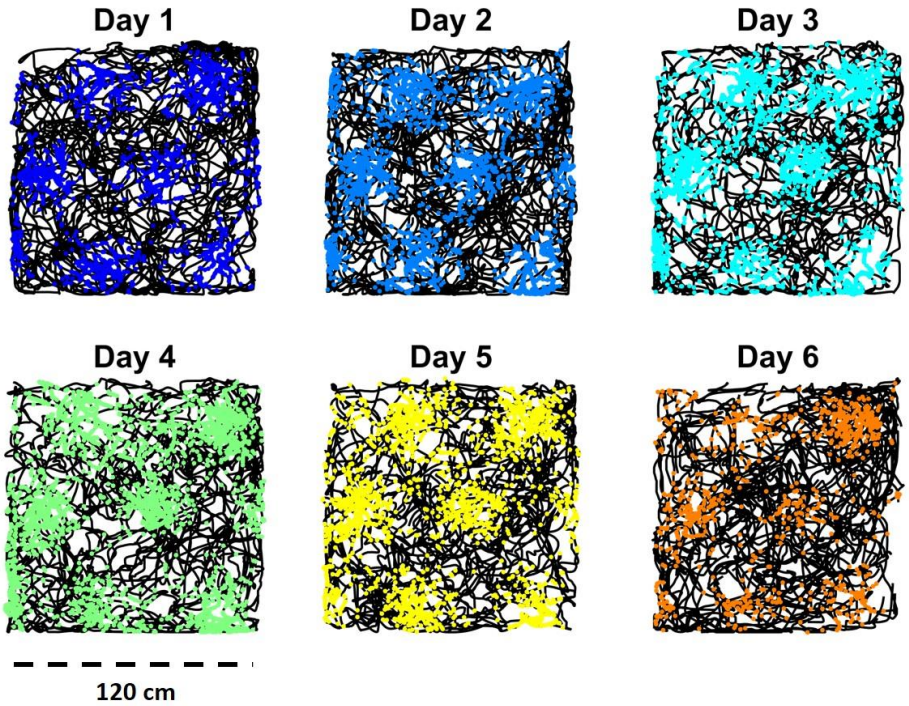

Figure 7-13 Spatial firing of a grid cell recorded across 6 days.

Open field recording sessions conducted across 6 consecutive days showing stable firing by the recorded grid cell. Note the hexagonal regularity exhibited in the open field and the stability of its spatial firing across days (color-coded for each day).

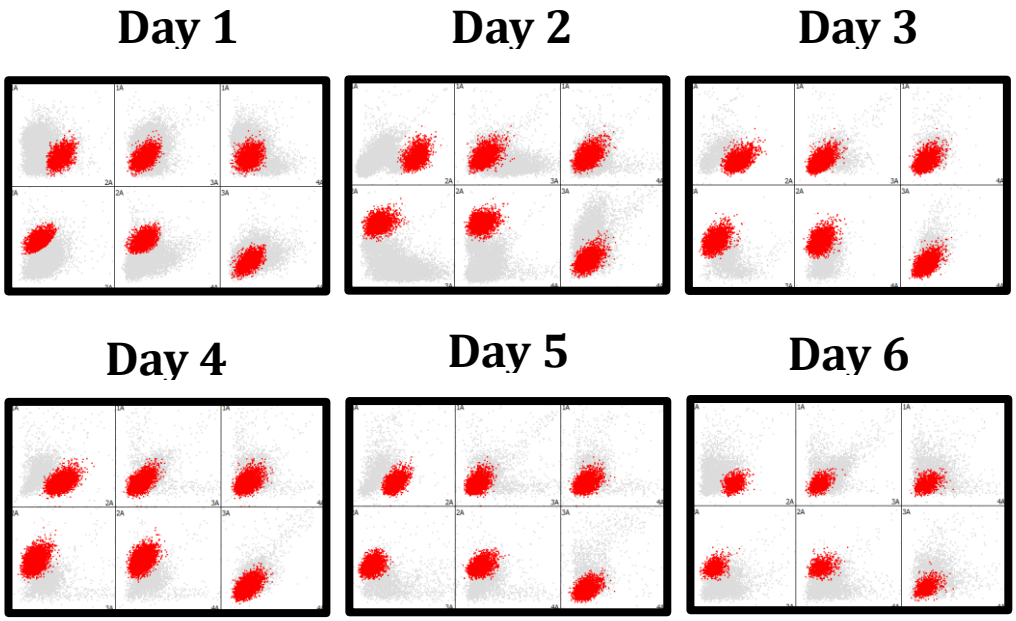

Figure 7-14 Cluster space of a grid cell recorded across 6 days.

To ensure that the same grid cell was recorded across the 6 consecutive days, a recording session in the open field was conducted before the large wall experiment was commenced. Each panel represents cluster space from tetrode 8 across 6 days. The grey dots represent all the individual spikes of all cells across 6 pairs of electrodes within the same tetrode (1A vs 2A, 1A vs 3A etc). The red dots represent the spikes from the grid cell forming the cell cluster which stayed stable across 6 consecutive days.

every day a screening session took place in the open field (5.2.1) and if a cell was assessed as present and stable by the experimenter after examination of the spatial firing in the open field (Figure 7-13) and corresponding cluster space (Figure 7-14) recordings on the large wall would begin immediately after.

7.2.4.2 *Results*

Only a single grid cell was successfully recorded from an animal showing satisfying spatial coverage of the large wall when 9 trials across 6 days were pooled together. Similarly, the spatial map of the cell was assessed by pooling together all the recorded trials. Like in the floor-wall experiment, the grid cell did not produce a vertical stripe but showed one large firing "patch" (mean firing rate 1.4 Hz, peak firing rate 9.4 Hz) which stayed stable across days (Figure 7.15A-C). To test the hypothesis that the grid cell exhibited six-fold symmetry in its spatial firing, the spatial autocorrelogram was obtained and the grid score determined (Figure 7.15) which showed a negative value (-0.3). Therefore, the firing pattern exhibited by only one cell recorded in this pilot experiment suggests that even on a very large surface, grid cells produce "blobs" of firing of larger size

compared to the open field, but the regular hexagonal pattern which characterizes grid cell firing on the horizontal plane is lacking in the vertical.

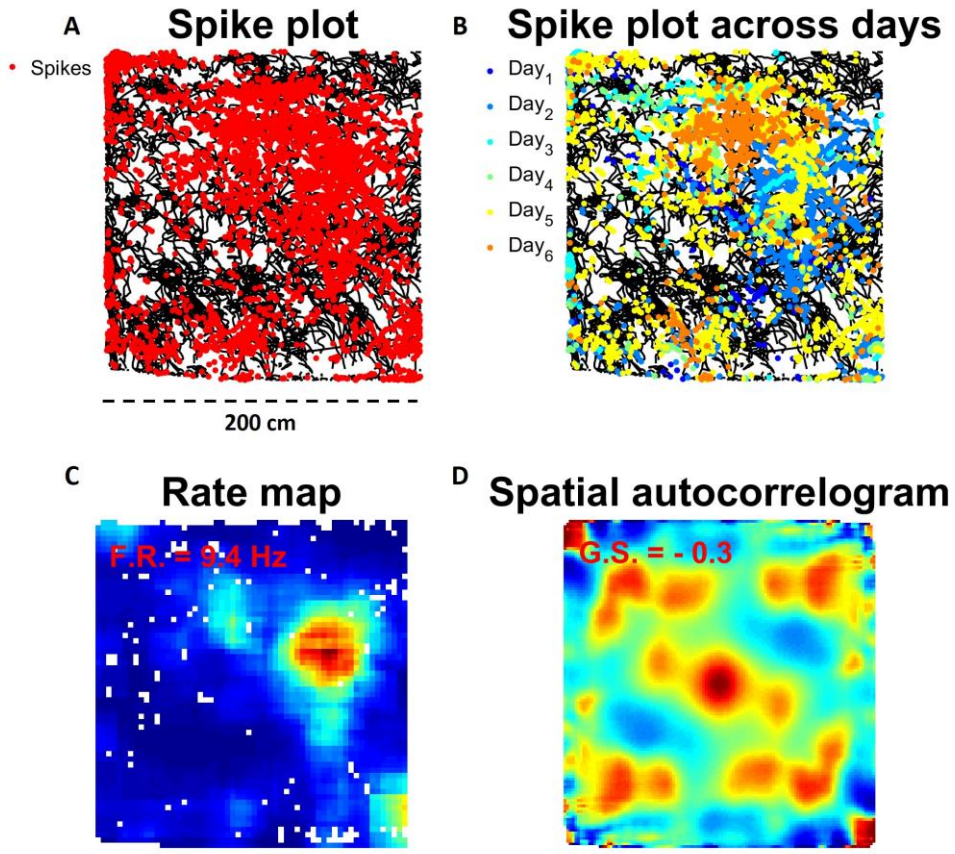

Figure 7.15 Grid cell on the large wall.

Multiple trials of a single grid cell across 6 consecutive days on the large wall. (**A**) Spike plot representing the cumulative track (black line) and the spikes (red dots) across trials from 6 days. (**B**) Similar to (**A**), color-coded spikes correspond to the day of the recording. Note the consistency in the spatial activity of the cell across days. (**C**) The rate map with the peak firing rate of the cell in the top left corner highlights the spatial firing of the cell. (**D**) The spatial autocorrelogram reveals the absence of periodic firing on the wall as quantified by the negative grid score represented in the top left corner in red.

7.2.5 Histology

Post-hoc histological analysis of the tracks confirmed that the target brain areas (HPC and MEC) were successfully hit by the electrodes during implantation (Figure 7-16).

7.3 Discussion

The aim of the floor-wall experiment was to address the spatial representation by place and grid cells in rats climbing on a vertical wall and compare their representation to

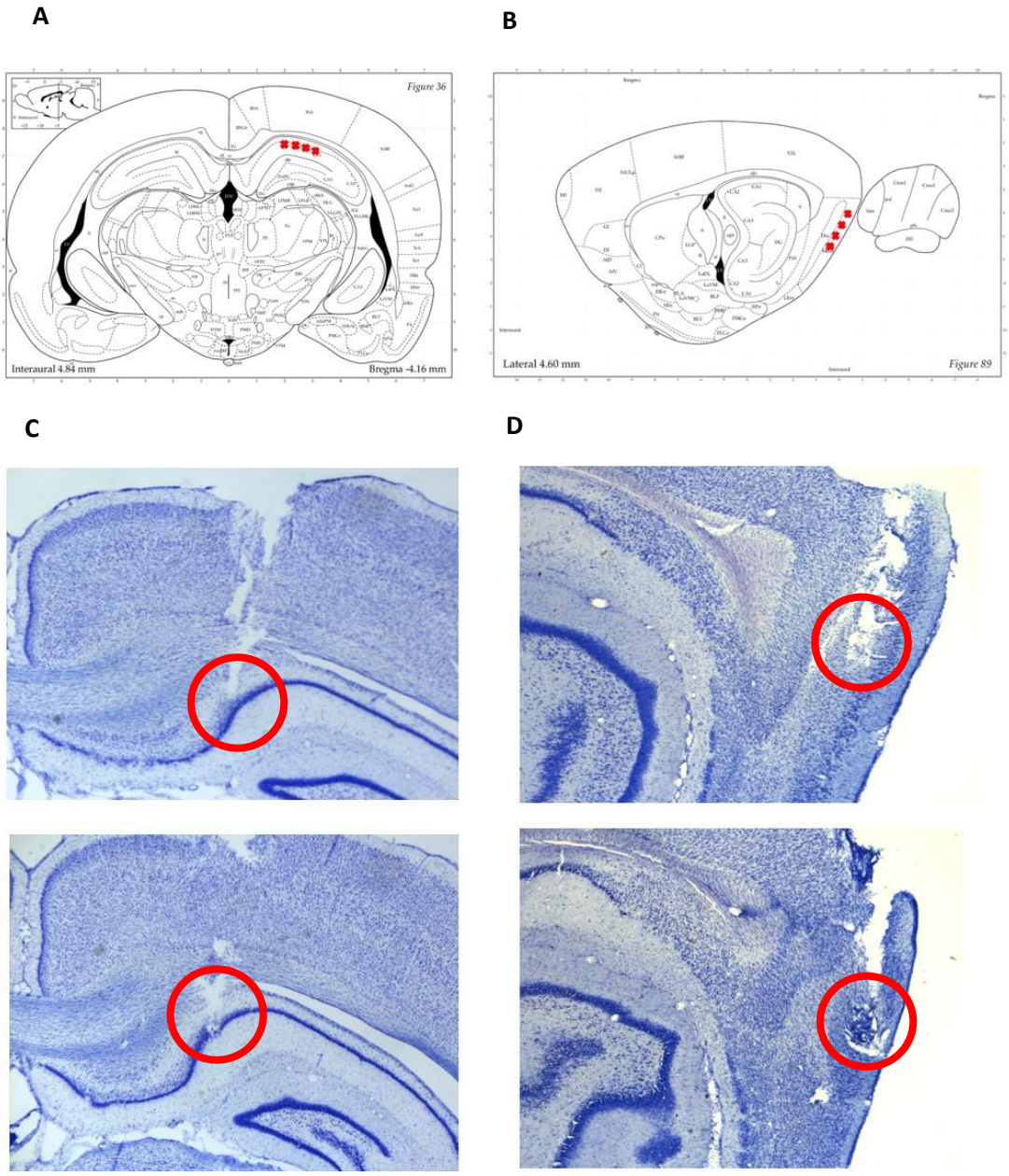

Figure 7-16 Target brain areas and histological confirmation.

Four representative examples of histology conducted using thionin solution for staining cell bodies. Schematic representation showing: (**A**) coronal view of the rat brain at the coordinates used for HPC implantation; (**B**) sagittal view of the rat brain at the coordinates used for MEC implantation. The red crosses represent the target area where tetrodes were aimed to
Representative histology conducted with thionin solution for staining cell bodies showing track of electrodes hitting the target area: (**C**) two coronal slices with clear tracks in the pyramidal layer of the hippocampus, and (**D**) two sagittal slices with clear tracks in the superficial layers of MEC.

the horizontal plane. In particular, this experiment was designed to test the reference frame hypothesis formulated in order to explain the stripe-like firing previously observed on the pegboard apparatus by Hayman et al., (2011) and observed in the experienced pegboard experiment (Chapter 6). The results showed that place and grid cells modified

their activity on the wall, suggesting that the spatial representation of space across dimensions is not identical. In the following paragraphs, the interpretation of the results obtained from the floor-wall experiment only will be discussed here. The general discussion of the results from both experiments presented in this thesis will be provided in chapter 9 where a more general and synthetic approach to the findings will be attempted.

7.3.1 Place cells on the wall

The first unexpected finding reported in this thesis concerning place cells on the vertical plane is that they were mostly silent as the majority of them did not produce spatially modulated firing on the wall. Accordingly, a dramatic drop in the mean and peak firing rate of cells was observed on the wall compared to the floor, suggesting that the whole hippocampal network showed significant reduction in its firing activity. This finding suggests that during locomotion on the wall, a smaller subset of place cells is actively recruited and contribute to the representation of vertical space. Nonetheless, spatial firing on the vertical plane mostly did not show significant changes, meaning that the more limited recruitment did not seem to interfere with the "quality" of place cell encoding. Indeed, place cells displaying spatial activity on the vertical plane showed no significant differences in the firing rate (both mean and peak firing rate of active cells was not different) nor in spatial firing (both spatial information and coverage). Moreover, place field properties on the wall were mostly similar to the floor. This finding thus suggests that the spatial inputs to place cells did not carry information substantially different between surfaces.

Overall these findings support several theoretical considerations. First, movements on the wall do not qualitatively disrupt place cell firing but reduce the number of neurons which are recruited during vertical locomotion. This represents an interesting and unexpected result as place cell responses have been tested under a variety of circumstances involving geometrical (Gothard et al., 1996; O'Keefe and Burgess, 1996), contextual (Anderson and Jeffery, 2003; Leutgeb et al., 2004) and reward-related (Dupret et al., 2010; Hok et al., 2007) manipulations but, to the best of our knowledge, there are no situations where place cell firing has been shown to silence so dramatically. This finding raises relevant questions regarding the nature of the spatial inputs turning off during vertical locomotion.

In conclusion, these results show that place cell ensemble activity was affected by vertical locomotion, but when they did form place fields, their representation was not

different compared to the horizontal plane.

7.3.2 Grid cells on the wall

A radically different scenario was exhibited by grid cells on the vertical plane. Indeed, different from place cells, grid cells always produced spatially modulated firing on the wall. Moreover, grid cells did not show the columnar firing pattern reported by Hayman et al., (2011) and also seen in the horizontal configuration of the "experienced pegboard experiment" (for a more general discussion of both experiments see below). However, the spatial firing pattern displayed by grid cells on the wall strongly differed from the one on the horizontal plane in three key features:

i) the hexagonal regularity of the spatial maps on the wall was dramatically impaired;
ii) grid cells overall showed substantial reduction in the number of grid fields on the wall;
iii) the fewer fields on the wall had a larger size compared to the floor. Importantly, the last two observations explain the lack of significant effect in the spatial coverage between floor and wall.

The initial hypothesis raised to explain these results was that, consistent with the smaller number of fields but of increased size, the spatial scale of grid cells on the vertical plane was substantially increased. Given that the methods to assess regularity (i.e. grid score) depends on a minimum number of 3 fields to work, it was speculated that on another wall of larger size, where more grid fields could appear, an expanded grid could then be displayed. Therefore, this rationale motivated the pilot study "large wall experiment" aimed to test the hypothesis that on a 2 m square wall grid cells could form regular grids of expanded size compared to the horizontal plane. Given the combined difficulties in carrying long-lasting recordings while keeping the animal engaged in the task and keeping the same ensemble of cells stable for several consecutive days, only one grid cell from one animal was recorded across 6 consecutive days. Consistent with the floor-wall experiment, the grid cell did not produce vertical stripes as reported on the pegboard (Hayman et al., 2011) but showed one large "patch" of firing and no evidence of a regular grid. Therefore, even though one cell only is available at the moment, this pilot experiment indicates that even on a very large vertical plane, grid cells may not produce vertical grids.

Put together, the combined findings of the “floor-wall experiment” and the pilot “large wall experiment” lead to the conclusion that the overall regularity of the grid cell spatial firing pattern on the vertical plane is impaired compared to the horizontal. Given that grid cell periodic firing is hypothesized to provide invariant metrics of space, and such metrics are heavily altered on the wall, it is possible to conclude that the spatial metrics encoded by grid cells on the wall are thus altered. It should be noted that the spatial maps exhibited by grid cells on the climbing wall showed a lack of regular firing and enlarged firing fields, a finding which resembles the expansion of the grids responding to spatial novelty (Barry et al., 2012a). However, across repeated exposures, grid cell representation has been shown to shrink down to the familiar scale along with the increasing regularity of the grid (Barry et al., 2012a). Importantly, rats used in this study were already extensively familiarized with the experimental apparatus before the first recordings of grid cells, so the bias of novelty on the vertical plane cannot account for the firing patterns observed here. Accordingly, these results argue that the global impairment on the wall is a permanent feature of grid cell firing in the vertical plane.

7.3.3 Working hypothesis

The overall results presented so far show that grid cell firing on the wall was not disrupted by movements along gravity but maintained highly spatial spiking modulation. However, the regularity of grid cell firing dramatically dropped and showed substantial increases in the spatial scale compared to the horizontal. Overall these results generated the hypothesis that the expanded and altered pattern on the wall reflected an impaired ability to perform path integration on the vertical plane is suggested. The combined findings of the reduced spatial coverage, reduced number of fields and expanded firing pattern suggests that grid cells may not be able to compute distances in the vertical but instead they underestimate them (encode smaller distances compared to actual movements during climbing). Based on this reasoning, the following hypothesis was proposed: the underestimation in the encoding of instantaneous displacement depends on an impaired input signalling instantaneous speed. In other words, the increase in the scale of the spatial representation on the wall could be driven by a substantial miscomputation of the instantaneous speed during climbing which ultimately affected the ability of grid cells to track an animal’s displacement. Therefore, based on this working hypothesis the following prediction was made: the neural codes for the encoding of instantaneous speed will be affected during climbing and specifically that speed is underestimated compared to

the horizontal. This hypothesis was tested by examining two neural codes for the encoding of instantaneous speed: i) LFP theta, of which frequency is well documented to correlate with running speed; ii) speed cells, recently described neurons which have been hypothesized to provide the context-invariant speed signal useful for grid cell capacity to perform odometry. Consistently, the speed modulation of grid cells, as well as their temporal encoding has been addressed and compared between floor and wall. In the next chapter, all the results from a number of temporal analyses of LFP theta, grid cells, and the simultaneously recorded speed cells, aimed to test this working hypothesis, will be shown and interpreted.

8 Neural encoding of speed on the vertical plane

The capacity to perform effective path integration depends on a number of types of spatial information which include instantaneous speed and heading direction. Previous experiments have shown that head direction cells, neurons that are thought to signal directional heading during navigation, maintain their encoding on the vertical plane. Therefore, the hypothesis that the encoding of speed could be similarly maintained during climbing or instead, similarly to grid cells, impaired on the wall, was explored. Based on the underestimation of speed hypothesis, the prediction that the speed signal upstream of grid cells underestimates the instantaneous speed during movements on the vertical plane compared to horizontal ones was made. Accordingly, the activity of the neural correlates of speed so far identified, namely LFP theta oscillation, grid cell speed modulation and the recently described speed cells, were examined.

8.1 Theta oscillation

The first set of analyses addressed LFP theta oscillation. Overall, 41/42 sessions from 12 rats used in the study from Chapter 7 with tetrodes in the MEC and 10/11 sessions from 4 rats with electrodes in the HPC were included in all the following analyses. The mean theta frequency computed with the power spectrum analysis (5.6.2.1) showed no significant differences between MEC and HPC in the open field (mean theta frequency: MEC = 8.6 ± 0.08 Hz, HPC = 8.9 ± 0.18 Hz; two-tailed un-paired: t_{50} = -1.75, p = 0.086). Therefore, recordings of LFP theta from both HPC and MEC were pooled together for all following analyses.

In the next paragraphs, all the results between surfaces were obtained by pooling recordings from different animals (n = 16) (see 10.3 for extra analyses addressing grid cell properties between animals).

8.1.1 Theta oscillation across speed

Given the substantial difference in the speed of movements between floor and wall, all the following analyses further investigated the differences in LFP theta frequency between surfaces as a function of running speed (Figure 8-1A). A repeated measure ANOVA revealed a significant effect of speed ($F_{8,408}$ = 113, p < 0.0001), a significant effect of surface

($F_{1,51}$ = 99.0, p < 0.0001) and a significant interaction ($F_{8,408}$ = 74.8, p < 0.0001). *Post-hoc* comparisons adjusted with Bonferroni corrections (p < 0.0055) revealed a significant decrease on the wall across all speeds. Consistent with previous results and the specific hypothesis made, these findings indicate that theta oscillation was affected and its frequency specifically reduced during climbing on the wall.

The next step addressed whether also the power of theta oscillation changed between surfaces and that was assessed by comparing the signal to noise ratio (Figure 8-1B) of theta power across 3 speed bins (width = 6 cm/s). A repeated measure ANOVA revealed a significant effect of speed ($F_{2,102}$ = 18.2, p < 0.0001), a significant effect of surface ($F_{1,51}$ = 15.5, p < 0.0001) and a significant interaction ($F_{2,102}$ = 10.4, p < 0.0001). *Post-hoc* comparisons adjusted with Bonferroni corrections (p < 0.017) revealed a significant decrease on the wall across all speeds.

In summary, consistent with the underestimation of speed hypothesis, the results of LFP theta comparison between floor and wall showed that at least at the population level, the encoding of instantaneous speed was underestimated on the wall compared to the floor.

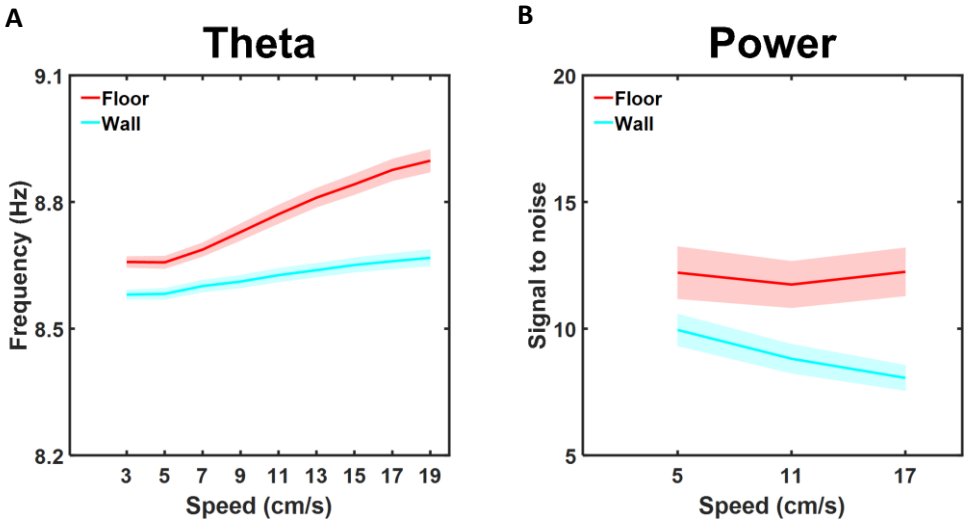

Figure 8-1 LFP theta between floor and wall.

Effects of vertical locomotion on LFP theta compared to horizontal in the 2-20 cm/s speed range.
(**A**) Plots representing the mean ± S.E.M. theta frequency during climbing on the wall (turquoise) compared to the floor (red).
(**B**) Plots representing the mean ± S.E.M theta power (assessed as signal to noise ratio) during climbing on the wall (turquoise) compared to the floor (red).

8.1.2 Properties of LFP theta between surfaces

To better characterize the substantial reduction in theta frequency observed on the wall (Figure 8-1), LFP theta properties such as the correlation value, intercept and slope of

the speed to theta relationship (5.6.2.2.2) were compared between surfaces.

Comparisons in the slope of LFP theta revealed a dramatic drop on the wall compared to the floor (Figure 8.2A; floor = 0.016 ± 0.001 cm^{-1}, wall = 0.0006 ± 0.001 $^{-1}$, t_{51} = 11.2, p < 0.0001). This result provides preliminary evidence that at least type I theta oscillation (Kramis et al., 1975), which is thought to be involved with path integration processes (Wells et al., 2013), was significantly impaired on the wall compared to the floor.

To address whether also type II theta showed similar effects between surfaces, the next step was to compare the intercept of the speed to theta relationship which was weakly but significantly reduced on the wall compared to the floor (Figure 8.2B; floor = 8.59 ± 0.01 Hz, wall = 8.56 ± 0.01 Hz, t_{51} = 2.45, p = 0.018).

Finally, to address LFP theta encoding of speed, the z-fisher transformation (5.6.2.2) of the r correlation values of the speed-theta relationship were compared. The analysis revealed a significant decrease on the wall compared to the floor (Figure 8.2C; floor = 1.97 ± 0.12, wall = 0.95 ± 0.12, t_{51} = 9.21, p < 0.0001).

Therefore, consistent with the underestimation of speed hypothesis, these findings suggest that during climbing the encoding of the instantaneous speed by LFP theta oscillation was affected compared to the horizontal and it was underestimated on the wall as predicted. Importantly, the intercept was mildly affected compared to the slope of the speed-theta relationship which was substantially decreased.

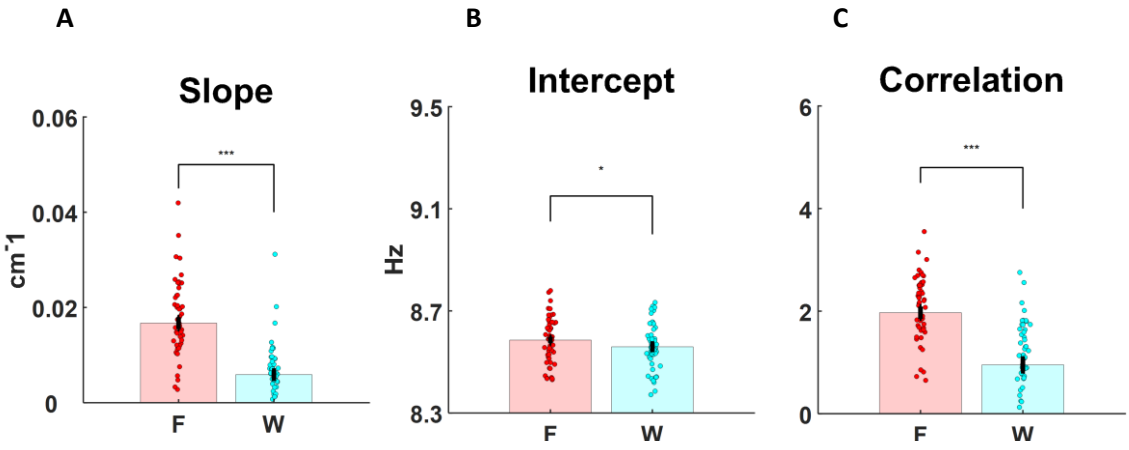

Figure 8.2 Speed-LFP theta properties.

Speed-LFP theta properties represented as coloured bars showing the mean ± S.E.M. with superimposed dots for each data point between floor (F) and wall (W).
The comparisons revealed significant decrease in the slope (**A**), intercept (**B**) and correlation (**C**) of the speed-LFP theta relationship.

8.2 Relationship between grid cell firing and speed

Two major classes of computational models aimed at explaining grid cell firing pattern formation have been proposed so far (Giocomo et al., 2011a). The first class, referred to as CANMs, posits that the regular grid cell pattern derives from the global network activity of the MEC, as a result of the operation of a 2D neural attractor (McNaughton et al., 2006). Specifically, thanks to the reciprocal phase-dependent interactions between grid cells, a bump of activity is stabilized in the 2D sheet of neurons (3.2.3.2). Different mechanisms have been proposed to explain the shift of the bump of activity around the attractor reflecting the animal movements in real space. However, an important requirement emerging from these models is that along with the directional information, the input moving the bump must be also incorporating information about the speed of the animal (Burak and Fiete, 2009; McNaughton et al., 2006). Importantly, consistent with CANMs, a number of studies focusing on grid cell firing found that a substantial proportion of them show significant speed modulation (Sargolini et al., 2006; Wills et al., 2012).

The second class of computational models proposed for grid cell firing pattern formation is the OIM (3.2.3.1) which posits that grid cell periodic firing is generated in the cell soma from the integration of upstream inputs oscillating in the theta band (Burgess et al., 2007; Bush and Burgess, 2014; Jeewajee et al., 2008a). While some of these theta modulated cells display intrinsic firing frequency modulated by running speed (Welday et al., 2011), termed basal oscillators, other theta cells show combined modulation by both running speed and heading direction, and are termed velocity-controlled oscillators, (Welday et al., 2011). Therefore, when the rat is heading towards the direction that a VCO is maximally tuned to, the frequency of that VCO is higher than that of the basal oscillator. The two upstream theta oscillators drive the grid cell membrane potential to oscillate in the theta range explaining the theta modulation of the grid spike train (Jeewajee et al., 2008a). Based on this theoretical framework, the following considerations can be made. As a natural consequence of the discrepancy between the oscillatory inputs, grid cell firing frequency is higher than that of the basal oscillators. At the large ensemble level, this signal is thought to coincide with the LFP theta, explaining phase precession in grid cells (Hafting et al., 2008; Jeewajee et al., 2008a; O'Keefe and Recce, 1993).

In summary, both models predict that grid cell firing should show modulation by speed, both at the firing rate level (Sargolini et al., 2006; Wills et al., 2012) and in theta intrinsic firing frequency (Jeewajee et al., 2008a; Wills et al., 2012). Importantly, one recent study showed that these two signals are independent (Hinman et al., 2016), suggesting that

they may depend on segregated speed signals upstream of grid cells. To explain the spatial enlargement of grid fields on the wall, the underestimation of speed hypothesis was formulated. The reduction of LFP theta in encoding speed on the wall provides preliminary evidence for this view. However, a prediction of this hypothesis is that grid cells also showed reduced modulation by speed. According to CANMs and OIMs, the underestimation of speed information by grid cells occurs respectively at the level of firing rate and intrinsic firing frequency (spike train theta frequency). In the next paragraphs, grid cell speed modulation was addressed following both approaches.

8.2.1 Speed modulation between floor and wall

Consistent with CAN models, the hypothesis that grid cell speed modulation was reduced during vertical navigation was tested. To address this question, speed lines representing mean firing rate across speed were produced (Figure 8-3) for all cells and the corresponding p-value obtained (Wills et al., 2012). Overall 70/119 (69 %) grid cells showed significant speed modulation on the floor in contrast to the 55/119 (46 %) on the wall. McNemar's test determined that there was not a statistically significant difference in the proportion of speed modulated cells between floor and wall ($p = 0.069$). The properties of grid cell speed modulation between floor and wall were then characterized. To do this, only those cells showing significant speed modulation on at least one surface between floor and wall (90/119, 76 %) were included in the analyses.

To test whether locomotion on the vertical plane affected the strength of the speed modulation, the z-fisher transformations of the speed line scores (5.6.6.2) between speed modulated cells (n = 90) were compared and the analyses revealed a significant decrease on the wall compared to the floor (Figure 8-4A; floor = 1.25 ± 0.08, wall = 0.69 ± 0.11, $t_{89} = 4.41$, $p < 0.0001$). Moreover, both the intercepts and slopes were significantly decreased (Figure 8-4B-C; intercepts: floor = 0.94 ± 0.07 Hz, wall = 0.71 ± 0.06 Hz, $t_{89} = 3.85$, $p < 0.0001$; slope: floor = 0.024 ± 0.0025 cm^{-1}, wall = 0.013 ± 0.0028 cm^{-1}, $t_{89} = 3.60$, $p < 0.001$). Put together, these findings show that grid cell speed modulation was affected during climbing on the wall, as the correlation in the speed modulation was decreased and their firing rate reduced across all speeds. Importantly, according to CANMs, the significant reduction in the mean firing rate across speed observed on the wall is consistent with the global expansion of the spatial metrics carried by grid cells. Therefore, together with the reduced LFP theta oscillation, grid cell firing suggests that the encoding of speed on the wall was reduced.

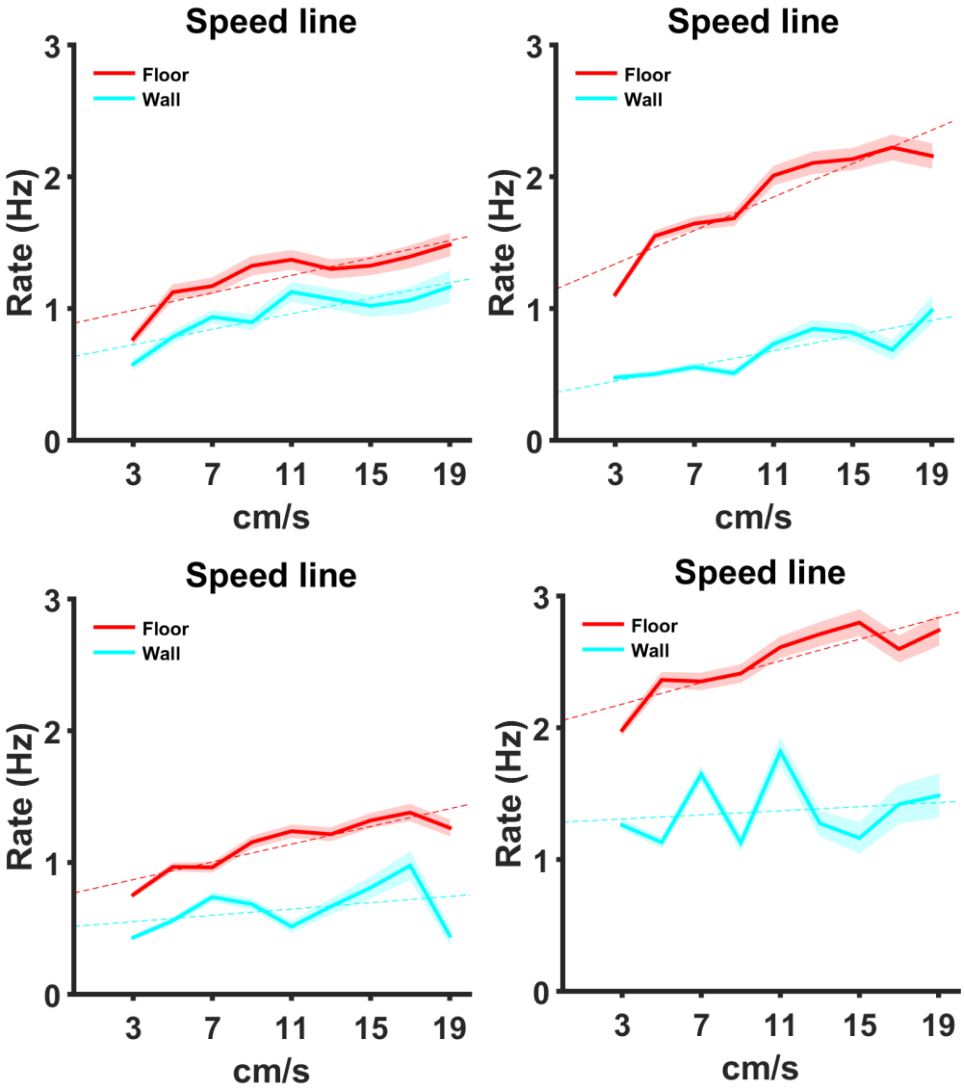

Figure 8-3 Examples of grid cells speed modulation.

A large subset of grid cells showed significant speed modulation of their firing rate as s. Four examples of speed lines are here shown representing the mean ± S.E.M. firing rate across speed bins (2 cm/s) on the floor (red) and wall (turquoise).

8.2.2 Intrinsic firing frequency between floor and wall

The oscillatory interference model (OIM) is a prominent model proposed to explain grid cell firing patterns which is based on the integration of multiple oscillatory signals converging onto the grid cell soma. Relevant for this thesis, the relative difference between the frequency of the basal oscillators and VCOs plays a crucial role in setting the scale of grid cells (Jeewajee et al., 2008a). In particular, the OIM predicts that a greater frequency difference drives grid cells to display smaller scale, in contrast to a reduced frequency difference which drives grid cells to display a larger scale grid (Giocomo et al., 2011b;

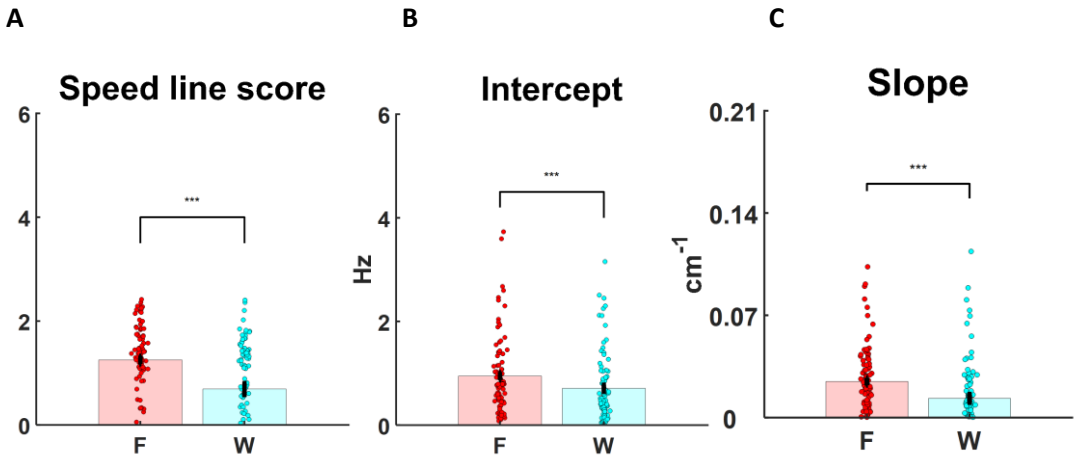

Figure 8-4 Speed line properties of grid cells between surfaces.

Speed line properties represented as coloured bars showing the mean ± S.E.M. with superimposed dots for each data point between floor (F) and wall (W).
The comparisons revealed significant decrease in speed line score (**A**), intercept (**B**) and slope (**C**) of speed lines on the wall compared to the floor.

Jeewajee et al., 2008a). The observation that during vertical locomotion on the wall the slope of the speed-theta relationship is decreased and the grid cell firing pattern is enlarged, is consistent with the OIM. However, the OIM predicts that the difference between grid cell intrinsic firing frequency and LFP theta correlates with the spatial scale of the cell (Jeewajee et al., 2008a). Accordingly, the hypothesis that grid cell intrinsic firing frequency was reduced as well as the difference with the ongoing LFP theta frequency was tested.

First, the number of grid cells showing significant theta modulation between surfaces was compared and the analyses revealed that 78/119 (66 %) of grid cells showed significant rhythmicity on the floor compared to 57/119 (48 %) on the wall. The McNemar's test determined that there was a statistically significant difference in the proportion of theta modulated grid cells between floor and wall, ($p < 0.001$).

Next, the hypothesis that theta modulated grid cells showed reduced frequency on the wall was tested. Consistent with the prediction from the OIM, the comparisons revealed a significant decrease in the intrinsic firing frequency on the wall compared to the floor (Figure 8-5; 9.3 ± 0.1 Hz on the floor and 8.9 ± 0.1 Hz on the wall, two-tailed paired: $t_{78} = 3.98$, $p < 0.001$).

Overall these results show that, similar to LFP theta oscillation, theta modulation of grid cell firing was still present on the wall but its occurrence and frequency were reduced compared to the floor. It should be pointed out though that because frequency is modulated by speed (Jeewajee et al., 2008a), the slower movements displayed on the wall

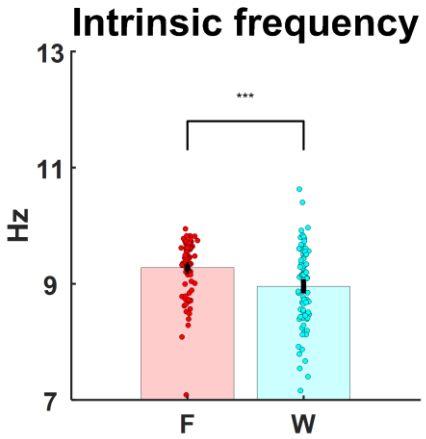

Figure 8-5 Intrinsic firing frequency between floor and wall.

Intrinsic firing frequency of rhythmic grid cells represented as coloured bars showing the mean ± S.E.M. with superimposed dots for each data point between floor (F) and wall (W). The comparisons revealed a significant decrease on the wall compared to the floor.

could be a reason for the observed reduction during climbing. To rule out this possibility, future analyses are therefore needed. Specifically, what remains to be elucidated is whether on each surface the relationship between the intrinsic firing frequency and speed was changed. Moreover, addressing whether the difference between grid cell intrinsic firing frequency and the LFP theta is reduced on the wall across speed will ultimately show whether the main predictions of the OIM are met and possibly provide further evidence for it.

8.3 Speed cells

Both classes of computational models, OIM's and CANMs, posit the existence of a context-invariant signal encoding the instantaneous speed of the animal which directly or indirectly terminates onto grid cells. A new cell-type of spatially-modulated neuron was recently reported in the HPC and MEC and due to their encoding of speed they were termed speed cells (Kropff et al., 2015). Consistent with theoretical models, preliminary evidence showed that at least a subset of these cells are theta modulated cells and may indeed be upstream of grid cells (Buetfering et al., 2014; Kropff et al., 2015).

The finding described in this thesis that grid cells show enlarged firing fields and reduced speed modulation on the wall raised the hypothesis that during climbing, the speed signal is underestimated (i.e. underestimation of speed hypothesis). The findings so far obtained support this view, both at the large cell ensemble level, as shown by LFP theta oscillation, and at the level of grid cell firing, as shown by reduced grid cell speed modulation and reduced intrinsic firing frequency. In the present section, the hypothesis that speed cells would also show impairment in the encoding of speed was addressed, specifically that at the cellular-level representation of speed during climbing on the wall would be underestimated.

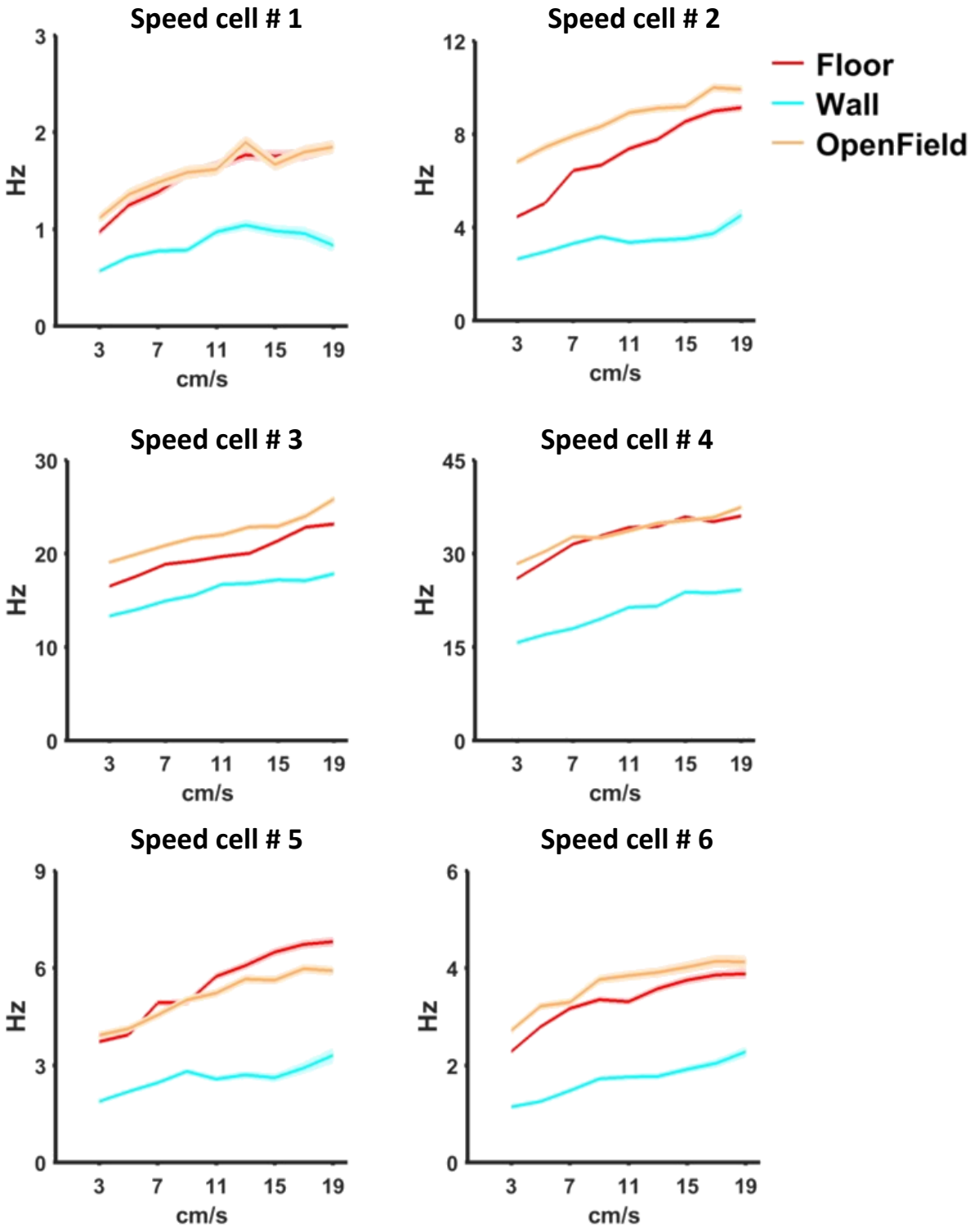

Figure 8.6 Examples of speed lines by across surfaces.

Six examples of speed cells showing speed lines representing mean firing rate ± S.E.M. across speed.
Note the linear relationship expressed by speed cells across three surfaces (floor in red, wall in turquoise and open field in orange). Note the similarity in the speed lines between floor and open field in contrast to the speed line on the wall always showing reduced firing rate compared to both horizontal planes.

8.3.1 Speed encoding between surfaces.

Consistent with a previous study (Hinman et al., 2016), a total number of 35 neurons (2% of the overall MEC population) recorded on the floor-wall apparatus and subsequently in the open field passed criteria for negatively-modulated speed cells (i.e. negative slope) having both speed and speed line score values lower than cut-off threshold derived from the 1st percentile of the shuffling distribution.

In contrast, a total number of 363 neurons from 9 rats for positively modulated speed cells having both speed and speed line score values lower than cut-off threshold derived from the 99th percentile of the shuffling distribution (5.6.8.2.3). In this thesis, only positively-modulated speed cells were included in the analysis.

As expected, these speed cells showed neither spatial nor heading modulation on any of the experimental *apparatus*, but displayed typical speed lines (3.2.4) representing the increase of the mean firing rate with running speed (Figure 8.6). On the floor 266/363 (73 %) of overall speed cells passed criteria for significance compared to 132/363 (36 %) on the wall. The McNemar's test determined that there was a statistically significant difference in the proportion of speed cells maintaining speed encoding between floor and wall ($p < 0.0001$). This result thus reveals that fewer cells functioned as effective speed cells during climbing on the wall compared to the floor. Consistent with the observation that a conspicuous number of speed cells lost speed encoding on the wall, the comparisons of both speed score and speed line score (after z-fisher transformation) between surfaces revealed a significant decrease on the wall compared to the floor (Figure 8.7A; speed score: floor = 0.083 ± 0.003, wall = 0.061 ± 0.003, $t_{362} = 9.60$, $p < 0.0001$; Figure 8.7B; speed line score: floor = 1.73 ± 0.03, wall = 1.37 ± 0.04, $t_{362} = 7.47$, $p < 0.0001$). These findings thus

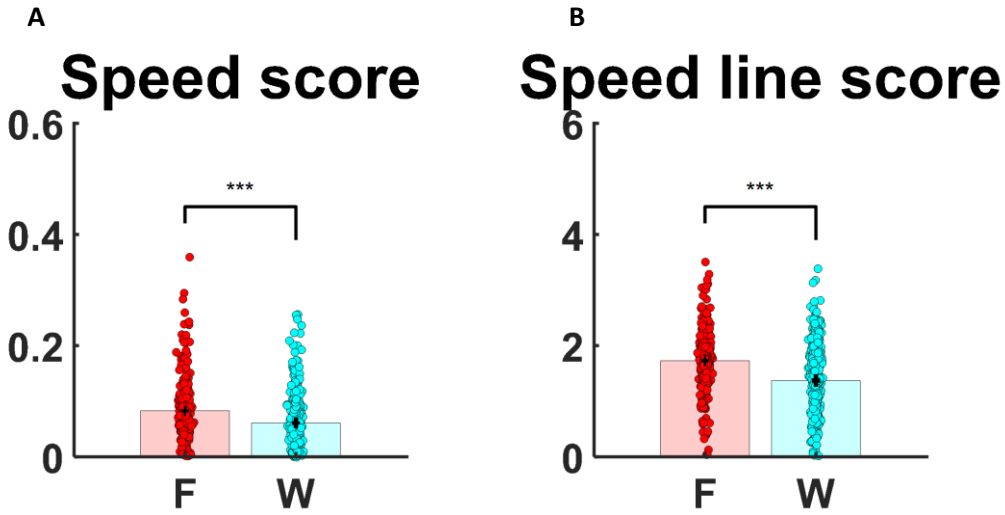

Figure 8.7 Speed encoding between surfaces.

The encoding of speed by speed cells on the wall was significantly reduced compared to the floor. Speed score (**A**) and speed line score (**B**) represented as coloured bars showing the mean ± S.E.M. with superimposed dots for each data point between floor (F) and wall (W).

suggest that the representation of speed on vertical was affected compared to the floor as fewer cells showed significant speed modulation during climbing on the wall.

8.3.2 Speed line properties between surfaces

Having shown the reduction in the number of functioning speed cells on the wall, the next step was to describe the properties of the speed lines (intercept and slope) between surfaces. Both comparisons revealed a significant decrease on the wall compared to the floor (Figure 8-8A; intercept: floor = 4.2 ± 0.3 Hz, wall =3.5 ± 0.3 Hz, t_{362} = 7.29, p < 0.0001; Figure 8-8B; slope: floor = 0.093 ± 0.007 cm^{-1}, wall =0.075 ± 0.007 cm^{-1}, t_{362} = 5.32, p < 0.0001). These results thus suggest that not only the encoding of speed was impaired on the wall, but also the firing rate of the cells was likely to be reduced on the wall compared to the floor.

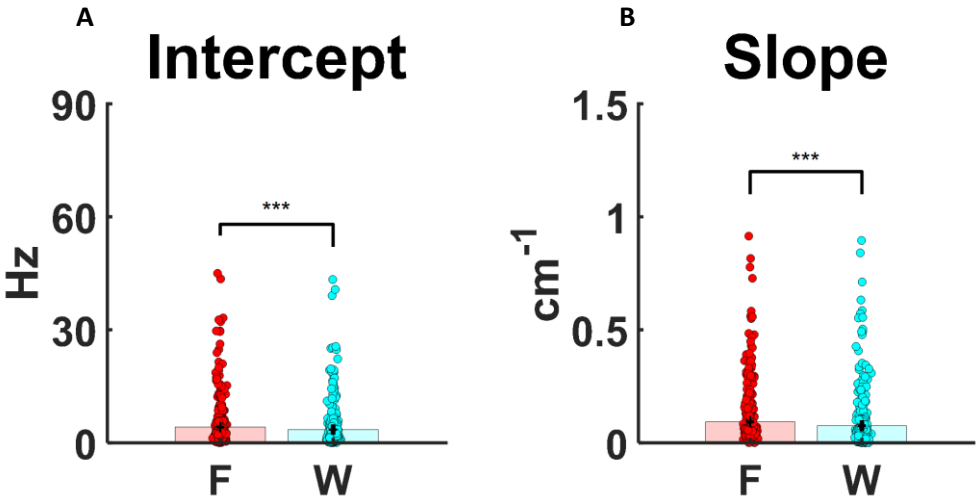

Figure 8-8 Intercepts and slopes of the speed lines between surfaces.

Intercepts and slopes of the speed lines represented as coloured bars showing the mean ± S.E.M. with superimposed dots for each data point between floor (F) and wall (W). For both the intercept and the slope, the comparisons revealed a significant decrease on the wall compared to the floor.
a significant decrease on the wall compared to the floor.

8.3.3 Speed cell firing rate between surfaces.

Similar to grid cells, speed cell firing rate was compared between surfaces and there was a significant decrease in the mean firing rate of the cells on the wall compared to the floor (mean firing rate: floor = 5.2 ± 0.4 Hz, wall = 4.2 ± 0.3, t362 = 9.68, p < 0.0001). To rule out the potential confound of the reduced speed exhibited by animals on the wall (7.2.1.2), speed cell firing rate across speed was compared between surfaces (Figure 8-9). A repeated measure ANOVA confirmed the main effect of speed ($F_{8, 2896}$ = 156.4, p < 0.0001) and

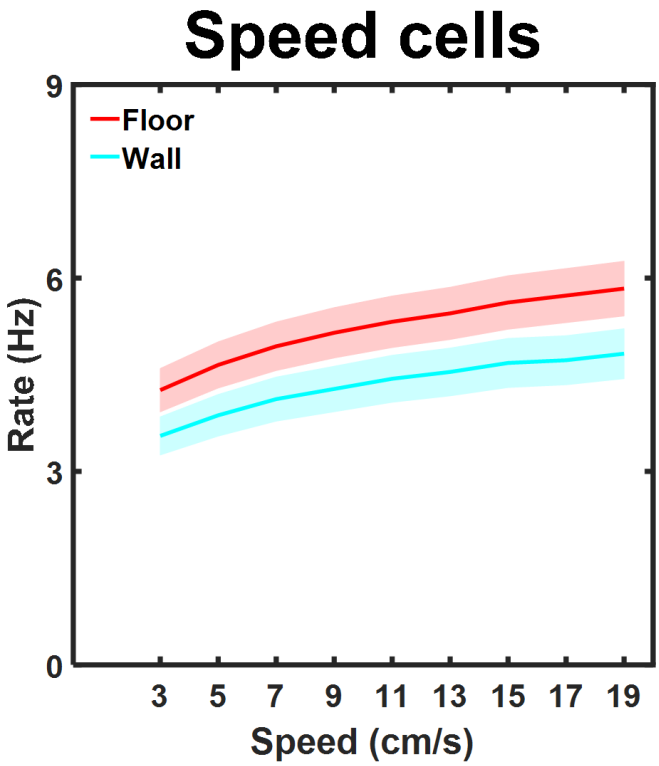

Figure 8-9 Speed cell firing rate between surfaces.

Plots representing the mean ± S.E.M firing rate of speed cells on the floor (red) and wall (turquoise). Note the reduction if the firing rate on the wall compared to the floor across the whole speed range.

revealed a main effect between surfaces ($F_{1, 362}$ = 77.0, p < 0.0001), and a significant interaction ($F_{8, 2896}$ = 15.5, p < 0.0001). *Post-hoc* comparisons adjusted with Bonferroni corrections (p < 0.017) revealed significant decrease on the wall (all speeds p < 0.001). Therefore, consistent with the underestimation of speed hypothesis, these results suggest that speed cell firing rate was reduced and so the representation of speed was underestimated during climbing on the wall.

In conclusion, overall these results suggest that consistent with the "underestimation of speed hypothesis", the neural computation of speed by speed cells on the wall was profoundly impaired. In particular, the firing rate of the cells was substantially reduced, supporting the hypothesis that the instantaneous speed during climbing on the wall was underestimated.

8.4 Discussion

In the next paragraphs, the results shown in this chapter will be discussed. For a more general discussion addressing all experiments and results presented in this thesis see Chapter 9 below.

The results obtained on LFP theta support the initial hypothesis that the neural representation of speed on the wall was underestimated. This hypothesis was initially

raised in light of the severely altered firing pattern of grid cells on the wall, particularly the enlargement of their firing fields. This observation led to the speculation that during movements on the wall the instantaneous representation of speed was miscomputed.

Three lines of evidence emerged and will be discussed in turn: a) grid fields expanded during climbing on the wall and the frequency of LFP theta oscillation was reduced across all speeds; b) consistent with both classes of computational models (CAN and OIM) grid cell firing showed similar reduction in its speed modulation; c) the firing rate of speed cells was reduced suggesting an underestimation of the instantaneous speed.

8.4.1 Theta oscillation and its relationship to grid cells

The observation that the frequency of LFP theta was reduced on the wall provided the first evidence towards the "underestimation of speed hypothesis (Figure 8-1A). Importantly, on the wall LFP theta showed substantial decrease in theta power (Figure 8-1B), suggesting that the on the whole theta functioning was partially impaired during climbing.

More detailed analyses of the speed-to LFP theta relationship revealed several aspects of the LFP theta impairments during climbing. Firstly, the slope of the speed-theta correlation was substantially reduced on the wall, unlike the intercept which had a weak (though significant) reduction (Figure 8.2A-B). Moreover, there was a significant reduction in the correlation values between speed and theta frequency on the wall compared to the floor, suggesting that the strength of the speed-theta frequency relationship was affected during climbing on the wall (Figure 8.2C). This result suggests that the putative encoding of speed by LFP theta oscillation was generally noisier during vertical movements.

The stronger reduction in the slope compared to the intercept between floor and wall poses several theoretical considerations. As discussed earlier, both experimental and theoretical studies suggested that the baseline frequency of theta oscillation (intercept of speed-theta relationship) is linked to type II theta or "alert immobility-related", and may be involved in attentional, anxiety and arousal states (Vanderwolf, 1969; Wells et al., 2013); see also 3.1.1). The observation that the intercept of theta frequency was mildly reduced on the vertical plane, suggests that neither attentional nor arousal processes were substantially affected on the vertical plane (Vanderwolf, 1969; Wells et al., 2013). In contrast, the dramatic decrease in the slope of the speed to theta frequency reveals a clear effect of the vertical plane on type I theta (Kramis et al., 1975; Wells et al., 2013).

A number of both experimental and theoretical studies suggest a link between theta

oscillation type I in path integration processes and specifically on grid cell firing (Giocomo et al., 2011a). Indeed, temporary inactivation of the medial septum, where theta frequency is thought to be primarily generated, has been shown to disrupt grid cell firing patterns (Brandon et al., 2011; Koenig et al., 2011). Moreover, during novelty, theta frequency is significantly reduced (Jeewajee et al., 2008b), and, as mentioned before, grid cells normally show expanded firing pattern along with a less regular grid (Barry et al., 2012a). The significant reduction in the slope of the speed-theta correlation observed on the wall has strong theoretical implications. First, it suggests that the putative encoding of the instantaneous speed during climbing is affected compared to the movements on the horizontal plane across all speeds. Even though a correlation is not proof of causality, the parallel underestimation of the speed signalled by LFP theta along with the increased and distorted representation by grid cells on the wall further corroborates the notion that these two processes may be linked together. Addressing the relationship between grid cell firing and theta oscillation is beyond the scope of this thesis, but these results thus provide additional evidence for linking LFP theta type I with grid cell firing patterns (see below).

8.4.2 Grid cell firing as a function of speed

A number of studies focusing on grid cell firing properties have shown that grid cell firing rate is modulated by running speed (Sargolini et al., 2006), and this computation is present from early developmental stages (Wills et al., 2012). The observation in the present thesis that on the wall grid cells maintained significant speed modulation thus suggests that several properties of the grid cell network were functioning also during climbing. However, the correlation value between speed and firing rate of grid cells is significantly impaired on the wall and so is the intercept of the regression line, in contrast to the slope which is instead unaffected. These findings are in line with the prediction generated by CANMs in which the position of the animal in physical space is represented on a 2D neural sheet as a bump of activity (Burak and Fiete, 2009; McNaughton et al., 2006; Samsonovich and McNaughton, 1997). Importantly, these models postulate different mechanisms by which the bump is translated in order to track the actual movements of the animal. Early models (McNaughton et al., 2006; Samsonovich and McNaughton, 1997) proposed that the translation of the bump is achieved by the integration of speed and directional information from conjunctive grid cells of layer III and V (Sargolini et al., 2006). More recent models hypothesize that the afferent speed signal, which is now thought to be carried by speed cells (Kropff et al., 2015), combined with the heading information from head direction cells

(Ranck, 1984; Taube, 2007) actively drives the bump of activity around the attractor network (Burak and Fiete, 2009; Fuhs and Touretzky, 2006). Relevant for this thesis is the situation where the speed of the animal is underestimated, like on the climbing wall. According to all CANMs, the computation of distance should also be underestimated. Intuitively, this can be seen as if the bump of firing was moving more slowly on the wall than on the floor or alternatively as if the animal had to move further in space on the wall compared to the floor to cause the same shift of the activity bump. Therefore, the natural prediction of the CANMs is that grid cells produce larger fields on the wall as result of the underestimation of speed. Therefore, while the reduced correlation value in the speed line by grid cells between floor and wall probably suggests that the general encoding is partially affected, the reduced intercept fits with the theoretical scenario proposed. Thus, these findings provide additional evidence for the CANMs as one prominent class of computational models for grid cell pattern formation.

In contrast to CANMs, another class of computational models for grid cell firing, termed OIMs (Burgess, 2008; Burgess et al., 2007; Bush and Burgess, 2014; Jeewajee et al., 2008a), relies on the oscillatory pattern of several cell-types recorded across the HF (Brandon et al., 2011). The majority of grid cells are also theta modulated neurons and as discussed earlier, their firing pattern has been postulated to emerge from two oscillatory signals at slightly different frequencies (Bush and Burgess, 2014; Jeewajee et al., 2008a). The results obtained between floor and wall support also the OIM. Importantly, the expansion observed on the wall is concomitant with a significant decrease in the intrinsic firing frequency of grid cells spiking as predicted by the model. However, further analyses addressing: a) the relationships between intrinsic firing frequency and speed; b) the difference between LFP theta and intrinsic grid cell firing frequency are needed before drawing ultimate conclusions. Precisely, whether the reduced intrinsic firing frequency depends on the slower speed on the wall and whether the difference between the intrinsic firing frequency and LFP theta is reduced on the wall compared to the floor needs to be elucidated. Future analyses addressing spike-train theta frequency relationship with speed (Climer et al., 2015), will provide relevant insights for a deeper understanding of these findings and perhaps shed light on the nature of grid cell firing pattern.

8.4.3 Speed cells between floor and wall.

Consistent with the underestimation of speed hypothesis, the firing rate of speed cells was substantially reduced and there was a substantial decrease in the number of cells

maintaining speed modulation. Together, these results suggest that speed cell representation was affected, supporting the hypothesis that the inner sense of speed was impaired and speed cells on the wall underestimated velocity compared to the floor. Importantly, these findings fit with the majority of the computational models of grid cell firing. Indeed, both oscillatory and attractor network-based classes of computational models require a stable, reliable and invariant code for speed to generate grid cell firing (Giocomo et al., 2011a). The recent description of the speed cells - a substantial portion of which are theta modulated– also fits well with both classes of models (Kropff et al., 2015). Indirect evidence from Kropff and colleagues (2015) suggests that the integration of the neural code for speed carried by speed cells could be functional for the establishment of the neural code for distance carried by grid cells (Kropff et al., 2015). However, a clear demonstration that the speed signal conveyed by speed cells targets grid cells is still lacking and needs further experimentation. Nonetheless, all the results shown in this thesis support this hypothesis. Indeed, the underestimation of speed by LFP theta co-occurs with the expanded firing pattern by grid cells, supporting the following speculation: on the wall, the underestimation of speed conveyed by speed cells drives grid cells to underestimate distances on the vertical plane. The nature of the speed-grid relationship remains to be elucidated and further experiments will be hugely helpful for a comprehensive understanding of grid cell pattern formation. Even though these results do not provide direct evidence to this matter, they are consistent with both classes of models for grid cells. Indeed, OIM predicts increased scale, and henceforth grid field size, in a situation where the slope of the speed-theta correlation is reduced. Similarly, CANMs also predict increased scale in the field size if the velocity at which the bump moved around the toroidal attractor is reduced (McNaughton et al., 2006). Therefore, these results add to the growing body of evidence that neural code for detecting instantaneous speed may serve for the generation of the inner sense of distance computed by grid cells. The upstream perturbation of the speed code is thus reflected to downstream outputs and grid cells distorted representation on the wall is consistent with the here proposed model.

9 General discussion

The background question driving the work in the present thesis was to elucidate the neural representation of vertical space in rats. In this thesis, two sets of experiments were presented. The first experiment, termed “experienced pegboard”, was a pilot study aimed at testing two hypotheses: a) that extensive experience with 3D navigation modulates grid cells’ representation on the horizontal configuration of the pegboard (i.e. the experience-dependent hypothesis); b) that grid cell spatial representation is robust to the orientation of the locomotion pattern relative to the vertical axis (the reference frame hypothesis). The second experiment, termed “floor-wall experiment”, further investigated the reference frame hypothesis, and in particular whether place and grid cells recorded from animals climbing on a vertical wall would produce the same spatial firing pattern as on the horizontal plane. In the next section, all the results combined will be first reviewed and discussed in light of the initial hypotheses and then combined into a synthetic theoretical framework. In the second section, a number of general considerations based on the overall findings will be finally discussed and summarized before the conclusion of this thesis.

9.1 Towards a coherent model of vertical locomotion

In this chapter, all the findings on the question as to the nature of spatial representation on the vertical plane will be reviewed and discussed. First, the hypotheses formulated from previous studies (Hayman et al., 2011) will be briefly reviewed (Jeffery et al., 2013a, 2015). Second, the theoretical framework emerging from all the results together will be then described. At the end, the general conclusions on the matter of the neural encoding of space on the vertical plane will be provided as a synthetic theory recapitulating all the findings at our disposal.

9.1.1 Review of the hypotheses

At the end of the Chapter 4, a large overview of the hypotheses generated by the previous studies was provided to explain the designs of the experiments conducted here. In particular, two sets of experiments aimed to test the hypotheses previously formulated.

9.1.1.1 *Experience-dependent hypothesis*

The overall findings presented in this thesis mostly contradict the experience-

dependent hypothesis (4.5.1.1 Experience-dependent). Thus, the prediction yielded by this hypothesis was a differential firing pattern depending on the level of experience, but the results showed no difference between groups: grid cells produced vertical stripes on the pegboard regardless of prior 3D experience. Formally, one could speculate that raising animals in the enriched environment is not a necessarily sufficient level of experience with 3D locomotion which *per se* is able to affect the spatial representation of laboratory rats. Another factor to address would be the temporal window when neural circuits for space are wired. Developmental studies show that within the first 2-3 weeks after birth, a period during which all the animals used in this study were not housed in the parrot cage but in laboratory cages with their lactating mother, are crucial for the maturation of a functional spatial system (Langston et al., 2010; Wills et al., 2012, 2010). Therefore, one follow-up experiment testing environmental influence on development could be done by housing pregnant mothers in the parrot cage so that young pups could experience 3D space from the onset of locomotion. Results from such experiments will conclusively reveal whether a differential level of experience with 3D space could modulate its neural representation. However, all the results collected so far speak against the experience-dependent hypothesis and so currently must be rejected.

9.1.1.2 *Anisotropic encoding hypothesis*

The observation that grid cells on the pegboard produced vertical stripes of firing spanning the entire height of the apparatus (Hayman et al., 2011) led to the formulation of the anisotropic encoding hypothesis (Hayman et al., 2011; Jeffery et al., 2013a, 2015). Briefly, it posits that grid cells do not perform path integration along the vertical axis as they are only sensitive to horizontal movements (4.5.1.2).

An important finding of the experienced pegboard experiment is that grid cells from an experienced animal produced vertical stripes of firing, qualitatively and quantitatively identical to those of the naïve animal and the study from Hayman et al., (2011). This result could be interpreted as evidence in favour of the anisotropic encoding hypothesis, but the results of both the diagonal configuration in the experienced pegboard experiment (where grid cells no longer produce vertical stripes but disorganized firing) and the overall floor-wall experiment (where grid cells produce large fields on the wall) strongly disagree with the anisotropic encoding hypothesis. Indeed, in both situations, grid cells did not produce vertical stripes as in the horizontal configuration of all groups of animals but respectively spatially disorganized firing on the pegboard and clear firing fields on the climbing wall.

Even though both the spatial firing patterns differ from the strikingly regular array of fields that grid cells normally show on the horizontal plane, the fact that the vertical stripes do not persist in these two conditions leads to two main considerations. The first consideration is that the anisotropic hypothesis, as it was initially conceived and described, simply does not account for the results on the diagonal configuration of the pegboard and the vertical wall so it should be also rejected. The second consideration is that the vertical stripes seem to be the general response of grid cells only in the paired-horizontal-pegs condition of the pegboard. This finding raises one new interesting question: indeed, if grid cells are not insensitive to movements along height, why do they produce vertical stripes only on this apparatus? The reference frame hypothesis may help answer this question.

9.1.1.3 *Reference frame hypothesis*

In the original study by Hayman et al., (2011), the fact that during locomotion on the pegboard animals kept the orientation of the body mostly horizontal was proposed to be one possible explanation for the observed anisotropic encoding (Hayman et al., 2011). Several studies highlighted this factor (Hayman et al., 2011; Jeffery et al., 2013a, 2015; Taube and Shinder, 2013) and proposed the reference frame hypothesis as a possible cause for the vertical stripes found on the pegboard (4.5.1.3). Briefly, this hypothesis posits that the orientation of the body (and hence the locomotor plane) sets the reference frame of an essentially planar representation in the spatial cognitive system. Therefore, according to the authors, the animals which mostly moved across pairs of pegs in the horizontal configuration on the pegboard were navigating with a horizontal earth-referenced frame despite being on the vertical plane. Accordingly, vertical stripes should be considered as a stack of horizontal fields along the height of the apparatus. The results from the other two experiments in the present study mostly support the reference frame hypothesis. Thus, the diagonal condition of the experienced-pegboard experiment, where animals did not keep the body plane horizontal, was found to disrupt both the hexagonal grid pattern and the columnar representation. This preliminary observation therefore suggests that by tilting the angle of the body plane, from horizontal as in the horizontal condition, to 45° (i.e. the angle of the pegs in the diagonal condition), grid cells not only changed their spatial representation, but fail to produce a clear spatial pattern.

The conclusion seems apparently inconsistent with the findings from a recent study addressing grid cell firing on a tilted slope (Hayman et al., 2015). In that experiment, animals were allowed to forage between two continuous planes, one horizontal and one

tilted by 45°. Comparisons of grid cell activity between planes showed that parameters such as the coverage, spatial regularity and interfield-distance were slightly affected during non-flat locomotion (Hayman et al., 2015). However, overall grid cells still exhibited a clear spatial pattern on the sloped surface in contrast to the noisy firing displayed by grid cells on the diagonal configuration of the pegboard in the current study. It should be pointed out though that a radical difference exists between these two conditions: in the study on the slope (Hayman et al., 2015) animals moved on a single tilted plane, whereas on the diagonal configuration of the pegboard animals could move along two planes (45° and 135° from horizontal reference). According to the reference frame hypothesis, two reference frames, one for each plane of locomotion, would be competing for influence, and so the noisy firing pattern displayed by grid cells could be the result of two interfering representations.

The results from the floor-wall experiment provide additional evidence for the reference frame hypothesis. The fact that grid cells, differently from the pegboard, did not form stripes but rather almost-circular fields shows that the orientation of the body indeed modulates grid cell firing. Consistent with the general hypothesis, during climbing the reference plane was set to vertical, so grid cells responded accordingly, producing local foci of firing which did not span the entire height of the apparatus as in the pegboard (Hayman et al., 2015). Thus, when the animal's plane of locomotion was oriented vertically, grid cells produced grid fields in the vertical plane.

However, as stated in the introduction of this thesis (4.5.2), the prediction made for the reference frame hypothesis was that grid cells on the wall would provide spatial metrics essentially indistinguishable from the floor. In contrast, drastic differences were displayed by spatial neurons during floor and wall locomotion. First, place cells showed a substantial reduction in the number of active place cells on the wall. Second, grid cells showed a significant decrease in the mean and peak firing on the wall. Moreover, the majority of grid cell properties were heavily altered, with a dramatic drop in the regular hexagonal pattern on the wall and a mild but significant bias along the vertical axis. Moreover, there was a substantial decrease in the number of grid fields on the wall and finer analyses focused on the geometrical characteristics of grid cells firing found that the grid fields were enlarged and less rounded compared to the floor. Overall these features demonstrate that the spatial encoding on the wall is radically different from the floor but also different from that one observed on the pegboard (Hayman et al., 2011).

The simultaneous decrease in the number of fields and increase in field size, lead to

the speculation that perhaps the global grid cell firing pattern was expanded but would be equally regular if tested on a larger wall. However, in the pilot study "large wall experiment", where only one grid cell was successfully recorded across multiple trials throughout 6 consecutive days, even on a large vertical surface the grid cell did not produce a regular hexagonal array of fields but, instead, large patches of firing. Therefore, put together, all the findings from experienced-pegboard and floor-wall experiments lead to the following conclusion: while the experience-dependent and anisotropic hypotheses are inconsistent with both the experimental findings *in toto*, the reference frame hypothesis turned out to be accurate in predicting differential firing between the pegboard and climbing wall. However, the reported lack of a grid pattern on the wall is inconsistent with the main prediction that a normal, metrically similar hexagonal grid pattern would emerge. These results thus require further thinking on the matter and the results focused on the encoding of speed may help in disentangling this puzzling scenario.

9.1.2 Considerations on the underestimation of speed hypothesis

As mentioned before, even though the reference frame hypothesis was the theoretical model which generally fitted the majority of the results obtained, the dramatic difference in the spatial encoding by grid cells between floor and wall has prompted the generation of a new theoretical framework which accounts for the reduction in spatial activity of grid cells on the wall and simultaneous enlargement of their place fields. For a system performing odometry, these two phenomena would be the consequence of an underestimation of distances travelled which, in turn, may derive from an underestimation in the encoding of speed. This simple theoretical scenario was explored by focusing on the neural traces of speed so far documented.

Theta, the most prominent oscillation (7-11 Hz) recorded in the LFP across the hippocampal formation, is a brain rhythm which theoretical and experimental studies have suggested to play major role in path-integration processes (Brandon et al., 2011; Burgess, 2008; Jeewajee et al., 2008a; O'Keefe and Recce, 1993). In particular, its frequency has been shown to correlate with running speed (Jeewajee et al., 2008a; McFarland et al., 1975) on flat horizontal environments, and a major class of computational models is based on the oscillatory pattern in the theta band of neurons recorded throughout the hippocampal formation (Burgess, 2008; Giocomo et al., 2011a; Jeewajee et al., 2008a).

The findings obtained on the wall support both the hypotheses that path integration processes are linked with theta oscillation, and that the encoding of speed was

underestimated. The power and strength of theta oscillations were partially affected during climbing on the wall, suggesting an intrinsic impairment of theta functioning. In addition, the reduced slope (but not intercept) of the speed-theta relationship suggests that at a large ensemble level, the representation of speed was affected on the wall, driving a reduction in the encoding of speed compared to horizontal surfaces at all speeds.

Consistent with LFP theta frequency reduction on the wall, the results from both grid and speed cells on the climbing wall corroborate the hypothesis that instantaneous speed was both noisy and underestimated. Grid cell speed modulation was still present on the wall but was reduced, as predicted by the underestimation of speed hypothesis. The results suggest that the putative speed signal (see below) upstream of grid cells affected their firing rate, both quantitatively (reduced intercept) and qualitatively (reduced correlation value). This finding is consistent with CANMs which posit that path integration is achieved by grid cells via speed and directional information from conjunctive grid cells of layer III and V of MEC. This finding may suggest that the movements of the bump of activity predicted by CANMs also occurred more slowly on the wall than on the floor. In other words, for the bump to move, rats had to cover greater distances on the wall compared to the floor and that phenomenon may possibly explain why fields are enlarged on the vertical plane.

The results from LFP theta provide evidence that speed encoding was underestimated. Additional support comes from the evidence that speed cells also show substantial changes in their encoding of speed during climbing on the wall. Importantly, similarly to grid cells, their speed modulation is less accurate on the wall (as evidenced by the reduced correlation values of the linear regression) and the intercept but not the slope of the speed lines were reduced during climbing. However, the reduced consistency between orthogonal but not horizontal planes provides evidence for the underestimation of speed hypothesis. This finding suggests two things. First, the speed code is context-invariant across horizontal planes (Kropff et al., 2015). The recordings on the floor and in the open field occurred in different rooms where cues, light and overall speed of the animal substantially differed, nonetheless speed cells displayed remarkably similar profiles. Consistent with a previous study (Kropff et al., 2015), these neurons fulfil the experimental requirements for acting as universal speedometers and are thus likely to contribute to path integration processes. Second, the speed code stays stable across horizontal planes but it is severely perturbed during locomotion in the vertical plane. Importantly, it does not show complete disruption, as most cells still keep speed encoding while climbing on the wall, but fewer cells maintained speed encoding compared to the floor, the general accuracy (speed

line score) was reduced and overall the firing rate was reduced across all speeds. This is an unexpected observation and it raises several questions on the input of the speed signal (see below).

9.1.3 A synthetic theory for the vertical encoding of space

Throughout this thesis, a particular emphasis has been given to the intrinsic relationship between the theoretical and experimental components this study took into account. As mentioned before, previous findings on the pegboard (Hayman et al., 2011) led to a number of hypotheses on the nature of the vertical encoding of space which ultimately motivated the experiments described in this thesis. The results obtained mostly disagreed with two hypotheses (experience-dependent) while the reference frame is consistent with the majority of the results but did not predict the substantial scaling effect shown between floor and wall. The underestimation of speed hypothesis may account for the significant change in the spatial metrics of grid cells in the vertical plane. Even though further investigation on this matter is required before drawing premature conclusions, it is useful to propose a synthetic approach reconciling all the data into a unified theoretical framework. One hypothesis is that both the reference frame and the underestimation of speed hypothesis are valid, as there is no *a priori* reason for them to be mutually exclusive. Both hypotheses combined together generate a new coherent theory for the vertical encoding of space. In essence, the fact that the locomotion plane of the animal sets the grid cell reference frame is experimentally validated and is a necessary pre-requisite for establishing a symmetric representation of space across dimensions. Nonetheless, grid cells in the vertical plane do not provide the same spatial metrics as on the horizontal plane because of an intrinsic property of the system, which is the underestimation of speed, which drives grid cells to display irregular and expanded firing patterns. Combined together, the reference frame and the underestimation of speed hypotheses provide a sensible framework which, paradoxically, ultimately rescue the anisotropic hypothesis. Indeed, the miscomputation of speed seems to be an intrinsic feature of the spatial cognitive system responding to movements in the vertical plane. This observation thus leads to the conclusion that the vertical encoding of space is simply different from the horizontal and the spatial cognitive system is therefore intrinsically anisotropic.

To summarize, the initial results from the pegboard led to the formulation of a “first generation” anisotropic encoding hypothesis positing that grid cells are insensitive to movements along vertical axis (Hayman et al., 2011). Here a “second generation”

anisotropic encoding hypothesis, based on both the reference frame and the underestimation of speed hypotheses, is proposed. The major difference between them is that the former posits a *qualitative* anisotropy across dimensions (no sensitivity to movements along height) whereas the latter posits a *quantitative* difference (decreased accuracy) but not complete disruption in the ability to provide spatial information. Further data, possibly from the large-wall experiment, may shed light on this new proposed synthetic theoretical framework. An unlikely, but still not-disproved, possibility is that a regular grid pattern of enlarged scale may indeed emerge if the available vertical surface is sufficient for a minimum number of fields. However, it should be noted that: a) the only cell recorded on the large-wall experiment did not show a regular pattern; b) results from the encoding of speed showed not only an underestimation in the encoded instantaneous speed, but also in the "goodness" (r value) of the encoding of speed. Indeed, together with the underestimation of instantaneous speed, LFP theta oscillation, grid and speed cells showed a significant drop in the correlation value between speed and firing rate. Based on these findings, it is reasonable to predict that even if a high number of fields could be produced on a vertical wall, the combined effect of the noisier and reduced encoding of instantaneous speed may essentially avoid the formation of a regular pattern and overall disrupt the regular grid cell firing pattern. At the moment, the results obtained from the floor-wall experiment speak in favour of this as the most likely scenario.

9.2 General considerations on the nature of the network of space

The original aim of this thesis was to elucidate the nature of spatial representation during navigation in the vertical plane, and the results show that the spatially-modulated neurons respond to movements on the vertical plane differently from movements on the horizontal one (i.e. second generation anisotropic hypothesis). The main findings combined are: on the wall place cells are more silent, grid cells produce less rounded fields than on the floor and expanded irregular maps, theta is still speed-modulated but with a lower slope, and speed cells underestimate the instantaneous speed on the wall. These results were largely discussed in the previous section with respect to the question of spatial coding in the vertical plane. However, aside from the original aim of the experiments, the findings presented in this thesis lead to more general considerations on the nature of the neural network for the representation of space.

While no strong theoretical link ties the results of place and grid cells, the results of grid and speed cells suggest a strong coupling between these two classes of cells.

Consistent with several computational models (Giocomo et al., 2011a), it has been hypothesized that speed cells in the MEC may be functional for path integration, possibly by direct connections onto grid cells (Buetfering et al., 2014; Cao et al., 2015; Kropff et al., 2015) and the results on the wall further support this view. According to the hypothesized speed-grid connection, the finding that speed cells show severely reduced firing rates on the wall compared to the floor accounts for the expanded and irregular representation by grid cells during climbing. However, it should be pointed out that the results presented in this thesis do not provide evidence for connections between speed and grid cells but they do show that the representation between these two classes of cells is similarly affected. Experiments aiming to better characterize the speed cell population, as well as their connections with grid cells, will help solving several questions on the matter and also assist with respect to grid cells pattern formation (Cao et al., 2015).

The "second generation anisotropic encoding hypothesis" is the general model proposed to describe the representation of space on the vertical plane and it raises several questions on the nature of the spatial encoding. For instance, with respect to the speed signal targeting grid cells, an unanswered question is: where it is computed and whether or not this occurs locally in the MEC or elsewhere and what is the relationship between speed cells and LFP theta oscillation? The observation that a substantial proportion of speed cells are theta modulated (Buetfering et al., 2014; Kropff et al., 2015) and that LFP theta frequency correlates with speed, suggests an intrinsic link between these two phenomena. Moreover, another important question addresses the nature of the signal responsible for generating speed cells. Which cue does it rely on, external sensory information (e.g. optic flow) or self-motion cues (proprioceptive, vestibular)? The combined observation that grid cells display effective path integration also in darkness (Hafting et al., 2005) and speed cells are not affected by lack of visual cues (Kropff et al., 2015) suggests that the speed code inputting to grid cells may be independent of visual cues (Chen et al., 2016; Pérez-Escobar et al., 2016). Recent studies suggested that the vestibular system may be (at least one) source for LFP theta rhythmic firing encoding of speed in the HF (Jacob et al., 2014; Ravassard et al., 2013). It is well known that the vestibular system is sensitive to both angular acceleration (semi-circular canals) and linear acceleration (otolith organs) and together they enable the distinguishing of head movements (such as tilt, yaw) from body translation (Angelaki and Cullen, 2008), by using the computed gravity vector. The reversible inactivation of the vestibular system results in a transient but severe disruption of the speed-theta relationship but, consistent with models positing a dissociation in type I

and type II theta (Wells et al., 2013), not in its basal oscillation (Jacob et al., 2014). The notions that the speed signal (at least partially) depends on vestibular information, and it is integrated by grid cells is far from being demonstrated. However, indirect evidence comes from studies in virtual reality (V-R) (Aronov and Tank, 2014; Domnisoru et al., 2013). However, during V-R navigation, spatial coding is computed in absence of vestibular cues as the animal is head fixed (Chen et al., 2013; Domnisoru et al., 2013; Ravassard et al., 2013) or can turn its head but not move forward (Aronov and Tank, 2014). According to the speed-grid model, a reduced speed signal drives grid cells to underestimate distances. Recordings of grid cells in V-R indeed show large fields across the whole extent of MEC and also from areas where the scale of cells during locomotion in the real world is 2/3 times smaller (Aronov and Tank, 2014). Consistent with the enlargement of fields, during V-R navigation, LFP theta frequency is reduced compared to real world navigation (Aronov and Tank, 2014; Ravassard et al., 2013). Therefore, the results obtained on the V-R partially resemble the scenario described on the climbing wall where larger fields are displayed and LFP theta frequency is reduced. However, a crucial difference between vertical plane and V-R is present: the lack of regular arrangement. While in V-R grid cells form large but remarkably regular grids (Aronov and Tank, 2014), on the climbing wall grid cells produced few and both irregularly arranged and deformed fields. Based on these findings, the following scenario can be hypothesized: during climbing on the wall, the gravity vector affects the representation of the instantaneous linear acceleration encoded by the otolith organs (Angelaki and Cullen, 2008). This impairment affects the computation of speed which is always reduced compared to horizontal movements and ultimately increases grid cell scale. Preliminary evidence, such as the flattening of the speed-theta relationship following temporary otolith inactivation, support this hypothesis (Jacob et al., 2014). Future experiments aimed to characterize the relationship between the vestibular system and grid cell scale are therefore needed to verify this theoretical framework.

9.3 Conclusions and future directions

More than four decades of research have helped build a comprehensive theoretical framework describing the neural encoding of space in flat horizontal surfaces, but similar investigations of the spatial representation during vertical locomotion was missing. A number of reasons motivate the present scientific question. First, the z-axis is part of the 3D space, so for every freely-moving animal, including surface-dwelling animals, encoding height is a necessary computation in order to perform efficient navigation. Real

environments provide a number of complex features, which the brain needs to cope with and encoding position along the z-axis is definitely one of those. Therefore, addressing how the spatial cognitive system incorporates information relative to height fills many gaps in our understanding of the general principles of the spatial system functioning. Indeed, relevant insights on the mechanisms of the neural networks dedicated for the encoding of space can be gained. Further investigation on the matter will help answer many general questions on the nature of the wiring and functioning of the hippocampal spatial-cognitive system.

Moreover, the findings presented in this thesis provide evidence on how the spatial representation in the vertical plane may be encoded in rodents. The substantial differences reported between the horizontal and vertical plane speak against the possibility that, at least in rats, grid cell representation may be symmetrical across dimensions and hence be truly volumetric. However, it should be noted that in the floor-wall experiment the representation in 3D space was not specifically addressed but rather: what kind of neural maps were exhibited on two 2D maps, one horizontal and one vertical, and how do they differ? Therefore, the reported findings do not rule out the hypothesis that in a situation where a rat navigates in a 3D environment grid cells may respond the same as they did on the climbing wall. Recording grid cells during navigation on a volumetric lattice (Jovalekic et al., 2011), experiment which is currently under way in Jeffery's lab, will help answer several questions on the nature of the 3D encoding of space.

In conclusions, this thesis addressed the functioning of the hippocampal spatial-cognitive system during locomotion in the vertical plane. The results showed that place and grid cell firing is modulated by the orientation of the plane of locomotion but their firing responses strongly differ during movements on a climbing wall. Whereas the majority of place cells stayed silent during climbing, grid cells always produced spatial firing but with a number of altered features such as a drop in the firing rate, hexagonal symmetry and spatial coverage in parallel to substantial expansion of the grid field. This result may derive from an altered computation of speed which we hypothesized is dependent on upstream speed cell signals that have been shown to underestimate instantaneous speed during climbing. According to this theoretical framework, both place and grid cells, although in different ways, showed that their spatial representation was not symmetric across dimensions and the neural representation of space is to be considered as anisotropic. Therefore, overall these findings raise several questions on the nature of the 3D representation of space which becomes a matter for future research.

10 Appendix

All the results presented in Chapter 7 and Chapter 8 were obtained by comparing spatial coding between surfaces after pooling together cells and LFP theta recordings from different rats. However, this approach violates the independence assumption, as individual datapoints obtained from the same animal do not share the same degree of indepedence with those from another animal. Similarly, different cells from a single animal were recorded across multiple sessions. Therefore, to avoid potential confounds, the same data presented in the chapter were analysed taking into account potential differences across animals.

10.1 Place cells

To address potential differences between rats, a mixed two-way repeated measure ANOVA comparing place cell properties between surfaces as a within subjects factor and rat identity as a between subjects factor was conducted.

Mean firing rate: main effect of surface: $F_{1,96} = 9.21$, $p < 0.01$, main effect of rats: $F_{3,96} = 2.44$, $p = 0.069$; surface by rat interaction: $F_{3,96} = 0.69$, $p = 0.98$.

Peak firing rate: main effect of surface: $F_{1,96} = 6.04$, $p = 0.05$, main effect of rats: $F_{3,96} = 7.12$, $p < 0.001$; surface by rat interaction: $F_{3,96} = 0.28$, $p = 0.84$.

Spatial information (bits/spike): main effect of surface: $F_{1,96} = 40.0$, $p < 0.0001$, main effect of rats: $F_{3,96} = 6.30$, $p < 0.001$; surface by rat interaction: $F_{3,96} = 3.45$, $p = 0.020$.

Coverage: main effect of surface: $F_{1,96} = 19.9$, $p < 0.0001$, main effect of rats: $F_{3,96} = 3.94$, $p = 0.011$; surface by rat interaction: $F_{3,96} = 0.81$, $p = 0.49$.

The results obtained by pooling cells from different rats were also robust when only the subset of active place cells was tested and the rat identity was included in the analysis. A factorial ANOVA comparing the surface (floor vs. wall) and rat identity revealed the following results:

Mean firing rate: main effect of surface: $F_{1,98} = 0.70$, $p = 0.41$, main effect of rats: $F_{3,98} = 1.51$, $p = 0.22$; surface by rat interaction: $F_{3,98} = 0.50$, $p = 0.68$.

Peak firing rate: main effect of surface: $F_{1,98} = 3.75$, $p = 0.055$, main effect of rats:

$F_{3,98}$ = 4.50, p = 0.005; surface by rat interaction: $F_{3,98}$ = 0.26, p = 0.86.

Spatial information (bits/spike): main effect of surface: $F_{1,98}$ = 0.22, p > 0.05, main effect of rats: $F_{3,98}$ = 2.34, p > 0.05; surface by rat interaction: $F_{3,98}$ = 1.72, p > 0.05.

Coverage: main effect of surface: $F_{1,98}$ = 1.26, p = 0.26, main effect of rats: $F_{3,98}$ = 2.07, p = 0.11; surface by rat interaction: $F_{3,98}$ = 1.10, p = 0.35.

The place field properties of place cells were also robust when only the subset of active place cells was tested and the rat identity was included in the analysis. A factorial ANOVA comparing the surface (floor vs. wall) and rat identity revealed the following results:

Place field area: main effect of surface: $F_{1,98}$ = 4.06, p = 0.47, main effect of rats: $F_{3,98}$ = 2.71, p = 0.49; surface by rat interaction: $F_{3,98}$ = 1.85, p = 0.14.

Place field major axis: main effect of surface: $F_{1,98}$ = 0.31, p = 0.58, main effect of rats: $F_{3,98}$ = 6.47, p < 0.001; surface by rat interaction: $F_{3,98}$ = 2.31, p = 0.08.

Place field minor axis: main effect of surface: $F_{1,98}$ = 3.61, p = 0.06, main effect of rats: $F_{3,98}$ = 1.00, p = 0.40; surface by rat interaction: $F_{3,98}$ = 0.80, p = 0.49.

Place field aspect ratio: main effect of surface: $F_{1,98}$ = 6.67, p = 0.011, main effect of rats: $F_{3,98}$ = 5.71, p < 0.001; surface by rat interaction: $F_{3,98}$ = 1.07, p = 0.37.

As shown here, overall, these results mostly agree with the results obtained by pooling place cells from different rats altogether. To further validate these results, an additional analysis was conducted by comparing the median value of each rat between surfaces.

10.2 Grid cells

Similar to place cells, a mixed two-way repeated measure ANOVA comparing grid cell properties between surfaces as a within subject factor and rat identity as a between subject factor was conducted.

Mean firing rate: main effect of surface: $F_{1,108}$ = 11.5, p < 0.001, main effect of rats: $F_{10,108}$ = 1.47, p = 0.16; surface by rat interaction: $F_{10,108}$ = 2.41, p = 0.013.

Peak firing rate: main effect of surface: $F_{1,108}$ = 5.80, p = 0.018, main effect of rats: $F_{10,108}$ = 1.75, p = 0.080; surface by rat interaction: $F_{10,108}$ = 0.98, p = 0.47.

Grid score: main effect of surface: $F_{1,108}$ = 11.2, p < 0.001, main effect of rats: $F_{10,108}$ = 0.728, p = 0.70; surface by rat interaction: $F_{10,108}$ = 1.54, p = 0.14.

Stripe score: main effect of surface: $F_{1,108}$ = 10.2, p < 0.01, main effect of rats: $F_{10,108}$ = 1.90, p = 0.053; surface by rat interaction: $F_{10,108}$ = 1.91, p = 0.052.

Coverage: main effect of surface: $F_{1,108}$ = 2.01, p = 0.16, main effect of rats: $F_{10,108}$ = 1.50, p = 0.15; surface by rat interaction: $F_{10,108}$ = 1.58, p = 0.16.

Scale: main effect of surface: $F_{1,108}$ = 5.50, p = 0.021, main effect of rats: $F_{10,108}$ = 3.54, p < 0.001; surface by rat interaction: $F_{10,108}$ = 3.75, p < 0.001.

Number of grid fields (normalized by available area): main effect of surface: $F_{1,108}$ = 14.9, p < 0.0001, main effect of rats: $F_{10,108}$ = 4.85, p < 0.001; surface by rat interaction: $F_{10,108}$ = 2.59, p = 0.01.

Grid field area: main effect of surface: $F_{1,108}$ = 5.92, p = 0.017, main effect of rats: $F_{10,108}$ = 1.74, p = 0.08; surface by rat interaction: $F_{10,108}$ = 1.36, p = 0.21.

Grid field major axis: main effect of surface: $F_{1,108}$ = 13.3, p < 0.0001, main effect of rats: $F_{10,108}$ = 2.04, p = 0.036; surface by rat interaction: $F_{10,108}$ = 0.76, p = 0.67.

Grid field minor axis: main effect of surface: $F_{1,108}$ = 1.28, p = 0.26, main effect of rats: $F_{10,108}$ = 2.52, p < 0.01; surface by rat interaction: $F_{10,108}$ = 3.81, p < 0.001.

Grid field aspect ratio: main effect of surface: $F_{1,108}$ = 13.5, p < 0.0001, main effect of rats: $F_{10,108}$ = 0.85, p = 0.59; surface by rat interaction: $F_{10,108}$ = 0.75, p = 0.68.

As shown here, overall these results mostly agree with the results obtained by pooling grid cells from different rats altogether. Whereas weak significant interactions exist between surfaces and rats in the mean and peak firing rate of grid cells, the grid scores, stripe scores and coverage showed no significant interaction but strong significant differences between surfaces. The scale and the number of grid fields showed significant interactions. However, as mentioned before, the scale is a meaningless value given the lack of regularity whereas the difference in the number of grid fields might be due to the fact that a different number of grid cell modules were recorded across animals (not tested though). Importantly, all grid field properties, except for the grid field minor axis, did not show significant interaction between surfaces and rat identity. Therefore, similar to place cells, results from grid cells were mostly robust to between-rat differences.

Moreover, given the larger number of animals implanted in MEC (n = 11) compared to HPC (n = 4), additional analyses on the grid cell dataset were conducted using one-

sample *t*-tests of the median of the difference between surfaces within each animal.

Mean firing rate: floor = 0.96 ± 0.13 Hz, wall = 0.64 ± 0.09 Hz, t_{10} = 4.41, p < 0.01;

Peak firing rate: floor = 8.6 ± 1.4 Hz, wall = 6.3 ± 1.3 Hz, t_{10} = 2.09, p = 0.063;

Grid score: floor = 0.33 ± 0.08, wall = -0.56 ± 0.06, t_{10} = 2.83, p = 0.018;

Stripe score: floor = 1.08 ± 0.03, wall = 1.80 ± 0.40, t_{10} = -1.77, p = 0.11;

Coverage: floor = 0.18 ± 0.01, wall = 0.15 ± 0.02, t_{10} = 1.97, p = 0.07;

Scale: floor = 54.9 ± 7.00 cm, wall = 43.7 ± 3.77 cm, t_{10} = 1.72, p = 0.12;

Number of grid fields (normalized by available area): floor = 0.0055 ± 0.0010 cm^{-2}, wall = 0.0039 ± 0.0006 cm^{-2}, t_{10} = 2.74, p = 0.02;

Grid field area: floor = 1966 ± 934 cm^2, wall = 3761 ± 1460 cm^2, t_{10} = -1.14, p = 0.28;

Grid field major axis: floor = 48.5 ± 9.6 cm, wall = 105 ± 23.4 cm, t_{10} = -3.22, p < 0.01;

Grid field minor axis: floor = 39.1 ± 8.1 cm, wall = 42.2 ± 9.0 cm, t_{10} = 0.25, p = 0.81;

Grid field aspect ratio: floor = 1.26 ± 0.03 cm, wall = 2.34 ± 0.33 cm, t_{10} = -3.09, p = 0.011;

Consistent with the results previously shown, these comparisons revealed a significant decrease in the mean firing rate and the grid scores in contrast to the peak firing rate (p = 0.063), stripe score and coverage (p = 0.07) which instead showed no significant changes. Similarly, the analyses on grid fields revealed a significant decrease in the number of grid fields, and a significant increase in the length of the major axis and the aspect ratio. In contrast the area of the grid fields and the minor axis did not show significant increase on the wall. Therefore, overall these results including rat identity (mixed repeated measure ANOVA) and the median within each animal mostly agree with what has been previously reported.

10.3 LFP theta

A mixed two-way repeated measure ANOVA comparing LFP theta properties between surfaces as a within subject factor and rat identity as a between subject factor was conducted.

LFP theta mean frequency: main effect of surface: $F_{1,36}$ = 94.9, p < 0.0001, main effect of rats: $F_{15,36}$ = 10.5, p < 0.0001; surface by rat interaction: $F_{15,36}$ = 2.85, p < 0.01.

LFP theta power signal to noise ratio: main effect of surface: $F_{1,36}$ = 10.2, p < 0. 01,

main effect of rats: $F_{15,36}$ = 9.47, p < 0.0001; surface by rat interaction: $F_{15,36}$ = 12.7, p < 0.001.

LFP theta intercept: main effect of surface: $F_{1,36}$ = 6.45, p = 0.016, main effect of rats: $F_{15,36}$ = 5.54, p < 0.001; surface by rat interaction: $F_{15,36}$ = 2.46, p = 0.014.

LFP theta slope: main effect of surface: $F_{1,36}$ = 116.5, p < 0.0001, main effect of rats: $F_{15,36}$ = 18.6, p < 0.0001; surface by rat interaction: $F_{15,36}$ = 2.69, p = 0.010.

LFP theta correlation: main effect of surface: $F_{1,36}$ = 69.7, p < 0.0001, main effect of rats: $F_{15,36}$ = 13.9, p < 0.0010; surface by rat interaction: $F_{15,36}$ = 2.01, p = 0.044.

As shown here, overall these results mostly agree with the results obtained by pooling together LFP recordings from different rats. The analyses revealed significant differences between surfaces even when the rat identity was included in the analysis. In addition, there were substantial differences between animals for the all the parameters tested (all p < 0.001). However, the interactions between surfaces and rat identity were all mildly significant except for the LFP theta power signal to noise ratio. Importantly, the correlation between speed and LFP-theta frequency, which most of all represents the encoding of speed by LFP theta, showed a weak – although significant – interaction (p = 0.044).

In addition, similarly to grid cell dataset, LFP theta was also addressed by comparing the median within each animal.

LFP theta mean frequency: floor = 8.74 $\pm$ 0.06 Hz, wall = 8.45 $\pm$ 0.07 Hz, t_{15} = 6.37, p < 0.001;

LFP theta power signal to noise ratio: floor = 19.3 $\pm$ 2.6, wall = 16.4 $\pm$ 1.7, t_{15} = 1.44, p = 0.17;

LFP theta intercept: floor = 8.58 $\pm$ 0.02 Hz, wall = 8.55 $\pm$ 0.02 Hz, t_{15} = 1.53, p = 0.14;

LFP theta slope: floor = 0.016 $\pm$ 0.002 Hz/cm/s, wall = 0.0057 $\pm$ 0.0016 Hz/cm/s, t_{15} = 7.22, p < 0.001;

LFP theta correlation: floor = 1.80 $\pm$ 0.22, wall = 0.87 $\pm$ 0.22, t_{15} = 7.11, p < 0.001;

Consistent with what previously reported, these results revealed the reduction in the LFP theta frequency during climbing on the wall compared to the floor. Moreover, this seems to be mostly dependent on the substantial reduction in the slope of the speed-theta correlation rather than intercept which instead was not affected by movements on the

vertical plane. Moreover, theta power (determined as the signal to noise ratio) was not significantly reduced compared to the floor in contrast to the LFP theta correlation which instead was significantly decreased on the wall compared to the floor.

10.4 Speed cells

A mixed two-way repeated measure ANOVA comparing speed cell properties between surfaces as a within subject factor and rat identity as a between subject factor was conducted.

Speed score: main effect of surface: $F_{1,354} = 43.1$, $p < 0.001$, main effect of rats: $F_{8,355} = 11.5$, $p < 0.001$; surface by rat interaction: $F_{8,355} = 7.40$, $p < 0.0001$.

Speed line score: main effect of surface: $F_{1,354} = 31.7$, $p < 0.001$, main effect of rats: $F_{8,354} = 5.87$, $p < 0.001$; surface by rat interaction: $F_{8,354} = 6.11$, $p < 0.0001$.

Intercept: main effect of surface: $F_{1,354} = 29.2$, $p < 0.001$, main effect of rats: $F_{8,354} = 1.84$, $p = 0.068$; surface by rat interaction: $F_{8,354} = 2.53$, $p = 0.011$.

Slope: main effect of surface: $F_{1,354} = 10.7$, $p < 0.001$, main effect of rats: $F_{8,354} = 4.72$, $p < 0.001$; surface by rat interaction: $F_{8,354} = 2.43$, $p < 0.014$.

Together, these results confirm the significant changes between surfaces observed and also reveal significant differences between rats. Interestingly, there were significant interactions in both the speed score and the speed line score of speed cells between surfaces and rats, whereas the intercept and slope of the speed lines returned weak – though still significant - changes.

In addition, similarly to grid cell dataset, speed cell properties were also addressed by comparing the median within each animal.

Speed score: floor = 0.076 ± 0.009, wall = 0.057 ± 0.010, $t_8 = 3.50$, $p < 0.01$;

Speed line score: floor = 1.71 ± 0.08, wall = 1.36 ± 0.14, $t_8 = 3.43$, $p < 0.01$;

Intercept: floor = 1.92 ± 0.19 Hz, wall = 1.48 ± 0.18, $t_8 = 5.58$, $p < 0.001$;

Slope: floor = 0.058 ± 0.006 Hz/cm/s, wall = 0.037 ± 0.007 Hz/cm/s, $t_8 = 5.68$, $p < 0.001$;

Consistent with what previously reported, these results indicate substantial differences between surfaces by speed cells across animals. Indeed, the encoding of speed

was substantially impaired as revealed by the significant reduction in the speed score and speed line score between surfaces (both $p < 0.01$). Moreover, consistent with the underestimation of speed hypothesis, both the intercept and the slope of the speed lines were significantly reduced (both $p < 0.001$), suggesting that the representation of speed was underestimated compared to the floor.

11 References

Alme, C.B., Miao, C., Jezek, K., Treves, A., Moser, E.I., and Moser, M.-B. (2014). Place cells in the hippocampus: Eleven maps for eleven rooms. Proc. Natl. Acad. Sci. *111*, 18428–18435.

Amaral, D., and Lavenex, P. (2006). Hippocampal Neuroanatomy. In The Hippocampus Book, P. Andersen, R. Morris, D. Amaral, T. Bliss, and J. O'Keefe, eds. (Oxford University Press), pp. 37–114.

Amaral, D.G., Ishizuka, N., and Claiborne, B. (1990). Neurons, numbers and the hippocampal network. Prog. Brain Res. *83*, 1–11.

Amaral, D.G., Dolorfo, C., and Alvarez-Royo, P. (1991). Organization of CA1 projections to the subiculum: a PHA-L analysis in the rat. Hippocampus *1*, 415–435.

Amaral, D.G., Scharfman, H.E., and Lavenex, P. (2007). The dentate gyrus: fundamental neuroanatomical organization (dentate gyrus for dummies). Prog. Brain Res. *163*, 3–22.

Andersen, P., Bliss, T.V.P., and Skrede, K.K. (1971). Lamellar organization of hippocampal excitatory pathways. Exp. Brain Res. *13*, 222–238.

Andersen, P., Richard, M., David, A., Tim, B., and John, O. (2006). The Hippocampal Formation. In The Hippocampus Book, P. Andersen, R. Morris, D. Amaral, T. Bliss, and J. O'Keefe, eds. (Oxford University Press), pp. 3–8.

Anderson, M.I., and Jeffery, K.J. (2003). Heterogeneous Modulation of Place Cell Firing by Changes in Context. J. Neurosci. *23*, 8827–8835.

Angelaki, D.E., and Cullen, K.E. (2008). Vestibular System: The Many Facets of a Multimodal Sense. Annu. Rev. Neurosci. *31*, 125–150.

Aranzi, G.C. (1587). Julii Caesaris Arantii,... de humano foetu liber : tertio editus, ac recognitus ; [ejusdem] Anatomicarum observationum liber ; [ac] De tumoribus secundum locos affectos liber : nunc primum editi ([Reprod.]).

Aronov, D., and Tank, D.W. (2014). Engagement of Neural Circuits Underlying 2D Spatial Navigation in a Rodent Virtual Reality System. Neuron *84*, 442–456.

Barry, C., and Bush, D. (2012). From A to Z: a potential role for grid cells in spatial navigation. Neural Syst. Circuits *2*, 1.

Barry, C., Lever, C., Hayman, R., Hartley, T., Burton, S., O'Keefe, J., Jeffery, K., and Burgess, N. (2006). The boundary vector cell model of place cell firing and spatial memory. Rev. Neurosci. *17*, 71.

Barry, C., Hayman, R., Burgess, N., and Jeffery, K.J. (2007). Experience-dependent rescaling of entorhinal grids. Nat. Neurosci. *10*, 682–684.

Barry, C., Ginzberg, L.L., O'Keefe, J., and Burgess, N. (2012a). Grid cell firing patterns signal environmental novelty by expansion. Proc. Natl. Acad. Sci. *109*, 17687–17692.

Barry, C., Bush, D., O'Keefe, J., and Burgess, N. (2012b). Models of grid cells and theta oscillations. Nature *488*, E1–E1.

Bartesaghi, R., and Ravasi, L. (1999). Pyramidal neuron types in field CA2 of the guinea pig. Brain Res. Bull. *50*, 263–273.

Bear, M.F., and Abraham, W.C. (1996). Long-term depression in hippocampus. Annu. Rev. Neurosci. *19*, 437–462.

Bingman, V.P., Gagliardo, A., and Ioalé, P. (1996). Hippocampal participation in the sun compass orientation of phase-shifted homing pigeons. J. Comp. Physiol. [A] *179*, 695–702.

Bird, C.M., and Burgess, N. (2008). The hippocampus and memory: insights from spatial processing. Nat. Rev. Neurosci. *9*, 182–194.

Bland, B.H. (1986). The physiology and pharmacology of hippocampal formation theta rhythms. Prog. Neurobiol. *26*, 1–54.

Bland, B.H., Bird, J., Jackson, J., and Natsume, K. (2006). Medial septal modulation of the ascending brainstem hippocampal synchronizing pathways in the freely moving rat. Hippocampus *16*, 11–19.

Bland, B.H., Derie-Gillespie, D., Mestek, P., Jackson, J., Crooks, R., and Cormican, A. (2007). To move or not: Previous experience in a runway avoidance task determines the appearance of hippocampal Type 2 sensory processing theta. Behav. Brain Res. *179*, 299–304.

Bliss, T.V., and Collingridge, G.L. (1993). A synaptic model of memory: long-term potentiation in the hippocampus. Nature *361*, 31–39.

Bliss, T.V., and Gardner-Medwin, A.R. (1971). Long-lasting increases of synaptic influence in the unanesthetized hippocampus. J. Physiol. *216*, 32P – 33P.

Bliss, T.V., and Lomo, T. (1970). Plasticity in a monosynaptic cortical pathway. J. Physiol. *207*, 61P.

Bliss, T.V.P., and Lømo, T. (1973). Long-lasting potentiation of synaptic transmission in the dentate area of the anaesthetized rabbit following stimulation of the perforant path. J. Physiol. *232*, 331–356.

Boccara, C.N., Sargolini, F., Thoresen, V.H., Solstad, T., Witter, M.P., Moser, E.I., and Moser, M.-B. (2010). Grid cells in pre- and parasubiculum. Nat. Neurosci. *13*, 987–994.

Bonnevie, T., Dunn, B., Fyhn, M., Hafting, T., Derdikman, D., Kubie, J.L., Roudi, Y., Moser, E.I., and Moser, M.-B. (2013). Grid cells require excitatory drive from the hippocampus. Nat. Neurosci. *16*, 309–317.

Borhegyi, Z., Varga, V., Szilágyi, N., Fabo, D., and Freund, T.F. (2004). Phase Segregation of Medial Septal GABAergic Neurons during Hippocampal Theta Activity. J. Neurosci. *24*, 8470–8479.

Bostock, E., Muller, R.U., and Kubie, J.L. (1991). Experience-dependent modifications of hippocampal place cell firing. Hippocampus *1*, 193–205.

Brandon, M.P., Bogaard, A.R., Libby, C.P., Connerney, M.A., Gupta, K., and Hasselmo, M.E. (2011). Reduction of Theta Rhythm Dissociates Grid Cell Spatial Periodicity from Directional Tuning. Science *332*, 595–599.

Brown, T.H., Kairiss, E.W., and Keenan, C.L. (1990). Hebbian synapses: biophysical mechanisms and algorithms. Annu. Rev. Neurosci. *13*, 475–511.

Buckmaster, P.S., Strowbridge, B.W., and Schwartzkroin, P.A. (1993). A comparison of rat hippocampal mossy cells and CA3c pyramidal cells. J. Neurophysiol. *70*, 1281–1299.

Buetfering, C., Allen, K., and Monyer, H. (2014). Parvalbumin interneurons provide grid cell-driven recurrent inhibition in the medial entorhinal cortex. Nat. Neurosci. *17*, 710–718.

Burak, Y., and Fiete, I.R. (2009). Accurate Path Integration in Continuous Attractor Network Models of Grid Cells. PLOS Comput Biol *5*, e1000291.

Burgalossi, A., Herfst, L., von Heimendahl, M., Förste, H., Haskic, K., Schmidt, M., and Brecht, M. (2011). Microcircuits of Functionally Identified Neurons in the Rat Medial Entorhinal Cortex. Neuron *70*, 773–786.

Burgess, N. (2008). Grid cells and theta as oscillatory interference: Theory and predictions. Hippocampus *18*, 1157–1174.

Burgess, N., and O'Keefe, J. (2011). Models of place and grid cell firing and theta rhythmicity. Curr. Opin. Neurobiol. *21*, 734–744.

Burgess, N., Barry, C., and O'Keefe, J. (2007). An oscillatory interference model of grid cell firing. Hippocampus *17*, 801–812.

Burwell, R.D., and Agster, K.L. (2008). 3.03 - Anatomy of the Hippocampus and the Declarative Memory System A2 - Byrne, John H. In Learning and Memory: A Comprehensive Reference, (Oxford: Academic Press), pp. 47–66.

Burwell, R.D., and Amaral, D.G. (1998). Cortical afferents of the perirhinal, postrhinal, and entorhinal cortices of the rat. J. Comp. Neurol. *398*, 179–205.

Bush, D., and Burgess, N. (2014). A Hybrid Oscillatory Interference/Continuous Attractor Network Model of Grid Cell Firing. J. Neurosci. *34*, 5065–5079.

Bush, D., Barry, C., Manson, D., and Burgess, N. (2015). Using Grid Cells for Navigation. Neuron *87*, 507–520.

Buzsáki, G. (2002). Theta Oscillations in the Hippocampus. Neuron *33*, 325–340.

Buzsáki, G., and Moser, E.I. (2013). Memory, navigation and theta rhythm in the hippocampal-entorhinal system. Nat. Neurosci. *16*, 130–138.

Cacucci, F., Yi, M., Wills, T.J., Chapman, P., and O'Keefe, J. (2008). Place cell firing correlates with memory deficits and amyloid plaque burden in Tg2576 Alzheimer mouse model. Proc. Natl. Acad. Sci. *105*, 7863–7868.

Calton, J.L., and Taube, J.S. (2005). Degradation of Head Direction Cell Activity during Inverted Locomotion. J. Neurosci. *25*, 2420–2428.

Canto, C.B., Wouterlood, F.G., and Witter, M.P. (2008). What does the anatomical organization of the entorhinal cortex tell us? Neural Plast. *2008*, 381243.

Cao, Q., Miao, C., Moser, M.B., and Moser, E.I. (2015). Spatially periodic firing in grid cells requires local inhibition through parvalbumin interneurons. (Chicago, USA),.

Carpenter, F., Manson, D., Jeffery, K., Burgess, N., and Barry, C. (2015). Grid Cells Form a Global Representation of Connected Environments. Curr. Biol. *25*, 1176–1182.

Caruana, D.A., Alexander, G.M., and Dudek, S.M. (2012). New insights into the regulation of synaptic plasticity from an unexpected place: hippocampal area CA2. Learn. Mem. Cold Spring Harb. N *19*, 391–400.

C. Gauss (1831). Besprechung des Buchs von L. A. Seeber: Intersuchungen über die Eigenschaften der positiven ternären quadratischen Formen usw. Göttingsche Gelehrte Anzeigen *2*, 188–196.

Chen, G., King, J.A., Burgess, N., and O'Keefe, J. (2013). How vision and movement combine in the hippocampal place code. Proc. Natl. Acad. Sci. *110*, 378–383.

Chen, G., Manson, D., Cacucci, F., and Wills, T.J. (2016). Absence of Visual Input Results in the Disruption of Grid Cell Firing in the Mouse. Curr. Biol.

Chen, L.L., Lin, L.H., Green, E.J., Barnes, C.A., and McNaughton, B.L. (1994). Head-direction cells in the rat posterior cortex. I. Anatomical distribution and behavioral modulation. Exp. Brain Res. *101*, 8–23.

Cho, J., and Sharp, P.E. (2001). Head direction, place, and movement correlates for cells in the rat retrosplenial cortex. Behav. Neurosci. *115*, 3–25.

Citri, A., and Malenka, R.C. (2008). Synaptic plasticity: multiple forms, functions, and mechanisms. Neuropsychopharmacol. Off. Publ. Am. Coll. Neuropsychopharmacol. *33*, 18–41.

Climer, J.R., Newman, E.L., and Hasselmo, M.E. (2013). Phase coding by grid cells in unconstrained environments: two-dimensional phase precession. Eur. J. Neurosci. *38*, 2526–2541.

Climer, J.R., DiTullio, R., Newman, E.L., Hasselmo, M.E., and Eden, U.T. (2015). Examination of rhythmicity of extracellularly recorded neurons in the entorhinal cortex. Hippocampus *25*, 460–473.

Cohen, N.J., and Eichenbaum, H. (1991). The theory that wouldn't die: a critical look at the spatial mapping theory of hippocampal function. Hippocampus *1*, 265–268.

Colom, L.V., Castaneda, M.T., Reyna, T., Hernandez, S., and Garrido-Sanabria, E. (2005). Characterization of medial septal glutamatergic neurons and their projection to the hippocampus. Synap. N. Y. N *58*, 151–164.

Corkin, S. (2002). What's new with the amnesic patient H.M.? Nat. Rev. Neurosci. *3*, 153–160.

Corkin, S., Amaral, D.G., González, R.G., Johnson, K.A., and Hyman, B.T. (1997). H. M.'s

Medial Temporal Lobe Lesion: Findings from Magnetic Resonance Imaging. J. Neurosci. *17*, 3964–3979.

Couey, J.J., Witoelar, A., Zhang, S.-J., Zheng, K., Ye, J., Dunn, B., Czajkowski, R., Moser, M.-B., Moser, E.I., Roudi, Y., et al. (2013). Recurrent inhibitory circuitry as a mechanism for grid formation. Nat. Neurosci. *16*, 318–324.

Danik, M., Cassoly, E., Manseau, F., Sotty, F., Mouginot, D., and Williams, S. (2005). Frequent coexpression of the vesicular glutamate transporter 1 and 2 genes, as well as coexpression with genes for choline acetyltransferase or glutamic acid decarboxylase in neurons of rat brain. J. Neurosci. Res. *81*, 506–521.

Dannenberg, H., Pabst, M., Braganza, O., Schoch, S., Niediek, J., Bayraktar, M., Mormann, F., and Beck, H. (2015). Synergy of Direct and Indirect Cholinergic Septo-Hippocampal Pathways Coordinates Firing in Hippocampal Networks. J. Neurosci. *35*, 8394–8410.

Day, L.B., and Schallert, T. (1996). Anticholinergic effects on acquisition of place learning in the Morris water task: spatial mapping deficit or inability to inhibit nonplace strategies? Behav. Neurosci. *110*, 998–1005.

Derdikman, D., and Moser, E.I. (2010). A manifold of spatial maps in the brain. Trends Cogn. Sci. *14*, 561–569.

Derdikman, D., Whitlock, J.R., Tsao, A., Fyhn, M., Hafting, T., Moser, M.-B., and Moser, E.I. (2009). Fragmentation of grid cell maps in a multicompartment environment. Nat. Neurosci. *12*, 1325–1332.

Deshmukh, S.S., and Knierim, J.J. (2011). Representation of non-spatial and spatial information in the lateral entorhinal cortex. Front. Behav. Neurosci. *5*, 69.

Doeller, C.F., Barry, C., and Burgess, N. (2010). Evidence for grid cells in a human memory network. Nature *463*, 657.

Dolorfo, C.L., and Amaral, D.G. (1998). Entorhinal cortex of the rat: organization of intrinsic connections. J. Comp. Neurol. *398*, 49–82.

Dombeck, D.A., Harvey, C.D., Tian, L., Looger, L.L., and Tank, D.W. (2010). Functional imaging of hippocampal place cells at cellular resolution during virtual navigation. Nat. Neurosci. *13*, 1433–1440.

Domnisoru, C., Kinkhabwala, A.A., and Tank, D.W. (2013). Membrane potential dynamics of grid cells. Nature *495*, 199–204.

Eichenbaum, H. (2000). A cortical-hippocampal system for declarative memory. Nat. Rev. Neurosci. *1*, 41–50.

Eichenbaum, H., Stewart, C., and Morris, R.G. (1990). Hippocampal representation in place learning. J. Neurosci. Off. J. Soc. Neurosci. *10*, 3531–3542.

Eichenbaum, H., Otto, T., and Cohen, N.J. (1992). The hippocampus--what does it do? Behav. Neural Biol. *57*, 2–36.

Ekstrom, A.D., Kahana, M.J., Caplan, J.B., Fields, T.A., Isham, E.A., Newman, E.L., and Fried,

I. (2003). Cellular networks underlying human spatial navigation. Nature *425*, 184–188.

Erdem, U.M., and Hasselmo, M. (2012). A goal-directed spatial navigation model using forward trajectory planning based on grid cells. Eur. J. Neurosci. *35*, 916–931.

Etienne, A.S., and Jeffery, K.J. (2004). Path integration in mammals. Hippocampus *14*, 180–192.

Eyre, M.D., Freund, T.F., and Gulyas, A.I. (2007). Quantitative ultrastructural differences between local and medial septal GABAergic axon terminals in the rat hippocampus. Neuroscience *149*, 537–548.

Fenton, A.A., and Muller, R.U. (1996). Using digital video techniques to identify correlations between behavior and the activity of single neurons. J. Neurosci. Methods *70*, 211–227.

Fenton, A.A., Lytton, W.W., Barry, J.M., Lenck-Santini, P.-P., Zinyuk, L.E., Kubík, S., Bures, J., Poucet, B., Muller, R.U., and Olypher, A.V. (2010). Attention-like modulation of hippocampus place cell discharge. J. Neurosci. Off. J. Soc. Neurosci. *30*, 4613–4625.

Fiete, I.R., Burak, Y., and Brookings, T. (2008). What Grid Cells Convey about Rat Location. J. Neurosci. *28*, 6858–6871.

Finch, D.M., Nowlin, N.L., and Babb, T.L. (1983). Demonstration of axonal projections of neurons in the rat hippocampus and subiculum by intracellular injection of HRP. Brain Res. *271*, 201–216.

Finkelstein, A., Derdikman, D., Rubin, A., Foerster, J.N., Las, L., and Ulanovsky, N. (2015). Three-dimensional head-direction coding in the bat brain. Nature *517*, 159–164.

Freund, T.F. (2003). Interneuron Diversity series: Rhythm and mood in perisomatic inhibition. Trends Neurosci. *26*, 489–495.

Freund, T.F., and Antal, M. (1988). GABA-containing neurons in the septum control inhibitory interneurons in the hippocampus. Nature *336*, 170–173.

Freund, T. f., and Buzsáki, G. (1996). Interneurons of the hippocampus. Hippocampus *6*, 347–470.

Frotscher, M., and Léránth, C. (1985). Cholinergic innervation of the rat hippocampus as revealed by choline acetyltransferase immunocytochemistry: a combined light and electron microscopic study. J. Comp. Neurol. *239*, 237–246.

Fuchs, E.C., Neitz, A., Pinna, R., Melzer, S., Caputi, A., and Monyer, H. (2016). Local and Distant Input Controlling Excitation in Layer II of the Medial Entorhinal Cortex. Neuron *89*, 194–208.

Fuhrmann, F., Justus, D., Sosulina, L., Kaneko, H., Beutel, T., Friedrichs, D., Schoch, S., Schwarz, M.K., Fuhrmann, M., and Remy, S. (2015). Locomotion, Theta Oscillations, and the Speed-Correlated Firing of Hippocampal Neurons Are Controlled by a Medial Septal Glutamatergic Circuit. Neuron *86*, 1253–1264.

Fuhs, M.C., and Touretzky, D.S. (2006). A Spin Glass Model of Path Integration in Rat Medial Entorhinal Cortex. J. Neurosci. *26*, 4266–4276.

Fyhn, M., Molden, S., Witter, M.P., Moser, E.I., and Moser, M.-B. (2004). Spatial Representation in the Entorhinal Cortex. Science *305*, 1258–1264.

Fyhn, M., Hafting, T., Treves, A., Moser, M.-B., and Moser, E.I. (2007). Hippocampal remapping and grid realignment in entorhinal cortex. Nature *446*, 190–194.

Fyhn, M., Hafting, T., Witter, M.P., Moser, E.I., and Moser, M.-B. (2008). Grid cells in mice. Hippocampus *18*, 1230–1238.

Geisler, C., Robbe, D., Zugaro, M., Sirota, A., and Buzsáki, G. (2007). Hippocampal place cell assemblies are speed-controlled oscillators. Proc. Natl. Acad. Sci. *104*, 8149–8154.

Geva-Sagiv, M., Las, L., Yovel, Y., and Ulanovsky, N. (2015). Spatial cognition in bats and rats: from sensory acquisition to multiscale maps and navigation. Nat. Rev. Neurosci. *16*, 94–108.

Gibson, B., Butler, W.N., and Taube, J.S. (2013). The head-direction signal is critical for navigation requiring a cognitive map but not for learning a spatial habit. Curr. Biol. CB *23*, 1536–1540.

Ginosar, G., Finkelstein, A., and Ulanovsky, N. (2014). 3-D grid cells in flying bats. (Washington, USA),.

Ginosar, G., Finkelstein, A., Rubin, A., Las, L., and Ulanovsky, N. (2015). 3D grid cells and border cells in flying bats. (Chicago, USA),.

Giocomo, L.M., Moser, M.-B., and Moser, E.I. (2011a). Computational Models of Grid Cells. Neuron *71*, 589–603.

Giocomo, L.M., Hussaini, S.A., Zheng, F., Kandel, E.R., Moser, M.-B., and Moser, E.I. (2011b). Grid Cells Use HCN1 Channels for Spatial Scaling. Cell *147*, 1159–1170.

Giocomo, L.M., Stensola, T., Bonnevie, T., Van Cauter, T., Moser, M.-B., and Moser, E.I. (2014). Topography of head direction cells in medial entorhinal cortex. Curr. Biol. CB *24*, 252–262.

Gloveli, T., Dugladze, T., Schmitz, D., and Heinemann, U. (2001). Properties of entorhinal cortex deep layer neurons projecting to the rat dentate gyrus. Eur. J. Neurosci. *13*, 413–420.

Gonzalez-Sulser, A., and Nolan, M.F. (2017). Grid cells' need for speed. Nat. Neurosci. *20*, 1–2.

Gonzalez-Sulser, A., Parthier, D., Candela, A., McClure, C., Pastoll, H., Garden, D., Sürmeli, G., and Nolan, M.F. (2014). GABAergic Projections from the Medial Septum Selectively Inhibit Interneurons in the Medial Entorhinal Cortex. J. Neurosci. *34*, 16739–16743.

Goodridge, J.P., and Taube, J.S. (1995). Preferential use of the landmark navigational system by head direction cells in rats. Behav. Neurosci. *109*, 49–61.

Gordon, J.A., Lacefield, C.O., Kentros, C.G., and Hen, R. (2005). State-Dependent Alterations in Hippocampal Oscillations in Serotonin 1A Receptor-Deficient Mice. J. Neurosci. *25*, 6509–6519.

Gothard, K.M., Skaggs, W.E., and McNaughton, B.L. (1996). Dynamics of Mismatch Correction in the Hippocampal Ensemble Code for Space: Interaction between Path Integration and Environmental Cues. J. Neurosci. *16*, 8027–8040.

Goutagny, R., Jackson, J., and Williams, S. (2009). Self-generated theta oscillations in the hippocampus. Nat. Neurosci. *12*, 1491–1493.

Gray, E.G. (1959). Axo-somatic and axo-dendritic synapses of the cerebral cortex: an electron microscope study. J. Anat. *93*, 420–433.

Gray, J.A., McNaughton, N., James, D.T., and Kelly, P.H. (1975). Effect of minor tranquillisers on hippocampal theta rhythm mimicked by depletion of forebrain noradrenaline. Nature *258*, 424–425.

Green, J.D., and Arduini, A.A. (1954). Hippocampal Electrical Activity in Arousal. J. Neurophysiol. *17*, 533–557.

Grieves, R.M., Jenkins, B.W., Harland, B.C., Wood, E.R., and Dudchenko, P.A. (2016). Place field repetition and spatial learning in a multicompartment environment. Hippocampus *26*, 118–134.

Guanella, A., Kiper, D., and Verschure, P. (2007). A model of grid cells based on a twisted torus topology. Int. J. Neural Syst. *17*, 231–240.

Guzowski, J.F., McNaughton, B.L., Barnes, C.A., and Worley, P.F. (1999). Environment-specific expression of the immediate-early gene Arc in hippocampal neuronal ensembles. Nat. Neurosci. *2*, 1120–1124.

Haeften, T. van, Wouterlood, F.G., Jorritsma-Byham, B., and Witter, M.P. (1997). GABAergic Presubicular Projections to the Medial Entorhinal Cortex of the Rat. J. Neurosci. *17*, 862–874.

van Haeften, T., Baks-te-Bulte, L., Goede, P.H., Wouterlood, F.G., and Witter, M.P. (2003). Morphological and numerical analysis of synaptic interactions between neurons in deep and superficial layers of the entorhinal cortex of the rat. Hippocampus *13*, 943–952.

Hafting, T., Fyhn, M., Molden, S., Moser, M.-B., and Moser, E.I. (2005). Microstructure of a spatial map in the entorhinal cortex. Nature *436*, 801–806.

Hafting, T., Fyhn, M., Bonnevie, T., Moser, M.-B., and Moser, E.I. (2008). Hippocampus-independent phase precession in entorhinal grid cells. Nature *453*, 1248–1252.

Hajós, M., Hoffmann, W.E., Robinson, D.D., Yu, J.H., and Hajós-Korcsok, E. (2003). Norepinephrine but not serotonin reuptake inhibitors enhance theta and gamma activity of the septo-hippocampal system. Neuropsychopharmacol. Off. Publ. Am. Coll. Neuropsychopharmacol. *28*, 857–864.

Hajós, M., Siok, C.J., Hoffmann, W.E., Li, S., and Kocsis, B. (2008). Modulation of hippocampal theta oscillation by histamine H3 receptors. J. Pharmacol. Exp. Ther. *324*, 391–398.

Hamam, B.N., Kennedy, T.E., Alonso, A., and Amaral, D.G. (2000). Morphological and electrophysiological characteristics of layer V neurons of the rat medial entorhinal cortex. J.

Comp. Neurol. *418*, 457–472.

Hangya, B., Borhegyi, Z., Szilágyi, N., Freund, T.F., and Varga, V. (2009). GABAergic Neurons of the Medial Septum Lead the Hippocampal Network during Theta Activity. J. Neurosci. *29*, 8094–8102.

Hardcastle, K., Ganguli, S., and Giocomo, L.M. (2015). Environmental Boundaries as an Error Correction Mechanism for Grid Cells. Neuron *86*, 827–839.

Hargreaves, E.L., Rao, G., Lee, I., and Knierim, J.J. (2005). Major dissociation between medial and lateral entorhinal input to dorsal hippocampus. Science *308*, 1792–1794.

Harris, K.D., Hirase, H., Leinekugel, X., Henze, D.A., and Buzsáki, G. (2001). Temporal Interaction between Single Spikes and Complex Spike Bursts in Hippocampal Pyramidal Cells. Neuron *32*, 141–149.

Hartley, T., Lever, C., Burgess, N., and O'Keefe, J. (2014). Space in the brain: how the hippocampal formation supports spatial cognition. Phil Trans R Soc B *369*, 20120510.

Harvey, C.D., Collman, F., Dombeck, D.A., and Tank, D.W. (2009). Intracellular dynamics of hippocampal place cells during virtual navigation. Nature *461*, 941–946.

Hasselmo, M.E. (2006). The role of acetylcholine in learning and memory. Curr. Opin. Neurobiol. *16*, 710–715.

Hasselmo, M.E., Bodelón, C., and Wyble, B.P. (2002). A Proposed Function for Hippocampal Theta Rhythm: Separate Phases of Encoding and Retrieval Enhance Reversal of Prior Learning. Neural Comput. *14*, 793–817.

Hasselmo, M.E., Giocomo, L.M., and Zilli, E.A. (2007). Grid cell firing may arise from interference of theta frequency membrane potential oscillations in single neurons. Hippocampus *17*, 1252–1271.

Hayman, R., Verriotis, M.A., Jovalekic, A., Fenton, A.A., and Jeffery, K.J. (2011). Anisotropic encoding of three-dimensional space by place cells and grid cells. Nat. Neurosci. *14*, 1182–1188.

Hayman, R.M.A., Casali, G., Wilson, J.J., and Jeffery, K.J. (2015). Grid cells on steeply sloping terrain: evidence for planar rather than volumetric encoding. Front. Psychol. *6*.

Hebb, D.O. (1949). The organisation of behavior : a neuropsychologicaltheory. (New York: Wiley and Sons).

Hetherington, P.A., and Shapiro, M.L. (1997). Hippocampal place fields are altered by the removal of single visual cues in a distance-dependent manner. Behav. Neurosci. *111*, 20–34.

Hinman, J.R., Brandon, M.P., Climer, J.R., Chapman, G.W., and Hasselmo, M.E. (2016). Multiple Running Speed Signals in Medial Entorhinal Cortex. Neuron *91*, 666–679.

Horiuchi, T.K., and Moss, C.F. (2015). Grid cells in 3-D: Reconciling data and models. Hippocampus *25*, 1489–1500.

Huh, C.Y.L., Goutagny, R., and Williams, S. (2010). Glutamatergic Neurons of the Mouse Medial Septum and Diagonal Band of Broca Synaptically Drive Hippocampal Pyramidal Cells: Relevance for Hippocampal Theta Rhythm. J. Neurosci. *30*, 15951–15961.

Insausti, R., Herrero, M.T., and Witter, M.P. (1997). Entorhinal cortex of the rat: cytoarchitectonic subdivisions and the origin and distribution of cortical efferents. Hippocampus *7*, 146–183.

Ishizuka, N., Weber, J., and Amaral, D.G. (1990). Organization of intrahippocampal projections originating from CA3 pyramidal cells in the rat. J. Comp. Neurol. *295*, 580–623.

Jackson, J., Amilhon, B., Goutagny, R., Bott, J.-B., Manseau, F., Kortleven, C., Bressler, S.L., and Williams, S. (2014). Reversal of theta rhythm flow through intact hippocampal circuits. Nat. Neurosci. *17*, 1362–1370.

Jacob, P.-Y., Poucet, B., Liberge, M., Save, E., and Sargolini, F. (2014). Vestibular control of entorhinal cortex activity in spatial navigation. Front. Integr. Neurosci. *8*.

Jacob, P.-Y., Casali, G., Spieser, L., Page, H., Overington, D., and Jeffery, K. (2016). An independent, landmark-dominated head-direction signal in dysgranular retrosplenial cortex. Nat. Neurosci. *advance online publication*.

Jarrard, L.E. (1983). Selective hippocampal lesions and behavior: effects of kainic acid lesions on performance of place and cue tasks. Behav. Neurosci. *97*, 873–889.

Jeewajee, A., Barry, C., O'Keefe, J., and Burgess, N. (2008a). Grid cells and theta as oscillatory interference: Electrophysiological data from freely moving rats. Hippocampus *18*, 1175–1185.

Jeewajee, A., Lever, C., Burton, S., O'Keefe, J., and Burgess, N. (2008b). Environmental novelty is signaled by reduction of the hippocampal theta frequency. Hippocampus *18*, 340–348.

Jeewajee, A., Barry, C., Douchamps, V., Manson, D., Lever, C., and Burgess, N. (2014). Theta phase precession of grid and place cell firing in open environments. Philos. Trans. R. Soc. Lond. B Biol. Sci. *369*, 20120532.

Jeffery, K.J., and Burgess, N. (2006). A metric for the cognitive map: found at last? Trends Cogn. Sci. *10*, 1–3.

Jeffery, K.J., Donnett, J.G., Burgess, N., and O'Keefe, J.M. (1997). Directional control of hippocampal place fields. Exp. Brain Res. *117*, 131–142.

Jeffery, K.J., Jovalekic, A., Verriotis, M., and Hayman, R. (2013a). Navigating in a three-dimensional world. Behav. Brain Sci. *36*, 523–543.

Jeffery, K.J., Jovalekic, A., Verriotis, M., and Hayman, R. (2013b). Navigating in a three-dimensional world. Behav. Brain Sci. *36*, 523–543.

Jeffery, K.J., Wilson, J.J., Casali, G., and Hayman, R.M. (2015). Neural encoding of large-scale three-dimensional space—properties and constraints. Front. Psychol. *6*.

Jovalekic, A., Hayman, R., Becares, N., Reid, H., Thomas, G., Wilson, J., and Jeffery, K.

(2011). Horizontal biases in rats' use of three-dimensional space. Behav. Brain Res. *222*, 279–288.

Jung, R., and Kornmüller, A.E. (1938). Eine Methodik der Ableitung Iokalisierter Potentialschwankungen aus subcorticalen Hirngebieten. Arch. Für Psychiatr. Nervenkrankh. *109*, 1–30.

Jung, M.W., Wiener, S.I., and McNaughton, B.L. (1994). Comparison of spatial firing characteristics of units in dorsal and ventral hippocampus of the rat. J. Neurosci. *14*, 7347–7356.

Justus, D., Dalügge, D., Bothe, S., Fuhrmann, F., Hannes, C., Kaneko, H., Friedrichs, D., Sosulina, L., Schwarz, I., Elliott, D.A., et al. (2017). Glutamatergic synaptic integration of locomotion speed via septoentorhinal projections. Nat. Neurosci. *20*, 16–19.

Kadir, S.N., Goodman, D.F.M., and Harris, K.D. (2014). High-dimensional cluster analysis with the Masked EM Algorithm. Neural Comput. *26*, 2379–2394.

Kandel, E.R., and Tauc, L. (1965a). Mechanism of heterosynaptic facilitation in the giant cell of the abdominal ganglion of Aplysia depilans. J. Physiol. *181*, 28–47.

Kandel, E.R., and Tauc, L. (1965b). Heterosynaptic facilitation in neurones of the abdominal ganglion of Aplysia depilans. J. Physiol. *181*, 1–27.

Kerr, K.M., Agster, K.L., Furtak, S.C., and Burwell, R.D. (2007). Functional neuroanatomy of the parahippocampal region: the lateral and medial entorhinal areas. Hippocampus *17*, 697–708.

Killian, N.J., Jutras, M.J., and Buffalo, E.A. (2012). A map of visual space in the primate entorhinal cortex. Nature *491*, 761–764.

King, C., Recce, M., and O'Keefe, J. (1998). The rhythmicity of cells of the medial septum/diagonal band of Broca in the awake freely moving rat: relationships with behaviour and hippocampal theta. Eur. J. Neurosci. *10*, 464–477.

Kinney, G.G., Patino, P., Mermet-Bouvier, Y., Starrett, J., and Gribkoff, V.K. (1999). Cognition-enhancing drugs increase stimulated hippocampal θ rhythm amplitude in the urethane-anesthetized rat. J. Pharmacol. Exp. Ther. *291*, 99–106.

Klausberger, T., and Somogyi, P. (2008). Neuronal Diversity and Temporal Dynamics: The Unity of Hippocampal Circuit Operations. Science *321*, 53–57.

Klausberger, T., Roberts, J.D.B., and Somogyi, P. (2002). Cell type- and input-specific differences in the number and subtypes of synaptic GABA(A) receptors in the hippocampus. J. Neurosci. Off. J. Soc. Neurosci. *22*, 2513–2521.

Klausberger, T., Magill, P.J., Márton, L.F., Roberts, J.D.B., Cobden, P.M., Buzsáki, G., and Somogyi, P. (2003). Brain-state- and cell-type-specific firing of hippocampal interneurons in vivo. Nature *421*, 844–848.

Klink, R., and Alonso, A. (1997). Morphological characteristics of layer II projection neurons in the rat medial entorhinal cortex. Hippocampus *7*, 571–583.

Kloosterman, F., Van Haeften, T., Witter, M.P., and Lopes da Silva, F.H. (2003). Electrophysiological characterization of interlaminar entorhinal connections: an essential link for re-entrance in the hippocampal–entorhinal system. Eur. J. Neurosci. *18*, 3037–3052.

Knierim, J.J., and McNaughton, B.L. (2001). Hippocampal place-cell firing during movement in three-dimensional space. J. Neurophysiol. *85*, 105–116.

Knierim, J.J., Lee, I., and Hargreaves, E.L. (2006). Hippocampal place cells: parallel input streams, subregional processing, and implications for episodic memory. Hippocampus *16*, 755–764.

Koenig, J., Linder, A.N., Leutgeb, J.K., and Leutgeb, S. (2011). The Spatial Periodicity of Grid Cells Is Not Sustained During Reduced Theta Oscillations. Science *332*, 592–595.

Köhler, C., Shipley, M.T., Srebro, B., and Harkmark, W. (1978). Some retrohippocampal afferents to the entorhinal cortex. Cells of origin as studied by the HRP method in the rat and mouse. Neurosci. Lett. *10*, 115–120.

Kramis, R., Vanderwolf, C.H., and Bland, B.H. (1975). Two types of hippocampal rhythmical slow activity in both the rabbit and the rat: Relations to behavior and effects of atropine, diethyl ether, urethane, and pentobarbital. Exp. Neurol. *49*, 58–85.

Kropff, E., and Treves, A. (2008). The emergence of grid cells: Intelligent design or just adaptation? Hippocampus *18*, 1256–1269.

Kropff, E., Carmichael, J.E., Moser, M.-B., and Moser, E.I. (2015). Speed cells in the medial entorhinal cortex. Nature *523*, 419–424.

Krupic, J., Bauza, M., Burton, S., Lever, C., and O'Keefe, J. (2014). How environment geometry affects grid cell symmetry and what we can learn from it. Phil Trans R Soc B *369*, 20130188.

Krupic, J., Bauza, M., Burton, S., Barry, C., and O'Keefe, J. (2015). Grid cell symmetry is shaped by environmental geometry. Nature *518*, 232–235.

Langston, R.F., Ainge, J.A., Couey, J.J., Canto, C.B., Bjerknes, T.L., Witter, M.P., Moser, E.I., and Moser, M.-B. (2010). Development of the Spatial Representation System in the Rat. Science *328*, 1576–1580.

Laurberg, S. (1979). Commissural and intrinsic connections of the rat hippocampus. J. Comp. Neurol. *184*, 685–708.

Laurberg, S., and Sørensen, K.E. (1981). Associational and commissural collaterals of neurons in the hippocampal formation (hilus fasciae dentatae and subfield CA3). Brain Res. *212*, 287–300.

Lawrence, J.J. (2008). Cholinergic control of GABA release: emerging parallels between neocortex and hippocampus. Trends Neurosci. *31*, 317–327.

Lee, M.G., Chrobak, J.J., Sik, A., Wiley, R.G., and Buzsáki, G. (1994). Hippocampal theta activity following selective lesion of the septal cholinergic system. Neuroscience *62*, 1033–1047.

Leutgeb, S., and Leutgeb, J.K. (2007). Pattern separation, pattern completion, and new neuronal codes within a continuous CA3 map. Learn. Mem. *14*, 745–757.

Leutgeb, S., Leutgeb, J.K., Treves, A., Moser, M.-B., and Moser, E.I. (2004). Distinct Ensemble Codes in Hippocampal Areas CA3 and CA1. Science *305*, 1295–1298.

Leutgeb, S., Leutgeb, J.K., Barnes, C.A., Moser, E.I., McNaughton, B.L., and Moser, M.-B. (2005). Independent Codes for Spatial and Episodic Memory in Hippocampal Neuronal Ensembles. Science *309*, 619–623.

Lever, C., Burton, S., Jeewajee, A., O'Keefe, J., and Burgess, N. (2009). Boundary Vector Cells in the Subiculum of the Hippocampal Formation. J. Neurosci. *29*, 9771–9777.

Lever, C., Burton, S., Jeewajee, A., Wills, T.J., Cacucci, F., Burgess, N., and O'Keefe, J. (2010). Environmental novelty elicits a later theta phase of firing in CA1 but not subiculum. Hippocampus *20*, 229–234.

Lomo, T. (1971a). Potentiation of monosynaptic EPSPs in the perforant path-dentate granule cell synapse. Exp. Brain Res. *12*, 46–63.

Lomo, T. (1971b). Patterns of activation in a monosynaptic cortical pathway: the perforant path input to the dentate area of the hippocampal formation. Exp. Brain Res. *12*, 18–45.

Manseau, F., Goutagny, R., Danik, M., and Williams, S. (2008). The Hippocamposeptal Pathway Generates Rhythmic Firing of GABAergic Neurons in the Medial Septum and Diagonal Bands: An Investigation Using a Complete Septohippocampal Preparation In Vitro. J. Neurosci. *28*, 4096–4107.

Marozzi, E., Ginzberg, L.L., Alenda, A., and Jeffery, K.J. (2015). Purely Translational Realignment in Grid Cell Firing Patterns Following Nonmetric Context Change. Cereb. Cortex *25*, 4619–4627.

Mathis, A., Herz, A.V.M., and Stemmler, M. (2012). Optimal Population Codes for Space: Grid Cells Outperform Place Cells. Neural Comput. *24*, 2280–2317.

Mathis, A., Stemmler, M.B., and Herz, A.V. (2015). Probable nature of higher-dimensional symmetries underlying mammalian grid-cell activity patterns. eLife *4*, e05979.

McFarland, W.L., Teitelbaum, H., and Hedges, E.K. (1975). Relationship between hippocampal theta activity and running speed in the rat. J. Comp. Physiol. Psychol. *88*, 324–328.

McNaughton, B.L., Barnes, C.A., and O'Keefe, J. (1983). The contributions of position, direction, and velocity to single unit activity in the hippocampus of freely-moving rats. Exp. Brain Res. *52*, 41–49.

McNaughton, B.L., Battaglia, F.P., Jensen, O., Moser, E.I., and Moser, M.-B. (2006). Path integration and the neural basis of the "cognitive map." Nat. Rev. Neurosci. *7*, 663–678.

Megías, M., Emri, Z., Freund, T.F., and Gulyás, A.I. (2001). Total number and distribution of inhibitory and excitatory synapses on hippocampal CA1 pyramidal cells. Neuroscience *102*, 527–540.

Monmaur, P., Collet, A., Puma, C., Frankel-Kohn, L., and Sharif, A. (1997). Relations between acetylcholine release and electrophysiological characteristics of theta rhythm: A microdialysis study in the urethane-anesthetized rat hippocampus. Brain Res. Bull. *42*, 141–146.

Morris, R.G.M. (1981). Spatial localization does not require the presence of local cues. Learn. Motiv. *12*, 239–260.

Morris, R.G., Garrud, P., Rawlins, J.N., and O'Keefe, J. (1982). Place navigation impaired in rats with hippocampal lesions. Nature *297*, 681–683.

Moser, E.I., and Moser, M.-B. (2008). A metric for space. Hippocampus *18*, 1142–1156.

Moser, E.I., Kropff, E., and Moser, M.-B. (2008). Place cells, grid cells, and the brain's spatial representation system. Annu. Rev. Neurosci. *31*, 69–89.

Moser, M.B., Moser, E.I., Forrest, E., Andersen, P., and Morris, R.G. (1995). Spatial learning with a minislab in the dorsal hippocampus. Proc. Natl. Acad. Sci. U. S. A. *92*, 9697–9701.

Muller, R. (1996). A quarter of a century of place cells. Neuron *17*, 813–822.

Muller, R.U., and Kubie, J.L. (1987). The effects of changes in the environment on the spatial firing of hippocampal complex-spike cells. J. Neurosci. *7*, 1951–1968.

Muller, R.U., Kubie, J.L., and Ranck, J.B. (1987). Spatial firing patterns of hippocampal complex-spike cells in a fixed environment. J. Neurosci. Off. J. Soc. Neurosci. *7*, 1935–1950.

Naber, P.A., Lopes da Silva, F.H., and Witter, M.P. (2001). Reciprocal connections between the entorhinal cortex and hippocampal fields CA1 and the subiculum are in register with the projections from CA1 to the subiculum. Hippocampus *11*, 99–104.

Nagode, D.A., Tang, A.-H., Karson, M.A., Klugmann, M., and Alger, B.E. (2011). Optogenetic Release of ACh Induces Rhythmic Bursts of Perisomatic IPSCs in Hippocampus. PLOS ONE *6*, e27691.

Nagode, D.A., Tang, A.-H., Yang, K., and Alger, B.E. (2014). Optogenetic identification of an intrinsic cholinergically driven inhibitory oscillator sensitive to cannabinoids and opioids in hippocampal CA1. J. Physiol. *592*, 103–123.

Neves, G., Cooke, S.F., and Bliss, T.V.P. (2008). Synaptic plasticity, memory and the hippocampus: a neural network approach to causality. Nat. Rev. Neurosci. *9*, 65–75.

O'Keefe, J. (1976). Place units in the hippocampus of the freely moving rat. Exp. Neurol. *51*, 78–109.

O'Keefe, J. (2006). Hippocampal Neurophysiology in the Behaving Animal. In The Hippocampus Book, P. Andersen, R. Morris, D. Amaral, T. Bliss, and J. O'Keefe, eds. (Oxford University Press), pp. 475–548.

O'Keefe, J., and Burgess, N. (1996). Geometric determinants of the place fields of hippocampal neurons. Nature *381*, 425–428.

O'Keefe, J., and Conway, D.H. (1978). Hippocampal place units in the freely moving rat: why

they fire where they fire. Exp. Brain Res. *31*, 573–590.

O'Keefe, J., and Dostrovsky, J. (1971). The hippocampus as a spatial map. Preliminary evidence from unit activity in the freely-moving rat. Brain Res. *34*, 171–175.

O'Keefe, J., and Nadel, L. (1978). The Hippocampus as a Cognitive Map (Oxford : New York: Oxford University Press).

O'Keefe, J., and Recce, M.L. (1993). Phase relationship between hippocampal place units and the EEG theta rhythm. Hippocampus *3*, 317–330.

Ólafsdóttir, H.F., and Barry, C. (2015). Spatial Cognition: Grid Cell Firing Depends on Self-Motion Cues. Curr. Biol. *25*, R827–R829.

Olton, D.S., and Papas, B.C. (1979). Spatial memory and hippocampal function. Neuropsychologia *17*, 669–682.

Olton, D.S., and Samuelson, R.J. (1976). Remembrance of places passed: Spatial memory in rats. J. Exp. Psychol. Anim. Behav. Process. *2*, 97–116.

Olton, D.S., Walker, J.A., and Gage, F.H. (1978). Hippocampal connections and spatial discrimination. Brain Res. *139*, 295–308.

Pastoll, H., Solanka, L., van Rossum, M.C.W., and Nolan, M.F. (2013). Feedback Inhibition Enables Theta-Nested Gamma Oscillations and Grid Firing Fields. Neuron *77*, 141–154.

Paz-Villagràn, V., Lenck-Santini, P.-P., Save, E., and Poucet, B. (2002). Properties of place cell firing after damage to the visual cortex. Eur. J. Neurosci. *16*, 771–776.

Pérez-Escobar, J.A., Kornienko, O., Latuske, P., Kohler, L., and Allen, K. (2016). Visual landmarks sharpen grid cell metric and confer context specificity to neurons of the medial entorhinal cortex. eLife *5*, e16937.

Petilla Interneuron Nomenclature Group, Ascoli, G.A., Alonso-Nanclares, L., Anderson, S.A., Barrionuevo, G., Benavides-Piccione, R., Burkhalter, A., Buzsáki, G., Cauli, B., Defelipe, J., et al. (2008). Petilla terminology: nomenclature of features of GABAergic interneurons of the cerebral cortex. Nat. Rev. Neurosci. *9*, 557–568.

Petsche, H., Stumpf, C., and Gogolak, G. (1962). [The significance of the rabbit's septum as a relay station between the midbrain and the hippocampus. I. The control of hippocampus arousal activity by the septum cells]. Electroencephalogr. Clin. Neurophysiol. *14*, 202–211.

Peyrache, A., Lacroix, M.M., Petersen, P.C., and Buzsáki, G. (2015). Internally organized mechanisms of the head direction sense. Nat. Neurosci. *18*, 569–575.

Poucet, B., Thinus-Blanc, C., and Muller, R.U. (1994). Place cells in the ventral hippocampus of rats. Neuroreport *5*, 2045–2048.

Quirk, G.J., Muller, R.U., and Kubie, J.L. (1990). The firing of hippocampal place cells in the dark depends on the rat's recent experience. J. Neurosci. Off. J. Soc. Neurosci. *10*, 2008–2017.

Ranck, J. (1984). Head direction cells in the deep layer of dorsal presubiculum in freely

moving rats.

Ranck, J.B. (1973). Studies on single neurons in dorsal hippocampal formation and septum in unrestrained rats. I. Behavioral correlates and firing repertoires. Exp. Neurol. *41*, 461–531.

Raudies, F., Brandon, M.P., Chapman, G.W., and Hasselmo, M.E. (2015). Head direction is coded more strongly than movement direction in a population of entorhinal neurons. Brain Res. *1621*, 355–367.

Ravassard, P., Kees, A., Willers, B., Ho, D., Aharoni, D., Cushman, J., Aghajan, Z.M., and Mehta, M.R. (2013). Multisensory Control of Hippocampal Spatiotemporal Selectivity. Science *340*, 1342–1346.

Ray, S., Naumann, R., Burgalossi, A., Tang, Q., Schmidt, H., and Brecht, M. (2014). Grid-Layout and Theta-Modulation of Layer 2 Pyramidal Neurons in Medial Entorhinal Cortex. Science *343*, 891–896.

Robinson, J., Manseau, F., Ducharme, G., Amilhon, B., Vigneault, E., Mestikawy, S.E., and Williams, S. (2016). Optogenetic Activation of Septal Glutamatergic Neurons Drive Hippocampal Theta Rhythms. J. Neurosci. *36*, 3016–3023.

Rolls, E.T., Miyashita, Y., Cahusac, P.M., Kesner, R.P., Niki, H., Feigenbaum, J.D., and Bach, L. (1989). Hippocampal neurons in the monkey with activity related to the place in which a stimulus is shown. J. Neurosci. Off. J. Soc. Neurosci. *9*, 1835–1845.

Rowland, D.C., Roudi, Y., Moser, M.-B., and Moser, E.I. (2016). Ten Years of Grid Cells. Annu. Rev. Neurosci. *39*, null.

Rubin, A., Yartsev, M.M., and Ulanovsky, N. (2014). Encoding of head direction by hippocampal place cells in bats. J. Neurosci. Off. J. Soc. Neurosci. *34*, 1067–1080.

Sainsbury, R.S., Heynen, A., and Montoya, C.P. (1987). Behavioral correlates of hippocampal type 2 theta in the rat. Physiol. Behav. *39*, 513–519.

Saleem, A.B., Ayaz, A., Jeffery, K.J., Harris, K.D., and Carandini, M. (2013). Integration of visual motion and locomotion in mouse visual cortex. Nat. Neurosci. *16*, 1864–1869.

Samsonovich, A., and McNaughton, B.L. (1997). Path Integration and Cognitive Mapping in a Continuous Attractor Neural Network Model. J. Neurosci. *17*, 5900–5920.

Sargolini, F., Fyhn, M., Hafting, T., McNaughton, B.L., Witter, M.P., Moser, M.-B., and Moser, E.I. (2006). Conjunctive Representation of Position, Direction, and Velocity in Entorhinal Cortex. Science *312*, 758–762.

Save, E., Cressant, A., Thinus-Blanc, C., and Poucet, B. (1998). Spatial Firing of Hippocampal Place Cells in Blind Rats. J. Neurosci. *18*, 1818–1826.

Schmidt-Hieber, C., and Häusser, M. (2013). Cellular mechanisms of spatial navigation in the medial entorhinal cortex. Nat. Neurosci. *16*, 325–331.

Scoville, W.B., and Milner, B. (1957). Loss of recent memory after bilateral hippocampal lesions. J. Neurol. Neurosurg. Psychiatry *20*, 11–21.

Segal, M., and Landis, S. (1974). Afferents to the hippocampus of the rat studied with the method of retrograde transport of horseradish peroxidase. Brain Res. *78*, 1–15.

Seidenbecher, T., Laxmi, T.R., Stork, O., and Pape, H.-C. (2003). Amygdalar and Hippocampal Theta Rhythm Synchronization During Fear Memory Retrieval. Science *301*, 846–850.

Shepard, J.F. (1933). Higher Processes in the Behavior of Rats. Proc. Natl. Acad. Sci. U. S. A. *19*, 149–152.

Shin, J., Gireesh, G., Kim, S.-W., Kim, D.-S., Lee, S., Kim, Y.-S., Watanabe, M., and Shin, H.-S. (2009). Phospholipase C β4 in the Medial Septum Controls Cholinergic Theta Oscillations and Anxiety Behaviors. J. Neurosci. *29*, 15375–15385.

Shipston-Sharman, O., Solanka, L., and Nolan, M.F. (2016). Continuous attractor network models of grid cell firing based on excitatory–inhibitory interactions. J. Physiol. *594*, 6547–6557.

Skaggs, W.E., McNaughton, B.L., Gothard, K.M., and Markus, E.J. (1993). An Information-Theoretic Approach to Deciphering the Hippocampal Code. In In, (Morgan Kaufmann), pp. 1030–1037.

Solanka, L., Rossum, M.C. van, and Nolan, M.F. (2015). Noise promotes independent control of gamma oscillations and grid firing within recurrent attractor networks. eLife *4*, e06444.

Solstad, T., Boccara, C.N., Kropff, E., Moser, M.-B., and Moser, E.I. (2008). Representation of Geometric Borders in the Entorhinal Cortex. Science *322*, 1865–1868.

Somogyi, P., and Klausberger, T. (2005). Defined types of cortical interneurone structure space and spike timing in the hippocampus. J. Physiol. *562*, 9–26.

Speakman, A., and O'Keefe, J. (1990). Hippocampal Complex Spike Cells do not Change Their Place Fields if the Goal is Moved Within a Cue Controlled Environment. Eur. J. Neurosci. *2*, 544–555.

Spruston, N. (2008). Pyramidal neurons: dendritic structure and synaptic integration. Nat. Rev. Neurosci. *9*, 206–221.

Stackman, R.W., and Taube, J.S. (1998). Firing Properties of Rat Lateral Mammillary Single Units: Head Direction, Head Pitch, and Angular Head Velocity. J. Neurosci. *18*, 9020–9037.

Stackman, R.W., Tullman, M.L., and Taube, J.S. (2000). Maintenance of rat head direction cell firing during locomotion in the vertical plane. J. Neurophysiol. *83*, 393–405.

Stella, F., and Treves, A. (2015). The self-organization of grid cells in 3D. eLife *4*, e05913.

Stensola, H., Stensola, T., Solstad, T., Frøland, K., Moser, M.-B., and Moser, E.I. (2012). The entorhinal grid map is discretized. Nature *492*, 72–78.

Stensola, T., Stensola, H., Moser, M.-B., and Moser, E.I. (2015). Shearing-induced asymmetry in entorhinal grid cells. Nature *518*, 207–212.

Stewart, M., and Fox, S.E. (1989a). Two populations of rhythmically bursting neurons in rat medial septum are revealed by atropine. J. Neurophysiol. *61*, 982–993.

Stewart, M., and Fox, S.E. (1989b). Firing relations of medial septal neurons to the hippocampal theta rhythm in urethane anesthetized rats. Exp. Brain Res. *77*, 507–516.

Stewart, M., and Fox, S.E. (1989c). Detection of an atropine-resistant component of the hippocampal theta rhythm in urethane-anesthetized rats. Brain Res. *500*, 55–60.

Stoiljkovic, M., Kelley, C., Nagy, D., and Hajós, M. (2015). Modulation of hippocampal neuronal network oscillations by α7 nACh receptors. Biochem. Pharmacol. *97*, 445–453.

van Strien, N.M., Cappaert, N.L.M., and Witter, M.P. (2009). The anatomy of memory: an interactive overview of the parahippocampal–hippocampal network. Nat. Rev. Neurosci. *10*, 272–282.

Sürmeli, G., Marcu, D.C., McClure, C., Garden, D.L.F., Pastoll, H., and Nolan, M.F. (2015). Molecularly Defined Circuitry Reveals Input-Output Segregation in Deep Layers of the Medial Entorhinal Cortex. Neuron *88*, 1040–1053.

Swanson, L.W., Sawchenko, P.E., and Cowan, W.M. (1981). Evidence for collateral projections by neurons in Ammon's horn, the dentate gyrus, and the subiculum: a multiple retrograde labeling study in the rat. J. Neurosci. Off. J. Soc. Neurosci. *1*, 548–559.

Takács, V.T., Freund, T.F., and Gulyás, A.I. (2008). Types and synaptic connections of hippocampal inhibitory neurons reciprocally connected with the medial septum. Eur. J. Neurosci. *28*, 148–164.

Takahashi, M., Lauwereyns, J., Sakurai, Y., and Tsukada, M. (2009). Behavioral state-dependent episodic representations in rat CA1 neuronal activity during spatial alternation. Cogn. Neurodyn. *3*, 165–175.

Tamamaki, N., and Nojyo, Y. (1990). Disposition of the slab-like modules formed by axon branches originating from single CA1 pyramidal neurons in the rat hippocampus. J. Comp. Neurol. *291*, 509–519.

Tang, Q., Burgalossi, A., Ebbesen, C.L., Ray, S., Naumann, R., Schmidt, H., Spicher, D., and Brecht, M. (2014). Pyramidal and Stellate Cell Specificity of Grid and Border Representations in Layer 2 of Medial Entorhinal Cortex. Neuron *84*, 1191–1197.

Taube, J.S. (1995). Head direction cells recorded in the anterior thalamic nuclei of freely moving rats. J. Neurosci. *15*, 70–86.

Taube, J.S. (2007). The Head Direction Signal: Origins and Sensory-Motor Integration. Annu. Rev. Neurosci. *30*, 181–207.

Taube, J.S., and Shinder, M. (2013). On the nature of three-dimensional encoding in the cognitive map: Commentary on Hayman, Verriotis, Jovalekic, Fenton, and Jeffery. Hippocampus *23*, 14–21.

Taube, J.S., Muller, R.U., and Ranck, J.B. (1990a). Head-direction cells recorded from the postsubiculum in freely moving rats. I. Description and quantitative analysis. J. Neurosci. *10*, 420–435.

Taube, J.S., Muller, R.U., and Ranck, J.B. (1990b). Head-direction cells recorded from the postsubiculum in freely moving rats. II. Effects of environmental manipulations. J. Neurosci. *10*, 436–447.

Taube, J.S., Wang, S.S., Kim, S.Y., and Frohardt, R.J. (2013). Updating of the spatial reference frame of head direction cells in response to locomotion in the vertical plane. J. Neurophysiol. *109*, 873–888.

Thinus-Blanc, C. (1996). Animal spatial cognition : behavioural and brain approach (Singapore; River Edge, N.J.: World Scientific Pub. Co.).

Thompson, L.T., and Best, P.J. (1989). Place cells and silent cells in the hippocampus of freely-behaving rats. J. Neurosci. Off. J. Soc. Neurosci. *9*, 2382–2390.

Thorndike, E.L. (1898). Animal intelligence: An experimental study of the associative processes in animals. Psychol. Rev. Monogr. Suppl. *2*, i – 109.

Tolman, E.C. (1948). Cognitive maps in rats and men. Psychol. Rev. *55*, 189–208.

Tonegawa, S., Tsien, J.Z., McHugh, T.J., Huerta, P., Blum, K.I., and Wilson, M.A. (1996). Hippocampal CA1-region-restricted knockout of NMDAR1 gene disrupts synaptic plasticity, place fields, and spatial learning. Cold Spring Harb. Symp. Quant. Biol. *61*, 225–238.

Tóth, K., Borhegyi, Z., and Freund, T.F. (1993). Postsynaptic targets of GABAergic hippocampal neurons in the medial septum-diagonal band of broca complex. J. Neurosci. Off. J. Soc. Neurosci. *13*, 3712–3724.

Towse, B.W., Barry, C., Bush, D., and Burgess, N. (2014). Optimal configurations of spatial scale for grid cell firing under noise and uncertainty. Philos. Trans. R. Soc. Lond. B Biol. Sci. *369*, 20130290.

Tukker, J.J., Lasztóczi, B., Katona, L., Roberts, J.D.B., Pissadaki, E.K., Dalezios, Y., Márton, L., Zhang, L., Klausberger, T., and Somogyi, P. (2013). Distinct dendritic arborization and in vivo firing patterns of parvalbumin-expressing basket cells in the hippocampal area CA3. J. Neurosci. Off. J. Soc. Neurosci. *33*, 6809–6825.

Ulanovsky, N., and Moss, C.F. (2007). Hippocampal cellular and network activity in freely moving echolocating bats. Nat. Neurosci. *10*, 224–233.

Ulanovsky, N., and Moss, C.F. (2011). Dynamics of hippocampal spatial representation in echolocating bats. Hippocampus *21*, 150–161.

Valerio, S., Clark, B.J., Chan, J.H.M., Frost, C.P., Harris, M.J., and Taube, J.S. (2010). Directional learning, but no spatial mapping by rats performing a navigational task in an inverted orientation. Neurobiol. Learn. Mem. *93*, 495–505.

Vandecasteele, M., Varga, V., Berényi, A., Papp, E., Barthó, P., Venance, L., Freund, T.F., and Buzsáki, G. (2014). Optogenetic activation of septal cholinergic neurons suppresses sharp wave ripples and enhances theta oscillations in the hippocampus. Proc. Natl. Acad. Sci. *111*, 13535–13540.

Vanderwolf, C.H. (1969). Hippocampal electrical activity and voluntary movement in the rat. Electroencephalogr. Clin. Neurophysiol. *26*, 407–418.

Varga, V., Hangya, B., Kránitz, K., Ludányi, A., Zemankovics, R., Katona, I., Shigemoto, R., Freund, T.F., and Borhegyi, Z. (2008). The presence of pacemaker HCN channels identifies theta rhythmic GABAergic neurons in the medial septum. J. Physiol. *586*, 3893–3915.

Vertes, R.P., and Kocsis, B. (1997). Brainstem-diencephalo-septohippocampal systems controlling the theta rhythm of the hippocampus. Neuroscience *81*, 893–926.

Welday, A.C., Shlifer, I.G., Bloom, M.L., Zhang, K., and Blair, H.T. (2011). Cosine Directional Tuning of Theta Cell Burst Frequencies: Evidence for Spatial Coding by Oscillatory Interference. J. Neurosci. *31*, 16157–16176.

Wells, C.E., Amos, D.P., Jeewajee, A., Douchamps, V., Rodgers, J., O'Keefe, J., Burgess, N., and Lever, C. (2013). Novelty and Anxiolytic Drugs Dissociate Two Components of Hippocampal Theta in Behaving Rats. J. Neurosci. *33*, 8650–8667.

Whishaw, I.Q., and Vanderwolf, C.H. (1971). Hippocampal EEG and behavior: effects of variation in body temperature and relation of EEG to vibrissae movement, swimming and shivering. Physiol. Behav. *6*, 391–397.

Wills, T., Barry, C., and Cacucci, F. (2012). The abrupt development of adult-like grid cell firing in the medial entorhinal cortex. Front. Neural Circuits *6*, 21.

Wills, T.J., Cacucci, F., Burgess, N., and O'Keefe, J. (2010). Development of the Hippocampal Cognitive Map in Preweanling Rats. Science *328*, 1573–1576.

Wilson, M.A., and McNaughton, B.L. (1993). Dynamics of the hippocampal ensemble code for space. Science *261*, 1055–1058.

Winocur, G. (1982). Radial-arm-maze behavior by rats with dorsal hippocampal lesions: effect of cuing. J. Comp. Physiol. Psychol. *96*, 155–169.

Winter, S.S., Mehlman, M.L., Clark, B.J., and Taube, J.S. (2015a). Passive Transport Disrupts Grid Signals in the Parahippocampal Cortex. Curr. Biol. *25*, 2493–2502.

Winter, S.S., Clark, B.J., and Taube, J.S. (2015b). Disruption of the head direction cell network impairs the parahippocampal grid cell signal. Science *347*, 870–874.

Witter, M.P. (2007). Intrinsic and extrinsic wiring of CA3: Indications for connectional heterogeneity. Learn. Mem. *14*, 705–713.

Witter, M.P., and Amaral, D.G. (2004). CHAPTER 21 - Hippocampal Formation A2 - Paxinos, George. In The Rat Nervous System (THIRD EDITION), (Burlington: Academic Press), pp. 635–704.

Witter, M.P., Wouterlood, F.G., Naber, P.A., and Van Haeften, T. (2000). Anatomical organization of the parahippocampal-hippocampal network. Ann. N. Y. Acad. Sci. *911*, 1–24.

Yartsev, M.M. (2013). Eppendorf. Space bats: multidimensional spatial representation in the bat. Science *342*, 573–574.

Yartsev, M.M., and Ulanovsky, N. (2013). Representation of three-dimensional space in the hippocampus of flying bats. Science *340*, 367–372.

Yartsev, M.M., Witter, M.P., and Ulanovsky, N. (2011). Grid cells without theta oscillations in the entorhinal cortex of bats. Nature *479*, 103–107.

Yoder, R.M., and Pang, K.C.H. (2005). Involvement of GABAergic and cholinergic medial septal neurons in hippocampal theta rhythm. Hippocampus *15*, 381–392.

Yoganarasimha, D., Rao, G., and Knierim, J.J. (2011). Lateral entorhinal neurons are not spatially selective in cue-rich environments. Hippocampus *21*, 1363–1374.

Yoon, K., Buice, M.A., Barry, C., Hayman, R., Burgess, N., and Fiete, I.R. (2013). Specific evidence of low-dimensional continuous attractor dynamics in grid cells. Nat. Neurosci. *16*, 1077–1084.

Yoon, K., Lewallen, S., Kinkhabwala, A.A., Tank, D.W., and Fiete, I.R. (2016). Grid Cell Responses in 1D Environments Assessed as Slices through a 2D Lattice. Neuron *89*, 1086–1099.

Zilli, E.A. (2012). Models of Grid Cell Spatial Firing Published 2005–2011. Front. Neural Circuits *6*.

Ziv, Y., Burns, L.D., Cocker, E.D., Hamel, E.O., Ghosh, K.K., Kitch, L.J., Gamal, A.E., and Schnitzer, M.J. (2013). Long-term dynamics of CA1 hippocampal place codes. Nat. Neurosci. *16*, 264–266.